The University Of Sheffield.

Access to Electronic Thesis

Author:	Richard Wells
Thesis title:	The roles of JAK / STAT pathway and Fasciclin III within epithelial structures during Drosophila development
Qualification:	PhD

This Thesis was embargoed until 20th July 2017.

If this electronic thesis has been edited by the author it will be indicated as such on the title page and in the text.

The roles of the JAK/STAT pathway and Fasciclin III in epithelial structures during Drosophila development

Richard Edward Wells

Submitted to the University for the Degree of

Doctor of Philosophy

January 2012

Abstract

The processes which drive morphogenesis during *Drosophila* development are well studied. However, the mechanisms employed to preserve the structures formed as a result of these events are poorly understood. The work of this thesis examines the role of localised cell signalling in effecting the morphogenesis of epithelial tissues.

The *Drosophila* embryonic hindgut is a curved epithelial tube which undergoes elongation and rotation to form a shepherd's crook shaped organ which breaks with the symmetry of the embryo. Work within this thesis describes how asymmetric JAK/STAT signalling, on the inside of the curve, positively regulates protein levels of the homophilic adhesion molecule Fasciclin III (FasIII). Increased levels of FasIII lead it to become asymmetrically distributed throughout the lateral cell membrane. Loss of either JAK/STAT signalling or FasIII leads to a reduction in the magnitude of the hindgut curve. Furthermore, preliminary data indicates that the spatial regulation of JAK/STAT signalling, and lateral FasIII, is also required for correct directional control of hindgut rotation.

Secondly, this thesis describes a role for localised JAK/STAT signalling and lateralised FasIII in maintaining the shape of folds within the prospective hinge of the 3rd instar larval wing disc. Further investigation of these folds indicates that their development is required for correct wing posture within the adult.

This thesis confirms FasIII as a mediator of cell-cell adhesion. It is therefore hypothesised that the lateralised FasIII domain increases tissue stability within the hindgut curve and the wing disc folds. Loss of this intrinsic support results in these structures being unable to maintain their form during development.

Declaration

I declare, that this thesis is the result of my own work except where the work of others is cited, either explicitly or via the list of references.

No part of this work has been submitted for a degree, diploma or other qualification at any other university.

Richard Edward Wells

June 2012

Acknowledgements

Firstly I would like to thank Mum and Dad for all their help and support over the years. I wouldn't have got to where I am without you.

I'd also like to thank my sister Rosie and my grandparents, Grandma, Pap, Gran and Grandad, as well as all my aunts, uncles and cousins for always being there for me.

It would have not been possible to undertake this work without the help, and advice, of my supervisors Martin Zeidler and David Strutt as well as members of the Zeidler and Strutt labs, past and present. Thank you for everything.

Over the years I have been lucky enough to live and study in a number of places. In each I have made countless friends who have always been there for me. A special mention goes to my friends in Leicester for being quick to learn, and kind enough, not to ask me "how work is going?" Also, to my friends in Sheffield who gave me a reason to leave the lab at the end of the day, and not to come in at the weekends (too often…).

Acknowledgements

This work is dedicated to Pap, 1st April 1923 – 13th September 2011.

Abbreviations

Genes and Proteins

α-catenin	α-cat	**Abdominal B**	Abd-b
aeroplane	ae	**Antennapedia**	Antp
apontic	apt	**apterous**	ap
armadillo	arm	**bazooka**	baz
brother of odd with entrails limited	bowl	**brachyenteron**	byn
coracle	cora	**crumbs**	crb
dally-like	dlp	**daughterless**	da
dead ringer	dri	**DE-cadherin**	DE-cad
decapentaplegic	dpp	**Delta**	Dl
Dichaete	D	**discs large**	dlg
Distal-less	Dll	**division abnormally delayed**	dally
domeless	dome	***Drosophila* Protein Inhibitors of Activated Stats**	dPIAs
drumstick	drm	**engrailed**	en
Epidermal Growth Factor Receptor	EGFR	**even-skipped**	eve
eye transformer	et	**eyes absent**	eya
Fasciclin II	FasII	**Fasciclin III**	FasIII
fork head	fkh	**four-jointed**	fj
G-Coupled Protein Receptors	GPCRs	**Gliotactin**	Gli
Green Fluorescent Protein	GFP	**hedgehog**	hh
head involution defective	hid	**heparan sulfate proteoglycipians**	HSPGs
Histone Deacetylase	HDAC	**hopscotch**	hop
huckabien	hkb	**Insulin gene enhancer protein**	Isl-1
Interferons	IFN	**inversion**	inv
Janus Kinase	JAK	**ken and barbie**	ken
knirps	kni	**knirps-related**	kni
kune-kune	kune	**Lachesin**	Lac
latran	lat	**lethal giant larvae**	lgl
lines	lin	**Megatrachea**	Mega

Genes and Proteins - continued

Melanotransferrin	MTf	**Myosin-31DF**	Myo31DF
Myosin-61F	Myo61F	**multiple ankyrin repeats single KH domain**	mask
Neurexin-IV	Nrx-IV	**Neuroglian**	Nrg
nuclear poly(A)-binding protein	PABPN1	**outstretched**	os
patched	ptc	**parkin**	park
Pituitary Homeobox 2	PITX2	**PTEN-induced putative kinase 1**	Pink1
rhomboid	rho	**scribble**	scrib
serpentine	serp	**Serrate**	Ser
shotgun	shg	**Sonic Hedgehog**	Shh
Signal Transducer and Activator of Transcription	STAT	**single-minded**	sim
sinuous	sinu	**sister of odd and bowl**	sob
slow border cells	slbo	**spread**	sprd
stardust	sdt	**Suppressor Of Cytokine Signalling**	Socs
tailless	tll	**taxi**	tx
teashirt	tsh	**torso**	tor
trachealess	trh	**Transforming Growth Factor ß**	TGF- ß
Ultrabithorax	Ubx	**unpaired**	upd
unpaired 2	upd2	**unpaired 3**	upd3
varicose	vari	**ventral veinless**	vll
vermiform	vemi	**vestigial**	vg
Wiskott-Aldrich syndrome protein	WASp	**wingless**	wg
zinc finger homeodomain protein-2	zfh-2		

Biological Structures

Anal Pads	ap	**Anterior midgut**	amg
Border Cells	BCs	**Dorsal Mesentery**	DM
Dorsal Mesocardium	DMC	**Epidermis**	e
Esophagus	es	**Extracellular Matrix**	ECM
Foregut	fg	**Heart Tube**	HT
Hindgut	hg	**Large Intestine**	LI
Large Intestine dorsal	LI-d	**Large Intestine ventral**	LI-v
Malpighian Tubules	mp	**Midgut**	mg
Omphalomesenteric veins	OVs	**Polar Cells**	PCs
Pharynx	ph	**Posterior midgut**	pmg
Posterior Spiracles	ps	**Proctodeum**	pr
Rectum	rec	**Ring Gland**	rg
Salivary gland	sg	**Septate Junction**	SJ
Small Intestine	SI	**Splanchnopleure**	SPL
Tracheal Placodes	tp	**Visceral Mesoderm**	vm

Miscellaneous

Adenosine TriPhosphate	ATP	**Atomic Force Microscopy**	AFM
Bovine Serum Albumin	BSA	**Chromatin Immuno-Precipitation**	ChIP
Co-immunoprecipitation	co-IP	**Complementary DNA**	cDNA
Cyanine dyes	Cy	**Developmental Studies Hybridoma Bank**	DSHB
Differential Adhesion Hypthesis	DAH	**Dionised water**	dH_20
Dithiothreitol	DTT	**Ethylenediaminetetraacetic acid**	EDTA
Electron Microscopy	EM	**Fetal Bovine Serum**	FBS
Fluorescein isothiocyanate	FITC	**Fluorescent Recovery After Photobleaching**	FRAP
Horse Radish Peroxidase	HRP	**Hour**	hr
Hour	hr	**Hydrochloric acid**	HCl
***In-vitro* Transcription**	IVT	**Luria-Betani**	LB
Magnesium chloride	$MgCl_2$	**Messenger RNA**	mRNA
Micro RNA	miRNA	**Minute**	min
Not Significant	ns	**Normal Horse Serum**	NHS
Planar Cell Chirality	PCC	**Planar Cell Polarity**	PCP

Miscellaneous - continued

Polymerase Chain Reaction	PCR	**Potassium Acetate**	KoAC
Potassium chloride	KCl	**Potassium ferricyanide**	$K_3Fe(CN)_6$
Potassium phosphate (dibasic)	$K_3Fe(CN)_6$	**Real Time-Quantitative PCR**	RT-qPCR
Region Of Interest	ROI	**RNA interference**	RNAi
Second	sec		
Sodium acetate	NaOAc	**Sodium bicarbonate**	$NaHCO_3$
Sodium chloride	NaCl	**Sodium citrate dihydrate**	Na_3citrate2 H_2O
Sodium Dodecyl Sulphate	SDS	**Sodium phosphate (monobasic)**	Na_2HPO_2
Total RNA	TRNA	**Upstream Activating Sequence**	UAS
Vienna *Drosophila* Resource Centre	VDRC		

Table of Contents

List of Figures

List of Tables

List of Videos

1 Introduction

1.1 Overview

The work in this thesis examines the effect of the JAK/STAT pathway on tissue morphology in *Drosophila* epithelia. As a general introduction I will be focusing on the components of the JAK/STAT pathway, its regulation and its roles in *Drosophila*. In addition, I will also give a brief overview of cellular junctions in epithelia. As a large body of the work concerns the embryonic hindgut I will then focus on its development, from patterning to morphogenesis. While the wing disc is also examined as part of this work, this will be discussed in the relevant results chapter (Chapter 6).

1.2 The JAK/STAT pathway

1.2.1 Components of the mammalian JAK/STAT pathway

The mammalian canonical JAK/STAT pathway consists of a set of core proteins required for signal transduction. Signalling occurs when an extra-cellular ligand binds to a transmembrane receptor. To date numerous ligands, divided into the IFN, gp130, yC, IL3 and Single Chain families, and receptors have been identified, (reviewed in, Schindler and Plumlee, 2008). Ligand binding results in a conformational change in the receptor activating a non-receptor tyrosine Janus Kinase (JAK) of which there are four JAK1, JAK2 (Wilks et al., 1991), JAK3 (Takahashi and Shirasawa, 1994) and Tyk2 (Firmbach-Kraft et al., 1990). Once activated, the JAK trans-phosphorylates other JAK molecules and receptors in the complex providing docking sites for Signal Transducer and Activator of Transcription (STAT) transcription factors (Sakatsume et al., 1995, Chen et al., 2002). In mammals there are seven STAT molecules, STAT1 (Shuai et al., 1992), STAT2 (Improta et al., 1994), STAT3 (Zhong et al., 1994), STAT4 (Yamamoto et al., 1994), STAT5a, STAT5b (Azam et al., 1995) and STAT6 (Quelle et al., 1995). Once phosphorylated, by JAK, STATs form homodimers, via SH2 domains (Shuai et al., 1994), and translocate to the nucleus (Koster and Hauser, 1999). When in the nucleus, STAT molecules act to positively and negatively regulate the transcription of genes (Bina

et al., 2010, Vogl et al., 2010). Aberrant pathway activity, through mutations in these key components, leads to numerous human disorders such as myeloproliferative cancers (reviewed in, Tefferi and Gilliland, 2005, Valentino and Pierre, 2006), vascular disease (reviewed in, Grote et al., 2005) and autoimmune disorders (reviewed in, Gee et al., 2009).

1.2.2 The model organism *Drosophila melanogaster*

The fruit fly *Drosophila melanogaster* was first introduced into the laboratory at the beginning of the 20th century by the eminent geneticist Thomas Morgan who won the 1933 Medicine Nobel Prize for his work on heredity (reviewed in, Raju, 1999). Concerted work over the last century has developed it as a laboratory genetic workhorse, driving the identification and characterisation of novel genes. This is largely due to its short generation time and ease of genetic manipulation, setting it apart from other vertebrate and amphibian model organisms. Over the years, *Drosophila* mutants lacking homologues of human disease relevant genes have led to breakthroughs in the study of various disorders including Parkinson's disease, (reviewed in, Whitworth, 2011), Alzheimer's (reviewed in, Cowan et al., 2010) and numerous cancers (reviewed in, Polesello et al., 2011).

As well as disease models, *Drosophila* is also extensively used to examine embryogenesis and the processes involved. The most striking of these studies examined mutants that caused embryonic lethality. This resulted in the discovery and mapping of numerous genes required for axis generation and segmentation (Nusslein-Volhard and Wieschaus, 1980). This alone generated a wealth of knowledge that has led to countless additional studies and resulted in the authors Christiane Nüsslein-Volhard and Eric Wieschaus being awarded the 1995 Nobel Prize in Physiology or Medicine (Raju, 2000). With regards to developmental processes the *Drosophila* embryo has nuances making it distinct from other model organisms. During its early life, a 4000 nuclei syncytium is formed prior to the synthesis of intercellular membranes (Hartenstein, 1993,Campos-Ortega and Hartenstein, 1997). This sets *Drosophila* apart from other organisms such as the nematode worm *Caenorhabditis elegans* (reviewed in, Bowerman, 2000) and higher

mammalian organisms (reviewed in, Wolpert et al., 2006). Furthermore, the process of germband extension, a combination of cell division and movement resulting in a large-scale epithelial migration, while conserved in long germband insects, does not occur in other organisms (Hartenstein, 1993,Campos-Ortega and Hartenstein, 1997). Despite the unique nature of these processes they have been extensively investigated, providing an invaluable insight into cellular biology. For example, study of the syncytium has led to a greater understanding of mechanisms controlling the subcellular localisation of RNA(reviewed in, Riechmann and Ephrussi, 2001) while germband extension has highlighted the roles of cell morphology and movement in large scale tissue migrations (Blankenship et al., 2006, Bertet et al., 2009, Simoes Sde et al., 2010).

1.2.3 The *Drosophila* JAK/STAT pathway

The *Drosophila* JAK/STAT pathway is a simple, low redundancy, homologue of the mammalian system (Table1.1). It is therefore, a good model in which to examine its regulation and function. This simplified cascade contains three ligands, Unpaired (Upd) (Harrison et al., 1998), Unpaired 2 (Upd2) (Gilbert et al., 2005, Hombria et al., 2005) and Unpaired 3 (Upd3) (Agaisse et al., 2003), a single receptor Domeless (Dome) (Brown et al., 2001), a single JAK kinase Hopscotch (Hop) (Binari and Perrimon, 1994) and a single transcription factor Stat92E (Hou et al., 1996), which binds the consensus sequence TTC(3n/4n)GAA (Rivas et al., 2008) (Fig1.1). In addition to canonical, ligand-dependent signalling, the *Drosophila* JAK/STAT pathway has also been found to function in a non-canonical manner, regulating chromatin structure (Shi et al., 2006) This is conserved in the mammalian system (Dawson et al., 2009, He and Zhang, 2010). In the absence of ligand-dependent signalling, monomeric unphosphorylated Stat92E binds chromatin-associated proteins promoting the formation of heterochromatin (Shi et al., 2008).

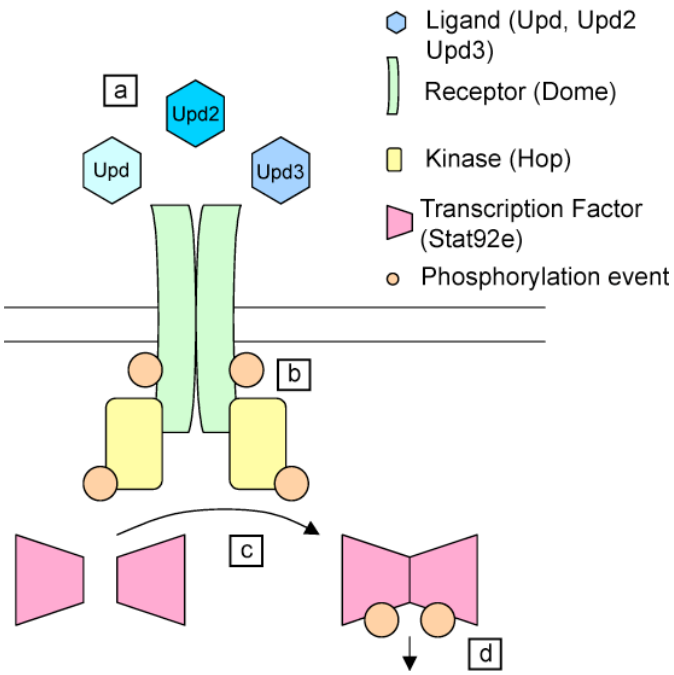

Figure 1.1: The *Drosophila* JAK/STAT pathway core components.
(a) Ligands Upd, Upd2 and Upd3 bind to the receptor, Dome. (b) Ligand binding causes cross phosphorylation by the kinase Hop of itself and Dome. (c) The Dome/Hop complex phosphorylates the transcription factor, Stat92E. (d) Stat92E forms dimers and translocates to the nucleus.

Regulation of the *Drosophila* JAK/STAT pathway occurs at multiple stages from ligand to transcription factor. Of the three ligands Upd and Upd2 display similar expression patterns while Upd3 is distinct (Harrison et al., 1998, Hombria et al., 2005). These differing expression patterns suggest a mechanism of spatial pathway regulation during development. Furthermore, Upd and Upd3 bind the ECM while Upd2 diffuses more freely (Hombria et al., 2005, Wright et al., 2011). This indicates that regulation of the ligands extracellular dynamics is likely to fine-tune the paracrine manner in which the pathway signals (Tsai and Sun, 2004).

In addition to Dome, there is a truncated JAK/STAT receptor Latran (Lat)/Eye transformer (Et) which negatively regulates the pathway by forming non-signalling heterodimers with Dome (Kallio et al., 2010, Makki et al., 2010). As with many signalling pathways, once ligand is bound to the receptor the complex is subject to endocytosis (reviewed in, Scita and Di Fiore, 2010). In the case of the JAK/STAT

pathway there is conflicting evidence whether this acts to positively (Devergne et al., 2007) or negatively (Vidal et al., 2010) regulate signal transduction.

Downstream of the receptor, numerous negative regulators have been identified, however, their mechanisms of inhibition are poorly understood in *Drosophila*. Proposed to function at the level of the receptor-kinase complex are Suppressor Of Cytokine Signalling (SOCS) Socs36E (Callus and Mathey-Prevot, 2002, Karsten et al., 2002), multiple ankyrin repeats single KH domain (Mask) (Muller et al., 2005) and the phosphatase Ptp61F (Baeg et al., 2005, Muller et al., 2005). Regulation at the level of the transcription factor is mediated by *Drosophila* Protein Inhibitors of Activated Stats (dPIAs) (Betz et al., 2001), Ken and Barbie (Ken) (Arbouzova et al., 2006, Hombria and Sotillos, 2006) and the truncated Stat molecule ΔNStat (Henriksen et al., 2002). In addition to direct inhibition at the protein level, the microRNA (miRNA), *miRNA-279* has been found to regulate levels of *stat92E* transcript by binding to its 3'UTR resulting in its degradation (Yoon et al., 2011).

Drosophila protein	Nearest mammalian homologue	Relevant references
Upd, Upd2 and Upd3	LIF	(Arbouzova and Zeidler, 2006)
Dome	LIFR	(Brown et al., 2001)
Hop	JAK2	(Binari and Perrimon, 1994)
Stat92E	STAT5	(Hou et al., 1996)
Et/Lat	IL-6, gp-130	(Kallio et al., 2010, Makki et al., 2010)
Socs36E	SOCS-5	(Karsten et al., 2002, Callus and Mathey-Prevot, 2002)
dPIAs	No clear homologue	(Betz et al., 2001)
Ken	Bcl-6	(Arbouzova et al., 2006)
Ptp61F	PTP-1B	(Baeg et al., 2005, Muller et al., 2005)

Table 1.1: *Drosophila* homologues of components of the mammalian JAK/STAT pathway

1.2.4 Roles of the JAK/STAT pathways in *Drosophila*

Despite its low redundancy, the *Drosophila* JAK/STAT pathway is involved in many aspects of the organism's development and homeostasis. Many JAK/STAT human disease relevant processes can be modelled using aspects of the fly's physiology from control of cell number (Hou et al., 1996, Bach et al., 2003, Tsai and Sun, 2004, Mukherjee et al., 2005, Betz et al., 2008), to immunity (Ekengren et al., 2001, Agaisse et al., 2003, Makki et al., 2010).

In this thesis, the embryonic hindgut, egg chamber and 3rd instar wing imaginal disc are used as model systems. The role of JAK/STAT signalling in the wing disc is largely uncharacterised, however, the relevant aspects of wing disc development will be

discussed in Chapter 6. The pathway does have known roles in hindgut morphogenesis, discussed in 1.4.5, and the egg chamber, discussed below.

The process of border cell migration, within the egg chamber during oogenesis, is a *Drosophila* model for cancer metastasis. During this process, six to eight cells, comprised of two polar cells (PCs) and between four to six specialised follicle cells, the border cells (BCs), delaminate from the anterior of the egg chamber and migrate through the nurse cells to the anterior of the oocyte (Fig1.2a). Here they form the micropyle which allows sperm access to the egg for fertilisation (reviewed in, Rorth, 2002). The JAK/STAT pathway is activated in a gradient with the ligand Upd being released from the PCs, signalling to the adjacent BCs (Xi et al., 2003), increasing the expression of *slow border cells* (*slbo*) and *shotgun* (*shg*), which encodes DE-cadherin (DE-cad) (Silver and Montell, 2001). Loss of both these targets affects BC migration (Montell et al., 1992, Niewiadomska et al., 1999) (Fig1.2b-c). The signalling gradient is established through the regulation of the pathway and its targets by the opposing action of *apontic* (*apt*), *eyes absent* (*eya*) and *miRNA-279* (Starz-Gaiano et al., 2008, Starz-Gaiano et al., 2009, Yoon et al., 2011) (Fig1.2b). Either loss of, or ectopic, JAK/STAT pathway activation results in a respective reduction or increase in the number of BCs as well as a failure to complete migration to the oocyte. As such, JAK/STAT signalling has an important role in both BC recruitment and migration (Silver and Montell, 2001, Ghiglione et al., 2002, Beccari et al., 2002, Silver et al., 2005).

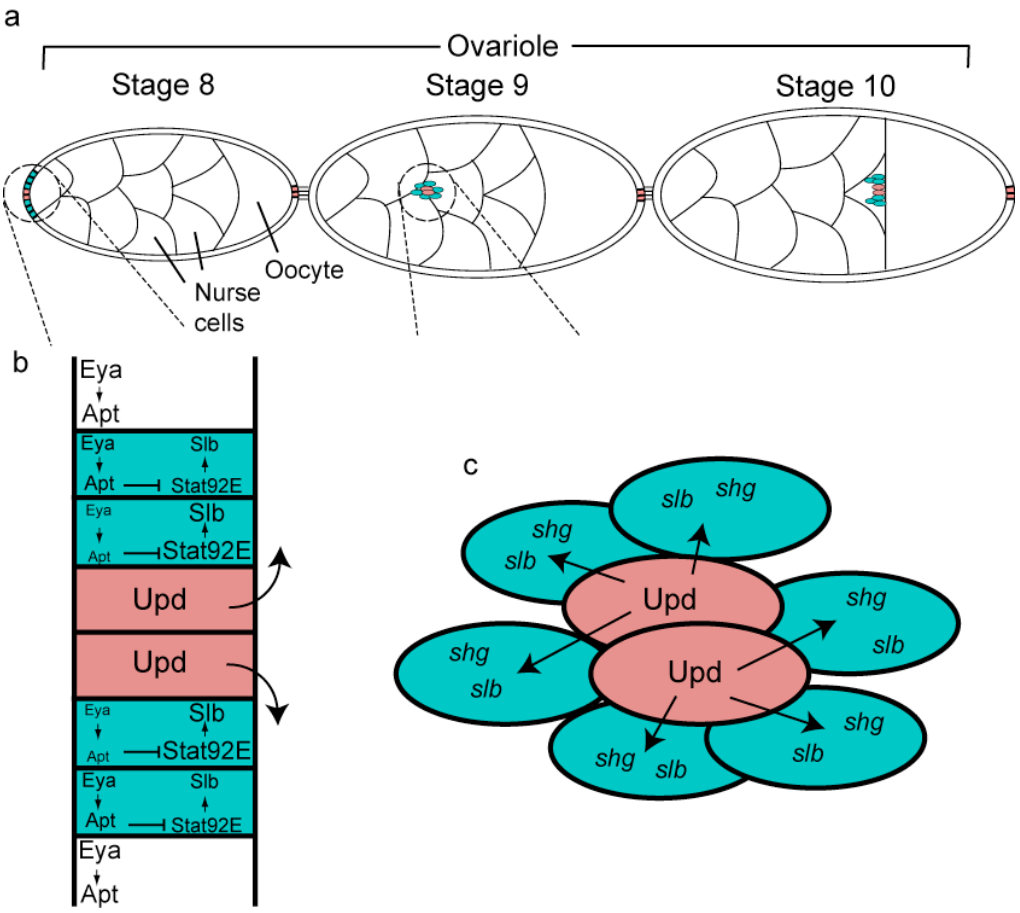

Figure 1.2: The role of JAK/STAT signalling in border cell migration.

(a) PCs, red, recruit BCs, blue, at the anterior of the egg chamber during stage 8 of oogenesis. As stage 9 progresses this clump of cells migrates through the nurse cells reaching the anterior of the oocyte at stage 10. (b) Upd is secreted from the pole cells increasing levels of *slbo* and *shg* (not shown), which defines presumptive border cells. This activity is repressed through an opposing gradient of Eya activating *apt* resulting in the inhibition of Stat92E via *miRNA279* (not shown). (c) During migration JAK/STAT signalling is still required to maintain correct border cell migration.

Of further relevance to the work of this thesis are the known roles of JAK/STAT signalling in embryo morphogenesis. In the embryo, loss of JAK/STAT signalling has been shown to cause aberrant morphogenesis of the posterior spiracles. These are the external structures required for gas exchange in larvae (Brown et al., 2001, Hombria et al., 2005). This defect is caused by a failure of the cells of the spiracular chamber, the internal tube that connects to the trachea, to fully elongate. Loss of JAK/STAT signalling causes a change in the expression of a number of adhesion molecules, DE-cad, Crumbs

(Crb), a Rho1 GTPase regulator RhoGEF64C and the un-conventional cadherins Cad88C and Cad96C (Lovegrove et al., 2006). While Crb, DE-cad, Cad88C and Cad96C appear to act in a largely redundant fashion (Lovegrove et al., 2006) the RhoGEF64C has a role in modulating the subcellular activity of Rho1, integral for MyosinII localisation and subsequent spiracular tube cell elongation (Simoes et al., 2006).

While less well characterised, the JAK/STAT pathway is also required for cell rearrangement in the foregut (Harrison et al., 1998, Josten et al., 2004). This is thought to be due to regulation of Notch signalling (Josten et al., 2004), which appears to be a downstream effector of cell movement (Fuss et al., 2004). A further role of JAK/STAT signalling is as an upstream regulator of tracheal placode invagination (Hou et al., 1996, Li et al., 2003) through the regulation of transcription factors *ventralveinless* (*vvl*) and *trachealess* (*trh*) (Sotillos et al., 2010). In addition, the pathway also modulates changes in cell shape during germband extension, through the regulation of Wiskott-Aldrich syndrome protein (WASp), resulting in changes in the localisation of actin (Bertet et al., 2009).

1.3 Cellular Junctions

1.3.1 Epithelial cellular junctions

In all multicellular organisms connections, junctions, between cells are integral for many processes. The formation, composition and function of these junctions is largely dependent on the properties of the cell. The work in this thesis focuses exclusively on epithelial tissues that often form the external boundaries of organs. Key to epithelial function is the maintenance of connections between cells mediated by cellular junctions (Fig1.3). These membrane domains are required to maintain a cohesive, polarised boundary, which is important for cellular functions such as signalling (Sotillos et al., 2008), endocytosis {Van (Wingen et al., 2009) and exocytosis (Van de Bor et al., 2011).

Key to generating a uniform membrane polarity is the establishment of apical-basal domains. This occurs early in the *Drosophila* embryo and requires the interactions of two

apically localised protein complexes, the Par complex (containing Par6, aPkc and Bazooka – Baz) and the Crb complex (containing Crb, Stardust – Sdt and Patj), with the basally localised Scrib complex (containing Scribbled – Scrib, Lethal giant Larvae – Lgl and Discs large – Dlg) (reviewed in, Assemat et al., 2008). A further junctional complex is the apically localised adherens, zonula, junction, which is comprised of DE-cad, α-catenin, β-catinin and P120, whose establishment is dependent on correct apical basal polarity (reviewed in, Tepass, 2002). Components of adherens junctions perform numerous functions, for example DE-cad establishes homophilic adhesive complexes between neighbouring cells (Nagafuchi et al., 1987), while Armadillo (Arm), *Drosophila* β-catenin*,* is a co-factor of the Wingless (Wg) signal transduction pathway (Noordermeer et al., 1994). Another junction that is integral to epithelial function is the septate junction (SJ) which contains multiple components, (Banerjee et al., 2006, Wu et al., 2007, Hijazi et al., 2009, Nelson et al., 2010, Tiklova et al., 2010), discussed in 1.3.2.

While often defined as self-contained membrane regions, there is much cross-talk occurs between junctional components. In *Drosophila* the genetics of these interactions have been extensively investigated. Examining protein localisation in mutants of junction components has revealed the epistasis of the interactions. Two important examples of this are the apical Par/Crb and basal Scrib complexes, which antagonistically define each others domains (Tanentzapf and Tepass, 2003), and SJ junction components restricting the apically localised Crb (Laprise et al., 2009). Furthermore, numerous proteins having been characterised as components in different junctions, most notable are the basal Scrib complex proteins within the SJs (Fig1.3) (Banerjee et al., 2006, Assemat et al., 2008). This indicates a level of plasticity in the system

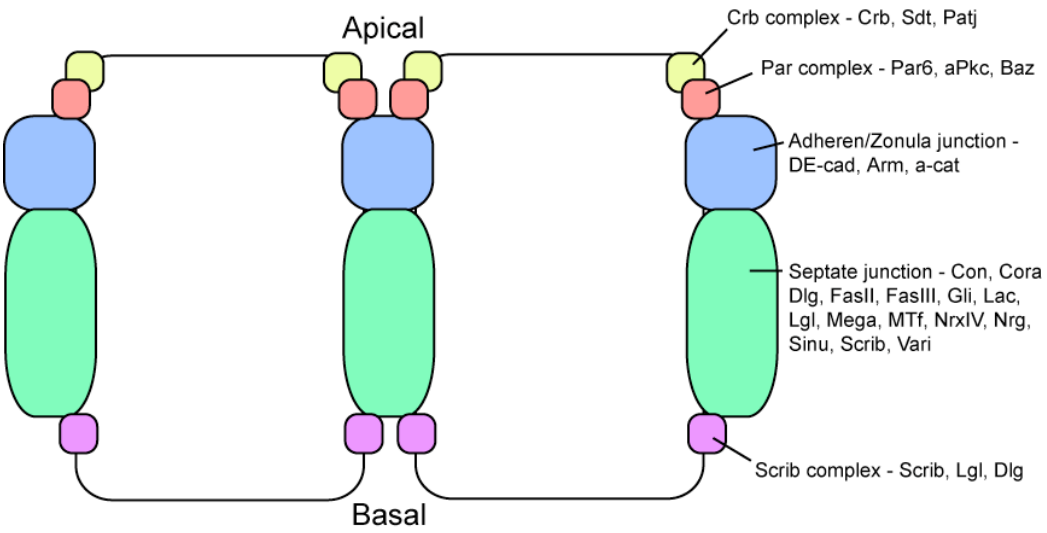

Figure 1.3: Schematic of epithelial cell junctions and their components.
At the apical cell surface are the Crb and Par complexes. Further basal are the adheren and SJs. Most basal is the Scrib complex.

1.3.2 Septate junctions

The work of thesis examines the SJ protein Fasciclin III (FasIII), discussed in 1.3.3, in *Drosophila* epithelia. While the majority of work examines the function prior to the formation of SJs a brief overview of this membrane domain is included. SJs, and their components, are homologous to vertebrate tight junctions (Banerjee et al., 2006). In ectoderm derived tissue FRAP analysis shows SJ components form progressively stable protein complexes from embryonic stage 13 (Oshima and Fehon, 2011) with SJs being visible from stage 14, by electron microscopy (EM) as intercellular junctions "pleated SJs" becoming fully mature septa in the 1st instar larvae (Tepass and Hartenstein, 1994).

Defects in SJs are associated with processes in which tight intercellular connections are required in epithelia. The function of SJs is best characterised in the *Drosophila* embryonic trachea. Numerous mutants of SJ proteins display abnormal, truncated, and in some cases broken, tracheal tubes causing an increase in transepithelial permeability (Behr et al., 2003, Paul et al., 2003, Faivre-Sarrailh et al., 2004, Wu et al., 2007, Hijazi et al., 2009, Nelson et al., 2010, Tiklova et al., 2010). Numerous hypotheses have been proposed for these defects including: a reduction in the secretion of ECM components

Vermiform (Verm) and Serpentine (Serp) (Wang et al., 2006, Luschnig et al., 2006, Laprise et al., 2010) and disruption of apical polarity (Laprise et al., 2009, reviewed in, Wu and Beitel, 2004). Due to the complex nature of SJs the defects are likely caused by a combination of the above. In addition to the embryonic trachea, correct SJ formation is required for the tight insulation of axons by glial cells, a primitive blood brain barrier. Loss of SJ proteins make this barrier permeable exposing nerves to the ions in the haemolymph (Baumgartner et al., 1996, Stork et al., 2008, Strigini et al., 2006, Hijazi et al., 2009).

1.3.3 Fasciclin III

Very little is known about FasIII function *in vivo*. Early characterisation of embryonic protein distribution noted it was present in a subset of neurons and axons as well as in the visceral mesoderm and numerous ectodermally derived structures (Patel et al., 1987). Despite its widespread expression, FasIII function has only been characterised in neuronal pathfinding. FasIII is expressed in the embryonic RP3 motor neuron and the muscles cells 6 and 7 which RP3 innervates. Loss of FasIII does not affect the fidelity of innervation, indicating a redundancy in function, however, ectopic expression of *FasIII* throughout the muscle results in the RP3 motor neuron innervating the incorrect muscle cells (Chiba et al., 1995). It was hypothesised that this process was due to the homophilic interactions between FasIII on both the neuron and muscles. This was confirmed through examination of neurons and muscles which do not normally innervate or express *FasIII*. Here, ectopic expression of *FasIII* in either the neurons or the muscles alone was not sufficient to mediate innervation, however, when expressed in both the neurons and muscles together innervation did occur (Kose et al., 1997).

1.4 The *Drosophila* embryonic hindgut

1.4.1 Overview of *Drosophila* embryonic digestive tract development

The *Drosophila* embryonic gut is divided into the anterior foregut and posterior hindgut, both derived from the ectoderm, and a central midgut, derived from the endoderm. The primordial gut tissue is defined by stage 5 of embryogenesis, the foregut and anterior midgut at the anterior extreme and the hindgut and posterior midgut at the posterior extreme of the embryo (Fig1.4a). At stage 7, after the tissue is defined, the gut undergoes three asynchronous cell divisions, regions of the hindgut, that have been specified as the Malpighian tubule cells, undergo a variable number of further cell divisions (Fig1.4b). These are the only mitoses observed in the gut for the whole of embryogenesis. At stage 13, the gut is still present in two halves, between stages 13 and 15 the midgut extends from the anterior and posterior fusing in the centre. This encompasses the yolk resulting in a continuous closed gut through the entire embryo (Fig1.4e-g). During the process of embryogenesis each gut compartment undergoes tightly regulated morphological movements, those involved in hindgut morphogenesis are described in 1.4.2-1.4.4 (Hartenstein, 1993, Campos-Ortega and Hartenstein, 1997).

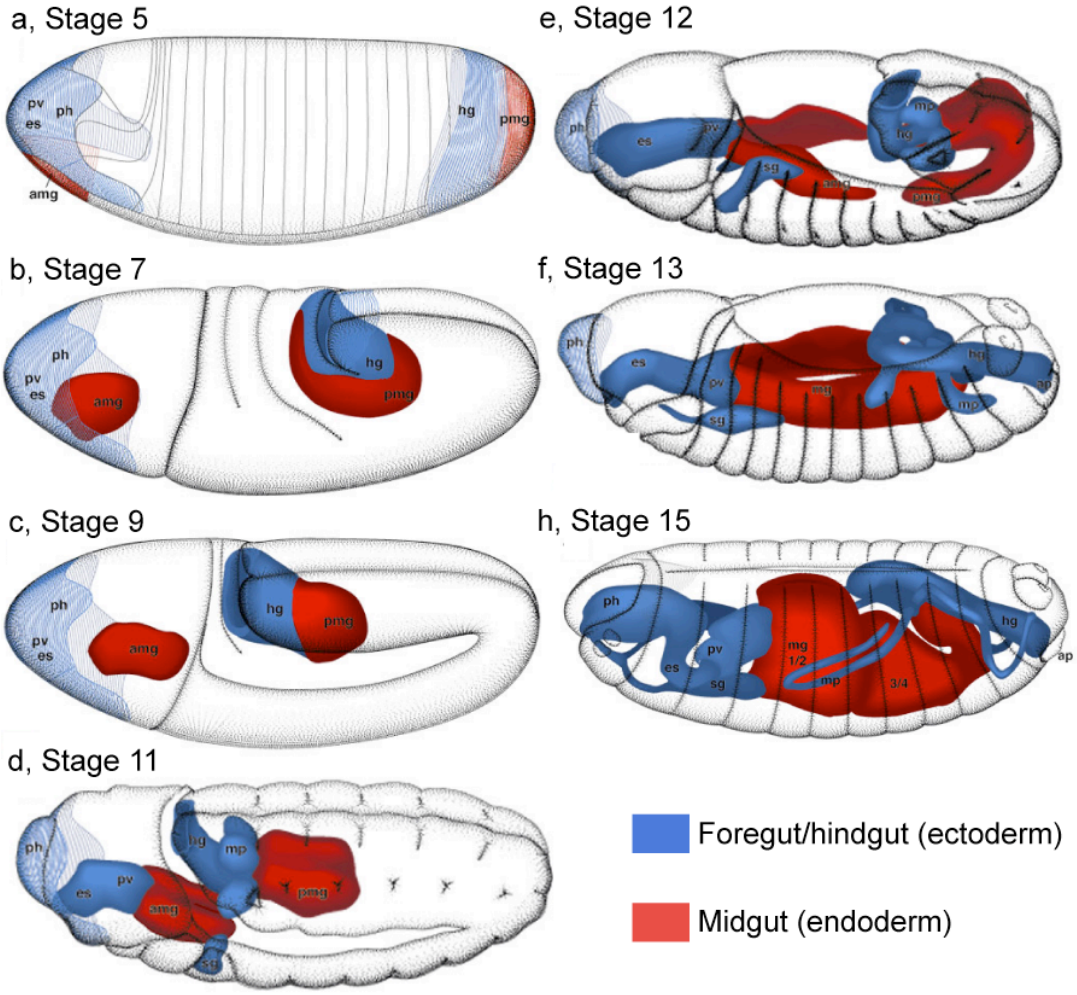

Figure 1.4: Development of the *Drosophila* digestive tract. (Adapted, with permission, from (Hartenstein, 1993).

(a) At stage 5, regions are fated to become the foregut, midgut and hindgut. (b-d) During stages 7-11 germband elongation occurs bringing the hindgut behind the embryonic head and (e) During stage 12 germband retraction occurs re-establishing the hindgut at the posterior of the embryo. (f) During stage 13 the midgut fuses. (h) By stage 15 the midgut has enveloped the yolk forming a contiguous closed gut through the embryo.

1.4.2 Morphogenesis of the *Drosophila* embryonic hindgut

The work in this thesis examines the morphogenesis of the hindgut compartment of the embryonic digestive tract. When fully developed this forms a shepherd's crook shape at the posterior of the embryo, characterised by a curve at the anterior, which breaks the symmetry of the embryo, bending from left to right (Fig1.5). This structure is further

divided into the anterior small intestine (SI), large intestine (LI) and posterior rectum (Rec) (Fig1.5) (Hartenstein, 1993,Campos-Ortega and Hartenstein, 1997). The patterning and definition of these regions is discussed in 1.4.3.

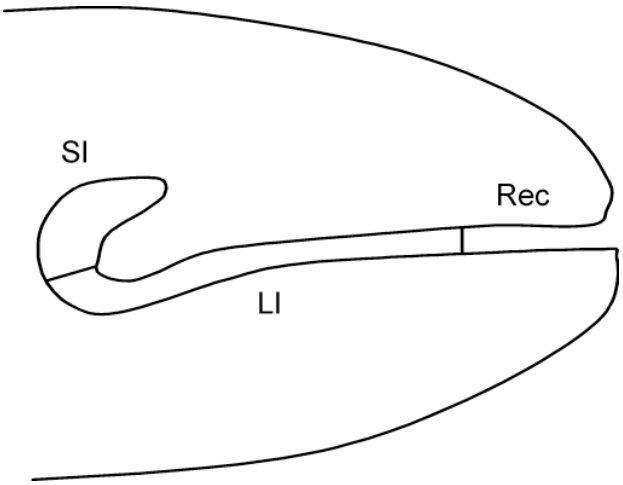

Figure 1.5: Schematic of the fully developed embryonic hindgut, as viewed from dorsal.
The embryonic hindgut lies at the posterior of the embryo. When fully formed, it is characterised by having an anterior curve. The hindgut is further subdivided into the anterior SI, LI and posterior Rec.

The hindgut undergoes several morphological processes to form the characteristic shepherd's crook shape. When the hindgut first becomes morphologically distinct at stage 10, post cell division, the anterior curve is already established (Hartenstein, 1993, Campos-Ortega and Hartenstein, 1997). Initial formation of the anterior curve is yet to be characterised, however, its structure is maintained unchanged through stage 11 and stage 12 of germband retraction. At this point the hindgut is bilateral with the curve bending into the centre of the embryo (Fig1.4d-e and Fig1.6 a-b)). Once the hindgut returns to the posterior of the embryo, stage 13 post germband retraction, it undergoes dextral rotation (Fig1.4f and Fig1.6c). After this dextral rotation, during stages 14 and 15 the hindgut undergoes elongation via convergent extension (Fig1.4g and Fig1.6d-e). (Hartenstein, 1993,Campos-Ortega and Hartenstein, 1997). These steps will be further described in Chapter three.

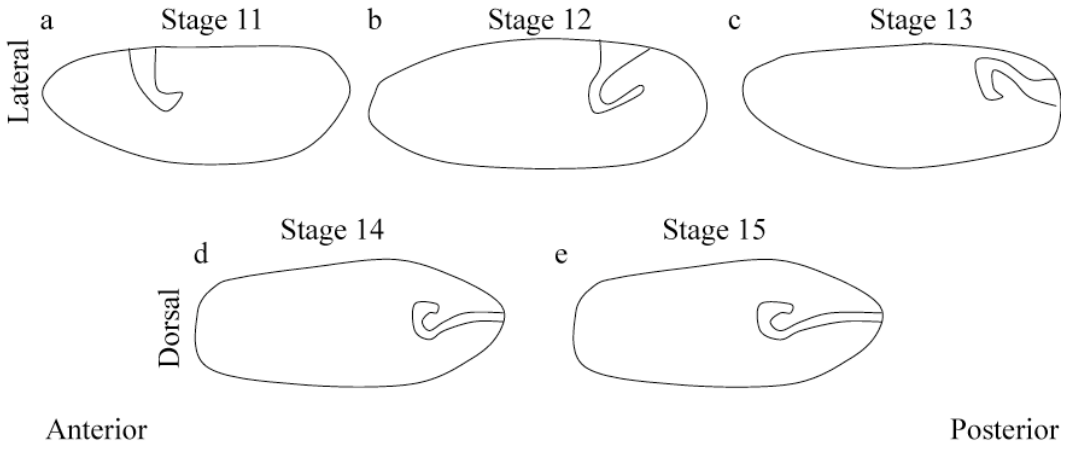

Figure 1.6: Schematic of hindgut morphogenesis during development.
(a) At stage 11, after germband extension, the hindgut forms a primordial curve whose topography is visible from lateral. This is found towards the anterior of the embryo behind the presumptive head. (b) During germband retraction the primordial hindgut curve remains constant and moves to the posterior of the embryo. (c) At stage 13 the primordial curve comes to rest at the posterior of the embryo and undergoes a dextral rotation. (d) At stage 14, after the stage 13 rotation, the hindgut curve is now visible bending from left to right when viewed from dorsal. During this period the hindgut begins to elongate. (e) During stage 15 hindgut elongation continues.

1.4.3 Patterning of the *Drosophila* embryonic hindgut

Cells destined to become the hindgut, initially known as the proctodeal primordia/ring, are established early in embryogenesis (Hartenstein, 1993,Campos-Ortega and Hartenstein, 1997). This is dependent on the regulation of the terminal gap genes *tailless* (*tll*) and *huckebein* (*hkb*) by the receptor tyrosine kinase Torso (Tor) (Fig1.7a) (Bronner et al., 1994, St Johnston and Nusslein-Volhard, 1992). Downstream of the gap genes are the transcription factors *brachyenteron* (*byn*) and *fork head* (*fkh*) which are expressed throughout the hindgut epithelium after invagination (Fig1.7b) (Weigel et al., 1989, Weigel et al., 1990, Kispert et al., 1994). Loss of either of these transcription factors results in widespread apoptosis (Singer et al., 1996, Wu and Lengyel, 1998).

Tll and Hkb are required for the expression of *hedgehog* (*hh)*, *wingless* (*wg*), *decapentaplegic* (*dpp*) and the transcriptional repressor *engrailed* (*en*) at stage 12 of embryogenesis (Hoch and Pankratz, 1996, Singer et al., 1996). These downstream genes are required to establish, and pattern, the three morphologically distinct compartments of

the hindgut, which arise at stage 13, the anterior SI (Fig1.7c), LI (Fig1.7d) and the posterior Rec (Fig1.7e). The boundaries between these compartments are marked with morphologically distinct border cells. The central LI is further split into dorsal (LI-d) and ventral (LI-v) by a further two rows of border cells which link the anterior SI/LI border cell ring and the posterior LI/Rec border cell ring (Fig1.7d). Much is understood about the signalling interplay that is required to establish these different compartments. To summarise: the most upstream factors Wg and Hh are expressed from the SI and Rec and are required for *dpp* expression in the LI. The LI is further patterned, defining the LI-d and LI-v, through the opposing action of En in the LI-d, restricting *dpp* and *Notch* to the LI-v (Takashima and Murakami, 2001). The border cell boundaries are then defined through the expression of *dead ringer* (*dri*) (Shandala et al., 1999), the nuclear steroid hormone receptors *knirps* (*kni*) and *knirps-related* (*knrl*) (Fuss et al., 2001), the transmembrane protein *rhomboid* (*rho*) (Fuss and Hoch, 2002) and *crb* (Tepass et al., 1990). The expression of these genes is largely due to the action of Delta signalling from the LI-v (Fig1.7c-e) (Iwaki and Lengyel, 2002, Fuss and Hoch, 2002).

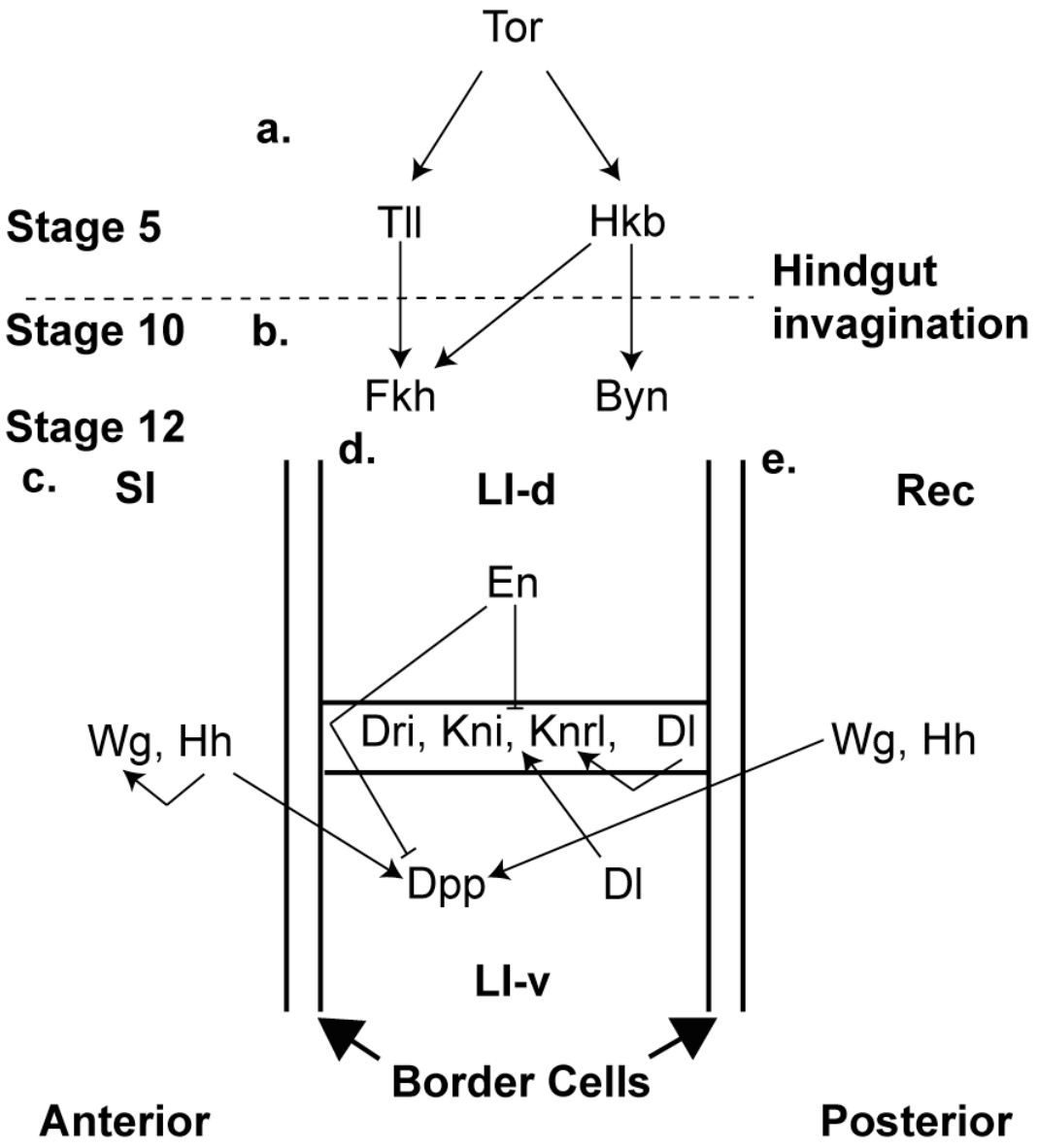

Figure 1.7: The regulation of hindgut patterning.

(a) The early function of Tor is required for the expression of *tll* and *hkb* which mediate early hindgut morphogenesis and later gene expression. (b) After invagination Fkh and Byn are required to maintain hindgut identity. (c-e) Signalling from the SI and Rec regulates genes in the LI which themselves define the LI-d and LI-v regions and the morphologically distinct boundaries, the border cells.

A key aspect of the work in this thesis is the spatial regulation of JAK/STAT signalling, through the localised expression of *upd*, at the anterior of the hindgut. This controlled by the zinc finger transcription factors *drumstick* (*drm*), *lines* (*lin*) and *brother of odd with entrails limited* (*bowl*). These are expressed in overlapping regions and operate in a "relief-of-repression" manner (Fig1.8). Bowl is the most downstream effector of transcription and is inhibited by Lin which is, in turn, inhibited by Drm (Fig1.8). Ectopic expression of these factors acts to re-pattern the hindgut resulting in the misexpression of *upd* (Liu et al., 1999, Iwaki et al., 2001, Green et al., 2002, Johansen et al., 2003a). In addition to the hindgut this regulation cassette is also required for the correct patterning of the embryonic foregut (Johansen et al., 2003a), embryonic epidermis (Hatini et al., 2005) and adult leg segmentation (Hao et al., 2003).

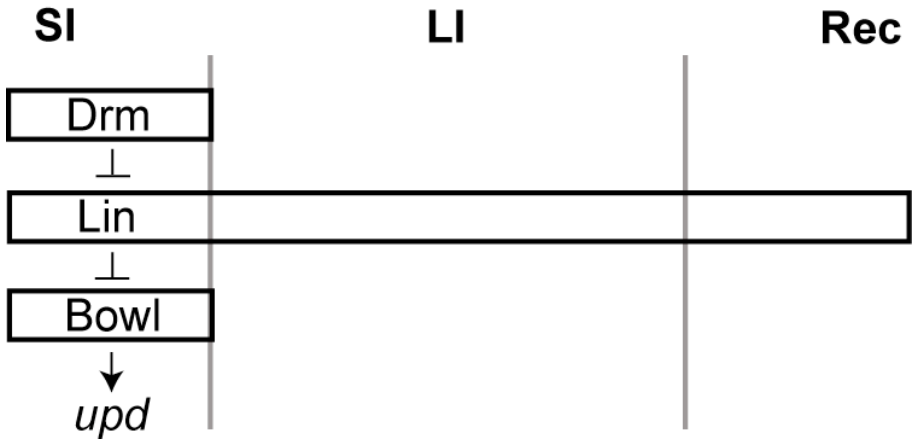

Figure 1.8: Restriction of *upd* expression to the SI.
The "relief-of-restriction" cascade of Drm, Lin and Bowl. Drm and Bowl are expressed in the SI with Lin being expressed throughout the hindgut. Bowl drives the expression of *upd*, the action of Lin inhibits Bowl while Lin is itself inhibited by Drm.

1.4.4 Rotation of the *Drosophila* embryonic hindgut

Hindgut rotation occurs during stage 13 at which time the anterior curve twists (from its bilateral position) 90° to the right, breaking the symmetry of the embryo and establishing "handedness" in the organ (Fig1.9) (Hartenstein, 1993,Campos-Ortega and Hartenstein, 1997).

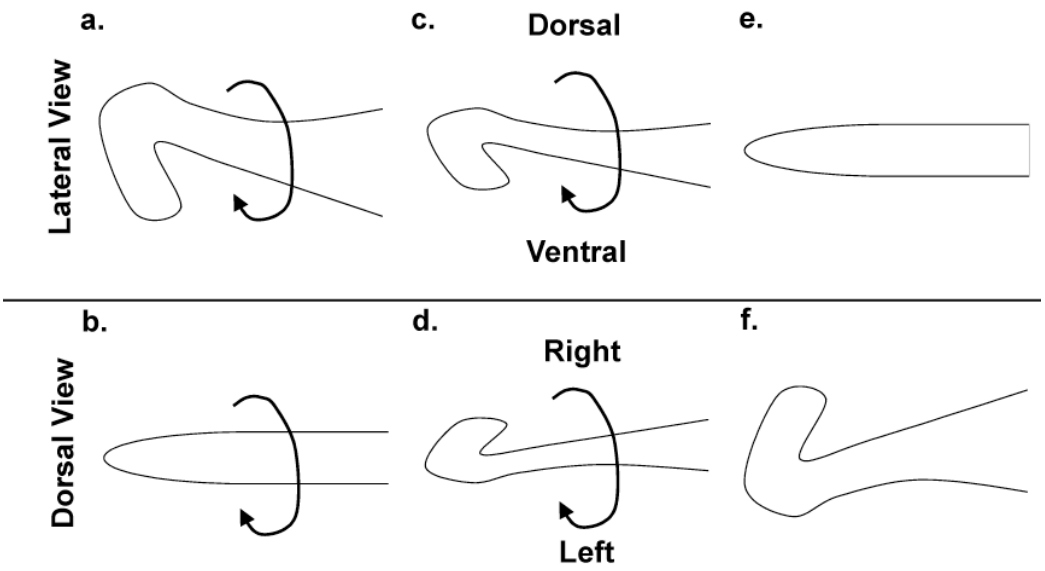

Figure 1.9: Schematic of hindgut rotation during stage 13.
(a) Prior to rotation, when viewed laterally, the hindgut curve bends down, ventrally, into the embryo. (b) If viewed dorsally at this time the profile of the curve is not visible. (c-d) The hindgut then undergoes a 90° rotation. (e) Once complete, the hindgut curve is no longer visible when viewed laterally. (f) However, when viewed dorsally, it can be seen bending from left to right breaking with the symmetry of the embryo.

The wildtype hindgut rotates to the right, dextral, with almost complete fidelity (Hayashi and Murakami, 2001). Several mutants have been identified which causes it to twist 90° to the left, sinistral. Interestingly, unlike the anterior/posterior and dorsal/ventral embryonic axis (reviewed in, Riechmann and Ephrussi, 2001) establishment of asymmetry is not believed to be due to a gradient of a morphogenetic signal (Tuinstra et al., 1990).

An initial study into this problem used a candidate approach examining genes known to be required for hindgut specification, and patterning, as well as genes required for embryonic patterning. This, however, yielded few results. Among the genes examined *wg* and *dpp* hindguts were judged too morphologically disrupted to judge direction of hindgut rotation while *hh* and *en* mutants did not cause errors in rotation (Hayashi and Murakami, 2001). Of all the genes found to be locally expressed only ubiquitous activation of the Notch pathway has been found to cause a small number of rotation

defects; this, however, was not investigate further (Iwaki and Lengyel, 2002). Further candidates examined were the homoeotic genes which pattern the anterior/posterior embryonic axis (reviewed in, Morata et al., 1990). Loss of *Antennapedia* (*Antp*), *Ultrabithorax* (*Ubx*) and *Abdominal-B* (*Abd-b*) did not affect hindgut rotation. This indicates that anterior/posterior patterning and left/right asymmetry are separable. One of the few genes known to be involved in hindgut patterning, and identified as affecting hindgut rotation was *hkb*. However, due to its upstream effect on hindgut specification this is likely to be through an, as yet, unidentified intermediate (Hayashi and Murakami, 2001).

In recent years our understanding of the factors that effect hindgut rotation has advanced greatly. This started with the discovery of the unconventional myosin *Myosin31DF* (*Myo31DF*), the loss of which causes hindgut inversions in the majority of embryos. Interestingly the effect of *Myo31DF* is not restricted to modulating the handedness of the hindgut, all asymmetrically positioned *Drosophila* organs are reversed (*situs inversus*) in the mutant (Hozumi et al., 2006, Speder et al., 2006). At the time, this was of great interest to the field as, after the mouse gene *inversin* (*inv*) (Morgan et al., 1998), it was the only gene found to cause *situs inversus*. *Myo31DF* is expressed uniformly in the hindgut between stages 12-14 (Hozumi et al., 2006). Temporally controlled rescues of *Myo31DF* mutants indicate that its function is required prior to rotation, at stage 12 and earlier (Hozumi et al., 2008). Myo31DF belongs to the myosin-1 protein family (Morgan et al., 1994) and is known to bind (Morgan et al., 1995) to and co-localise with actin (Hozumi et al., 2006) via its head region (Hozumi et al., 2008). Consistent with this, hindgut-specific disruption of the actin network is sufficient to cause inversions in handedness suggesting that Myo31DF requires an intact actin network to function (Hozumi et al., 2006).

Despite early models in which cell rearrangement was proposed to mechanistically cause rotation (Hozumi et al., 2006), it has recently been postulated that changes in cell shape mediate this process. Indeed examination of cell morphology preceding rotation indicates cell shape is distorted from its normal, symmetrical hexagonal shape in the direction of

the rotation (Taniguchi et al., 2011). This process has been termed Planar Cell Chirality (PCC). This shift in PCC is relaxed after rotation is complete at stage 14. Computer simulations have shown that PCC is sufficient to mediate rotation. Interestingly, in *Myo31DF* mutants the cells are distorted in the opposite manner following the direction of the inverted hindgut rotation. In the same study loss of the adherens junction protein DE-cad, was found to cause inversions in hindgut rotation and block PCC. Examination of the phenotype *shg*/*Myo31DF* mutants epistatically place DE-cad downstream of Myo31DF indicating they operate in the same pathway. Furthermore, DE-cad was found to accumulate at one edge of the cell prior to hindgut rotation with this bias in accumulation being reversed in the *Myo31DF* mutant (Taniguchi et al., 2011). This is perhaps consistent with previous reports that Myo31DF physically interacts with Arm, another component of adherens junctions (Speder et al., 2006). While Taniguchi and colleagues do not discuss the interaction with Arm they note that correct DE-cad localisation has been shown to be dependent on endocytic recycling (Langevin et al., 2005). Preliminary data showed that Myo31DF may be required to correctly recycle DE-cad and that this may result in its accumulation (Taniguchi et al., 2011). To date, the proposed model of hindgut rotation is that DE-cad is asymmetrically accumulated, in a Myo31DF dependent manner, causing cell shape changes which are sufficient to drive rotation (Fig1.10).

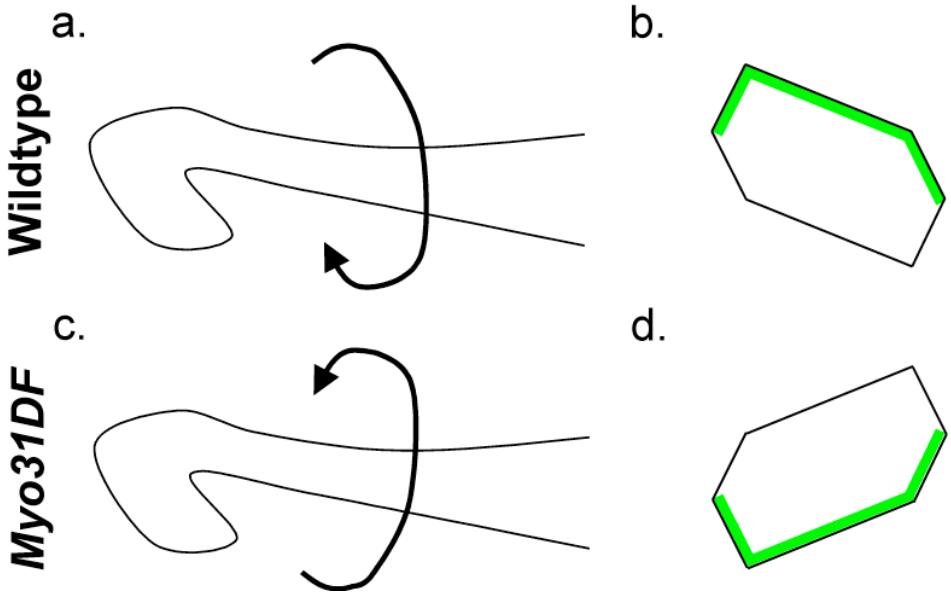

Figure 1.10: Taniguchi *et al.* 2011, model of hindgut rotation.
Hindgut as viewed laterally during rotation. (a) The wildtype hindgut undergoes dextral rotation, (b) this is driven by a shift in cell shape PCC caused by accumulated DE-cad – green. (c) In the *Myo31DF* mutant the hindgut undergoes a sinistral rotation. (d) The sinistral rotation is caused by an opposite shift in PCC driven by DE-cad accumulating on the opposite side of the cell.

While this model provides a good explanation for the mechanical force driving the rotation it leaves questions regarding the origin of left/right asymmetry. At first glance Myo31DF appears to be a master regulator of this process in *Drosophila,* however this cannot be the case. Hindgut rotation and DE-cad accumulation still occur in the absence of *Myo31DF*, albeit in the opposite direction, indicating a default mechanism, underlying Myo31DF function, which is capable of driving these processes.

In addition to the factors described, two further genes are known to cause inversions in hindgut rotation. *Myosin-61F* (*Myo61F*), also a member of the myosin-1 family (Morgan et al., 1994), when overexpressed causes sinistral hindgut rotations (Hozumi et al., 2006, Hozumi et al., 2008) as does loss of the transcription factor *single-minded* (*sim*) (Maeda et al., 2007). Neither of these, however, operate upstream of Myo31DF and their role in the PCC model of hindgut rotation is yet to be determined.

1.4.5 Elongation of the *Drosophila* embryonic hindgut via convergent extension

Hindgut elongation, via convergent extension, begins at stage 13 and progresses through stages 14 and 15. During this time the hindgut curve is pushed towards the anterior resulting in the organ extending over roughly a third of the embryo's total length (Hartenstein, 1993,Campos-Ortega and Hartenstein, 1997).

The most downstream effector of hindgut elongation is the JAK/STAT pathway (Johansen et al., 2003b, Li et al., 2003). Key to correct elongation is anterior polarised pathway activation through release of the ligands, Upd (Johansen et al., 2003b) and Upd2 (Hombria et al., 2005), from the anterior SI, regulation of which is discussed in 1.4.3. In addition to *upd* and *upd2*, higher levels of *dome*, *hop* and *stat92E* expression are found in the anterior of the hindgut, however, these are not as restricted exclusively to the SI (Johansen et al., 2003b). Despite the polarisation of all pathway components to the anterior, all the cells of the hindgut are competent to receive the JAK/STAT signal (Johansen et al., 2003b, Hombria et al., 2005, Wright et al., 2011). Both loss of JAK/STAT signalling, or ectopic activation throughout the length of the hindgut, results in a truncated structure, found not to be due to cell death. This shows that the spatial regulation of pathway activation is key for correct elongation to occur. In addition to being shorter, there are also more cells in the circumference of JAK/STAT mutant hindguts. It was therefore hypothesised that this phenotype was caused due a failure of correct cell rearrangements (Johansen et al., 2003b).

1.5 Summary

In this chapter I have introduced the JAK/STAT pathway, FasIII and the *Drosophila* embryonic hindgut as a model tissue. The following results chapters will discuss experimentation examining novel roles for the JAK/STAT pathway, and FasIII as a novel prospective pathway target, in the development of the hindgut. I will then proceed to examine if the processes characterised within the hindgut have roles elsewhere during *Drosophila* development.

2 Materials and Methods

2.1 Molecular Techniques

2.1.1 Primer sequences

Primer sequences were generated based on published sequences (Table2.1) (www.flybase.org) using the online tool Primer3 (Rozen and Skaletsky, 2000) and synthesised by either Sigma-Aldrich or Integrated Technologies Ltd.

Primer ID	Sequence
FasIII sense T7 Fwd	gaattaatacgactcactatagggaGAAGGTCATGTCCTCGACCAAC
FasIII sense Rev	AAAACACCATCGGCCAGTAG
FasIII anti-sense Fwd	AGGTCATGTCCTCGACCAAC
FasIII anti-sense T7 Rev	gaattaatacgactcactatagggaGAAAAACACCATCGGCCAGTAG
FasIII GW fwd	cacCATGTCACGGATCGTTTT
FasIII GW Rev	taaGTACAAGTTCAGCATAG
FasIII RT-qPCR Fwd	TATGTCTCGCAGCCATCTTA
FasIII RT-qPCR Rev	CGAAGAGCAGCCTTATTCAG
pUASt seq	TTAAAAGTAACCAGCAACC
rpl32 RT-qPCR Fwd	GACGCTTCAAGGGACAGTATCTG
rpl32 RT-qPCR Rev	AAACGCGGTTCTGCATGAG
s18 RT-qPCR Fwd	TCTAGCAATATGAGATTGAGCAATAAG
s18 RT-qPCR Rev	AATACACGTTGATACTTTCATTGTAGC
socs36E RT-qPCR Fwd	AGTTCCTCTTCTCGGTCACAT
socs36E RT-qPCR Rev	GTAGTGCTCCAAAAGTCCTGTC

Table 2.1: Primer sequences.

Gene-specific sequences represented in upper case, additional genetic sequences in lower case.

2.1.2 Polymerase Chain Reaction (PCR)

The Polymerase Chain Reaction (PCR) was used for the specific amplification of DNA fragments from either genomic DNA, isolation described in 2.1.8, or complementary DNA (cDNA), isolation described in 2.1.11. PCR mixes, for a 10µl volume, were made using either 0.5µl proofreading Pfu polymerase (Promega) or non-proofreading Tac polymerase (Promega), 1µl of appropriate 1x buffer (Promega), 0.5µl template DNA, 0.5mM dNTPs (NEB), 1nM forward and reverse primers and was undertaken using a PTC-200 cycler (MJ Research). The standard protocol was as follows: (1) 95°C for 5min, (2) 95°C for 30sec, (3) annealing temperature varied depending on primers used, for 30sec, (4) extension time varied depending on polymerase used, at 72°C (5) go to step 2 for 35 cycles, (6) 72°C for 10min.

2.1.3 Colony PCR

Colony PCR was used for rapid, high throughput, screening of transformed colonies for the correct plasmid insert. This used a dilute PCR mix with 1μl of Tac polymerase added to each 50μl of total reaction volume. Half a bacteria colony was picked from an agar plate, using a pipette tip, and dabbed in 10μl of PCR mix; the remaining half a colony was marked so it was identifiable later. The PCR was undertaken as described in 2.1.2 and the correct insert visualised through gel electrophoresis, described in 2.1.5.

2.1.4 Restriction digests

DNA was digested using specific restriction enzymes (NEB), with the appropriate buffer (NEB) and, when required, Bovine Serum Albumin (BSA) (NEB), for 1hr at 37°C.

2.1.5 Gel electrophoresis and band extraction

Gel electrophoresis was undertaken on 1% agarose (Agar Scientific) gels made with TAE buffer and SYBR® safe dye (Invitrogen). Bands were visualised using a Safe Illuminator (Invitrogen).

Specific bands were cut from the gel using a scalpel (Agar Scientific) and DNA was isolated using a QIAquick Gel Extraction Kit (Qiagen), following manufacturer's instructions.

1x TAE buffer: for 1 litre, 40mM Tris base (Sigma-Aldrich), 1.14ml acetic acid (Fisher Scientific), 1mM EDTA (Sigma-Aldrich) in dH_20.

2.1.6 Ligation reactions

Reactions, for a 20μl volume, used 1μl T4 ligase (Invitrogen), 1x ligase buffer (Invitrogen), 3:1 ratio of insert:plasmid and were incubated overnight at 18°C.

2.1.7 Bacterial transformation and culture

One Shot® TOP10 competent *E.coli* (Invitrogen) were thawed on ice for 20min. Plasmid DNA was then added followed by a heat shock for 30sec at 42°C. 250µl of SOC media (Sigma-Aldrich) was added and incubated at 37ºC for 1hr; 100µl of this was spread on Luria-Betani (LB) agar plates with the appropriate antibiotic. This was left to grow overnight at 37ºC, colonies were analysed as described in 1.1.2. Colonies containing the correct insert were then amplified within a larger liquid LB broth and appropriate antibiotic at 37ºC. Plasmid DNA was then isolated using either Miniprep (Qiagen), Midiprep (Qiagen) or Maxiprep (Qiagen) kits depending on the volume of overnight culture.

LB agar plate: for 1 litre, 15g agar (Agar Scientific), 10g tryptone (Sigma-Aldrich), 5g yeast extract (Sainsburys), 10g NaCl (Sigma-Aldrich) in dH_20
LB broth: for 1 litre, 10g tryptone, 5g yeast extract, 10g NaCl in dH_2O

2.1.8 Large scale isolation of genomic DNA from flies

50 flies were frozen and homogenised in 400µl extraction buffer using a pestle which, to retain all biological material, was rinsed with a further 400µl of extraction buffer. This was incubated at 65°C for 30min. Following this, 120µl of 8M KOAc

(Sigma-Aldrich) was added and incubated on ice for a further 30min followed by centrifugation at 13K rpm for 5min. Centrifugation steps, throughout Materials and Methods, were undertaken using a bench top centrifuge at room temperature unless otherwise stated. The supernatant was removed, mixed 1:1 with 100% ethanol (Fisher Scientific), incubated at room temperature for 5min and centrifuged at 13K rpm for 5min. The pellet was washed with 500µl 70% ethanol followed by a further centrifugation step at 13K rpm for 5min. The pellet was then resuspended in 400µl TE buffer. RNA was removed through the addition of 1ng/µl RNaseA (Qiagen) and incubation at 37°C for 30min. The RNaseA and residual protein contaminants were removed by the addition of 1:10 Strataclean beads (Stratagene). After incubating at room temperature for 1min the beads were removed via centrifugation at 3K rpm for 1min. The supernatant was removed and 1/10 5M NaCl plus 2 1/2 volumes of 100% ethanol were added. The DNA was then precipitated overnight at -80°C, pelleted by centrifuging at 13K rpm for 10min at 4°C and resuspended in 50µl TE buffer.

Extraction buffer: 0.1M NaCl (Sigma-Aldrich), 0.2M Sucrose (Sigma Aldrich), 0.1M Tris HCl pH9 (Sigma Aldrich), 50mM EDTA, 0.5% SDS (Sigma Aldrich).
TE buffer: 10mM Tris-Hcl (Sigma-Aldrich) pH 7.5, 1mM EDTA.

2.1.9 RNA extraction from embryos

Embryos were dislodged from the apple juice agar plate and washed on a mesh filter with water. The embryo's outer shell, the chorion, was removed in 50% bleach (Ottimo Supplies Ltd) for 3min. The embryos were then rinsed in water for 5min and moved to a 1.5ml micro-centrifuge to which 10x the volume of TRIzol reagent (Sigma-Aldrich) was added. The embryos were then homogenised using a pestle and stored at -80°C.

Embryos were thawed on ice, pooled and 2/5ths the volume of chloroform (Sigma-Aldrich) was added. This was followed by a 15sec vortex and centrifugation at 4°C, 12K rpm for 15min. The upper aqueous layer was removed, mixed 1:1 with 70%

ethanol and briefly vortexed. RNA was then isolated using the RNeasy kit (Qiagen) following manufacturer's instructions.

Apple juice agar plate: for 1 litre, 30g agar, 200ml apple juice (Sainsbury), 15ml Nipagin (Sigma-Aldrich) in dH_2O.

2.1.10 RNA extraction from cells

Media was removed and the cells were washed with ice cold 1xPBS. The cells were then lysed using RNeasy kit RLT buffer (Qiagen) with 1% ß-mercaptoethanol (Fisher Scientific) (350µl, per well, for a 24-well plate, 600µl, per well, for a 6-well plate), placed in a QIAshredder column (Qiagen) and centrifuged at 13K rpm for 2min. The eluate was mixed 1:1 with 70% ethanol and the RNA isolated using the RNeasy Kit (Qiagen) following manufacturer's instructions.

2.1.11 Reverse transcription reactions

Total RNA (TRNA) concentration was measured using a Nanodrop spectrophotometer (Thermo). 2µg of TRNA was used with the MEGAscript® T7 kit (Agilent) and the reaction set up following the manufacturer's instructions.

2.1.12 Real Time-Quantitative PCR (RT-qPCR)

10µl reactions using SYBR® green reagent (Invitrogen) were set up following manufacturer's instructions to include 1:10 dilutions of cDNA and primers as described in Table2.1. Primers were designed, using the online tool Primer3 with published transcript sequences (www.flybase.org), to be around 250bp in length preferably spanning an intron with an annealing temperature of around 60°C. Samples were loaded in triplicate into a white-bottomed 96 well plate (Biorad) and read on either a CFX96 touch reader (Biorad) or an iCycler (Biorad). The standard protocol was as follows: (1) 95°C for 3min, (2) 95°C for 10sec, (3) 64°C for 10sec, (4) repeat from step 2 for 39 cycles, (5) 65°C-95°C, at 0.5°C increments per cycle, for 10min. Differential expression of transcripts were calculated using Bio-Rad CFX software (Biorad), with the abundance of the experimental transcript compared to

the ubiquitous ribosomal s18 (Cavdar Koc et al., 2001) or rpl32 transcripts (Dostert et al., 2005).

2.1.13 Cloning of *Fasciclin III* into pUASt

FasIII full length cDNA (isoform E), RE66097 (DSC gold Berkley *Drosophila* Genome Project) was used as the source of the *FasIII* coding sequence. This was received as a small blot paper disk from which the plasmid DNA was eluted following the manufacturer's instructions, and transformed as described in 2.1.7. *FasIII* was directly cut from the plasmid with Not1 and Asp718 restriction enzymes, as described in 2.1.4. The *FasIII* digest was isolated via gel electrophoresis and gel extraction, as described in 2.1.5. This was then directly ligated into the pUASt vector, as described in 2.1.6, and sequenced to confirm correct sequence and insert orientation. The pUASt-*FasIII* plasmid was then sent for injection into wildtype, strain w^{1118} flies at BestGene Inc. A stock was generated with the insertion found to be on the second chromosome.

2.1.14 Cloning of *FasIII* into Gateway® vectors

The source of *FasIII* was the cDNA RE66097. This was amplified, as described in 2.1.2, using primers designed with 5'CAC and 3'TAA overhangs (Table2.1) allowing for orientated ligation into Gateway® Entry vector (Invitrogen) attL1 and attL2 recombination sites following manufacturer's instructions. The *FasIII* insert was then "flipped" into the Gateway® Destination vectors (Invitrogen) containing 5' HA and Flag epitope tags following manufacturer's instructions. Plasmids were sequenced to confirm the correct sequence.

2.1.15 Generation of *FasIII in situ* hybridisation probes

In situ hybridisation probes were generated from the *FasIII* cDNA, RE66097, using primers including the T7 polymerase consensus sequence (Table2.1). The specific sequence was amplified by PCR, as described in 2.1.2 and isolated by gel electrophoresis and gel extraction, described in 2.1.5. DIG-labelled probes were generated using an *in vitro* transcription (IVT) mix of: 2µl T7 polymerase (NEB),

0.5µl RNase inhibitor (NEB), 2µl DIG labelling mix (Roche) 5µl 5x PEG buffer (Roche) and 11.5µl DNA, incubated for 2hr at 37°C. Following this incubation the volume was made up to 50µl with RNase free water and the probe digested with 50µl 2x carbonate buffer at 60°C for 15min. The digestion was stopped by the addition of 100µl of neutralising buffer. To precipitate the probe 450µl of 100% ethanol was added and incubated overnight at -20°C followed by centrifugation at 13K rpm, for 30min at 4°C. The pellet was washed with 70% ethanol, centrifuged at 13K rpm for 30min at 4°C, air dried and resuspended in 200µl of RNase free water.

A dot blot was performed to confirm the incorporation of DIG-labelled nucleotides into the probe. 1µl of probe was pipetted onto a hybond membrane (GE Healthcare) and cross-linked using UV Stratalinker 2400 (Stratagene). The blot paper was blocked using standard block solution for 10min. It was then incubated at room temperature with 1:500 preabsorbed anti-DIG, diluted in PBT, for 30min followed by two 10min washes in standard block buffer then three 5min washes in HP buffer. The colourimetric reaction was undertaken using 0.1% BCIP (Promega) diluted in HP buffer until colour appeared.

2x Carbonate buffer: 40mM $NaHCO_3$ (Sigma-Aldrich), 60mM Na_2CO_3 (Sigma-Aldrich) in dH_20
2x Neutralising buffer: 200mM NaOAc (Sigma-Aldrich), pH6 in dH_20
1x PBS: for 1 litre, 137mM NaCl, 2.7mM KCl (Sigma-Aldrich), 10mM Na_2HPO_2 (Sigma-Aldrich), 2mM KH_2PO_4 (Sigma-Aldrich) in dH_20.
Standard block: 1xPBS, 0.1% Triton x-100 (Sigma-Aldrich), 5% Normal Horse Serum (NHS) (Vector Labs).
PBT: 1xPBS, 0.1% Triton X-100
HP buffer: 100mM Tris base pH9.5, 100mM NaCl, 50mM $MgCl_2$ (Sigma-Aldrich) and 1% Triton X-100 in dH_20.

2.1.16 Protein extraction from embryos

Embryos were collected and dechorionated, as described in 2.3.1 and 2.1.9, moved to a 1.5ml micro-centrifuge tube and washed in ice cold 1x PBS followed by ice cold lysis buffer. Post wash, the embryos were resuspended in 300μl protein lysis buffer and dissociated using a pestle. Embryo lysis was completed with a 5sec, 10 amplitude microns sonication using a Soniprep 150 (MSE) followed by centrifugation at, 3K rpm for 6min at, 4°C. The supernatant was transferred to a new micro-centrifuge tube and centrifuged for a further 1min at 14K, 4°C. The supernatant was then either used immediately or stored at -80°C.

Lysis buffer: 50mM Tris-Hcl pH 7.4, 250mM NaCl, 5mM EDTA, 0.3% Triton X-100 in dH_20. Prior to use one protein inhibitor tablet (Roche) was added to 10ml.

2.1.17 Co-immunoprecipitation (co-IP) and Western blot

100µl-150µl of protein lysate was mixed with antibody and incubated overnight at 4°C. 30µl of Dynabeads (Invitrogen) were isolated from their eluent using a magnetic bead separator Dynal (Invitrogen) and washed twice with ice cold 1xPBS. The overnight antibody-protein lysate was mixed with beads and incubated for 4hr at 4°C after which the beads were isolated and 30µl of sample buffer was added for each lane required. The protein was removed from the beads and denatured through heating to 99°C for 10min. Crude protein samples were also run, these were mixed 2:1 with 2x sample buffer, to a total of 25µl for each lane required. These samples were denatured for 5min at 99°C. After cooling on ice for 5min samples were loaded onto a pre-cast gradient polyacrylamide gel (Biorad) submerged in running buffer and run at 120V for 1hr using a Hoefer EPS2A200 power-pack. Following separation the proteins were transferred to a nitrocellulose membrane (GE healthcare) using a wet transfer in transfer buffer run at 80V for 1hr using a Hoefer EPs2A200 power-pack. Post transfer the membrane was washed three times for 10min in TBST then blocked for 30min with protein block. Primary antibody was diluted in protein block and left on the membrane at 4°C overnight. Following primary antibody incubation the membrane was washed three times for 10min in

TBST. Secondary Horse Radish Peroxidase (HRP) conjugated antibody, diluted 1:5000 in protein block, was added to the membrane for 2hr after which it was washed three times in TBST for 20min. The enzymatic visualisation reaction was then undertaken through the addition of ECL reagent (GE healthcare) following manufacturer's instructions. This was then wrapped in cling film and developed onto photo film (Thermo Scientific) use an Optimax 2010 ® developer (Protec).

2x Sample buffer: 0.1% bromophenol blue (Sigma-Aldrich), 10% SDS, 20% glycerol (Sigma-Aldrich), 0.125M Tris-Hcl pH6.8
10x Running buffer: for 1 litre, 250mM Tri Base, 1.29M glycine (Sigma-Aldrich), 0.1% SDS in dH_20.
10x Transfer buffer: for 1 litre, 250mM Tris Base, 1.29M in dH_20; 20% of 100% methanol added to 1xtransfer buffer prior to use.
20x TBS: 3M NaCl, 0.5M Tris Base, 40mM KCl in dH_20 pH 7.4; 0.05% of Tween-20 (Sigma-Aldrich) was added to 1xTBS prior to use to make TBST.
Protein block: TBST, 5% NHS.

2.1.18 Renilla luciferase assay

Cells were plated into a 24-well plate and transfected, as described in 2.5.2, with 250ng pAc Renilla luciferase and 250ng of additional plasmid DNA. This was left overnight after which the media containing Effectene reagents was replaced with fresh media. The cells were then seeded into a white-bottomed 96-well plate (Corning Inc) and left for a further two days. The media was removed and cells were then lysed with 40µl of lysis buffer for 10min. This was followed by the addition of 60µl Renilla luciferase reagent and the plate was immediately read using the 485 filter on the Milthras LB940 luminometer (Berthold Technologies).

BL buffer: for 1 litre, 50mM Hepes, 0.5mM EDTA, 0.36mM phenylacetic acid (Sigma-Aldrich) in dH_2O
Lysis buffer: BL buffer, 0.07mM oxalic acid (Sigma-Aldrich) with 3% Triton X-100.

Renilla luciferase reagent: BL buffer, 415mM DTT, 33mM ATP (Sigma-Aldrich), 1mM AMP (Sigma-Aldrich) and 0.2mM Coelenterazine (Apollo Scientific).

2.2 *Drosophila* techniques

2.2.1 Fly care

Drosophila stocks were maintained at 18°C on a standard fly cornmeal food. Crosses were undertaken at 25°C unless otherwise stated. Images of adult flies were captured using a Nikon Extended Focus stereomicroscope. Image processing was undertaken using ImageReady CS (Adobe) and Photoshop CS (Adobe).

2.2.2 Mutant Stocks

In this work the stock w^{1118}, mutant for *white* (*w*), was used as wildtype. The majority of transgenic *Drosophila* lines used were initially generated using *w* marked P-elements, in a *w* mutant background (Klemenz et al., 1987). The insertion of the P-element was then confirmed through a change of eye colour from white to red. As such, a *w* mutant is the true genetic background from which most *Drosophila* lines used was derived from.

Genotype	Source	Relevant Reference
w;P[w+,10xSTAT-GFP] on II	Lab Stocks	(Bach et al., 2007)
w;P[w+,10xSTAT-GFP] on III	Lab Stocks	(Bach et al., 2007)
$Df(1)os^{1a}/FM7$	Lab Stocks	(Ferrus et al., 1990)
$Df(1)os^{1a}/FM7[ftz\text{-}lacZ]$	Lab Stocks	(Ferrus et al., 1990)
PBac(w[+mC]=5Hpw[+])*Fas3[A142] /CyO*	Bloomington	(Bellen et al., 2004)
P[neoR,FRT]82B.STAT[56D3], 2/TM3, Sb	Lab Stocks	(Silver and Montell, 2003)
y.w.ubx-Flp FRT82B P[w+,arm-lacZ]	Lab Stocks	N/A
$Myo31DF^{K2}$	Stephane Noselli	(Speder et al., 2006)
os^{lol} *on X*	Lab Stocks	(Muller, 1930)
w;Stat92E[f],e/TM6b	Lab Stocks	(Baksa et al., 2002)
$vari^{48EP}/Cyo$	Roger Jacob	(Moyer and Jacobs, 2008)
w^{1118}	Lab Stocks	(Morgan, 1910)

Table 2.2: Mutant stocks.

Listed alphabetically by genotype including source and principal citation.

2.2.3 Gal4/UAS ectopic expression system

The strength of *Drosophila* as a model organism is through the ease of its *in vivo* genetic manipulation. Key to this is the Gal4/UAS system which provides temporal and spatial control of ectopic gene expression. This system utilises the *S.cerevisiae* derived transcriptional activator, Gal4 (Klar and Halvorson, 1974), and its consensus binding sequence, Upstream Activating Sequence (UAS) (Guarente et al., 1982). Gal4 constructs are made with identified cell-specific promoter sequences cloned upstream of *Gal4* within the pGawB vector. UAS constructs are made with an identified gene cloned downstream of five UAS sequences within the pUAST vector. These constructs are then injected into flies where they randomly integrate into the genome. When flies containing Gal4 and UAS constructs are crossed, the

gene controlled by UAS is expressed in the pattern of the Gal4 promoter (Brand and Perrimon, 1993).

2.2.4 UAS Stocks

Genotype	Source	Relevant Reference
w;P[w+,,UAS-CADH $^{5/9}$]	Bénédicte Sanson	(Sanson et al., 1996)
w;P[w+,,UAS-dome $^{\Delta cyt}$]3.1/Tm3[Sb]	Lab Stocks	(Brown et al., 2001)
w;P[w+,UAS-dome$^{\Delta\omega}$], UAS-P[w+,UASdome$^{\Delta\alpha}$]/TM3[Sb]	James Castelli-Gair Hombria	(Brown et al., 2003)
w;P[w+,UAS-FasIII]/CyO	This Work	N/A
w;P[w+,UAS-FasIIIRNAi] on II	VDRC	(Dietzl et al., 2007)
y,w,P[w+,UAS-FLP] on II	Lab Stocks	
y,w;P[w+,UAS-hop]/CyO	Lab Stocks	(Harrison et al., 1995)
y,w;P[w+,UAS-hop^{Tuml}]/CyO	Lab Stocks	(Harrison et al., 1995)
w;P[w+,UAS-Kaede] on II	Bloomington	(Grueber et al., 2007)
w;P[w+,UAS-RedStinger]on III	Lab Stocks	(Barolo et al., 2004)
w;P[w+,UAS–stat92ERNAi] on II	VDRC	(Dietzl et al., 2007)
w;P[UAS-upd]2b.2 on II	Lab Stocks	(Zeidler et al., 1999)
w;P[w+,UAS-updRNAi] on II	VDRC	(Dietzl et al., 2007)
w;P[w+,UAS-upd3RNAi] on II	VDRC	(Dietzl et al., 2007)

Table 2.3: UAS stocks.

Listed alphabetically by genotype including source and principal citation.

2.2.5 Gal4 Stocks

Genotype	Source	Relevant Reference
y,w;P[w+,10xSTAT-GFP] ,P[w+,ptc -Gal4],P[w+,UAS-DsRed]/Cyo	Lab Stocks	(Vidal et al., 2010)
w; 69B-Gal4 on II	Lab Stocks	(Brand and Perrimon, 1993)
y,w;P[Act>y+.Gal4]25,P[w+, UAS -RedStinger]4,P[w+,10x STAT-GFP]/Cyo	Lab Stocks	N/A
y,w;P[w+ap-Gal4]/Cyo	Lab Stocks	(Calleja et al., 1996)
y,w;P[w+byn-Gal4]/Tm3, Ser, Sb	Judith Lengyel	(Iwaki and Lengyel, 2002)
y,w;P[w+byn-Gal4],P[w+UAS-GFP]/Tm3, Ser, Sb	Judith Lengyel	(Iwaki and Lengyel, 2002)
y,w;P[w+byn-Gal4],P[w+,10x STAT-GFP]/Tm3, Ser, Sb	Lab Stocks	N/A
w;P[w+,da-Gal4,G32] on III	Lab Stocks	(Wodarz et al., 1995)
w;P[w+Dll-Gal4]^{md23}/Cyo	Lab Stocks	(Calleja et al., 1996)
w;P[w+,E132Gal4] on X	Lab Stocks	(Halder et al., 1995)
w;P[w+,MS1096Gal4]	Lab Stocks	(Capdevila and Guerrero, 1994)
w;P[w+,OSPC2-Gal4]#3/Cyo	Stephen Brown	N/A
w;P[w+,OSPC4-Gal4]#8	Stephen Brown	N/A
w;P[w+,OSPC5-Gal4]#18/MKRS	Stephen Brown	N/A
w;P[w+,OSPC7-Gal4]#30/Cyo	Stephen Brown	N/A
w;P[w+,OSPC8-Gal4]#13/Tm3, Ser, Sb	Stephen Brown	N/A
w;P[OSPC10-Gal4]#8	Stephen Brown	N/A
w;P[w+,PC11Gal4]#24/Cyo	Stephen Brown	N/A
w;P[w+,PC12Gal4]	Stephen Brown	N/A
w;P[w+,PC15Gal4]#5/MKRS	Stephen Brown	N/A
w;P[w+,slbo-Gal4],P[w+,UAS-GFP] on II	Lab Stocks	(Rorth et al., 1998)

Genotype	Source	Relevant Reference
w;P[w+,vg-Gal4] on II	Lab Stocks	(Simmonds et al., 1995)
zfh2^{MS209}Gal4/In(4)ci^{D},ci^{D} pan^{ciD}	Bloomington	(Whitworth and Russell, 2003)

Table 2.4: Gal4 stocks.
Listed alphabetically by genotype including source and principal citation.

2.2.6 Generation of clones

Wing disc clones were generated with a cross between P[neoR,FRT]82B.STAT[56D3] and .w.ubx-Flp FRT82B P[w+,arm-lacZ]. This resulted in a stochastic generation of *stat92E* mutation tissue towards the anterior of the larvae marked by a lack of arm-LacZ.

2.3 *In vivo* Histology

2.3.1 Embryo collection

Flies were housed in a closed cage placed on a standard supplemented apple juice agar plate with a thin spread of baker's yeast paste (Sainsburys). Cages were left inverted at 25°C.

2.3.2 Embryo fixation

Embryos were removed from apple juice plates and dechorionated as described in 2.1.9. Fixation was undertaken in a 50:50 embryo fix:heptane mixture (Fisher Scientific) with rapid shaking for 30min. To remove the vitelline membrane the fix solution was exchanged for methanol and the embryos vortexed for 30sec, followed by three washes in 100% methanol. The embryos were then stored, in methanol, at –20°C.

Embryo fix: 1x PBS, 5mM EGTA (Sigma-Aldrich), 10% formaldehyde (Sigma-Aldrich)

2.3.3 Antibody preabsorption

Where stated antibodies were preabsorbed with w^{1118} *Drosophila* embryos to improve their specificity. Embryos were rehydrated from methanol (Fisher Scientific) with 5min washes in 50:50 methanol 1xPBS mixture then 1xPBS. Antibodies were diluted in standard block, added to the embryos and incubated overnight at 4°C. The antibody mixture was then removed from the embryos and stored at 4°C.

2.3.4 Primary antibodies

Target Protein	Raised in	Concentration	Source	Relevant Reference
α-spectrin	Mouse	1:30	DSHB	(Dubreuil et al., 1987)
ß-galactosidase	Mouse	1:100	Abcam	N/A
ß-galactosidase	Rabbit	1:100	Abcam	N/A
Cleaved caspase 3	Rabbit	1:100	Abcam	N/A
Coracle	Mouse	1:50	DSHB	(Fehon et al., 1994)
Crumbs	Mouse	1:10	DSHB	(Tepass et al., 1990)
Digoxygenin	Sheep	1:2000	Roche	N/A
DE-cadherin	Rat	1:50	DSHB	(Oda et al., 1994)
Discs large	Mouse	1:50	DSHB	(Parnas et al., 2001)
Engrailed	Mouse	1:50	DSHB	(Patel et al., 1989)
Fasciclin II	Mouse	1:50	DSHB	(Snow et al., 1987)
Fasciclin III	Mouse	1:50	DSHB	(Patel et al., 1987)
Histone H3 (phospho-S10)	Rabbit	1:100	Abcam	N/A
Varicose	Rabbit	1:50	J, Roger Jacobs	(Moyer and Jacobs, 2008)

Table 2.5: Primary antibodies.
Listed alphabetically by name, including animal raised in, concentration used at, source and, where relevant, the principal citation.

2.3.5 Secondary antibodies

All secondary antibodies were used at 1:500 dilution. The anti-mouse HRP antibody was always used preabsorbed, as described in 2.3.3.

Antibody	Raised against	Raised in	Source
Alexa Fluor 568	Rat	Goat	Invitrogen
Alexa Fluor 647	Rat	Chicken	Invitrogen
Alexa Fluor 647	Mouse	Goat	Invitrogen
Alexa Fluor 647	Rabbit	Goat	Invitrogen
Cy2	Mouse	Donkey	Abcam
Cy2	Rat	Donkey	Abcam
Cy3	Mouse	Donkey	Abcam
Cy3	Rabbit	Donkey	Abcam
Cy5	Rabbit	Goat	Abcam
FITC	GFP	Goat	Abcam
HRP	Mouse	Goat	Dako

Table 2.6: Secondary antibodies.

Listed alphabetically by name, including animal raised against, animal raised in and source.

A selection of secondary antibodies was tested in embryos to identify any non-specific staining. While some auto-fluorescence was detected, largely in the embryonic yolk, no antibodies were found to exhibit non-specific staining patterns (Fig2.1).

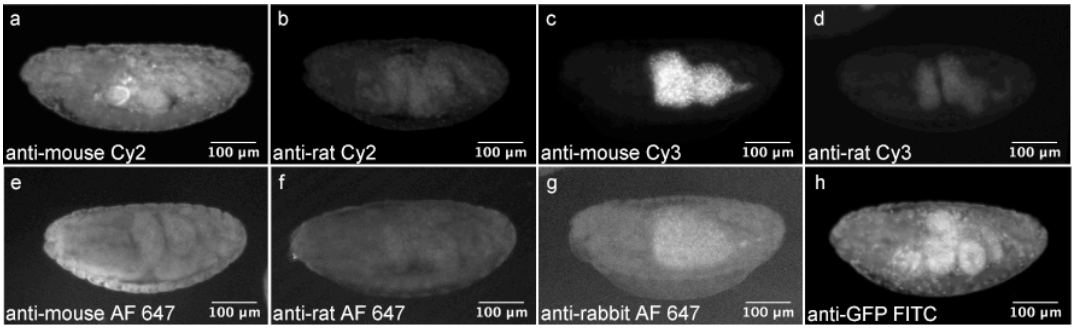

Figure 2.1: Background staining of secondary antibodies.

Stage 15 embryos viewed laterally. Apart from the embryonic yolk, no secondary antibodies caused non-specific staining.

2.3.6 Embryo whole mount immunohistochemical fluorescent staining

All incubation and wash steps in histology protocols were undertaken with gentle shaking at room temperature, unless stated otherwise. Embryos were collected and fixed as described in 2.3.1 and 2.3.2 They were then rehydrated with 5min washes of 50:50 methanol:1xPBS mixture followed by 1xPBS. They were then blocked in standard block solution at 4°C for 1hr. The primary antibody was diluted in standard block and added overnight at 4°C followed by three 15min washes with PBT. The secondary antibody was diluted in standard block and incubated at 4°C for 4hr. This was followed by three 15min washes with PBT and 20min washes of 25% glycerol, 50% glycerol and 85% glycerol, with 2.5% N-propyl galate (Fluka). 50µl of embryos were placed on a 22x22mm coverslip (Mezel-Glãzer) and then mounted on a microscope slide (Thermo Scientific), stored at 4°C overnight to settle before being sealed with nail vanish (Boots). Images were captured using a Zeiss 510 LSM confocal microscope. Image processing was undertaken using ImageJ (http://rsbweb.nih.gov/ij/).

2.3.7 Embryo whole mount immunohistochemical staining with colourimetric reaction

Embryos were collected fixed and treated with primary and secondary antibodies as previously described in 2.3.1, 2.3.2 and 2.3.6. After the secondary antibody was removed with three 10min PBT washes the colourimetric reaction was undertaken

using ImmPACT DAB (Vector Laboratories), following manufacturer's instructions, and incubated at room temperature until staining appeared. The embryos were then washed with copious PBT, all liquid waste and plasticware disposed of in 50% bleach. Embryos were dehydrated with 10min washes in an ethanol gradient of 35%, 50%, 75%, 95% and 100% and then incubated for 20min in methyl salicylate (Fisher Scientific) followed by equilibration in Canada balsam mounting medium (Sigma-Aldrich) for 2hr at 4°C. 100µl of embryos were placed on a 50x22mm coverslip (Mezel-Glãzer) and mounted on a microscope slide. Images captured using a Zeiss Axioskop 2 MOT light microscope, image processing was undertaken using ImageReady CS and Photoshop CS.

2.3.8 Embryo mRNA *in situ* hybridisation

Embryos were collected and fixed as described in 2.3.1 and 2.3.2. They were then rehydrated in a series of 5min methanol *in situ* fix mixture washes (ratios of 3:7, 5:5, 7:3) followed by a 20min wash in *in situ* fix and three 5min washes in PBT. Embryos were permeabilised with 4µg/ml proteinase K (Sigma-Aldrich) diluted in PBT for 2min followed by two 2min washes with 20µg/ml glycine in 1xPBS and five 5min washes in PBT. This was replaced with 1:1 PBT:hyb buffer for 20min followed by two washes in hyb buffer, one 20min at room temperature then another 1hr at 55°C. The *in situ* probes were diluted in hyb buffer, denatured at 95°C for 5min then added to embryos before incubation at 65°C overnight. This was followed by four 20min washes with hyb buffer, 10min hyb buffer:PBT washes (ratios of 4:1, 3:2, 2:3, 1:4) and three 5min washes with PBT. Preabsorbed anti-DIG was diluted with PBT and incubated overnight at 4°C followed by three 15min washes with PBT and three 15min washes with HP buffer. The colour reaction was undertaken with 0.2% BCIP diluted in HP until staining appeared; this was followed by washes with copious amounts of PBT. The embryos were dehydrated with 10min washes of 50%, 90% and 100% ethanol then mounted in Canada balsam, as described in 2.3.7. Image capture and processing was undertaken as described in 2.3.7.

In situ fix: 1xPBS, 2% formaldehyde

20x SSC buffer: 3M NaCl, 300mM Na_3Citrate (Sigma-Aldrich) in dH_2O.
Hyb buffer: 50% formamide (Sigma-Aldrich), 5xSSC, 100µg/ml denatured sonicated salmon sperm DNA (Sigma-Aldrich), 50µg/ml heparin (Sigma-Aldrich), 0.1% Tween 20, in dH_2O, pH 4.5.

2.3.9 Embryo ßlue-ßlau Dome dimerisation visualisation

A revised embryo fixation is required for this protocol as methanol disrupts the β-galactosidase enzymatic reaction. Embryos were dechorionated as described in 2.3.2. Fixation was undertaken using 1:1 ßlue-ßlau fix:heptane and shaken vigorously for 5min. The fix was replaced with 70% ethanol and the embryos vortexed for 30sec to remove the vitelline membrane. This was followed by three washes with 70% ethanol.

Embryos were rehydrated with 5min washes of 1:1 70% ethanol:1xPBS then 1xPBS followed by three 15min washes with X-gal buffer. The colourimetric reaction was undertaken in X-gal buffer 5mM $K_3Fe(CN)_6$ (Sigma-Aldrich) and 5mM K_3FeCN (Sigma-Aldrich) 50µl of this mixture was removed and replaced with 50µl of X-gal substrate (Invitrogen). The solution was pre-warmed at 37°C and passed through a Supatop 0.45µm filter (Anachem) connected to a 1ml syringe (Thermo) prior to use. The reaction was undertaken at 37°C until staining appeared, after which the embryos were washed in copious amounts of PBT followed by a series of 10min washes of glycerol 30%, 50% and 85%. The embryos were then mounted, as described in 2.3.6, on 50x22mm coverslips. Image capture and processing was undertaken as described in 2.3.7.

ßlue-ßlau fix: 1xPBS, 1% glutaraldehyde (Sigma-Aldrich)
X-gal buffer: 7.2mM Na_2HPO_4, 2.8mM NaH_2PO_4, 1mM $MgCl_2$, 15mM NaCl in dH_2O.

2.3.10 Embryo preparation for live imaging

Slides were made using a 60x20mm coverslip (Knittel glass) on which a square of Parafilm (Parafilm) with a hole in the middle was placed. 20µl of glue, made from Sellotape (Sellotape) dissolved in heptane, was added into the Parafilm hole and left for 6hr to allow the heptane to evaporate, laying down an adhesive surface.

Individual embryos were placed on double-sided tape and hand dechoriniated by gentle pushing with forceps. The dechoriniated embryo was placed on the pre-made coverslip and covered with halocarbon 700 oil (Polysciences Inc). Images were captured using a PerkinElmer UltraVIEWVoX spinning-disk confocal microscope. Image processing was undertaken using Volocity (PerkinElmer).

2.3.11 Kaede photoactivation experiments

Timed collections were made, ageing the embryos to late stage 13 after which they were prepared as described in 2.3.10, being placed dorsal side up on the coverslip. A Zeiss 510 LSM confocal microscope was used to photoconvert and image Kaede which fluoresces green until exposed to intense UV light after which it fluoresces red (Ando et al., 2002). Zeiss software was used to select regions of interest (ROI) which were photoconverted using the bleaching tool by 10 iterations of the 405 laser at 100% strength. The embryos were then aged to stage 15 to examine any movement in photoconverted Kaede. Image capture and processing was undertaken as described in 2.3.6.

2.3.12 Wing disc dissection, fixation and immunohistochemical staining from 3rd instar larvae

Forceps were used to turn the larvae inside out by grasping two thirds down its length and pulling off the posterior extreme. The anterior extreme of the larvae was then held and forceps were inserted into the body cavity which was opened and then pushed over the anterior. The carcass was placed in fix solution for 15min followed by three 10min washes in 1xPBS.

Carcasses were moved to standard block and left for 1hr at 4°C. This was replaced by primary antibody diluted in standard block overnight at 4°C followed by three 15min washes in PBT. Secondary antibody was diluted in standard block and added for 2hr followed by a 30min wash with Hoechst (Invitrogen) diluted 1:2000 in PBT. The carcasses were then washed three times for 15min in PBT, the wing discs dissected and mounted on 18x18mm coverslips (Mezel-Glãzer) in 85% glycerol with 2.5% N-propyl galate. Image capture and processing was undertaken as described in 2.3.6.

Fix solution: 1xPBS, 4% formaldehyde.

2.3.13 Ovary dissection, fixation and immunohistochemical staining

Female virgins were placed with males and fresh dried yeast (Sainsburys) for at least two days to optimise egg production. Dissections were undertaken in ice cold standard block with an incision made into the ventral abdomen using forceps. The epidermis was then folded back and both ovaries removed. The ovaries were placed in fix solution for 20min followed by three 15min washes with 1xPBS.

Ovaries were permeabilised for 1hr with 1% Triton in 1xPBS followed by three 5min washes with PBT. They were then placed in standard block for 30min followed by primary antibody, diluted in standard block, overnight at 4°C. Ovaries were then washed three times in PBT for 15min and incubated in secondary antibody, diluted in standard blocking solution, overnight at 4°C. This was followed by a 20min wash with Horescht, diluted 1:2000 in PBT, and three 15min washes in PBT. The ovaries were then washed for 2hr in 30% glycerol, then overnight in 50% glycerol after which they were mounted on lysine-coated slides (PolySciences Inc) in 85% glycerol with 2.5% N-propyl galate. Image capture and processing was undertaken as described in 2.3.6.

2.4 *In vivo* hindgut measurements

2.4.1 Hindgut curvature traces

To allow for the simultaneous comparison of different hindgut curves in the same figure traces of hindgut curves were made and overlayed. The lines were drawn by tracing a line down the centre of the hindgut lumen from the centre of the anus to the centre of the hindgut/midgut boundary.

2.4.2 Hindgut angle measurement

Two methods were used to measure the magnitude of the hindgut curve. The first was used to ascertain differences in hindgut curvature at stage 15. This measured the angle at which the distal point of the hindgut deviated from the embryonic midline. Embryos were viewed dorsally and the embryonic midline was defined by points at the anterior (Fig2.2 "1") and posterior (Fig2.2 "2") extremities of the embryo. Two further points were marked at the anterior (Fig2.2 "3") and distal (Fig2.2 "4") extremes of the hindgut. The angle was measured between point 1 and point 2 around point 3 using ImageJ (Fig2.2 θ).

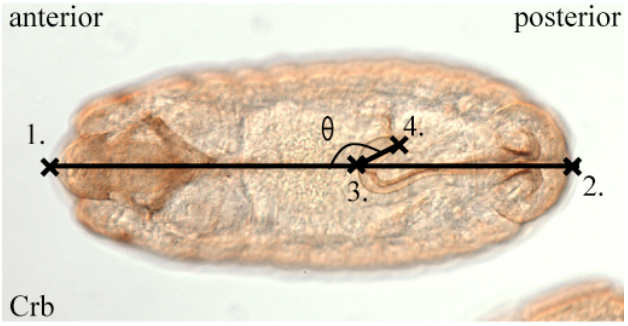

Figure 2.2: Measurement of hindgut curve magnitude, method one.

Dorsally viewed stage 15 embryo stained with Crb. The embryonic midline was defined between points 1 and 2, with further points marked at 3 and 4. The angle was measured between points 1 and 4 around point 3, θ.

A second method was used to measure hindgut curvature throughout development. Early in development the hindgut curve is visible when the embryo is viewed

laterally while later in development it is visible when the embryo is viewed dorsally. The points used to measure curvature when the embryo is viewed dorsally are no longer applicable when the embryo is viewed laterally. To address this a simplified measurement was made of the linear distance between the start and the distal extreme of the curve (Fig2.3). This distance was measured in pixels using ImageJ. While this should provide comparable data for each developmental stage the selection of points is less well defined than those in the first method and so, by definition, is more subjective.

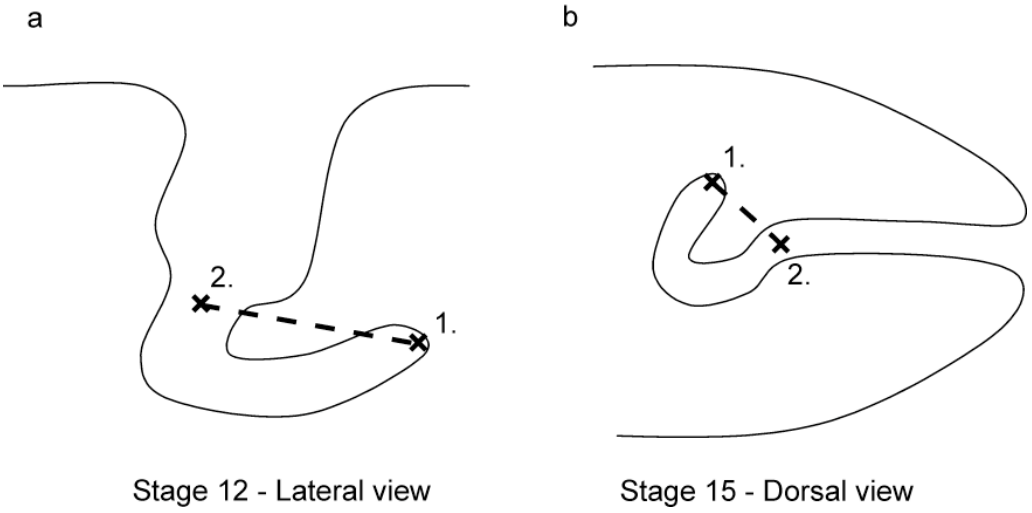

Figure 2.3: Measurement of hindgut curve magnitude, method two. Hindguts not drawn to scale.

(a) Schematic of a stage 12 hindgut, viewed laterally. In the early embryo, stage 12 and 13, the curve start point was defined as the region where the hindgut abruptly narrows, point 2. The distance between this and the end of the hindgut was measured, point 1. (b) Schematic of a stage 15 hindgut, viewed dorsally. In the later embryo, stage 14 and 15, the curve start point was defined as the region where the hindgut starts to turn, point 2. The distance between this and the end of the hindgut was measured, point 1. The distance between these points is measured in pixels using ImageJ.

2.4.3 Quantification of differences in *10xSTATGFP* either side of the hindgut curve

To calculate the difference in GFP on the inside and the outside of the hindgut curve a fluorescence intensity measurements were taken equidistant from the SI/LI

boundary using ImageJ (Fig2.4a). Due to the inherent variability of *in vivo* imaging it was not possible to generate comparable images between embryos while maintaining the confocal microscope setting the same. To overcome this, a ratio calculation of the intensity of GFP on the inside of the curve divided by that on the outside was made (Fig2.4b). Based on the assumption that there was little variation in a single confocal image this provided a single numerical value comparing GFP on either side of the hindgut lumen which could be compared between embryos.

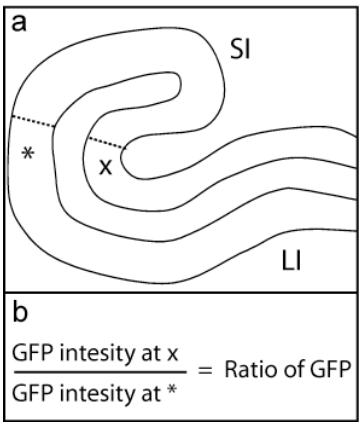

Figure 2.4: Calculating the ratio of GFP across the hindgut curve.
(a) GFP was measured equidistant from the SI/LI boundary using ImageJ. (b) A ratio was then calculated by dividing the GFP intensity value on the inside of the curve by that on the outside.

2.4.4 Statistical analysis

Statistical analysis was undertaken using Prism (Graphpad) or Excel (Microsoft). The tests used are defined for each experiment.

2.5 Tissue Culture

2.5.1 Cell maintenance

The haemocyte-derived Kc_{167} cell line (Bourouis and Jarry, 1983) was maintained in *Drosophila* Schneider's medium (Gibco), this was supplemented with 5% Fetal Bovine Serum (FBS) (Sigma). Cell lines were kept in a humidified 25°C incubator (Sanyo).

2.5.2 Transfection

Cells were seeded at a density of $1x10^6$ in 24-well plates (Corning Inc) or $5x10^6$ in 6-well plate (Corning Inc) and left to settle for at least 2hr. Plasmid DNA was transfected using the Effectene transfection system (Qiagen), 250ng into a 24-well plate, 2µg into a 6-well plate, following manufacturer's instructions.

2.5.3 Cell fixation and Immunohistochemistry

Cells were transfected, as described 2.5.2, and left for 4 days to allow for gene expression. They were then seeded onto 10mm circular coverslips (Thermo Scientific) at a density of 250,000 and left to settle for 2hr. Media was replaced with fix solution for 20min followed by three 5min washes with 1xPBS. Cells were permeabilised using 0.1% Triton in 1xPBS and washed in cell block for 30min. Cells were then incubated with primary antibody, diluted in cell block, without shaking at 4°C overnight. This was followed by three 10min washes with PBT. Coverslips were then incubated in secondary antibody, diluted in cell block, and 1:500 phalloidin (Alexa Fluor 488 (Invitrogen)) for 2hr. This was followed by a single 20min wash with PBT, a 20min wash of Hoechst, diluted 1:2000 in PBT, and a further wash in 10min wash in PBT. The cells were then mounted in Permafluor (Thermo Scientific).

Cell block: PBT, 3% BSA.

3 Characterisation of novel roles for the JAK/STAT pathway in hindgut curvature

3.1 Introduction

The *Drosophila* hindgut is a monolayer epithelial tube that forms a characteristic, asymmetrically positioned, shepherd's crook-shaped organ at the posterior of the embryo. Key to forming this final structure is the establishment of a curve at the anterior. When the curve is first visible it can be seen bending into the embryo; this then undergoes a dextral rotation to break with the symmetry of the embryo, discussed in 1.4.4. The formation and maintenance of the anterior curve, during morphogenesis, is yet to be described.

Development of the hindgut occurs independent of changes in cell number (Hartenstein, 1993,Campos-Ortega and Hartenstein, 1997) in an epithelial cell-autonomous manner, discussed in 1.4.2 (San Martin and Bate, 2001, Johansen et al., 2003b, Johansen et al., 2003a, Hozumi et al., 2006, Hozumi et al., 2008, Taniguchi et al., 2011). As such, morphogenesis is likely to be driven by localised changes in cell behaviour caused by localised cell signalling. As the characteristic hindgut curve is positioned at the anterior of the organ it is conceivable that patterning along the anterior/posterior axis is key in its formation and maintenance. In the hindgut the ligands of numerous signalling cascades have been described as being locally expressed. Of these Ser, Wg and Hh are expressed at both the anterior and posterior while Dl and Dpp are restricted to the LI-v, discussed in 1.4.3. The expression of the JAK/STAT ligands Upd and Upd2 appear unique being restricted to the anterior of the hindgut (Johansen et al., 2003b, Hombria et al., 2005). Given the proposed requirement for correct anterior/posterior patterning, localised JAK/STAT signalling provides a good candidate for having a role in the morphogenesis of the shepherds crook structure. While already described as being required for correct hindgut elongation (Johansen et al., 2003b) this chapter will investigate further roles for JAK/STAT signalling in hindgut curvature. This work will be undertaken by a closer

examination of the JAK/STAT mutant hindgut phenotype, as well as a characterisation of the manner in which the curve is affected during morphogenesis.

3.2 Results

3.2.1 Experimental description of hindgut morphogenesis

To confirm published descriptions of hindgut morphogenesis the process was examined by immunolabeling using the apical domain protein Crumbs to mark ectodermally-derived tissue (Tepass et al., 1990). The hindgut first becomes morphologically distinct at stage 10, around five hours post egg laying. At this stage the germband is fully extended with the posterior extremity of the embryo found dorsally behind the prospective head. The anterior hindgut curve is visible, has bilateral symmetry and is bent into the centre of the embryo (Fig3.1ai-aii). This structure is maintained unchanged over the next four hours, between stages 11-12, during germband retraction, (Fig3.1bi-cii). The most noticeable changes in hindgut morphology begin at stage 13. This lasts for an hour during which the hindgut curve rotates from a central, symmetric position (Fig3.1di-dii) turning 90° to the right (dextral) and, in doing so, breaking the symmetry of the embryo. The completion of this process is most visible at early stage 14 (Fig3.1ei-eii). Stage 13 also marks the start of hindgut elongation which occurs over a period of around four hours through stages 14 (Fig3.1ei-eii) and 15 (Fig3.1fi-fii). The anterior hindgut curve is maintained, largely unchanged, throughout the process of morphogenesis (Fig3.1 bi, fii).

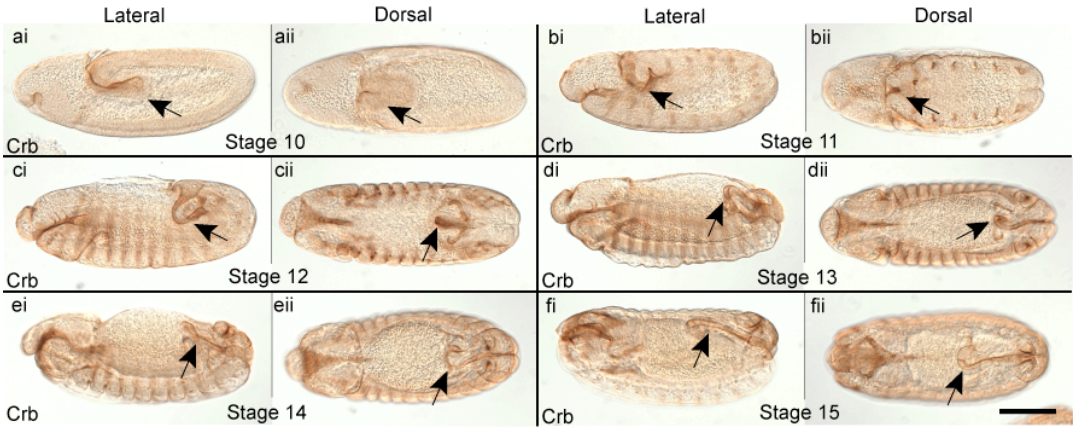

Figure 3.1: Drosophila hindgut morphogenesis. Embryonic development displayed both laterally and dorsally through stages 10-15, the hindgut indicated by a black arrow. Embryos are stained with the apical protein Crb which marks ectodermally-derived tissue.
(ai-bii) At stages 10 and 11 the hindgut first becomes morphologically distinct. (ci-cii) At stage 12 the curve persists during germband retraction. (di-dii) At stage 13 gut dextral rotation occurs and elongation, via convergent extension, begins. (ei-eii) At stage 14 hindgut elongation continues, (fi-fii) At stage 15 the hindgut is present as a fully formed shepherd's crook, Scale bar 100µm.

It has previously been described that, after initial rounds of cell division at stage 11, hindgut morphogenesis proceeds without changes in cell number via cell death or division (Hartenstein, 1993,Campos-Ortega and Hartenstein, 1997). To confirm this, cell death was examined using a marker of apoptosis, cleaved caspase 3 (reviewed in, Cohen, 1997). Staining showed that, from stage 12 onwards, there is no programmed cell death in the hindgut (Fig3.2a-d). Furthermore examination of cell division using a mitotic marker, Phospho-Histone H3 (phospho S10) (Hendzel et al., 1997), showed that there was cell division at stage 11, however, from stage 12 onwards there are no visibly dividing cells in the hindgut (Fig3.2e-h). This confirms that hindgut morphogenesis occurs in a fixed cell population.

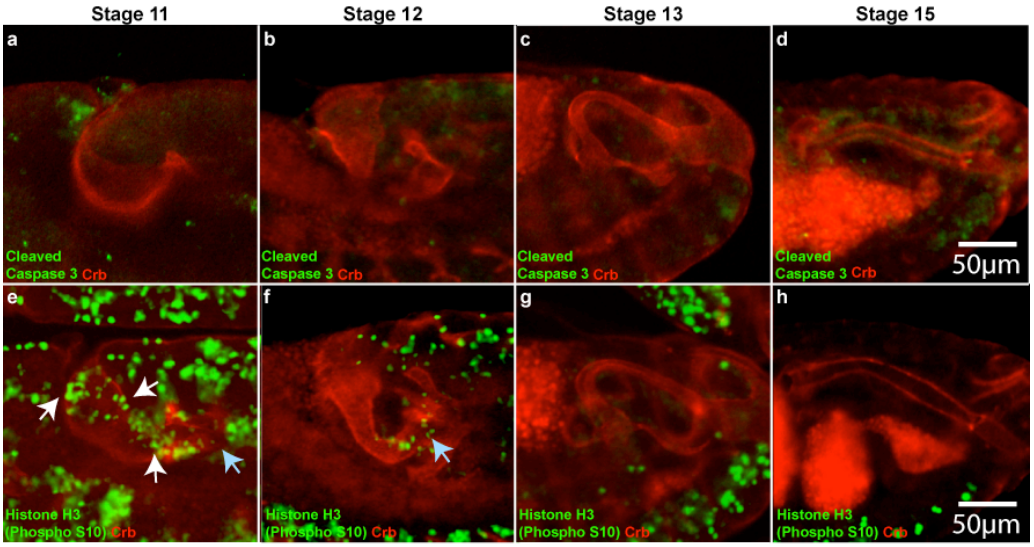

Figure 3.2: Hindgut development occurs independent of cell division and cell death. Embryos viewed laterally, hindgut indicated by a white arrow.

(a-d) Staining with cleaved caspase 3 shows no cells are undergoing apoptosis in the developing hindgut (e) Staining with Phospho-Histone H3 shows that there are dividing cells within the hindgut (white arrows) and malpighian tubules at stage 11. (f-h) After stage 11 there is no further cell division within the hindgut however there is some cell division within the Malpighian tubules at stage 12 (blue arrow).

The JAK/STAT ligand *upd* is expressed in the anterior of the hindgut (Johansen et al., 2003b). To confirm this, *upd* expression was examined throughout embryogenesis by *in situ* hybridisation (*upd* probe gift from Victoria Wright). Initial expression of *upd* is detected during early embryogenesis at stage 5 (Fig3.3a) where it activates the pair-rule gene *even-skipped* (*eve*) required for correct embryonic segmentation (Hou et al., 1996, Harrison et al., 1998). *Upd* expression is later detected at stage 9 in ectodermal stripes (Fig3.3b) where it is required to modulate changes in cell shape during germband extension (Bertet et al., 2009). At stage 10 expression is detected in the anterior hindgut, the prospective SI, as well as in the tracheal pits (Fig3.3c) where JAK/STAT signalling is required for correct tracheal placode invagination (Binari and Perrimon, 1994, Li et al., 2003). Expression of *upd* in the anterior hindgut persists through stages 11 to 15 (Fig3.3d-hii). During this period it is also detected in the foregut (Fig3.3e-h), where signalling is required for

correct morphogenesis (Johansen et al., 2003a, Josten et al., 2004), as well as in the ring gland (Fig3.3e-g).

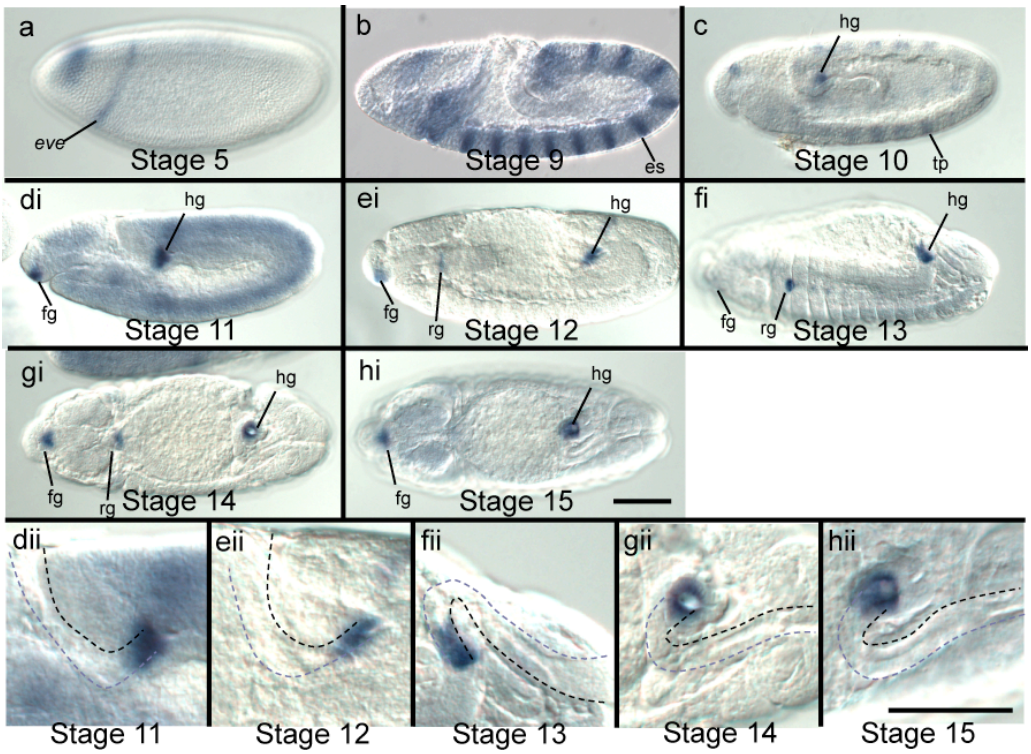

Figure 3.3: Expression pattern of *upd*. Embryos orientated to show hindgut curve topography. In dii-hii the black line indicates the inside of the hindgut while the grey indicates the outside. (a) At stage 5, early *upd* expression is found in a stripe (*eve*) (b) At stage 9, expression is found in ectodermal segments (e) and tracheal placodes (tp). (c) At stage 10, *upd* is initially found at the anterior of the hg. (di-hii) Through stages 11-15, *upd* expression persists in the hg and the foregut (fg). (ei-fi) At stages 12 and 13, *upd* expression is also found in the ring gland (rg). Scale bar 100µm.

A key tool used to genetically manipulate the hindgut is a Gal4 line inserted into the *byn* locus (Iwaki and Lengyel, 2002). Expression of the Gal4 in this line was visualised using GFP (UAS-*GFP*). GFP was detected as early as stage 10, (Fig3.4ai-aii) persisting through stage 11 (Fig3.4bi-bii), stage 12 (Fig3.4ci-cii) and during hindgut rotation and elongation during stages 13-14 (Fig3.4di-eii). Co-staining with Crb showed that the GFP protein is almost exclusively found in the hindgut tissue. However, in addition to the hindgut, GFP was also detected in the Malpighian

tubules (Fig3.4fi-fii), the developing *Drosophila* renal system, which arise from hindgut derived tissue near the hindgut/midgut boundary at stage 10. Malpighian tubule development then proceeds independently from hindgut morphogenesis (reviewed in, Ainsworth et al., 2000). It should be noted that experiments using *byn*-Gal4 were undertaken based on the assumption that the phenotypes observed were hindgut specific.

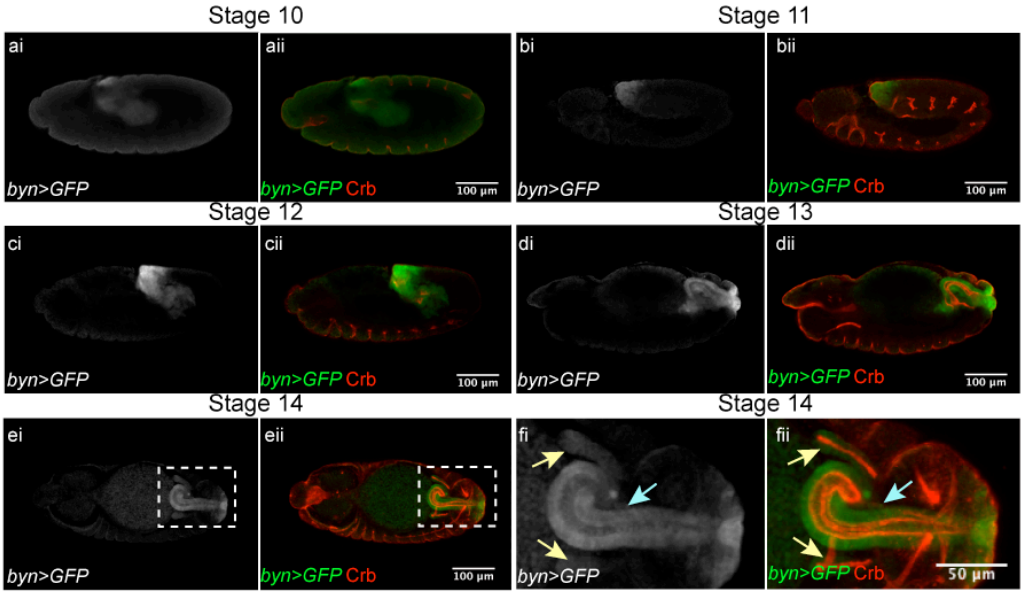

Figure 3.4: Expression pattern of *byn*-gal4. *Byn*-gal4 expression visualised using UAS-*GFP* (*byn>GFP*).

(ai-aii) GFP is first observed at stage 10, (bi-cii) through stages 11-12, germband retraction (di-eii) and stages 13-14, hindgut morphogenesis. (fi-fii) In addition to the hindgut, blue arrow, *byn>GFP* is observed in the embryonic Malpighian tubules, yellow arrows.

3.2.2 JAK/STAT signalling is required for correct hindgut curvature

Using stock w^{1118} used as a wildtype (discussed in 2.2.2), stage 15 embryos were found to have the characteristic shepherds crook morphology of the hindgut fully formed with the anterior curve bending back on itself (Fig3.5a) with complete fidelity (Fig3.5b). Loss of JAK/STAT signalling, through a deficiency lacking all pathway ligands, $Df(1)os^{1A}/y$, termed $Df(1)os^{1A}$ (Fig3.5c-d), or by hindgut-specific inhibition through the expression of a dominant negative pathway receptor,

byn>dome$^{\Delta cyt}$ (Fig3.5e-f), caused a marked reduction in the magnitude of the stage 15 curve. Furthermore, errors in curvature were also observed with ectopic JAK/STAT activation either by hindgut-specific expression of the ligand, *byn>upd* (Fig3.5g-h), or a constitutively active kinase, *byn>hop*^{Tuml} (Fig3.5i-j).

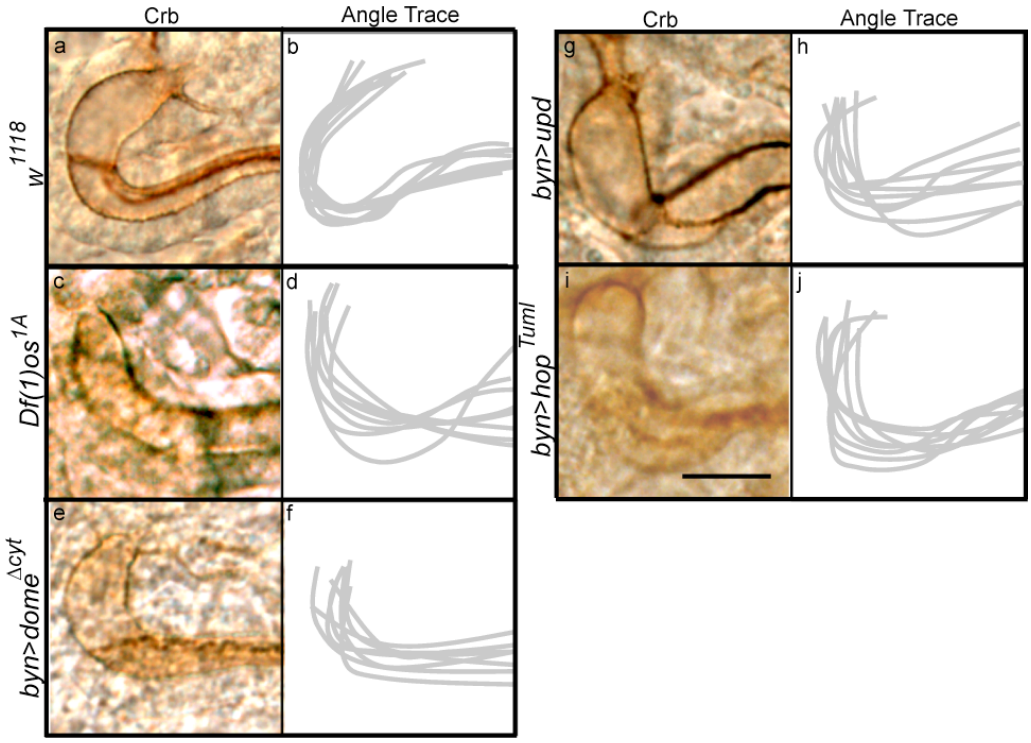

Figure 3.5: Loss of, and ectopic, JAK/STAT signalling causes a reduction in the magnitude of the stage 15 hindgut curve. For each genotype a Crb stained representative image is displayed accompanied by traced images of a further eight hindguts.
(a-b) In the wildtype the hindgut bends back on itself. (c-d) Loss of JAK/STAT signalling using either *Df(1)os*^{1A} or (e-f) *byn>dome*$^{\Delta cyt}$ causes a noticeable reduction in the magnitude of the hindgut curve. (g-h) Ectopic JAK/STAT activation throughout the hindgut using either *byn>upd* or (i-j) *byn>hop*^{Tuml} also causes a noticeable reduction in the magnitude of the hindgut curve. Scale bar represents 100µm.

To quantify this phenotype a measurement of the hindgut angle was made calculating the deviation of the hindgut curve from the embryonic midline, discussed in 2.4.1. This confirmed that the magnitude of the stage 15 hindgut curve was significantly reduced with both loss of JAK/STAT signalling, *Df(1)os*^{1A} and

byn>dome$^{\Delta cyt}$, and ectopic JAK/STAT activation, *byn>hop*^{Tuml} and *byn>upd* (Fig3.6).

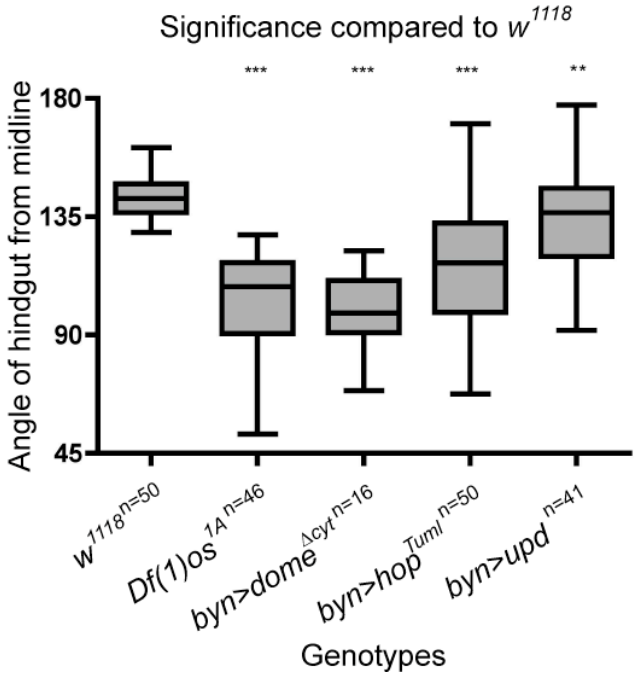

Figure 3.6: Quantification of hindgut curvature defects in JAK/STAT mutant embryos. Angle represents the deviation of the hindgut from the midline of stage 15 embryo, all statistical comparisons made between the wildtype and mutant. Loss of JAK/STAT signalling in *Df(1)os*^{1A} or *byn>dome*$^{\Delta cyt}$ causes a significant reduction in the magnitude of the hindgut curve (* p>0.0001). A significant reduction in the magnitude of the hindgut curve is also observed with ectopic JAK/STAT signalling via *byn>hop*^{Tuml} (*** p>0.0001) or *byn>upd* (** p>0.001). Statistical significance calculated using an unpaired t-test.**

3.2.3 JAK/STAT signalling is asymmetric in the hindgut

In the hindgut, genetic rescue studies have shown the requirement for non-autonomous JAK/STAT signalling for correct elongation. While the ligand *upd* is expressed in the SI, the JAK/STAT signal must be received in the LI (Johansen et al., 2003b). Studies have shown that Upd is capable of signalling in a paracrine manner over the distance of several cells in the *Drosophila* eye (Zeidler et al., 1999), oocyte (Silver et al., 2005) and testes (Kiger et al., 2001, Tulina and Matunis, 2001, Bach et al., 2007). To visualise the JAK/STAT transcriptional output in the hindgut

the 10xSTATGFP reporter was used. This is GFP under the transcriptional control of 10 Stat92E binding sites from the known pathway target *socs36E* (Karsten et al., 2002, Bach et al., 2007). Examination of this reporter, in the hindgut LI, indicates higher levels of GFP on the inside of the curve when compared to the outside (Fig3.7).

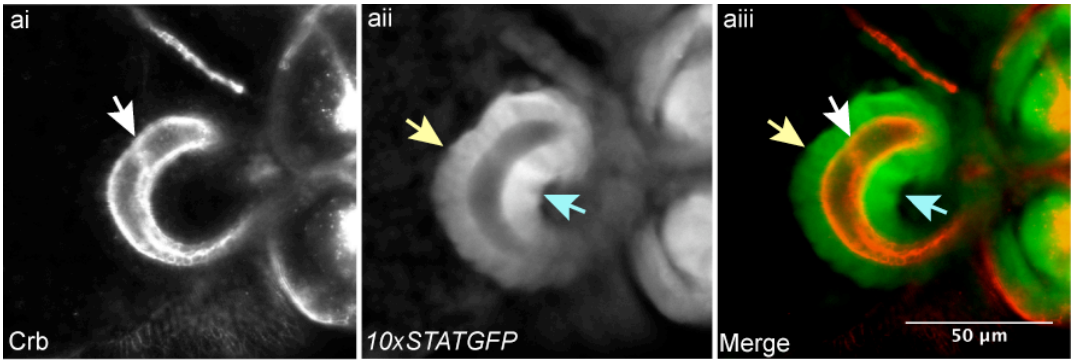

Figure 3.7: Asymmetry of JAK/STAT signalling in the hindgut. The Image represents a single confocal slice transecting the stage 14 hindgut curve. The yellow arrow indicates the outside of the curve and the blue indicates the inside.
(ai-aiii) Crb staining shows the SI/LI boundary, white arrow. where it is known that Upd release is limited to. (aii-aiii) The *10xSTATGFP* reporter in the LI appears higher on the inside of the curve than the outside.

To further investigate the asymmetry in *10xSTATGFP*, confocal cross-sections were generated through the LI at the curve of the stage 14 hindgut. Imaged in this manner *10xSTATGFP* can be seen to be higher on the inside of the hindgut curve (Fig3.8aii-aiii). Interestingly this appears to be largely within the lateral border cells on the inside of the gut (Fig3.8ai, aiii).

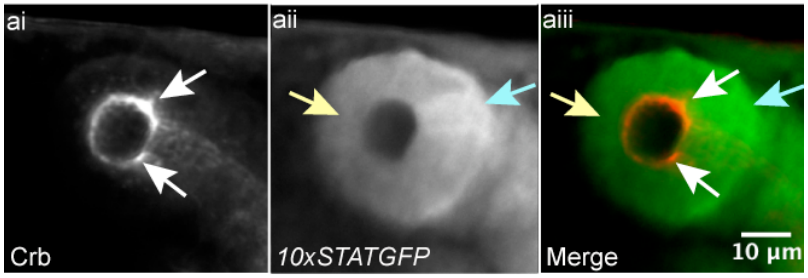

Figure 3.8: Asymmetry of JAK/STAT signalling in a lumen cross-section. Image represents a single confocal slice transecting a laterally orientated stage 14 embryo, the yellow arrow indicates the outside of the curve and blue the inside.
(ai-aiii) Enrichment of Crb marks the lateral border cells, white arrows. (aii-aii) The *10xSTATGFP* reporter appears higher on the inside of the curve.

Examination of the asymmetry of *10xSTATGFP* over time showed that it is present prior to hindgut rotation at stage 13 (Fig3.9ai-aiii) as well as after rotation and during elongation, stage 14 (Fig3.9bi-biii). Interestingly the asymmetry of JAK/STAT signalling appeared to persist after morphogenesis is completed, stage 15 (Fig3.9ci-ciii). Unfortunately, due to the depth of the hindgut in the stage 12 embryo, clear images of the *10xSTATGFP* reporter could not be obtained.

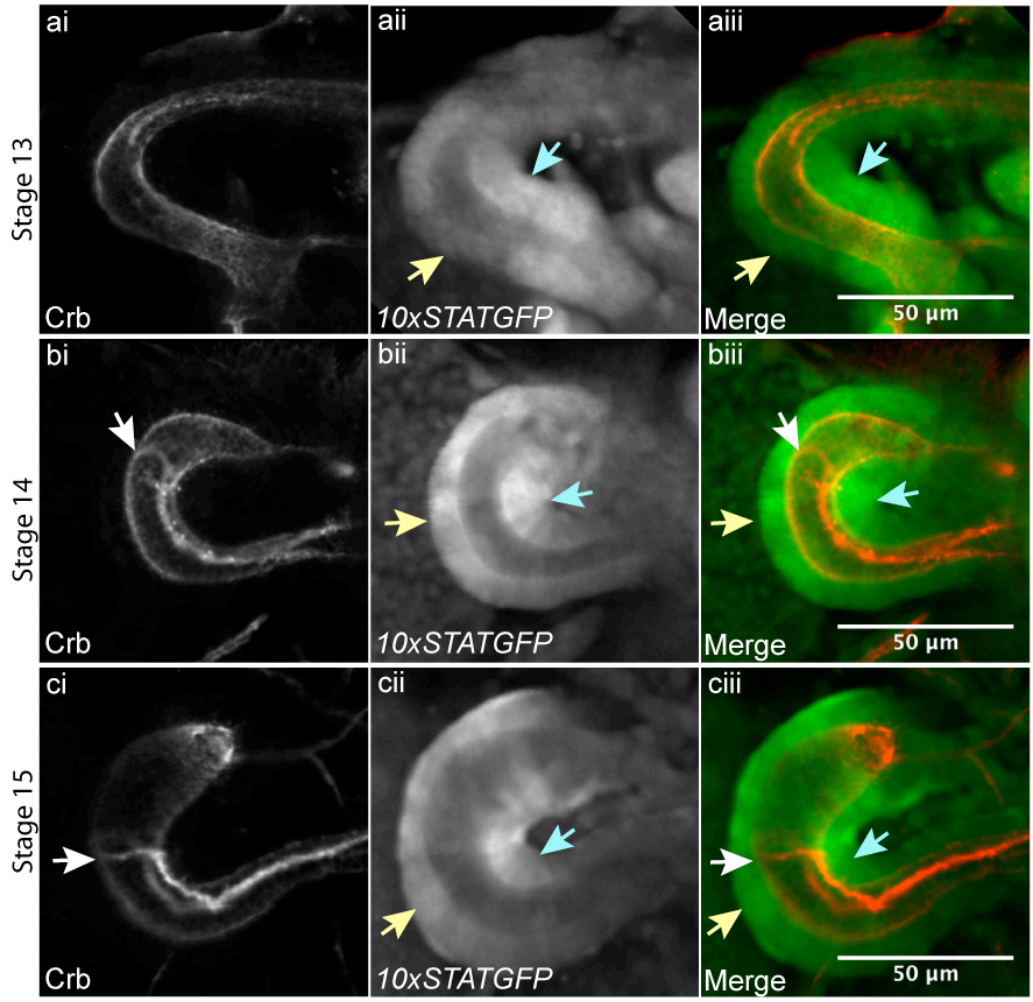

Figure 3.9: Asymmetry of JAK/STAT signalling throughout development. Images represent single confocal slices, stage 13 viewed laterally, stages 14 and 15 dorsally. The yellow arrow indicates the outside of the curve and blue the inside. White arrow indicates SI boundary when formed.

(ai-aiii) At stage 13 *10xSTATGFP* is higher on the inside of the hindgut in the presumptive LI. (bi-biii) At stage 14 and (ci-ciii) stage 15 *10xSTATGFP* is also found higher on the inside of the hindgut in the LI.

The observed asymmetry in the *10xSTATGFP* reporter indicates an asymmetry in JAK/STAT signalling. This may, however, be due to differing levels of GFP accumulation in cells on the inside and outside of the hindgut. To exclude this possibility, the intensity of the *10xSTATGFP* was measured on both sides of the hindgut curve and compared to a uniformly expressed GFP, *byn>GFP*. To do this

the ratio of GFP was measured on both the inside and outside of the curve, as described in 2.4.2, in early stage 14 embryos of both genotypes. The ratio was calculated as GFP intensity on the inside of the curve divided by the GFP intensity on the outside. Equal numbers will result in a ratio of one. The ratio of the *10xSTATGFP* reporter is greater than one showing that the intensity measurements on the inside of the hindgut are higher than on the outside. Conversely, the ratio of *byn>GFP* measurements is around one. This indicates that there is no intrinsic property of the hindgut cells on the inside of the curve which causes accumulation of GFP providing strong evidence that the observed difference in *10xSTATGFP* intensity represents an asymmetry in the strength of JAK/STAT signalling (Fig3.10).

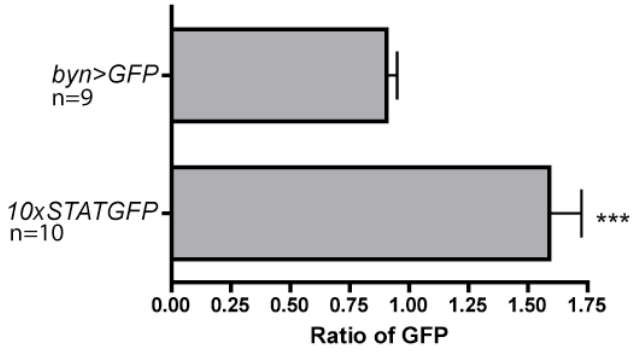

Figure 3.10: Quantification of asymmetry in *10xSTATGFP*.
The ratio of *10xSTATGFP* on the inside vs. the outside of the curve higher when compared to the uniformly expressed *byn>GFP* (* p>0.0001). Statistical significance calculated using an unpaired t-test.**

To further confirm an asymmetry of JAK/STAT signalling on the inside of the hindgut, the expression of the known JAK/STAT target *socs36E* was examined by *in situ* hybridisation (*socs36E* probe gift from Stephen Brown). *socs36E* expression, like *10xSTATGFP*, was higher on the inside of the hindgut than the outside. In addition to showing asymmetry at stages 13 and 14 (Fig3.11b-c) it was possible to see an asymmetry in signalling at stage 12 (Fig3.11a). Furthermore, this asymmetry appeared to diminish at stage 15 (Fig3.11d) after morphogenesis is complete. The symmetry of *socs36E* at stage 15 contradicts the observation made with the

10xSTATGFP reporter which still appears asymmetric at this stage (Fig3.9ci-ciii). The disparity in results may be due to a higher stability of the GFP protein which has a long half-life (Corish and Tyler-Smith, 1999) and is likely to persist longer than mRNA. With this in mind the *socs36E in-situ* hybridisation should provide a more accurate portrayal of the developmental dynamics in the asymmetry of JAK/STAT signalling.

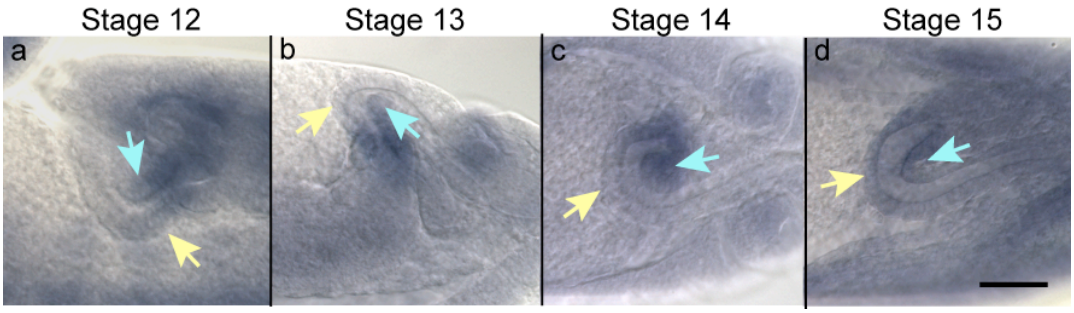

Figure 3.11: Asymmetry of *socs36E* expression. Images orientated to show curve topography, yellow arrow indicates outside of the curve and blue the inside.
(a) At stage 12 *socs36E* expression appears asymmetric in the hindgut. (b-c) The asymmetry in *socs36E* persists through stages 13 and 14. (d) At stage 15 *socs36E* expression is no longer asymmetric in the hindgut. Scale bar represents 50µm.

3.2.4 The role of JAK/STAT signalling in hindgut curvature

The asymmetric activation of JAK/STAT signalling in the hindgut curve places it in the correct context to effect curvature. The JAK/STAT ligand Upd is present (Fig3.4c) in the presumptive small intestine as early as stage 10 leading to the possibility that the pathway is required for initial curve formation. To assess if JAK/STAT signalling is required for the initial formation of the hindgut curve, wildtype and $Df(1)os^{1A}$ hindguts were compared at stage 12. Early in development the wildtype (Fig3.12a-b) and $Df(1)os^{1A}$ (Fig3.12c-d) curves appear to be of a similar magnitude. This is in stark contrast to the stage 15 hindgut in which the $Df(1)os^{1A}$ curve (Fig3.12g-h) has a reduced magnitude when compared to wildtype (Fig3.12e-f). These results show that loss of JAK/STAT signalling does not affect the initial formation of curvature.

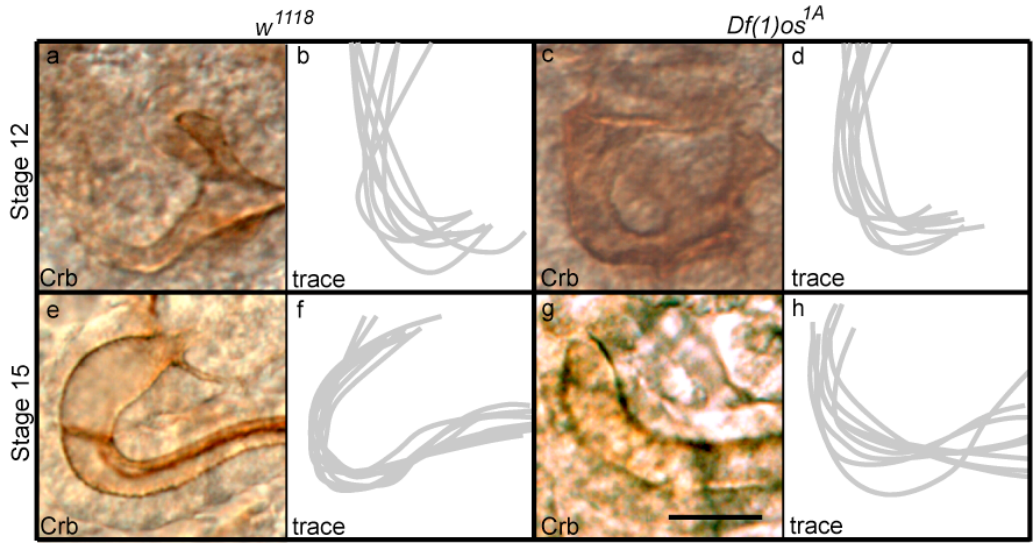

Figure 3.12: The effect of JAK/STAT loss-of-function on early hindgut curvature. For both genotypes and developmental stages a Crb-stained representative image is displayed, accompanied by traced images of a further eight hindguts.
(a-b) At stage 12 both the wildtype and (c-d) *Df(1)os*^{1A} hindguts curves are of similar magnitude. (e-f) At stage 15 the wildtype hindgut bends back on itself. Conversely (g-h) *Df(1)os*^{1A} shows a drastic reduction in curvature. Scale bar 100µm.

To more closely examine the developmental point at which loss of JAK/STAT signalling affects the magnitude of curvature, hindgut morphology was examined in the wildtype and *Df(1)os*^{1A} throughout embryogenesis. As shown in figure 3.12 the stage 12 *Df(1)os*^{1A} hindgut (Fig3.13e) appears similar to wildtype (Fig3.13a). At stage 13, after germband retraction, there appears to be a drastic reduction in the magnitude of the hindgut curve in *Df(1)os*^{1A} (Fig3.13f) when compared to wildtype (Fig3.13b). The observed reduction in hindgut curvature then persists through stages 14 (Fig3.13c, g), and 15 (Fig3.13g, h).

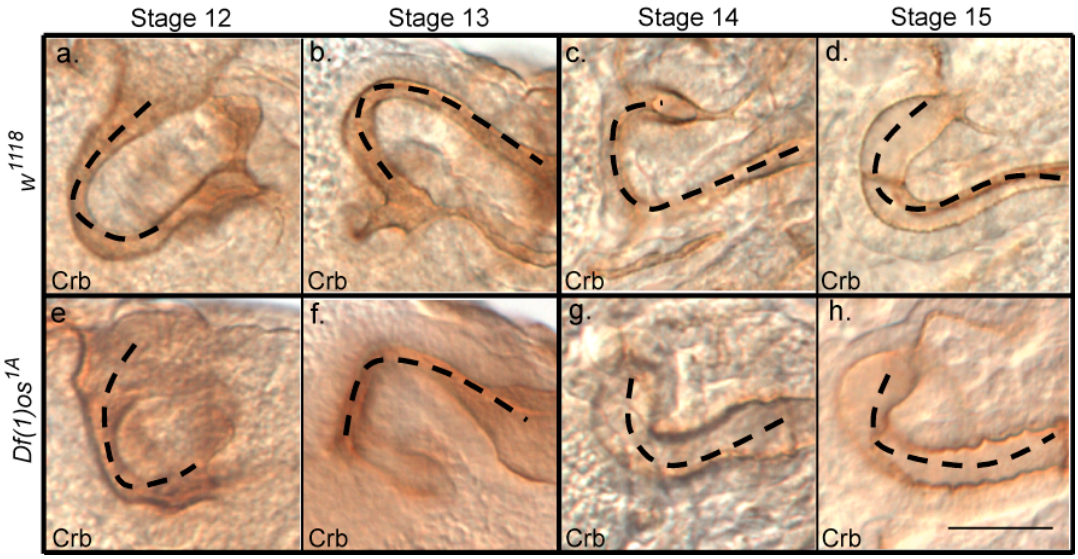

Figure 3.13: A timeline of hindgut curvature in wildtype and *Df(1)os^{1A}* hindguts. Hindguts are visualised with Crb staining.

(a) At stage 12 the wildtype and (e) *Df(1)os^{1A}* hindgut curvature appears to be of similar magnitude. (f) At stage 13 a marked reduction in the curvature of the *Df(1)os^{1A}* hindgut can be observed when compared to (b) wildtype. (g-h) This loss of curvature is visible in the *Df(1)os^{1A}* hindgut during stages 14 and 15 when compared to the (c-d) wildtype. Scale bar represents 50µm.

To confirm the observed changes in hindgut curvature between wildtype and *Df(1)os^{1A}* the anterior curve was measured during development. As the topography of the hindgut curve is visible laterally at stages 12 and 13 and dorsally at stages 14 and 15. For this reason the previous measurement of curvature, examining the angle of curve deviation from the midline, could not be used. An alternative method to quantify the magnitude of hindgut curvature was to measure the span of the curve, from its start to the tip, described in 2.4.1. One drawback of this method is the lack of fixed points, in the embryo, used to define the curve; this results in the generation of less stringent values. The method was, however, the only conceivable technique that could be devised to examine curvature during development. As cell movement does not appear to contribute to curvature, discussed later (video3.1, Fig3.15, Fig3.16), it was assumed that the effect of JAK/STAT signalling on convergent extension would not affect these measurements. Using this second method there is

no significance difference in the magnitude of the hindgut curve between wildtype and *Df(1)os*^{1A} embryos at stage 12. However, it was confirmed that at stage 13 there is a significant difference in curvature between the wildtype and *Df(1)os*^{1A}. This difference was maintained through stages 14 and 15 (Fig3.14). The apparent abrupt reduction in hindgut curvature at stage 13 (Fig3.13, Fig3.14), provides further evidence that this phenotype is not caused by errors in initial hindgut curve formation.

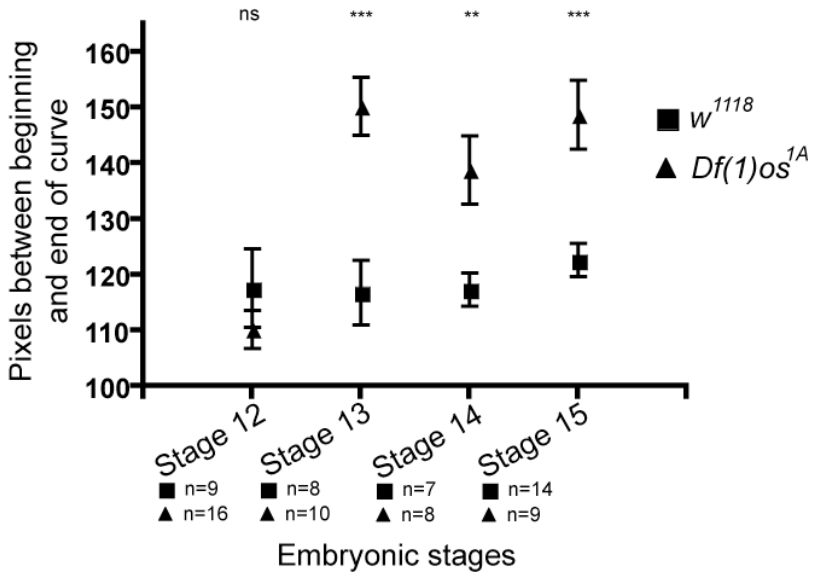

Figure 3.14: Quantification of the difference in hindgut curvature over time between wildtype and *Df(1)os*^{1A}. Measurement taken as distance between the start and finish of the curve.
At stage 12 the curvature of both the wildtype and *Df(1)os*^{1A} is not significantly different. From stage 13 onwards there is a significant difference (P>0.0001 at stage 13 and 15, P>0.001 at stage 14) in the span of the hindgut curve. Statistical significance calculated using an unpaired t-test.

JAK/STAT mutant hindguts show a loss of curvature as well as the documented errors in elongation (Johansen et al., 2003b). As such, the reduction in curvature may be due to the error in elongation. Assuming cells in the hindgut have comparable volumes it is likely that the curve would require more cells on the outside than the inside. Indeed, asymmetric convergent extension movements could contribute to this distribution of cells and, as a result, curvature. While data presented in figure 3.13 and figure 3.14 indicates this is likely not to be the case, as

loss of curvature occurs prior to the onset of the bulk of elongation, this hypothesis was still investigated further. To track cell movement hindgut nuclei were labelled with a nuclear-localised fluorophore, *byn>RedStinger*. The movement of nuclei was then examined in relation to their neighbours. There was, however, no evidence of any drastic asymmetric cell movements between stages 14 and 15 (Fig3.15). Examination of the complete process of elongation shows that the majority of cell rearrangement appeared to occur in the LI more posterior to the curve (video3.1).

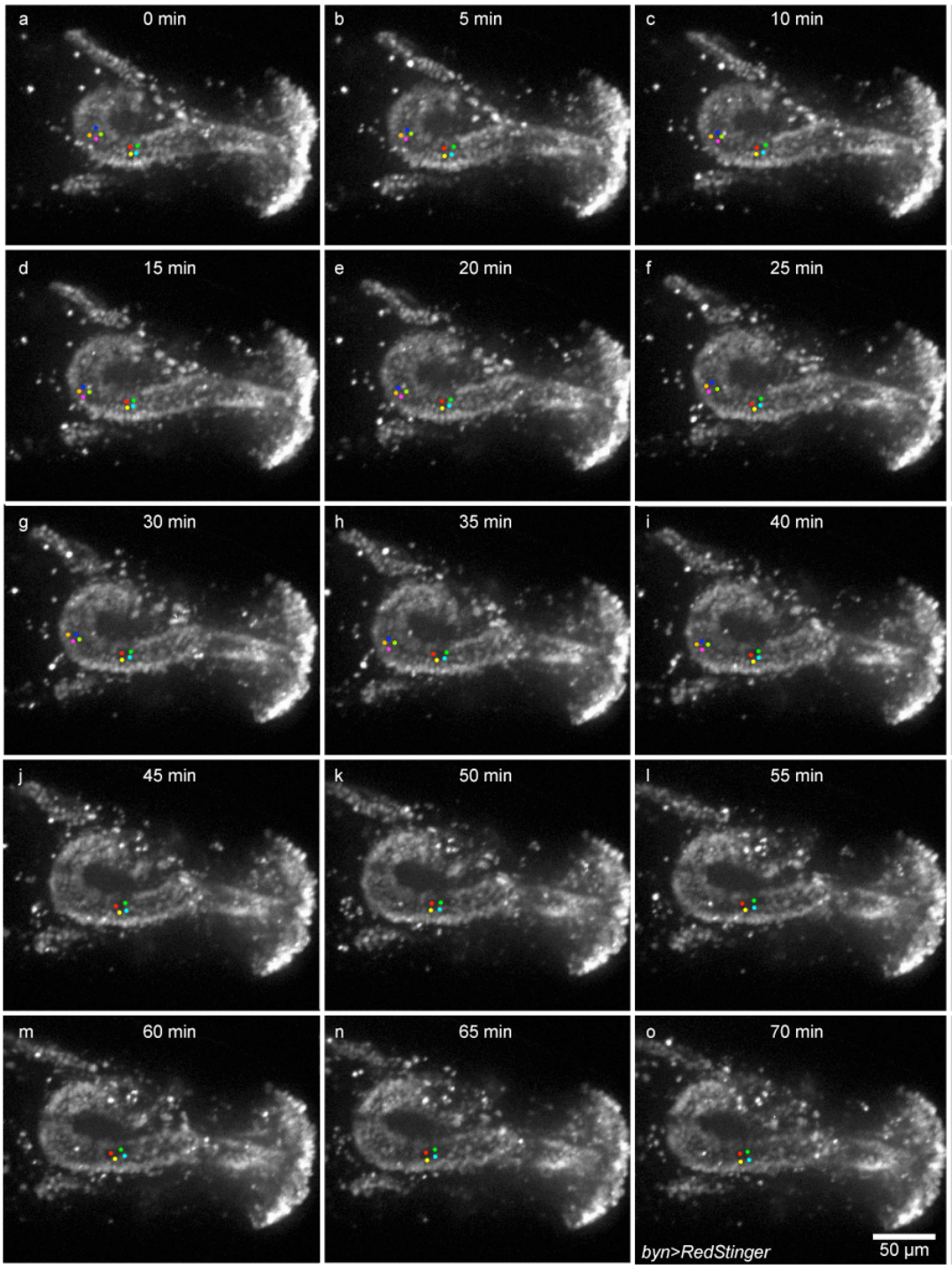
a
0 min
b
5 min
c
10 min
d
15 min
e
20 min
f
25 min
g
30 min
h
35 min
i
40 min
j
45 min
k
50 min
l
55 min
m
60 min
n
65 min
o
70 min
byn>RedStinger
50 µm

Figure 3.15: Stills of live hindgut development, video 3.1. Images represent maximum projections of a 70min timeframe, in five min intervals.
In a stage 14 embryo, nuclei marked with RedStinger, *byn>RedStinger*; individual nuclei tracked during development by coloured dots while visible in the field of view. During this period there appears to be little movement of the marked nuclei.

Video 3.1: The development of embryonic hindgut. The video is a maximum projection of hindgut morphogenesis from stage 12 to 15, viewed dorsally, white line highlights the region of presumed cell rearrangement. Images taken at one minute intervals. The hindgut is marked with RedStinger, *byn>RedStinger*.

To confirm the conclusions drawn from figure 3.15 and video 3.1 an alternative method to track cell movement was devised. This utilised the photoconvertible fluorophore Kaede which usually fluoresces green but is converted to red with exposure to UV light (Ando et al., 2002). The use of Kaede allowed regions of the hindgut to be marked and the movement of these cells tracked, discussed in 2.3.11. Photoconversion was undertaken after hindgut rotation, late stage 13/early stage 14, and the subsequent cell movement was examined at stage 15 after elongation had occurred. Unfortunately, due to the depth of the stage 12 and early stage 13 hindguts in the embryo accurate photoconversion could not be undertaken prior to rotation. Initial photoconversion generated a region of red Kaede equally distributed either side of the hindgut curve (Fig3.16bi-biii). After elongation red Kaede remained relatively even on each side of the hindgut (Fig3.16ci-ciii). If asymmetric cell movement did contribute to curvature it would be expected that cells containing red Kaede would be positioned further around the outside of the curve when compared to the inside. This provides further evidence that asymmetric cell movement does not contribute to curvature during elongation. As cell movement in the wildtype does not appear to contribute to curvature it is assumed that the failure of JAK/STAT mutants to correctly undergo convergent extension does not result in the reduction of curvature. Indeed, this is consistent with the observations that the hindgut curve is formed at stage 10 and that curvature is reduced prior to the majority of elongation during stage 14.

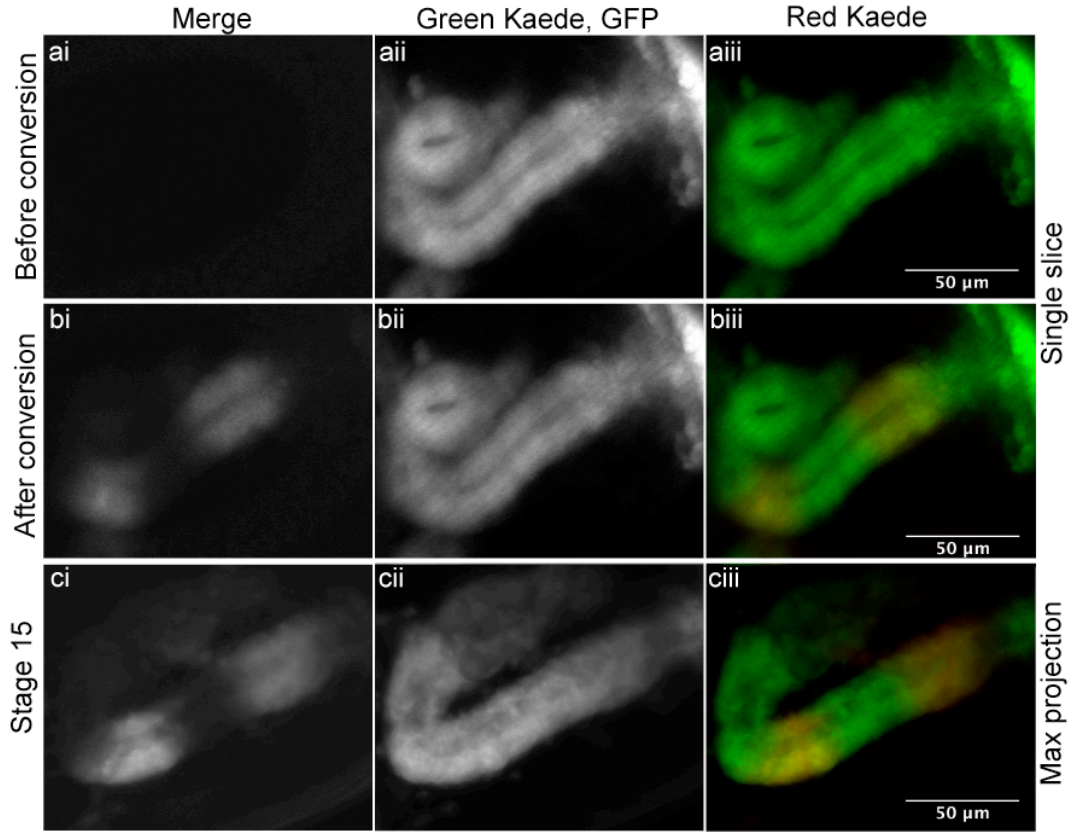

Figure 3.16: Tracking cell movement during hindgut elongation using Kaede. Undertaken in the *byn>GFP*, *Kaede* genetic background, photoconversion undertaken at early stage 14. Images ai-biii represent a single slice while ci-ciii are a maximum projection of multiple slices.
(ai-aiii) Prior to photoconversion no red signal is present. (bi-biii) Photoconversion undertaken in the curve and the LI. (ci-ciii) Embryos were aged to stage 15, there is no drastic difference in the movement of red Kaede on the outside of the hindgut.

A further process which may be disrupted with the loss of JAK/STAT signalling is the regulation of cell shape. Theoretically, the formation of a curved structure requires wedge shaped cells, with a larger apical than basal cell surface, on the inside of the hindgut curve. Examination of the hindgut curve in the wildtype does confirm the presence of these shaped cells (Fig3.17ai-aii). During germband extension the JAK/STAT pathway is known to increase the apical surface of the cell through mislocalising actin, via the repression of the Wiskott-Aldrich syndrome protein (WASp) (Bertet et al., 2009). Indeed, JAK/STAT regulation of cell shape on the inside of the curve in this manner could be sufficient to form wedge-shaped

cells. It thus follows that loss of JAK/STAT function could cause a reduction in the magnitude of the hindgut curve via changes in cell shape. However, examination of cell morphology in *Df(1)os*^{1A} shows that wedge-shaped cells are still present (Fig3.17bi-bii). Indeed, it is assumed that the majority of cell shape changes associated with curvature occur as the curve is forming, prior to the manifestation of the JAK/STAT phenotype. This indicates that JAK/STAT signalling is not likely to have a role in modulating cell shape in the hindgut and so is not a cause of the loss in curvature.

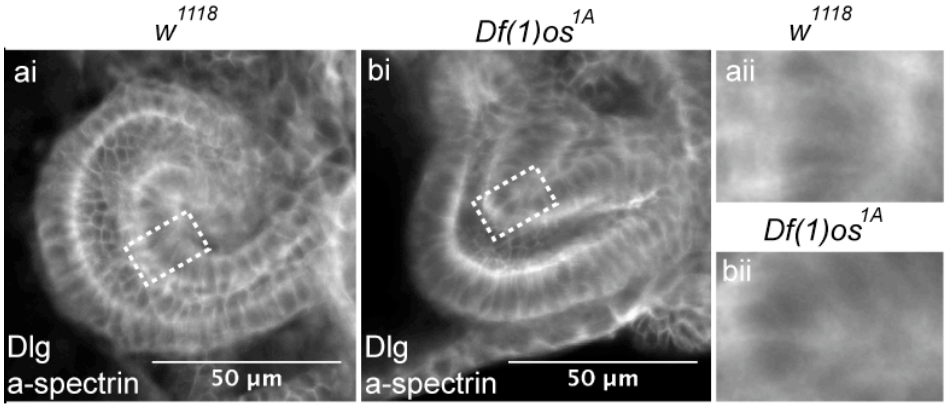

Figure 3.17: The occurrence of wedge-shaped cells in the hindgut curve. Stage 14 hindguts represent by a single slice. A combination of α-spectrin and Dlg staining was used to provide clear outlines of the cells.
(a-aii) In the wildtype wedge-shaped cells are present on the inside of the hindgut curve. (bi-bii) Wedge-shaped cells are also present on the inside of the *Df(1)os*^{1A}.

3.3 Discussion

In this chapter I have described a role for the JAK/STAT pathway in maintaining the anterior curvature in the *Drosophila* embryonic hindgut. Both loss of and ectopic, JAK/STAT signalling causes a reduction in the magnitude of the anterior curve. Examination of the transcriptional output of the pathway shows that, as well as being restricted to the anterior of the organ, there is an asymmetrical bias in signalling. High signalling initially forms on the inside of the anterior curve on the dorsal/ventral axis that becomes the left/right axis after hindgut rotation. As both loss-of-function and ectopic activation results in similar phenotypes it appears that

tight spatial regulation of pathway activation is required for correct curvature, a requirement that has been previously noted for JAK/STAT hindgut elongation defects (Johansen et al., 2003b).

The bias of JAK/STAT signalling on the inside of the hindgut curve places it in the correct spatial context to effect this phenotype. Given the localisation and known functions of JAK/STAT signalling, asymmetric cell movement or regulation of cell shape provided plausible hypotheses for pathway function. However, experimental data indicates this is unlikely to be the case, in the wildtype, as asymmetric cell movement does not occur around the hindgut curve and loss of JAK/STAT signalling does not cause the loss of wedge-shaped cells in the curve. Comparisons in the magnitude of curvature in the wildtype and JAK/STAT loss-of-function hindgut curves through development have indicated the temporal window in which the pathway is required. In the absence of JAK/STAT signalling the hindgut curve appears to form correctly, however, the magnitude of hindgut curvature rapidly reduces by stage 13, coinciding with the onset of rotation and elongation.

Given JAK/STAT signalling does not appear to be required for the initial formation of the hindgut curve it is hypothesised it acts to maintain curvature during development. It is presumed that hindgut morphogenesis is solely mediated by the hindgut epithelium as such, the processes of cell rearrangement (Hartenstein, 1993, Campos-Ortega and Hartenstein, 1997) and changes in cell morphology(Taniguchi et al., 2011) occurring at this time put the organ under an unknown, but potentially significant, biomechanical strain. Unfortunately no satisfactory experimental method to directly test *in vivo* "stress" in the hindgut was possible. Given the asymmetry of the JAK/STAT pathway activation on the inside of the curve it is hypothesised that it maintains curvature, through a downstream intermediate, by providing structural integrity in the anterior curve during morphogenesis. Indeed, the preservation of already formed structures is important during development. Embryogenesis must occur in a step-wise manner in which structures are formed and must be maintained through subsequent developmental processes.

While the evidence for the requirement of tight spatial regulation of JAK/STAT transduction in maintaining curvature is strong, more could be done to understand the nature and significance of the apparent asymmetry in signalling. Tools are available which would allow asymmetric misexpression in the LI-v, *dpp*-Gal4 and LI-d, *en*-Gal4. Cell autonomous downregulation (UAS-$dome^{\Delta cyt}$) or upregulation (UAS-hop^{Tuml}) of pathway activity in these domains would allow for a direct assessment of any asymmetric non-autonomous effects of JAK/STAT signalling in the LI.

To better characterise the manner in which JAK/STAT signalling maintains hindgut curvature the identification of downstream targets is critical. The function of these effectors will likely lead to a greater understanding of this phenotype. Furthermore the experimental data presented indicates that tight spatial regulation of JAK/STAT signalling is key for correct hindgut morphogenesis. While the relief-of-repression cassette of Drm, Bowl and Lin has been shown to restrict signalling to the anterior, through the regulation of *upd* (Johansen et al., 2003a), the novel asymmetry in signalling is yet to be characterised. The focus of the following chapter will be investigating these two problems, characterising a novel downstream effector of JAK/STAT signalling and examining the asymmetric regulation of pathway activation.

4 Characterisation of *Fasciclin III* acting downstream of JAK/STAT signalling in the hindgut curve

4.1 Introduction

Data presented in Chapter three described a novel role for the JAK/STAT pathway in the maintenance of the hindgut anterior curve. Either loss of, or ectopic pathway activation resulting in a similar phenotype. This suggests that the process requires correct spatial regulation of the pathway, at the anterior of the hindgut. In addition, non-autonomous pathway activation was further examined and a novel asymmetry in pathway signalling, on the inside of the hindgut curve, was described.

Key to understanding the mechanism by which the JAK/STAT pathway affects curvature is the identification and characterisation of downstream transcriptional targets. Known downstream targets, and roles, of JAK/STAT signalling in morphogenesis elsewhere in the embryo have been outlined in 1.2.4. These generally involve changes in cell shape, such as the elongation of cells in the posterior spiracle spiracular tube through regulation of RhoGEF (Lovegrove et al., 2006), or contractions in the apical cell surface of the epidermis during germband extension by regulation of WASp (Bertet et al., 2009). As the JAK/STAT pathway is not required for the original curvature of the hindgut, and is unlikely to effect changes in cell shape in this context, it is assumed that processes and targets, previously described, are not required downstream of JAK/STAT signalling in hindgut curvature. This chapter describes the characterisation of FasIII, discussed in 1.3.3, as a novel downstream effector of the pathway and its role in hindgut curvature.

4.2 Results

4.2.1 Fasciclin III abundance is affected by JAK/STAT signalling in the *Drosophila* embryo

FasIII is asymmetrically enriched, on the inside of the curve, at the anterior of the hindgut (Barry Denholm, Cambridge University, personal communication), an observation also found reported in the literature (Fraichard et al., 2006). Examination of the distribution of FasIII in the hindgut shows that it overlies the asymmetric expression of the JAK/STAT reporter, *10xSTATGFP*, (Fig4.1) placing it in the right spatial context to be downstream of JAK/STAT signalling.

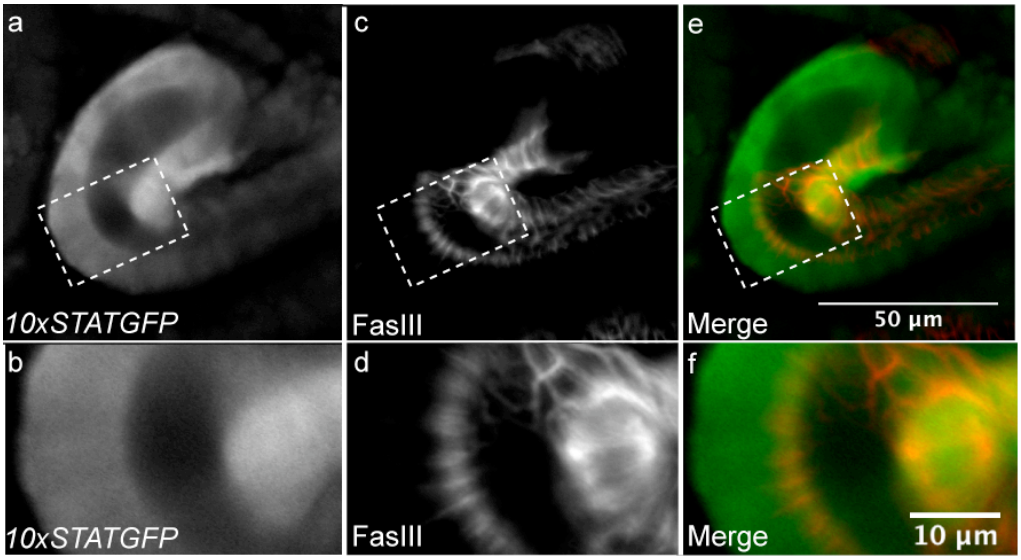

Figure 4.1: Asymmetric enrichment of FasIII overlies asymmetry in high JAK/STAT activity. Image represents a single confocal slice of a stage 14 hindgut. Dashed box shows the region of a,c,e magnified in b,d,e.
(a-b) Enrichment of *10xSTATGFP* on the inside of the hindgut curve. (c-d) Enrichment of FasIII on the inside of the hindgut curve. (e-f) Overlay of *10xSTATGFP* and FasIII.

Examination of *FasIII* expression by *in situ* hybridisation, shows it is not expressed before stage 10 (Fig4.2a-b). From stage 11 onwards *FasIII* mRNA expression appears in a number of locations in which the JAK/STAT pathway is known to be active. This includes the stage 12 tracheal placodes (Fig4.2d-e), the foregut

(Fig4.2d-e, g-h, j-k, m-n, p-q) and the posterior spiracles (Fig4.2j-k, m-n, p-q). Expression in the hindgut appears at stage 12 where it is present asymmetrically on the inside of the curve (Fig4.2g-h); this asymmetry persists through stages 13 (Fig4.2j-k) and 14 (Fig4.2m-n). The asymmetry of *FasIII* mRNA indicates that the observed asymmetry of FasIII protein (Fig4.1) is due to *de novo* protein production rather than protein stability. At stage 15 *FasIII* appears to be expressed uniformly throughout the hindgut (Fig4.2p-q). As described in Chapter three both *upd* expression and *10xSTATGFP* are anterior at stage 15. Hence, this shows a clear dissociation between signalling and *FasIII* expression at this point. Interestingly, this is the stage at which the majority of hindgut morphogenesis has ceased and is shortly after the formation of sSJs. Examination of the sense *FasIII* probe shows low levels of non-specific background staining; this indicates that the observed anti-sense staining is not due to non-specific effects (Fig4.2 c, f, i, l, o, r).

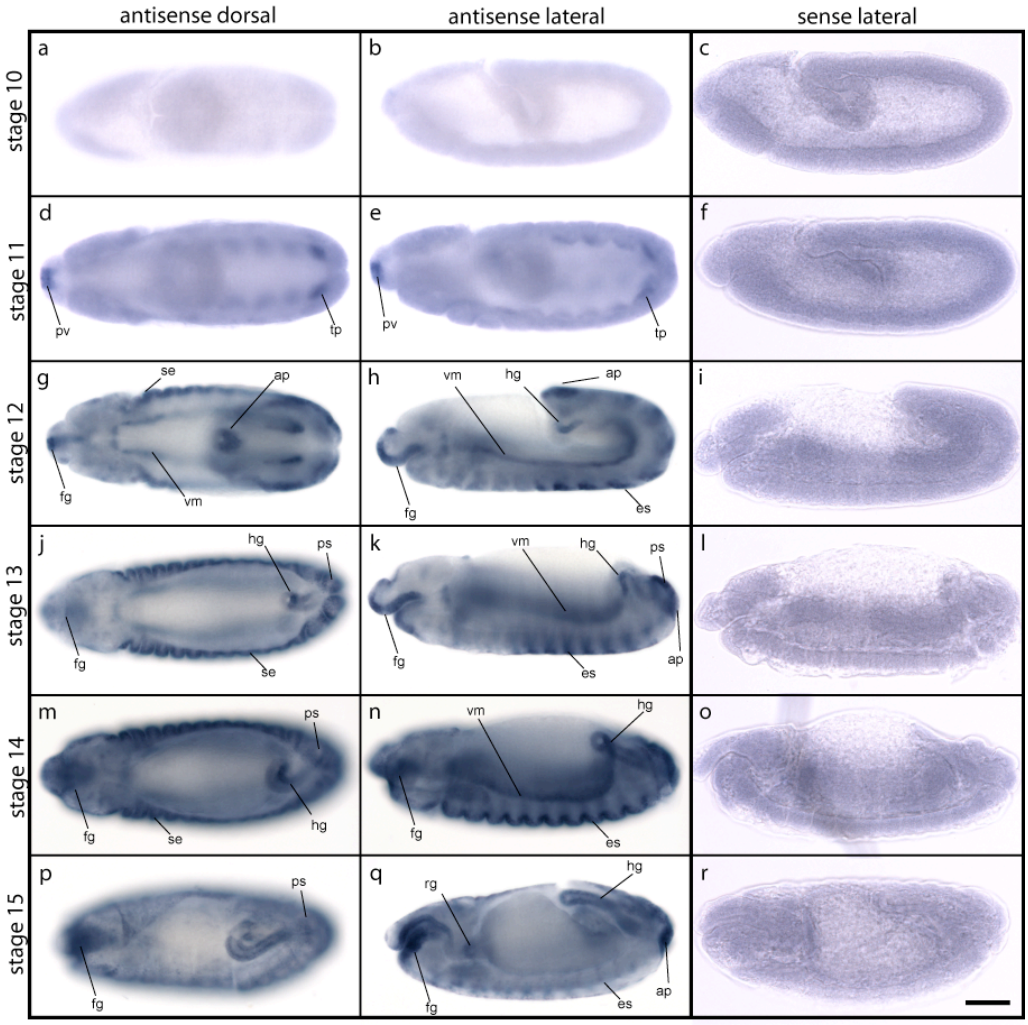

Figure 4.2: The embryo-wide expression pattern of *FasIII*. Embryos stained with the anti-sense probe are viewed from both dorsal and lateral while embryos stained with the sense probe are viewed from lateral.

(a-b) *FasIII* expression appears absent at stage 10. (d-e) From stage 11 early expression is detectable in foregut (fg) and tracheal placodes (tp). (g-h) From stage 12 expression is detectable in the fg, visceral mesoderm (vm), anal pads (ap), ectodermal segments (es), and asymmetrically in the hindgut (hg). (j-k, m-n) Through stages 13 and 14 expression remains in the fg, wm, ap, es and is also found in the posterior spiracles (ps). (p-q) At stage 15 staining in vm and es appears greatly reduced while staining in the hg appears uniform. (c, f, i, l, o, r). There was no background staining present with the sense probe. Scale bar represents 50µm.

Figure 4.2 indicates that FasIII is expressed in tissues known to also have high levels of JAK/STAT activity. To confirm this the distribution of FasIII protein was

compared to the expression of the *10xSTATGFP* reporter and also examined in the *Df(1)os*^{1A} mutant backgrounds. Mutant embryos were selected through absence of ß-galactosidase staining, due to a *LacZ* transgene on the balancer chromosome. Confocal levels were set in the FasIII channel based on the signal received from wildtype (ß-galactosidase positive) embryos and kept constant for imaging the mutant. As expected, the FasIII protein is found in the same locations as the *FasIII* mRNA. Furthermore it appears to coincide with the *10xSTATGFP* reporter in the hindgut, ectoderm stripes (Fig4.3aiii, ciii, eiii giii), foregut (Fig4.3aiii, ciii) and the posterior spiracles (Fig4.3giii). In *Df(1)os*^{1A} mutants lacking JAK/STAT signalling, global FasIII protein levels appear reduced. Low levels of FasIII staining are observed in the visceral mesoderm at stages 12 and 13 (Fig4.3d-f) as well as the ectoderm at stages 13 and 14 (Fig4.3f-h). FasIII staining was not detected in the *Df(1)os*^{1A} mutant hindgut until stage 14 (Fig4.3h). These data show that FasIII protein abundance is reduced with the loss of JAK/STAT signalling.

The reduction in FasIII levels in the visceral mesoderm of the *Df(1)os*^{1A} is confusing as neither the *10xSTATGFP* reporter nor *upd* are expressed there (Chapter three). A recent study has shown that, despite these markers of JAK/STAT signalling not being present, the pathway does have a role in cell specification in the embryonic heart tube, an organ derived from the visceral mesoderm (Johnson et al., 2011). It should be noted that the Stat92E consensus binding motifs in the *10xSTATGFP* reporter are derived from one known pathway target, *socs36E* (Bach et al., 2007). As such, this may therefore not be representative of the regulatory elements required for all JAK/STAT targets. This sets a precedent for JAK/STAT signalling in the visceral mesoderm providing an explanation for the reduction of FasIII in this tissue with the loss of JAK/STAT signalling.

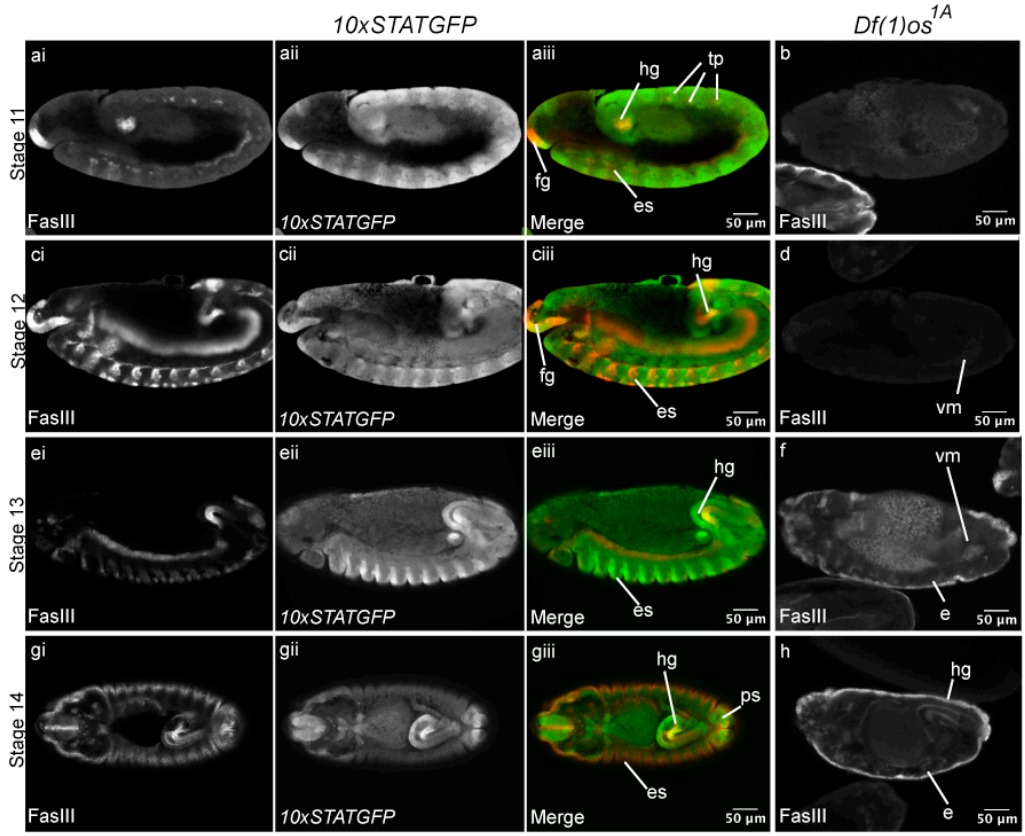

Figure 4.3: Embryo-wide association of FasIII and JAK/STAT signalling. Images represent a single confocal slice, embryos orientated to show hindgut curve topography.
(ai-aiii) FasIII protein is first detectable at stage 11 and coincides with *10xSTATGFP* in the hg, fg, tp and the es, (ci-ciii, ei-eiii) At stage 12 and 13 FasIII protein is more widespread but still shows coincidence with *10xSTATGFP* in the hg, fg and in es. (gi-giii) At stage 14 FasIII still coincides with *10xSTATGFP* in the hg and es but also in the ps (b, d, f, h) Loss of JAK/STAT signalling causes a global reduction in FasIII protein. Reduced staining is still detected in the vm at stages 12 and 13, epidermis (e) at stages 13 and 14 and hg at stage 14.

FasIII normally localises to SJs. To assess this Dlg protein abundance was also examined in the context of pathway activity. Dlg protein distribution was found to have specific co-localisation with the *10xSTATGFP* reporter, Dlg protein being more widely distributed than the restricted pathway activity (Fig4.4ai-aiii, ci-ciii, ei-eiii, gi-giii). Furthermore, Dlg protein levels are unaffected in *Df(1)os*^{1A} (Fig4.4b, d, e f).

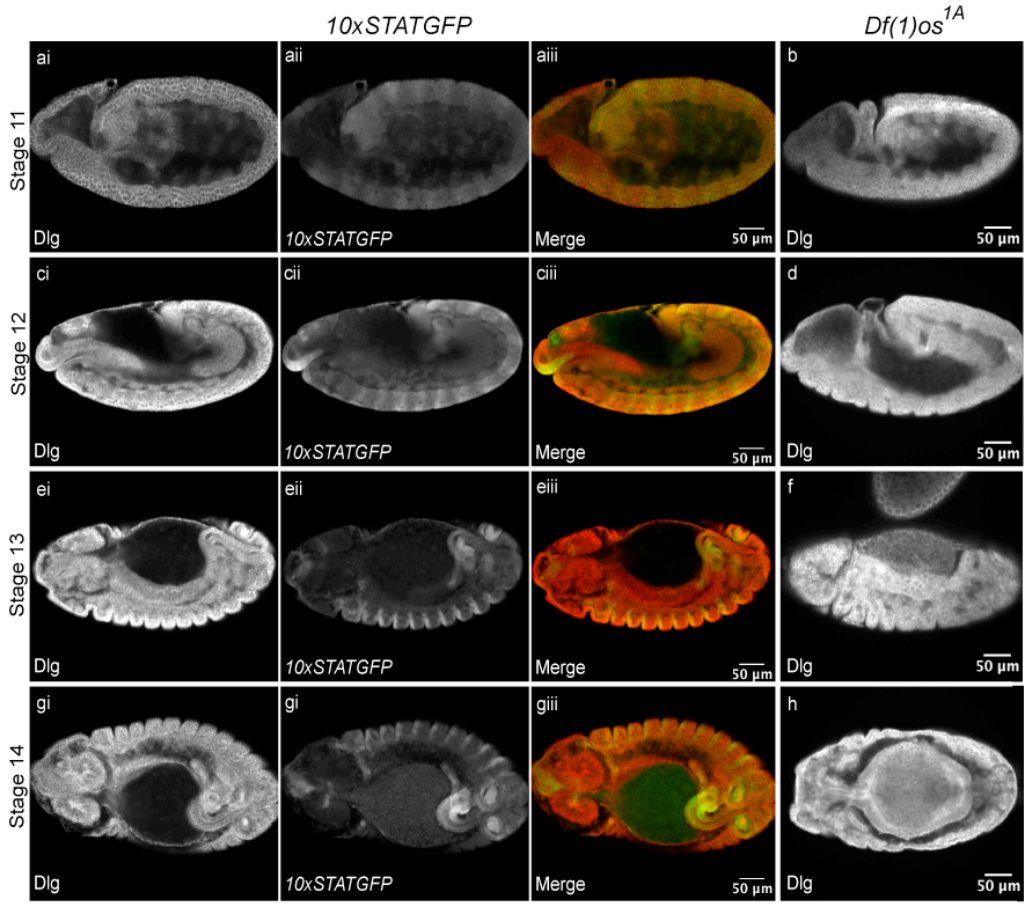

Figure 4.4: Embryo-wide association of Dlg and JAK/STAT signalling. Images represent a single confocal slice, embryos orientated to show hindgut curve topography.
(ai-aiii, ci-ciii, ei-eiii, gi-giii) Dlg and the *10xSTATGFP* reporter show no specific co-incidence in distribution through stages 11-14. (b, d, f, h) Loss of JAK/STAT signalling does not affect Dlg protein staining.

Given the global effect of JAK/STAT signalling on FasIII protein abundance (Fig4.3), the expression of *FasIII* mRNA in different JAK/STAT mutant backgrounds was examined in the hindgut by *in situ* hybridisation. In wildtype hindguts *FasIII* expression is restricted to the inside of the hindgut curve through stages 12-14 (Fig4.5a-c). A reduction of JAK/STAT signalling in the hindgut, *byn>dome*$^{\Delta cyt}$, causes a reduction in the amount and asymmetry of *FasIII* (Fig4.5d-e). Cell non-autonomous pathway activation, *byn>upd*, causes ectopic *FasIII* expression which extends beyond the inside of the curve but remains largely

asymmetric on the inside of the hindgut (Fig4.5f-h). Likewise, cell non-autonomous pathway activation, *byn>hop*^{Tuml}, also causes ectopic *FasIII* expression, however, this appears to be more symmetric (Fig4.5i-k). Therefore changes in FasIII protein abundance in the hindgut may be regulated at the mRNA level by JAK/STAT signalling. Furthermore, the changes in asymmetric expression of *FasIII,* with non-autonomous and autonomous pathway activation, may hint at the manner in which the pathway itself is asymmetrically regulated; this is discussed further in 4.2.3.

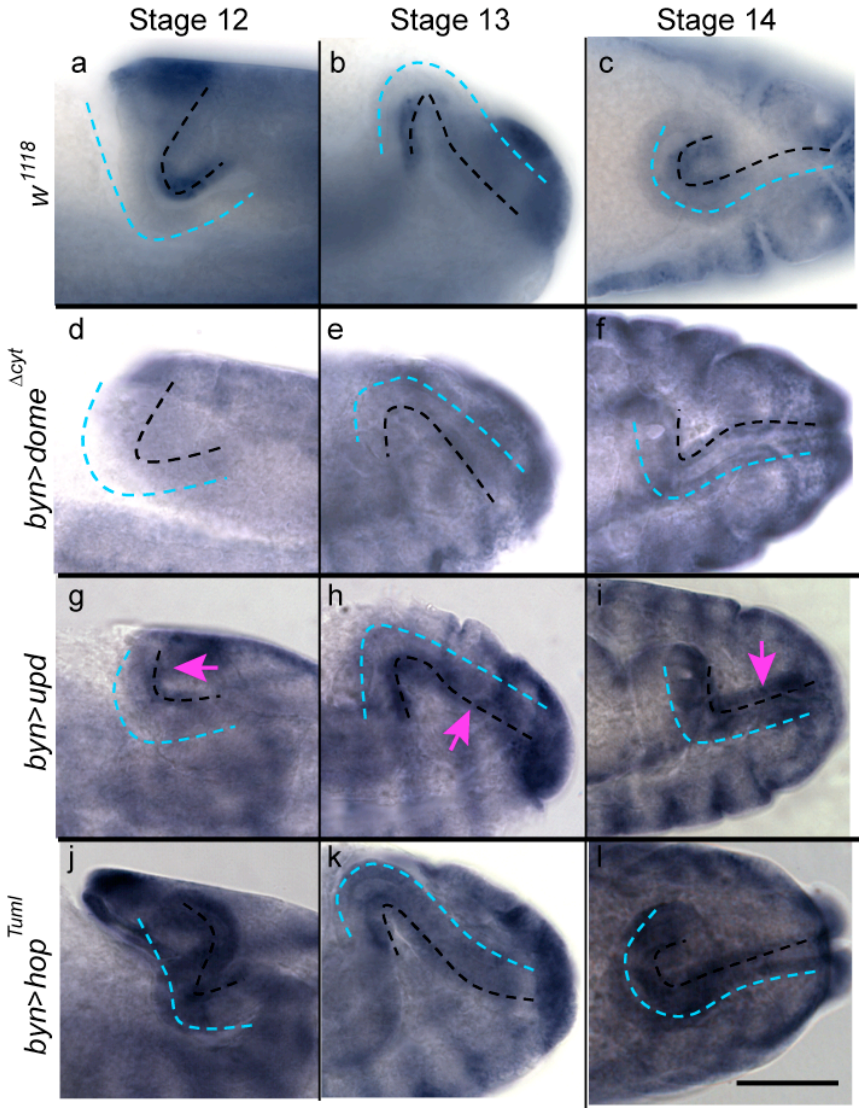

Figure 4.5: *FasIII* expression, visualised by *in situ* hybridisation, in the hindgut in different JAK/STAT mutant backgrounds. Images orientated to show curve topography through stages 12-14, the light blue line indicates the outside of the curve and the black line the inside.

(a-c) In the wildtype *FasIII* expression is found on the inside of the hindgut curve. (d-f) Loss of JAK/STAT activity, *byn>dome*$^{\Delta cyt}$, causes a reduction in *FasIII* and a loss in its asymmetry, (g-h) Ectopic non-autonomous pathway activation, *byn>upd*, causes ectopic pathway activation more posterior to the curve, purple arrow, however this is still largely asymmetric. (j-l) Ectopic autonomous pathway activation, *byn>hop*^{Tuml}, causes an increased uniform expression of *FasIII*. Scale bar represents 50µm.

To confirm that *FasIII* levels are affected in a JAK/STAT-dependent manner, Real Time quantitative PCR (RTqPCR) was attempted. Mixed embryo collections were used to generate cDNA, as a result, use of this technique was hampered by the heterogeneous nature of the biological material collected. It was not possible to detect changes in the expression of a known JAK/STAT target, *socs36E* (Karsten et al., 2002), in response to loss of JAK/STAT signalling. Therefore, no clear assessment of changes in *FasIII* expression could be made. Future investigation should be undertaken using single embryo RTqPCR (Ghanim and White, 2006), or by FACs sorting of GFP balanced embryos, guaranteeing a homogenous genetic sample.

Despite being unable to quantify changes in *FasIII* expression in response to JAK/STAT signalling, *in situ* hybridisation and immunohistochemistry data in various JAK/STAT mutant backgrounds show that FasIII abundance is affected by signalling. Changes in expression could occur either directly in response to Stat92E binding to *FasIII* regulatory elements, or through an immediate signalling effector. To examine this, Stat92E binding sites, both TTC(3n)GAA and TTC(4n)GAA (Rivas et al., 2008), were annotated in the *FasIII* locus and compared to that of a known pathway target *socs36E* and a gene never associated with JAK/STAT signalling, *rhodopsin4* (*rh4*) (annotation of the Stat92E binding sites undertaken by Micheal Moorhouse). Rh4 is a GPCR involved in the *Drosophila* visual system (reviewed in, Broeck, 2001). It may be expected that a known pathway target would be associated with a higher number of Stat92E binding sites. Each region examined is ~90kb; the *socs36E* locus contains 31 3n binding sites and 40 4n binding sites (Fig4.6a), the *FasIII* locus contains 37 3n binding sites and 34 4n binding sites (Fig4.6b) and the *rh4* locus contains 43 3n and 37 4n binding sites (Fig4.6c). From this comparison, there appears to be no obvious enrichment of Stat92E binding sites in the locus of a known target, *socs36E*, or the putative target *FasIII,* when compared to the non-interacting *rh4*. From these data no conclusions can be drawn relating to regulation based on association with Stat92E binding sites. Furthermore, a complication of this method is the variation of gene density in each locus. As a

result, relating the number of binding sites to a specific gene cannot be done in isolation.

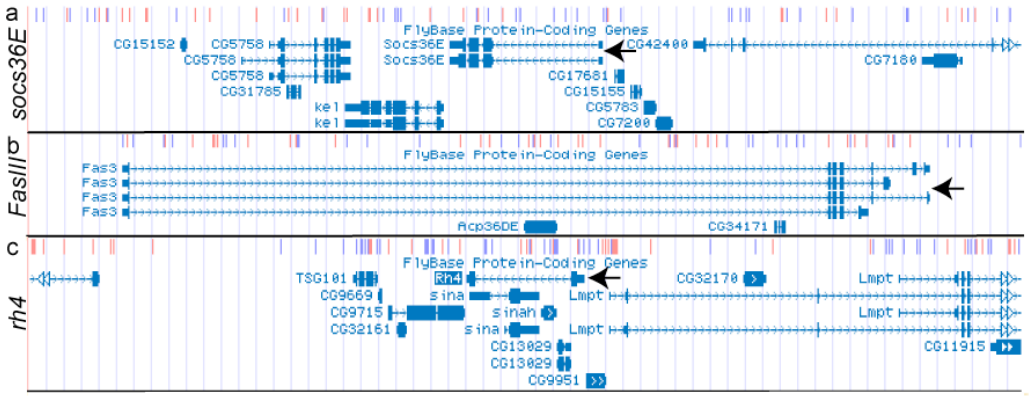

Figure 4.6: Annotation of Stat92E binding sites in the loci of *socs36E*, *FasIII* and *rh4*. A 90kb region of the genome including the genes, indicated by a black arrow, and surrounding area. Stat92E binding consensus sequence TCC(3n)GAA indicated by a red line while TCC(4n)GAA is indicated with a blue line.

(a) In the locus of a known pathway target, *socs36E* there are 31 3n and 40 4n STAT92E binding sites. (b) In the locus of *FasIII* there are 37 3n and 34 4n binding sites. (c) In the locus of *rh4* there are 43 3n and 37 4n binding sites.

Annotation of Stat92E consensus sequences is a simple method from which to infer regulation but does not take account of the context in which the binding site lies. A more definitive analysis of transcription factor binding is Chromatin Immuno-Precipitation (ChIP) which identifies, *in situ*, the DNA sequences which actually bind the transcription factor of interest (reviewed in, Collas, 2010). Mapping of Stat92E binding sites using ChIP has been undertaken as part of the modENCODE project (www.modencode.org) which is systematically characterising the *Drosophila* genome (Celniker et al., 2009). A recent study has utilised these data to examine potential pathway targets, generating a list of genes potentially regulated by JAK/STAT signalling due to their proximity to known Stat92E binding sites. This analysis identified the known pathway targets *socs36E* and *ventral veinless* (*vvl*) but not *FasIII* (Johnson et al., 2011). While no active Stat92E binding sites were found

in the *FasIII* loci this does not rule out the possibility the JAK/STAT pathway regulates its expression.

4.2.2 FasIII abundance leads to protein mis-localisation

In the wildtype hindgut, asymmetric JAK/STAT signalling coincides with an increase in FasIII protein on the inside of the curve (Fig4.1, Fig4.7ai). Data presented in 4.2.1 show that the asymmetry in FasIII is due to *de novo* protein production, dependent on JAK/STAT signalling; this does not occur with the SJ protein Dlg. To further examine the nature of FasIII asymmetry, in the context of the SJ, the distribution of additional SJ proteins was analysed. Varicose (Vari), Dlg, Coracle (Cor) and Fasciclin II (FasII) (Fig4.7aii, b-d) show no asymmetry in protein abundance. This analysis also highlights an important aspect of FasIII asymmetry. FasIII on the inside of the curve appears to span the entire lateral cell membrane. This is different when compared to sub-apical FasIII on the outside of the curve (Fig4.7ai) and sub-apical Vari, Dlg, Cora and FasII on both the inside and outside of the curve (Fig4.7aii-d).

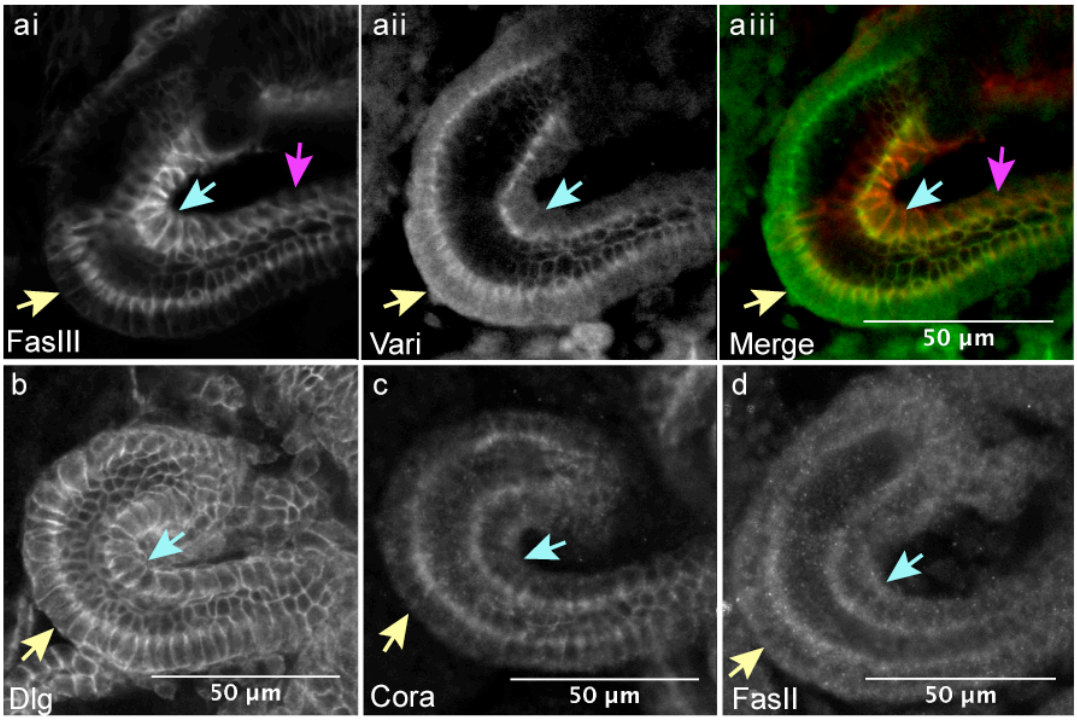

Figure 4.7: Asymmetry in FasIII sub-cellular localisation. Images represented are a single confocal slice through a stage 14 hindgut. The yellow arrow indicates the outside of the curve and blue, the inside.

(ai, aiii) FasIII spans the entire lateral membrane on the inside of the hindgut but is restricted to a sub-apical domain on the outside. Further posterior to the inside of the curve FasIII appears to be more sub-apical, magenta arrow, when compared to FasIII on the inside of the curve, blue arrow. (aii) Vari, (b) Dlg, (c) Cora and (d) FasII appear sub-apical on both sides of the hindgut curve.

To better understand the nature of FasIII lateralisation in the hindgut this phenomenon was examined throughout development. At stage 12 FasIII is exclusively detected on the inside of the hindgut curve where it is lateralised (Fig4.8a). At stage 13 FasIII is first detected, weakly, on the outside of the hindgut curve in a sub-apical membrane domain (Fig4.8b); this is also the case, albeit clearer, at stage 14 (Fig4.8c). While this difference is maintained at stage 15 a sub-apical domain of FasIII is visible on the inside of the curve indicating a reduction in the asymmetry of lateral and sub-apical FasIII either side of the hindgut (Fig4.8d). By stage 16 FasIII, on the inside of the curve, appears to be largely sub-apical, with

cells on the inside and outside of the curve displaying similar FasIII protein localisation and levels (Fig4.8e). The reduction in FasIII asymmetry over time is similar to that seen with the asymmetry in *FasIII* mRNA expression (Fig4.2) and is reminiscent of the asymmetry of *socs36E* mRNA expression (Fig3.11).

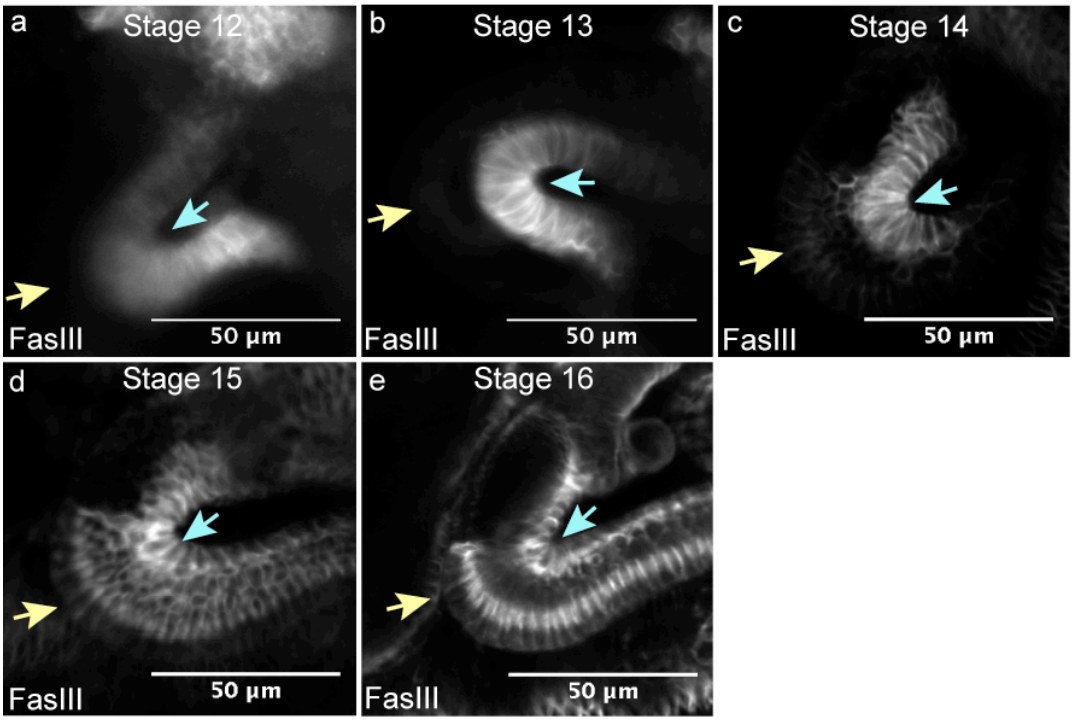

Figure 4.8: FasIII protein lateralisation during development. Images represent a single confocal slice, embryos orientated to show hindgut curve. The yellow arrow indicates the outside of the curve and blue, the inside.

(a) At stage 12 lateral FasIII is exclusively detected, lateralised, on the inside of the hindgut curve. (b) At stage 13 FasIII is faintly visible in a sub-apical domain on the outside of the hindgut curve and remains lateral on the inside, (c) this is clearer at stage 14. (d) At stage 15, FasIII is present in a sub-apical domain on the outside of the curve and is also visible in a sub-apical domain on the inside of the hindgut curve. (e) At stage 16 FasIII is present at nearly uniform levels either side of the hindgut curve.

Given the association between JAK/STAT signalling and FasIII abundance, sub-cellular localisation of FasIII protein was examined in different JAK/STAT mutant backgrounds. Loss of JAK/STAT signalling, *Df(1)os*^{1A}, results in a loss of lateral

FasIII on the inside of the hindgut (Fig4.9b), when compared to wildtype (Fig4.9a), an observation consistent with previous data showing that loss of JAK/STAT signalling results in a loss of *FasIII* expression (Fig4.3b, d, f, h, Fig4.5d-f). Furthermore, cell autonomous ectopic pathway activation, via *byn>hop*^{Tuml}, results in lateral FasIII on both the inside and the outside of the curve (Fig4.9c), while cell non-autonomous ectopic pathway activation, *byn>upd*, results in an increase of FasIII lateralisation posterior to the curve but not on the outside of the curve (Fig4.9d). This observation is broadly consistent with previous data (Fig4.5g-l) showing differences in the distribution of ectopic *FasIII* expression in response to autonomous and non-autonomous pathway activation. However, the levels of protein appear to be more stable than that of the mRNA. This is likely to be due to the protein being maintained within the sub-apical domain.

Taken together, these observations indicate that the effect of JAK/STAT signalling on FasIII abundance directly correlates with the sub-cellular localisation of FasIII. To confirm whether increased FasIII abundance is sufficient to result in protein lateralisation, *FasIII* was ectopically expressed in a JAK/STAT-independent manner, *byn>FasIII*, a condition that resulted in ectopic lateralised FasIII (Fig4.9e).

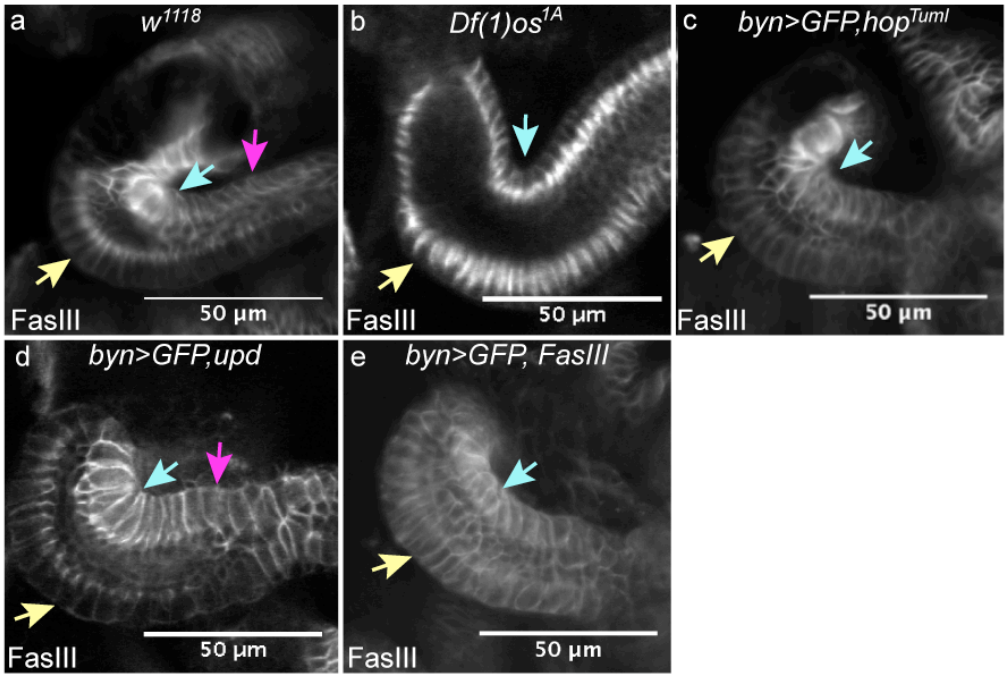

Figure 4.9: Changes in FasIII abundance affects protein lateralisation. Images represent a single confocal slice through a stage 14 hindgut. The yellow arrow indicates the outside of the curve and blue, the inside.

(a) In the wildtype FasIII is lateral on the inside of the curve. (b) Loss of JAK/STAT signalling, *Df(1)os*^{1A}, results in loss of lateral FasIII on the inside of the curve. (c) Ectopic cell autonomous pathway activation, *byn>hop*^{Tuml}, appears to cause FasIII lateralisation on both the inside and the outside of the curve. (d) Ectopic non-autonomous pathway activation, *byn>upd*, does not cause excess FasIII lateralisation on the outside of the curve, however lateralised protein extends further to the posterior; compare magenta arrows in (d) and (a). (e) Ectopic *FasIII* expression, *byn>FasIII*, results in protein lateralisation on both side of the hindgut.

4.2.3 Examination of the origin of JAK/STAT asymmetry

Data previously presented in 4.2.1 and 4.2.2 shows a difference in FasIII asymmetry in response to autonomous and non-autonomous ectopic JAK/STAT signalling. An asymmetry in *FasIII* expression is found in a *byn>upd* background (Fig4.5h-i, Fig4.9d, Fig410b) while it appears more symmetric in a *byn>hop*^{Tuml} background (Fig4.5j-l, Fig4.9c, Fig4.10c). While preliminary, this indicates that if activated at the level of the ligand then the transcriptional activation is asymmetric (Fig4.10d); this is consistent with the observed asymmetry in the *10xSTATGFP* reporter, *socs36E* mRNA and FasIII in the wildtype, as discussed in Chapter three. However,

activation downstream of the receptor, at the level of the kinase, causes the transcriptional activation to be symmetric (Fig4.10e). This indicates that the regulation of the asymmetry in JAK/STAT signalling in the hindgut may be at the level of the receptor.

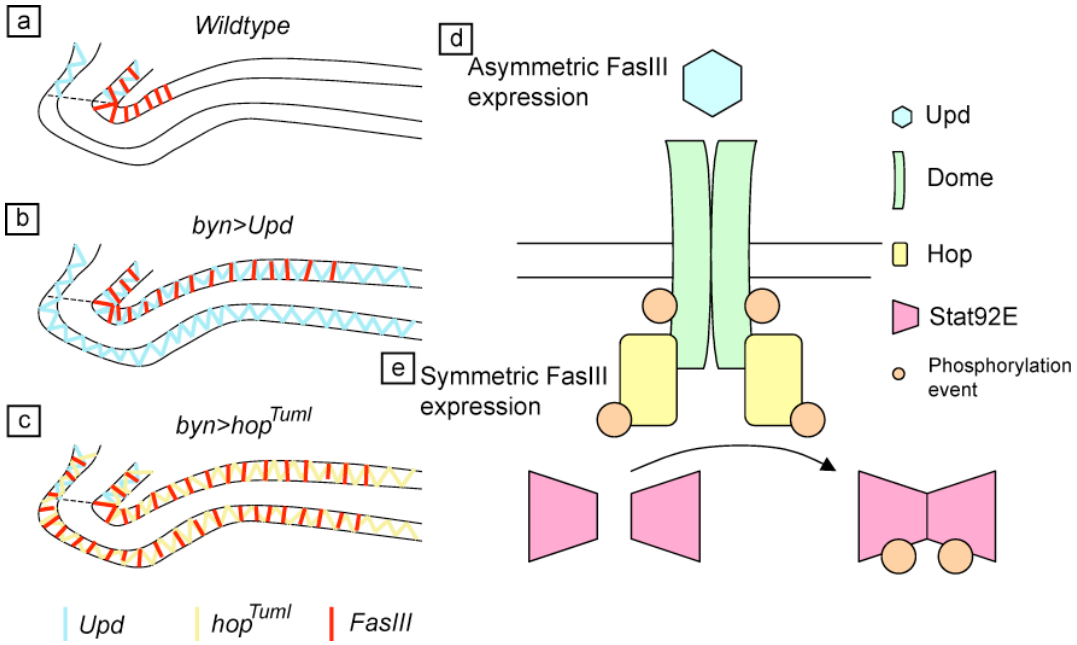

Figure 4.10: Schematic of asymmetric JAK/STAT regulation.

(a) In the wildtype, Upd released from the small intestine causes expression of FasIII on the inside of the curve. (b) Cell non-autonomous pathway activation throughout hindgut, *byn>upd,* causes an extension of the asymmetric expression of *FasIII* on the inside of the hindgut curve. (c) Cell autonomous pathway activation throughout the hindgut, *byn>hop^{Tuml}*, causes an extension in symmetric *FasIII* expression. (d) Asymmetric signalling appears to be maintained when ectopic activation occurs at the ligand level, (e) Symmetric signalling appears to occur when ectopic activation occurs at the kinase level.

An integral event in JAK/STAT signal transduction is the formation of a receptor dimer (Brown et al., 2003). A bias in Dome dimerisation on the inside of the curve may therefore be sufficient to cause a bias in non-cell autonomous signalling. To examine this the ßlue-ßlau *in vivo* dimer visualisation system was used (Mohler and Blau, 1996). Dome is fused to two mutant forms of ß-galactosidase that, in isolation, are enzymatically inactive. If both constructs are expressed in the same cell, when

Dome dimers form, the close proximity of the two ß-galactosidase mutants causes them to become enzymatically active (Brown et al., 2001). This activity can be visualised by the colourimetric processing of the ß-galactosidase substrate. Examination of Dome dimer formation at stages 13 and 14, the period of the most striking asymmetry in FasIII, shows that, as previously described, Dome appears localised to the apical cell surface (Brown et al., 2003, Sotillos et al., 2008). However, there is no apparent asymmetry in Dome dimerisation in the hindgut indicating this is unlikely to cause the asymmetry in pathway activity (Fig4.11).

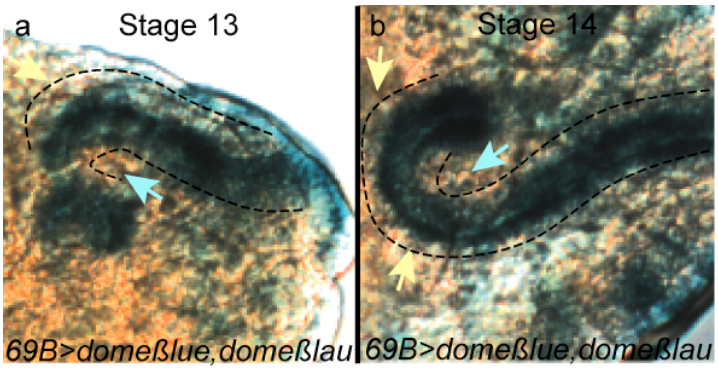

Figure 4.11: Visualisation of Dome dimerisation. Embryos orientated to show hindgut curve. The yellow arrow indicates the outside of the curve and blue, the inside, the black dotted line indicates the basal edge of the hindgut cells.
(a-b) At both stages 13 and 14 dimerised Dome appears equally distributed on both sides of the curve.

A further potential regulator of cell non-autonomous signalling are the heparan sulfate proteoglycans (HSPGs) of which there are two in *Drosophila, division abnormally delayed* (*dally*) (Nakato et al., 1995) and *dally-like* (*dlp*) (Khare and Baumgartner, 2000). Studies of numerous signalling pathways show that HSPGs may affect signalling at the level of the ligand in a number of ways. HSPGs have been shown to be required for ligand protein stability in the extracellular space, the physical movement of the ligand across cells and to mediate ligand transcytosis, ligand endocytosis and resecretion elsewhere (reviewed in, Blair, 2005). In the egg chamber it has been shown that Upd is unable to signal across *dlp* loss-of-function follicle cell clones (Doug Harrison, University of Kentucky, personal

communication). Furthermore *dlp* has also been found to be required for correct signal transduction by Dpp (Belenkaya et al., 2004), Wg (Baeg et al., 2001) and Hh (Han et al., 2004). It therefore may be hypothesised that a bias of Dlp protein distribution on the inside of the hindgut curve may cause a bias of JAK/STAT signalling. Dlp appears symmetrically distributed on each side of the hindgut curve between stages 11-14 (Fig4.12). From these data Dlp distribution alone cannot result in the asymmetry of JAK/STAT signalling.

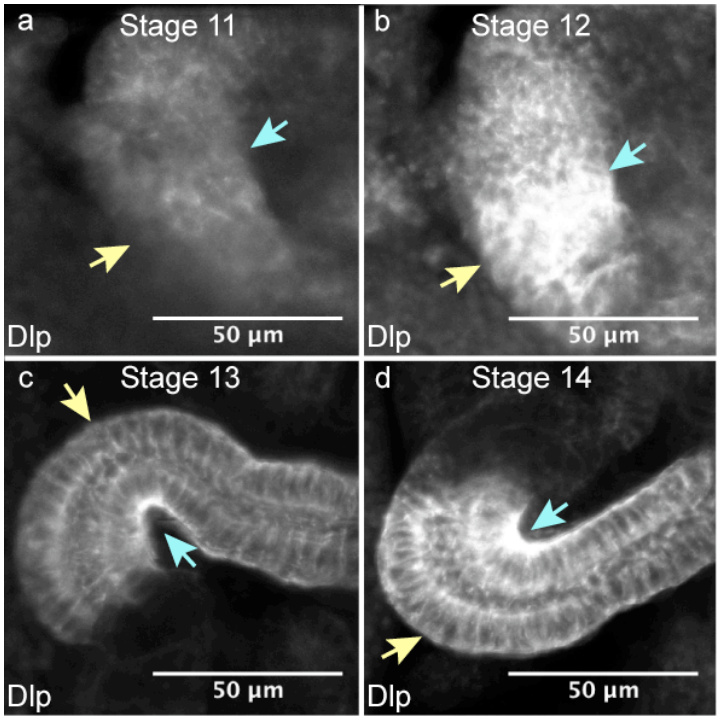

Figure 4,12: Dlp is not asymmetric in the hindgut. Images represent a single confocal slice, embryos orientated to show hindgut curve. The yellow arrow indicates the outside of the curve and blue, the inside.

(a-d) Throughout hindgut development Dlp does not show an asymmetry in protein localisation.

4.2.4 *In vitro* analysis of FasIII function

FasIII is a single-pass transmembrane immunoglobulin family protein which has previously been shown to act as a homophilic adhesion molecule in *Drosophila* S2 cells (Snow et al., 1989). To confirm these previous findings, the ability of FasIII to facilitate cell adhesion in the non-adhesive mesodermally derived Kc_{167} cell line was examined. Based on transcript profiling generated by the modENCODE project

FasIII is not expressed by Kc_{167} cells, searchable at the Harvard RNAi facility website (www.flyrnai.org). Consistent with this, *FasIII* is not detectable by RTqPCR in Kc_{167} cells transfected with an empty plasmid but is expressed in proportionally higher amounts when transfected with increasing amounts of *FasIII-HA* (Fig4.13).

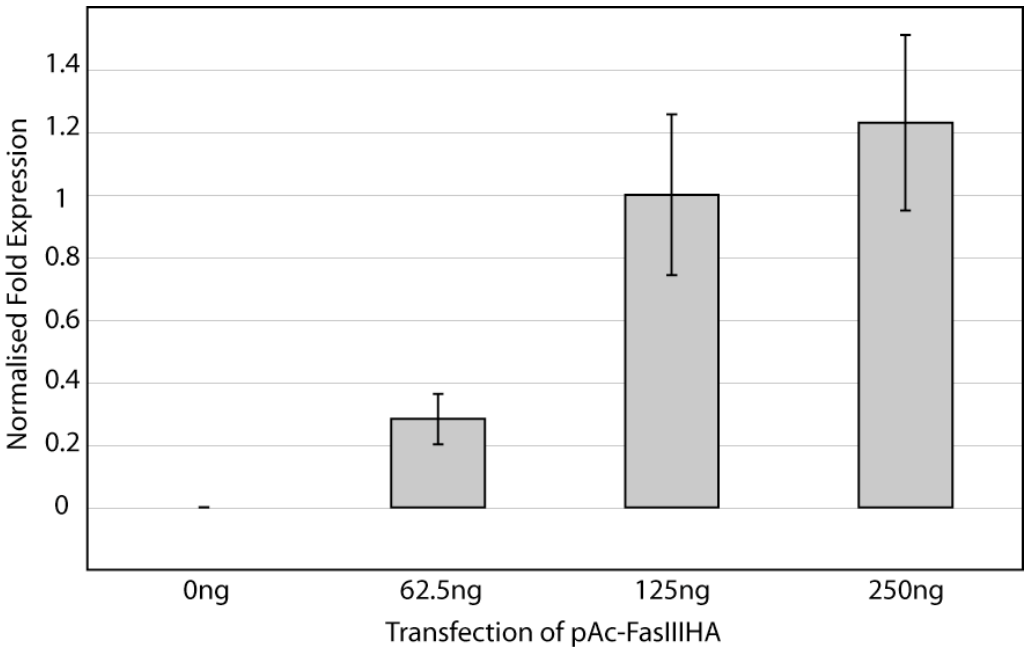

Figure 4.13: *FasIII* is not expressed in Kc_{167} cells.
In cells transfected with an empty plasmid no *FasIII* expression was detected. *FasIII* expression was detected in proportionally higher amounts with an increase in the amount of *FasIII* transfected. Expression normalised to the ubiquitously-expressed *s18*.

To assay the adhesive properties of FasIII, Kc_{167} cells were transfected with either *FasIII-HA* or *FasIII-Flag*. Strikingly *FasIII* expression caused the formation of large cell clumps when compared to cells transfected with an empty vector (Fig4.14).

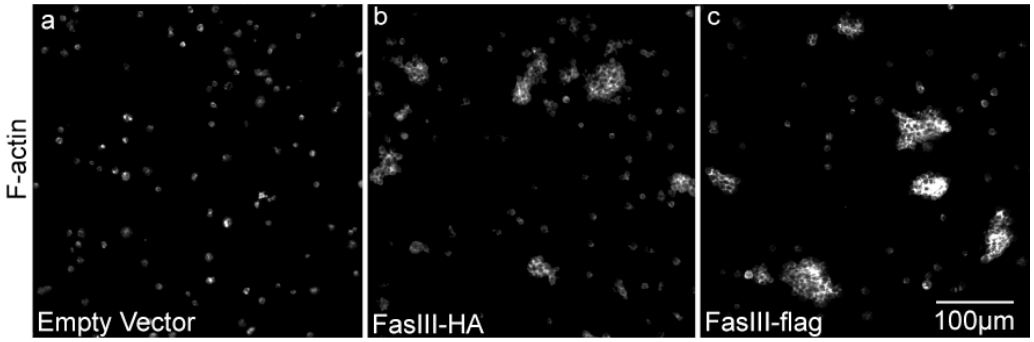

Figure 4.14: FasIII causes clumps in Kc^{167} cell populations. Cell transfections were left to express for 4 days.

(a) Transfection with an empty vector causes no clumps to form. (b) Transfection of *FasIII* either tagged with HA or (c) Flag causes the spontaneous formation of cell clumps.

Consistent with previous reports (Snow et al., 1989), FasIII protein is localised at the interfaces between adjacent cells in the clumps (Fig4.15aii-aiii). Cells not included in clumps did not appear to stain with FasIII (Fig4.15ai,aiii). This indicates that FasIII must be expressed in all cells of a clump, suggesting that interactions between cells are mediated by FasIII homotypic interactions.

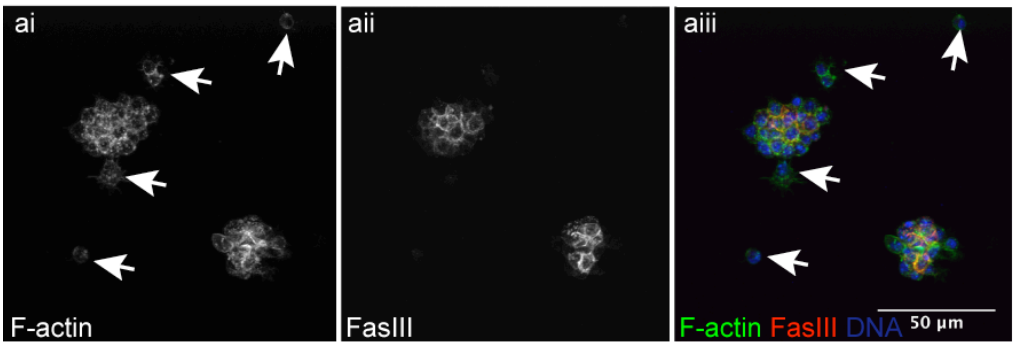

Figure 4.15: FasIII localises to the cell interfaces in clumps.

(aii, aiii) Cell aggregates show FasIII localisation primarily at the internal cell interfaces. (ai, aiii) Cells not expressing FasIII appear not be found in clumps, white arrows.

Given the known function of FasIII, it is highly likely that the observed cell clumps are forming through the interactions of adhesive homodimers. Another explanation for this type of clump formation is that FasIII may be acting as a mitogen, increasing cell division, with the observed aggregates being a product of clonal expansion. To

discount this hypothesis, quantification of cell number in response to transfection with *FasIII* was carried out. As the formation of clumps interfered with the ability to visualise cells to count, a Renilla luciferase assay was undertaken. Renilla placed under the transcriptional regulation of the ubiquitously-expressed promoter is widely used to assess cell viability (Muller et al., 2005). Cells transfected with increasing amounts of *FasIII* showed no increase in luminescence indicating that cell number was unaffected through exogenous expression of *FasIII* (Fig4.16). These data confirm that clumps are not formed due to a mitogenic effect of FasIII, indicating that they arise via cell adhesion.

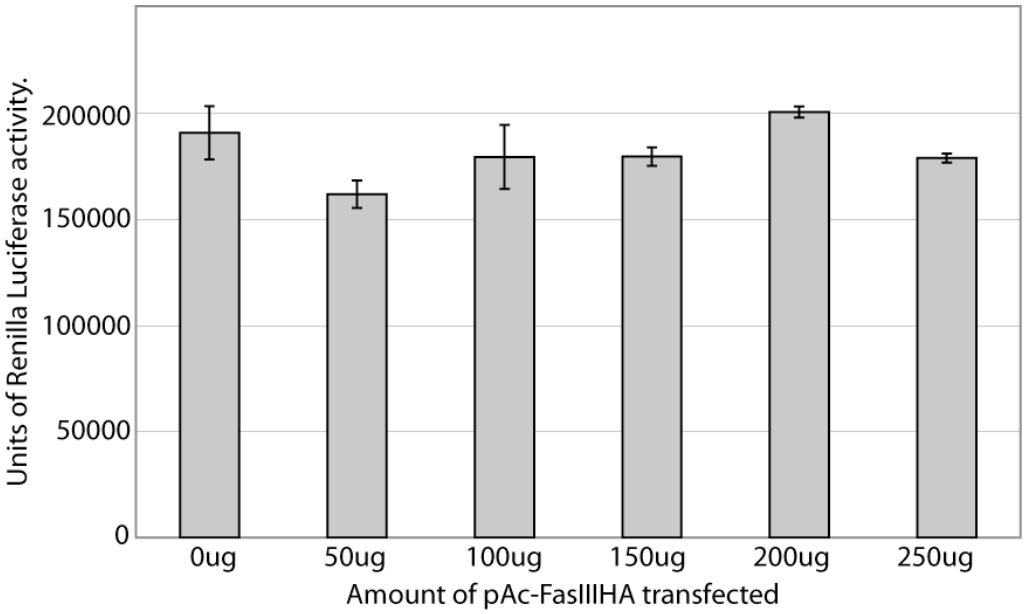

Figure 4:16: FasIII does not affect cell proliferation in Kc^{167} cells.
Using a cell viability reporter, Renilla luciferase, no increase in luminescence was detected with increasing transfection of *FasIII*.

4.2.5 Spatial regulation of FasIII lateralisation is required for correct hindgut curvature.

Data presented in Chapter three show that JAK/STAT signalling is required for maintenance of curvature during morphogenesis. FasIII is a provisional pathway target that appears lateralised on the inside of the hindgut in a JAK/STAT-dependent manner. Furthermore, the asymmetrical lateralisation of FasIII appears to reduce at

the completion of hindgut morphogenesis (Fig4.8). Taken together, FasIII may be a good candidate to act as a JAK/STAT effector in maintaining hindgut curvature.

An additional tool which can be utilised to examine the significance and effect of FasIII lateralisation is the MAGUK scaffold protein Vari (Wu et al., 2007). In SJs, Vari is required for the correct localisation of FasIII into the sub-apical domain (Moyer and Jacobs, 2008). Consistent with this, loss of *vari* causes FasIII to become lateralised on the outside of the hindgut (Fig4.17b). A higher amount of FasIII is still present on the inside of the curve, presumably due to the asymmetry of JAK/STAT-induced expression. The *vari* mutant, therefore, provides a JAK/STAT-independent tool in which to examine the effect of FasIII lateralisation on hindgut morphology.

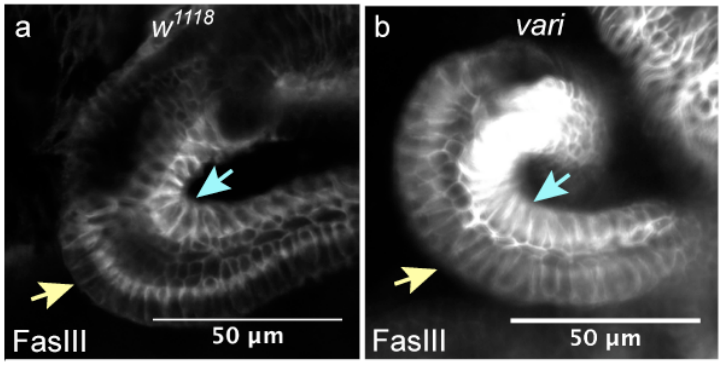

Figure 4.17: FasIII localisation in the *vari* mutant. Images represent a single confocal slice through a stage 14 hindgut curve. The yellow arrow indicates the outside of the curve and blue, the inside.
(a) In the wildtype FasIII is lateralised on the inside of the hindgut curve. (b) Loss of *vari* causes ectopic lateralisation of FasIII on the outside of the hindgut curve.

To further investigate the association of FasIII and Vari, a Co-IP was undertaken using wildtype embryo lysate. This showed that Vari can pull down the smallest FasIII isoform (Patel et al., 1987), isoform B (Fig4.18). Based on these data it is assumed that FasIII is physically held in the sub-apical domain through binding to Vari.

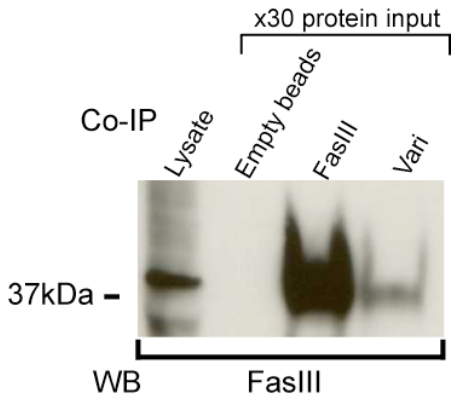

Figure 4.18: Vari physically associates with FasIII.
Western blot analysis using anti-FasIII shows a clear band at around 42kDa. This is absent with lysate incubated with no antibody but present if the lysate is incubated with either anti-FasIII or anti-Vari.

Hindgut curvature in stage 15 *FasIII* and *vari* mutant embryos appears to be reduced when compared to the wildtype (Fig4.19). These data indicate that FasIII must be present, and its lateralisation spatially regulated, for correct hindgut curvature.

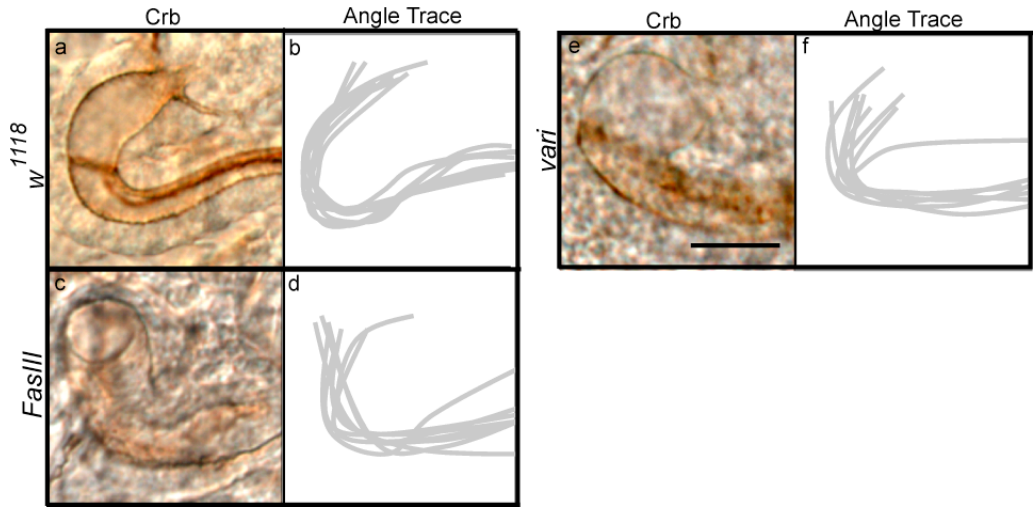

Figure 4.19: Loss of *FasIII* or *vari* causes a reduction in the magnitude of the stage 15 embryo hindgut curve. For each genotype a Crb-stained representative image is displayed accompanied by traced images of a further eight hindguts.
(a-b) The wildtype curves back on itself. (c-d) Loss of either *FasIII* or (e-f) *vari* causes a reduction in the magnitude of the hindgut curve. Scale bar represents 100µm.

Quantification of the deviation of the hindgut curve from the embryonic midline shows that the observed reduction in curve magnitude is significantly different from wildtype (Fig4.20). These data indicate that JAK/STAT signalling is likely to be operating through FasIII to maintain curvature during hindgut morphogenesis.

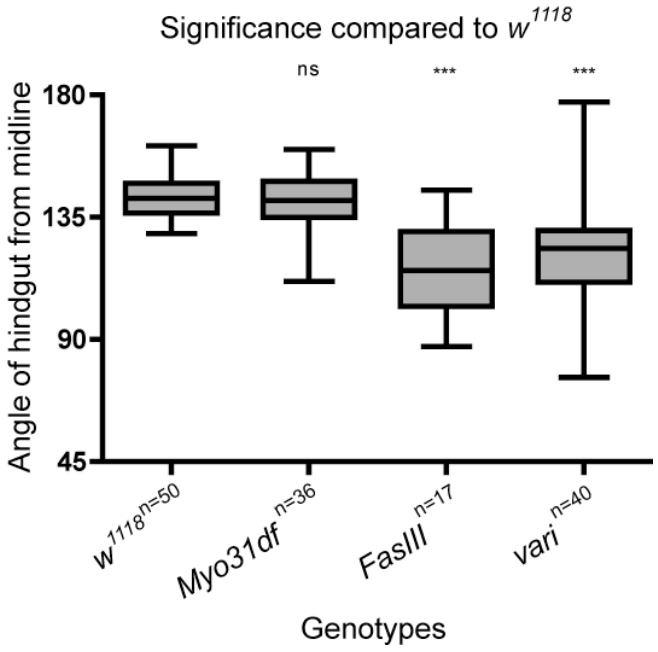

Figure 4.20: Quantification of hindgut curvature defects in *FasIII* and *vari* stage 15 mutants. Angle represents the deviation of the hindgut from the midline of the embryo. Angle of hindgut in *Myo31DF* mutant does not significantly differ from the wildtype, however, loss of *FasIII* and *vari* causes a significant reduction in magnitude (P>0.0001). Statistical significance calculated using an unpaired t-test.

Figures 4.19 and 4.20 show that, independent of changes in JAK/STAT signalling, FasIII must be present, and its lateralisation spatially regulated, for correct hindgut curvature. To further examine the role of FasIII in curvature, *FasIII* was expressed throughout the hindgut, *byn>FasIII*. This resulted in a drastically truncated hindgut structure which did have an established curve or rotation when fully formed (Fig4.21b). Ectopic cell-autonomous JAK/STAT signalling (Fig4.9c) and loss of *vari* (Fig4.19b) also results in ectopic lateral FasIII but not a truncated hindgut structure. It is likely that the expression directly driven by *byn*-Gal4 results in higher ectopic FasIII expression. Based on the known role of FasIII as a cell adhesion molecule these data appear to show that high, ectopic, cell adhesion is detrimental to hindgut morphogenesis. While this assumption is made there are many cell adhesion molecules, such as DE-cad, which also have roles in cell signalling. While this has not been shown for FasIII it may have a, as yet, uncharacterised additional role

which may cause this phenotype. Future work could undertake this experiment at lower temperatures, reducing the expression from the Gal4 UAS system, or use a weaker hindgut-specific Gal4 driver such as *fkh* (Lengyel and Iwaki, 2002).

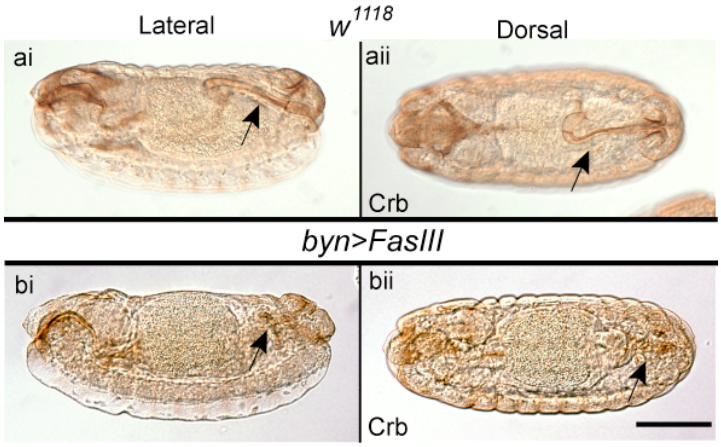

Figure 4.21: Overexpression of *FasIII* results in a truncated hindgut. Images represent a stage 15 embryo viewed from dorsal and lateral.
(ai-aii) The wildtype forms a Shepherd's crook morphology. (bi-bii) Overexpression of *FasIII*, *byn>FasIII* causes a greatly truncated structure.

The truncated hindgut phenotype, caused by overexpression of *FasIII*, is similar to the hindgut formed with increased expression of DE-cad, *byn>CADH*^{519} (Fig 4.22). Closer examination of the DE-cad overexpression phenotype shows that around stage 13, at the onset of elongation, cells appear to delaminate from the hindgut epithelium and undergo apoptosis. As both FasIII and DE-cad are homophilic adhesion molecules, these data appear to confirm the earlier hypothesis that a uniform increase in cell adhesion may affects hindgut morphogenesis.

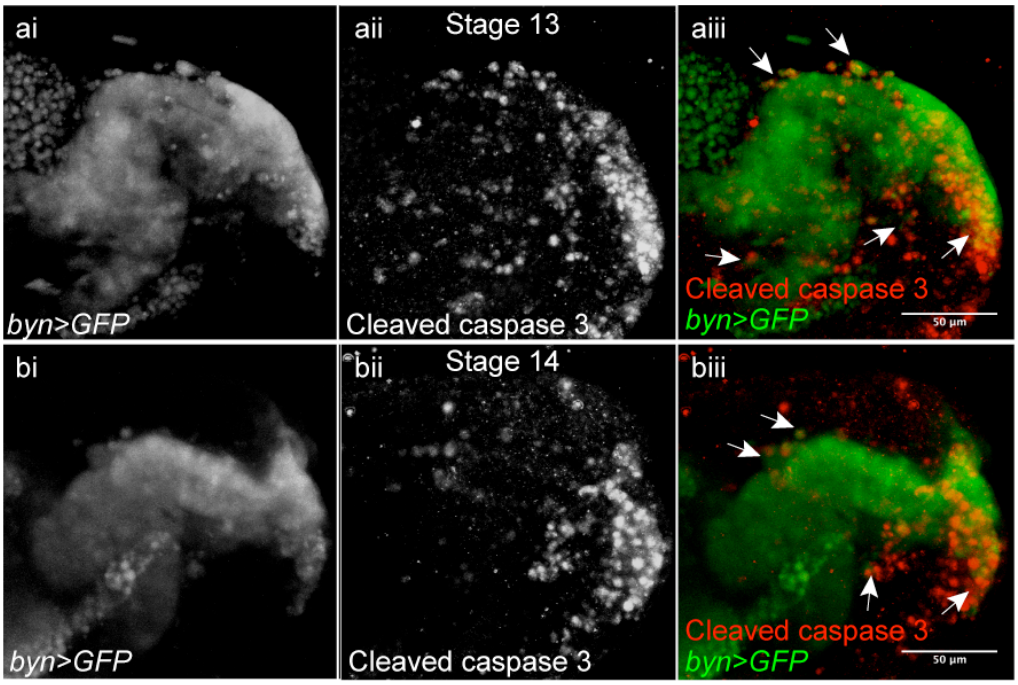

Figure 4.22: Overexpression of DE-cad (*shotgun-shg*) results in a truncated hindgut and apoptosis. Embryos viewed laterally, images represent a maximum projection of multiple slices. (ai-aii) Overexpression of full length *shg*, *byn>CADH*$^{5/9}$, results in a truncated structure with delaminated hindgut cells undergoing apoptosis, white arrows, at both stages 13 (bi-biii) and 14.

4.3 Discussion

In this chapter FasIII has been shown to be a potential novel downstream effector of JAK/STAT signalling. On the inside of the hindgut curve, overlying the asymmetry in JAK/STAT signalling, FasIII is found to span the entire lateral cell membrane. Loss of JAK/STAT signalling causes a loss of both mRNA and protein abundance resulting in a loss of FasIII lateralisation. Conversely, ectopic JAK/STAT signalling is sufficient to produce ectopic lateralised FasIII, presumably through an increase in *de novo* protein production. Curvature defects, with both loss of *FasIII* and loss of the spatial regulation of FasIII lateralisation through loss of *vari*, indicates that the JAK/STAT regulation of lateralised FasIII is likely to be key in maintaining the hindgut curve. Due to the demonstrated adhesive properties of FasIII it is assumed that lateralised protein on the inside of the hindgut curve provides a region of high tissue stability. This domain could provide rigidity to the curve structure during morphogenesis.

In vivo analysis of both FasIII protein and mRNA in various JAK/STAT backgrounds indicate its abundance is influenced by JAK/STAT signalling. The dynamics of *FasIII* expression and JAK/STAT activity show the largest association prior to stage 14. During stage 14, SJs form indicating that the JAK/STAT pathway has a pre-SJ effect on *FasIII* expression. After stage 14 *FasIII* expression appears more widespread and dissociated from JAK/STAT signalling (Fig4.3). Attempts to assess this interaction in a quantitative manner, using RTqPCR, and in a qualitative manner, using bioinformatics, were inconclusive. Furthermore, *FasIII* expression was not shown to be affected by JAK/STAT signalling in Kc_{167} cells (Bina et al., 2010), however, this study was undertaken in a mesodermally-derived hemocyte cell line while the hindgut is an epithelial tissue. It can be assumed that cells derived from separate germlayers would have different cell signalling outcomes reflecting their divergent functions.

The ideal manner in which to confirm transcriptional regulation is the *in vivo* identification and mutation of transcription factor consensus binding sequences. This is a technique which has been elegantly undertaken for JAK/STAT targets *trh* and *vvl* (Sotillos et al., 2010). In this study, conserved Stat92E binding sites were mapped in these loci and the regions containing them were cloned upstream of a *LacZ* reporter. In reporter constructs that replicated endogenous gene expression Stat92E binding sites were then mutated. The resulting loss of expression allowed for identification of specific consensus sequences required for gene expression in different embryonic organs (Sotillos et al., 2010). Similar promoter mutation studies have been used *in vitro* to confirm the JAK/STAT regulation of *Draf* (Kwon et al., 2000) and *in vivo* to confirm the regulation of *crb* (Lovegrove et al., 2006), *eve* (Yan et al., 1996) and *dome* (Rivas et al., 2008). While beyond the remit of this study future work examining the regulation of *FasIII* by JAK/STAT signalling could utilise a similar approach.

Closer analysis of *FasIII* asymmetry in the wildtype indicates that its expression is unlikely to be solely as a result of JAK/STAT signalling. FasIII is tightly spatially regulated on the inside of the hindgut curve in a region spanning the SI and LI. While FasIII in the LI overlies the asymmetry in JAK/STAT signalling, it is puzzling that FasIII is asymmetrically localised in the SI where JAK/STAT signalling appears to be uniform. While the JAK/STAT pathway undoubtedly plays a significant role in *FasIII* expression, either directly or indirectly, it is likely to do so in the context of an, as of yet, unknown asymmetrically-distributed factor. The only other known factors that affect *FasIII* expression are the RTKs Anaplastic Lymphoma Kinase (Alk) (Loren et al., 2003) and Epidermal Growth Factor Receptor (EGFR) (Dong et al., 1999). However, neither of these appear to be asymmetrically distributed in the hindgut and therefore are unlikely to cause asymmetric *FasIII* expression. While the work of this chapter focused of possible mediators of JAK/STAT asymmetry, Dome dimerisation and Dly distribution, it did not examine a contribution of the underlying asymmetry in the hindgut to JAK/STAT and FasIII asymmetry. Factors expressed in the *dpp* domain, the LI-v, would be correctly spatially distributed to positively regulate JAK/STAT signalling or act as a co-factor for *FasIII* expression. Conversely, factors expressed in the *en* domain, the LI-d, would be correctly spatially distributed to negatively regulate JAK/SAT signalling or FasIII expression, discussed in 1.4.3 (Takashima and Murakami, 2001, Iwaki and Lengyel, 2002). Indeed, regulation in either manner would be sufficient to generate an asymmetry in FasIII asymmetry. Therefore, examining FasIII asymmetry in response to misexpression experiments re-patterning the LI-v and LI-d would be of interest.

The JAK/STAT-dependent lateralisation of FasIII appears to be the key downstream effect of the pathway. To fully understand this it must be examined in the context of SJ formation and the sub-apical localisation of FasIII in a Vari dependent manner (Moyer and Jacobs, 2008). It is expected that the observed physical interaction between Vari and FasIII is required to retain FasIII within this sub-cellular region.

While the stoichoimetry of this interaction is unknown, it is likely that only a finite amount of FasIII can be accommodated within the sub-apical region. Fluorescent Recovery After Photobleaching (FRAP) analysis shows that, if excluded from the SJs, the cell adhesion molecules Neuroglian (Nrg) and Neurexin IV (NrxIV) can rapidly move throughout the lateral membrane (Laval et al., 2008). Therefore, there appears to be no innate physical barrier inhibiting SJ cell adhesion molecules, such as FasIII, from moving laterally in the cell membrane except their retention in the sub-apical domain. Based on these assumptions the gradual reduction of lateral FasIII on the inside of the hindgut curve during development can be explained. The observed JAK/STAT-dependent regulation of *FasIII* occurs prior to the formation of SJs, between stages 11-13, creating regions with a high abundance of lateral FasIII. From the onset of SJ formation, at stage 13 and onwards, FasIII expression is no longer limited to regions of high JAK/STAT signalling where it becomes immediately localised into a sub-apical region, a process dependent on Vari. While *FasIII* expression remains asymmetric during stage 14 its protein lateralisation remains asymmetric during stage 15, despite the uniform expression of *FasIII* mRNA, due to the excess asymmetric protein produced during the preceding stages. On the inside of the hindgut excess FasIII cannot be incorporated into the sub-apical domain and becomes lateralised by default rather than through an active re-distribution driven by JAK/STAT signalling (Fig4.23). As FasIII becomes uniformly expressed at stage 15 the excess protein on the inside of the hindgut curve is removed, presumably through a combination of degradation and sequestering into the sub-apical domain, resulting in a symmetrical sub-apical FasIII by stage 16. This process can be disrupted as increased ectopic FasIII protein production, either in a JAK/STAT-dependent manner or via *byn>FasIII*, results in ectopic FasIII lateralisation.

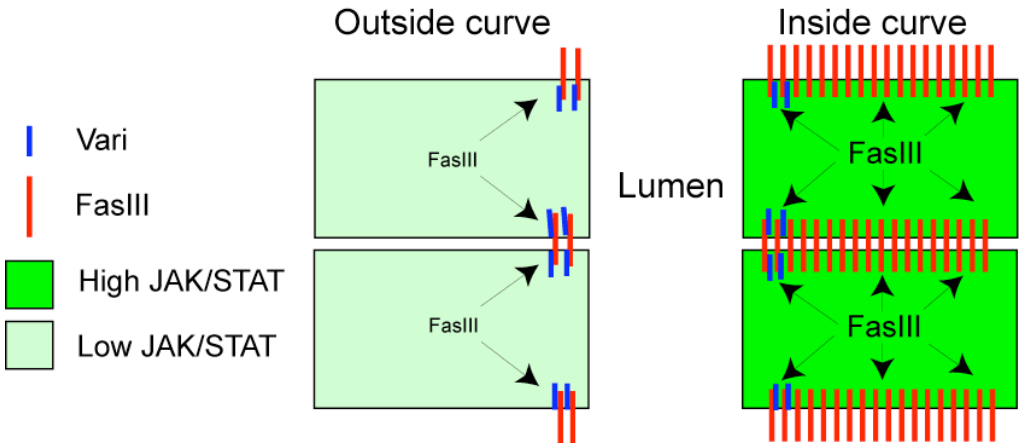

Figure 4.23: Schematic of the asymmetry of FasIII lateralisation in the hindgut.
Low levels of *FasIII* expression on the outside of the hindgut curve can be properly sub-apically localised by Vari. On the inside of the hindgut curve, high levels of JAK/STAT signalling result in high FasIII protein production which cannot be correctly localised to the sub-apical domain so extends throughout the lateral membrane.

Data presented in this chapter show that lateralised FasIII functions downstream of the JAK/STAT pathway in the maintenance of hindgut curvature, however the mechanism by which it operates is yet to be elucidated. *In vitro* data show that FasIII functions as a mediator of cell adhesion. Lateralisation of FasIII could therefore increase the surface area over which these interactions occur. It is proposed that increased adhesion may stabilise interactions between neighbouring cells leading to an increase in local tissue stability. Therefore, loss of or ectopic FasIII, either in a JAK/STAT dependent manner or through loss of *vari*, will affect the manner in which this stabilisation effect is distributed. As discussed in Chapter 3, loss of JAK/STAT signalling causes a loss of hindgut curvature at stage 13. It is assumed that this is due to the absence of a structural factor in the hindgut curve making it susceptible to the inherent stress of hindgut morphogenesis caused by cell rearrangement (Hartenstein, 1993,Campos-Ortega and Hartenstein, 1997) and changes in cell shape (Taniguchi et al., 2011). Indeed local tissue stability, mediated by lateral FasIII, may be integral to the maintenance of curvature during this period (Fig4.24a).

The tight asymmetrical regulation of FasIII is intriguing. Loss of FasIII or the loss of asymmetric FasIII, through the loss of JAK/STAT signalling, appears sufficient to cause a reduction in curvature (Fig4.24b). Furthermore, curvature defects in *vari* and *byn>hop*^{Tuml} mutant backgrounds, in which FasIII lateralisation appears bilateral, shows that if this stability is extended to the other side of the lumen, curvature is again disrupted (Fig4.24c). The juxtaposition between high and low tissue stability either side of the hindgut therefore appears critical for the maintenance of structural integrity in the hindgut curve. This rationale, however, does not explain the curvature defects in the *byn>upd* background where FasIII is ectopically lateralised towards the posterior of the gut but remains largely on the inside of the hindgut. This result indicates that excess lateral FasIII elsewhere, not only symmetrically, also affects the manner in which the hindgut curve is maintained. However, as the curvature defect with *byn>upd* is less severe than in the other JAK/STAT genotypes as it does not cause such a loss of curvature.

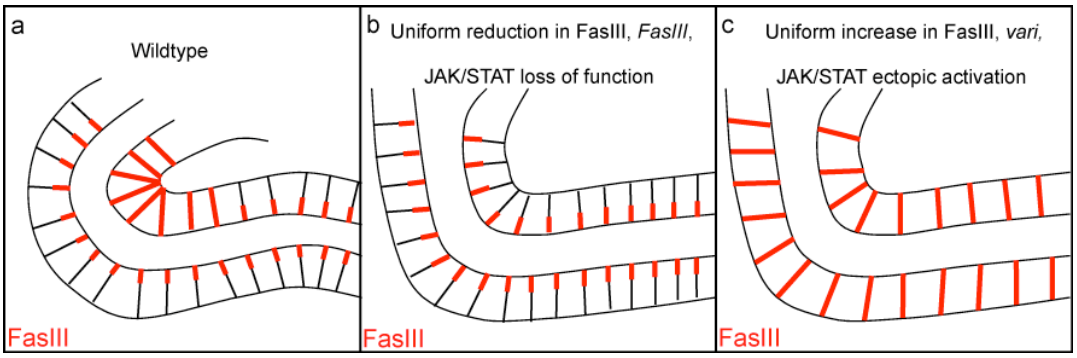

Figure 4.24: The role of FasIII spatial regulation in curvature. Schematic of a stage 14 hindgut curve.

(a) In the wildtype FasIII is lateralised on the inside of the hindgut curve. (b) With loss of JAK/STAT signalling FasIII is no longer asymmetric and results in a reduction in curvature. (c) Loss of *vari* or ectopic JAK/STAT activation, via *byn>hop*^{Tuml}, causes bilateral FasIII lateralisation also resulting in the reduction of curvature.

While these experiments provide an insight into the mechanisms downstream of the JAK/STAT pathway in hindgut curvature, additional work will be required to consolidate these findings. Indeed use of *vari* mutants to examine the role of the spatial regulation of FasIII in a JAK/STAT-independent manner, while convenient,

is undoubtedly an oversimplification of the system. In addition, Vari is also required to correctly localise Cora, Nrx IV, Sinuous (Sinu) and Na^+/K^+ ATPase into the sub-apical domain of mature SJs (Wu et al., 2007, Bachmann et al., 2008). Furthermore, SJs are complex protein aggregations containing, and requiring, the correct function of numerous components (reviewed in, Banerjee et al., 2006). Further work could be undertaken to examine if the effects on hindgut curvature are unique to Vari and FasIII and are indeed purely dependent on FasIII localisation, rather than a general disruption of SJ formation. In addition to the alleles used in this work, other null and hypomorphic *Drosophila* stocks for both *FasIII* (Patel et al., 1987, Bellen et al., 2011) and *vari* (Beitel and Krasnow, 2000, Wu et al., 2007, Bachmann et al., 2008) are available and could be analysed.

In this chapter I have described FasIII as a novel downstream effector of JAK/STAT signalling with a role in maintaining the curvature of the hindgut. During the course of this work errors in the direction of hindgut rotation were also observed in JAK/STAT mutants. Investigation into this aspect of hindgut morphogenesis will be described in the next chapter.

5 The role of JAK/STAT signalling and FasIII in hindgut rotation

5.1 Introduction

Data presented in Chapters three and four described a novel role for JAK/STAT signalling and the prospective pathway target *FasIII* in hindgut curvature. During this work errors in hindgut handedness, the direction of rotation, were also observed in JAK/STAT mutant embryos. While a number of mutants have been described in which hindgut handedness is reversed little is known about how the rotation occurs (Speder et al., 2006, Hozumi et al., 2006, Maeda et al., 2007, Taniguchi et al., 2011). Given the anterior localisation of JAK/STAT signalling, in the hindgut, the pathway may provide spatial regulation of rotation. This hypothesis will be examined in this chapter.

5.2 Results

5.2.1 JAK/STAT signalling is required for correct hindgut rotation

Hindgut rotation occurs during stage 13. The anterior curve is initially medially positioned, bending into the embryo (Fig5.1ai-aii), after which it undergoes a rotation to the right (dextral). As a result of this event the curve breaks the symmetry of the embryo, bending from left to right, when viewed dorsally (Fig5.1bi-bii).

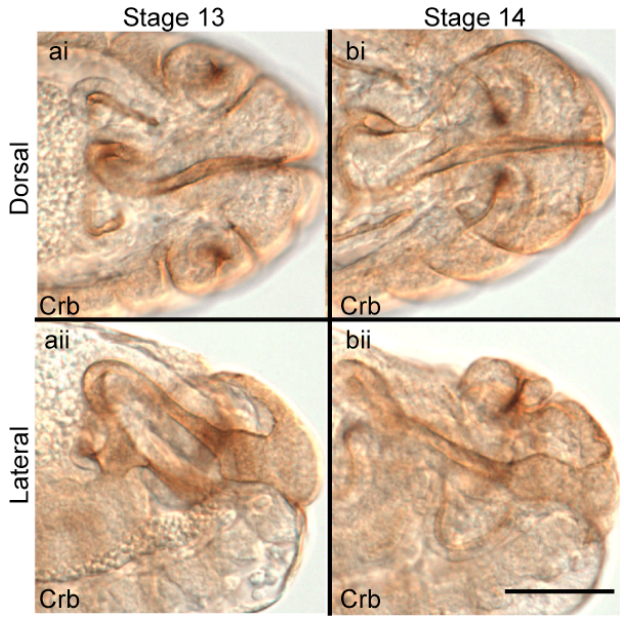

Figure 5.1: Hindgut rotation.

(ai) At stage 13 when viewed from dorsal the hindgut is symmetric. (aii) At stage 13 when viewed from lateral it can be seen to be curving into the embryo. (bi) At stage 14 when viewed from dorsal the hindgut is seen breaking with the symmetry of the embryo. (bii) At stage 14 when viewed from lateral the curve topography is no longer visible. Scale bar 50µm.

In the wildtype, the hindgut undergoes a dextral rotation with complete fidelity (Fig5.2a) (Hayashi and Murakami, 2001). The direction of rotation is largely reversed with frequent left (sinistral) rotations in the *Myo31DF* mutant (Fig5.2b) (Hozumi et al., 2006). Hindguts lacking JAK/STAT signalling, via either $Df(1)os^{1A}$ (Fig5.2c-d) or $byn>dome^{\Delta cyt}$ (Fig5.2e-f), display both dextral and sinistral hindgut rotation. In addition, ectopic pathway activation, via either *byn>upd* (Fig5.2g-h) or $byn>hop^{Tuml}$ (Fig5.2i-j), also resulted in both dextral and sinistral rotation.

Both loss of and ectopic JAK/STAT signalling results in a similar rotation phenotype. This suggests that spatial control of JAK/STAT signalling is required for correct rotation, an observation analogous to the role of JAK/STAT signalling in hindgut curvature (Chapter three) and elongation (Johansen et al., 2003). Furthermore, the phenotypes are observed when genetic manipulation is restricted to the hindgut in a cell-autonomous manner, i.e. $byn>dome^{\Delta cyt}$ and $byn>hop^{Tuml}$.

Therefore, the requirement for JAK/STAT signalling in rotation appears to be intrinsic to the hindgut epithelium. Again, this is consistent with JAK/STAT signalling in curvature (Chapter three) and elongation (Johansen et al., 2003) as well as studies into mediators of rotation (Hozumi et al., 2006, Hozumi et al., 2008, Maeda et al., 2007, Taniguchi et al., 2011).

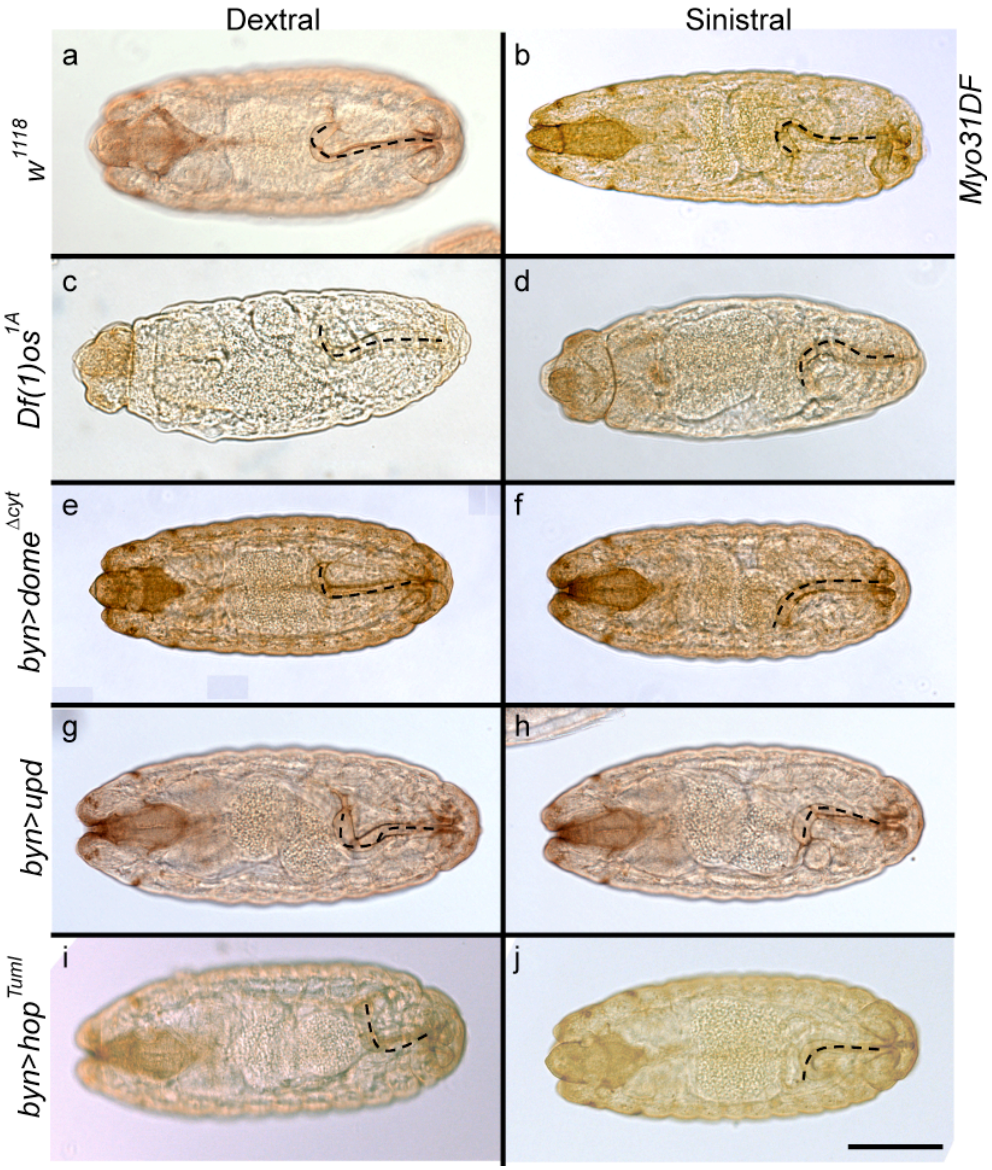

Figure 5.2: Loss of and ectopic JAK/STAT signalling cause defects in hindgut rotation. Stage 15 embryos orientated dorsally.

(a) In the wildtype embryo the hindgut undergoes a dextral rotation. (b) In the *Myo31DF* mutant it largely undergoes a sinistral rotation. (c-d) Loss of JAK/STAT signalling, using either *Df(1)os^{1A}* or (e-f) *byn>dome$^{\Delta cyt}$*, causes the hindgut to rotate in either a dextral or sinistral direction. (g-h) Ectopic JAK/STAT activation through either *byn>upd*, or (i-j) *byn>hop^{Tuml}* also causes the hindgut to rotate in either a dextral or sinistral direction. Scale bar 100µm.

The frequency of hindgut inversions shows that both loss of and ectopic JAK/STAT signalling is not as pentrant as loss of *Myo31DF* (Fig5.3). The strongest JAK/STAT

allele, *Df(1)os*^{1A}, shows the highest penetrance. Hindgut rotation in this allele with a half dosage of *Myo31DF* (*Df(1)os*^{1A}; *Myo31DF/+*) does not worsen the JAK/STAT phenotype. This indicates that JAK/STAT signalling may either be independent, or downstream, of *Myo31DF*.

A further observation is that loss of and ectopic JAK/STAT signalling results in a small proportion of hindguts that failed to rotate (Fig5.3). Failure of rotation was not observed in either the wildtype embryo or *Myo31DF* mutant, indicating that JAK/STAT signalling may affect rotation in a different manner to *Myo31DF*.

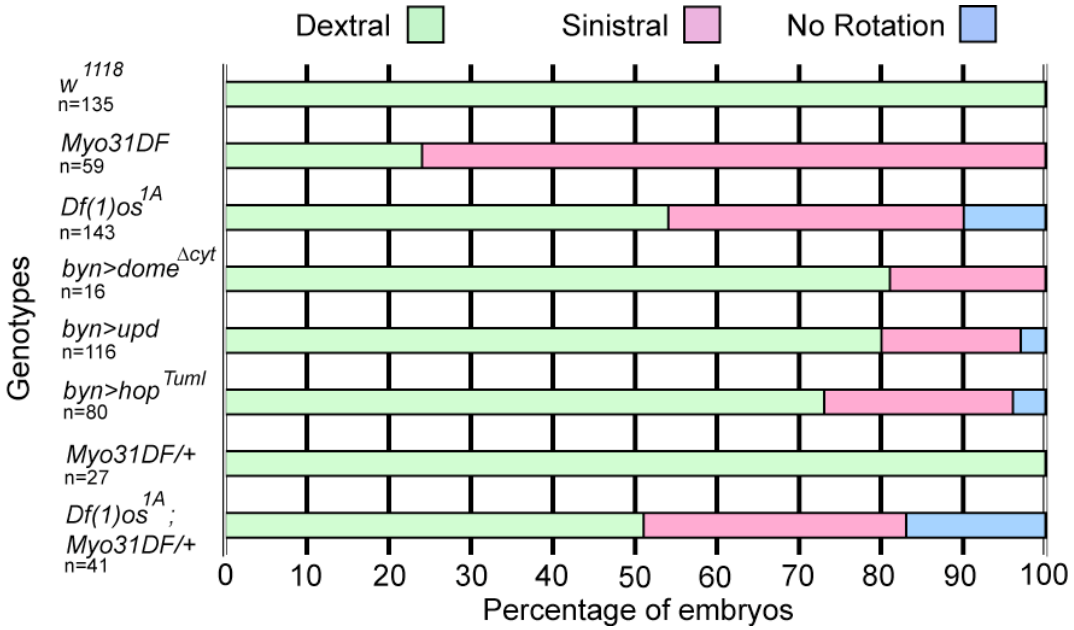

Figure 5.3: Quantification of JAK/STAT mutant hindgut rotation defects.
In the wildtype, *w*^{1118}, the hindgut undergoes dextral rotation with complete fidelity. Loss of *Myo31DF* causes the hindgut to largely undergo sinistral rotation. Loss of JAK/STAT signalling using either *Df(1)os*^{1a} or *byn>dome*$^{\Delta cyt}$ throughout the hindgut causes dextral and sinistral hindgut rotations. Ectopic pathway activation using either *byn>upd* or *byn>hop*^{Tuml} also causes dextral and sinistral hindgut rotations. The direction of rotation of heterozygous *Myo31DF*, *Myo31DF/+* and heterozygous *Myo31DF,* in a JAK/STAT loss-of-function background, *Df(1)os*^{1a};*Myo31DF/+*, appears similar to *w*^{1118} and *Df(1)os*^{1a} respectively.

Data presented in Chapter three show that JAK/STAT mutant hindguts display a reduction in curvature. To see if errors in hindgut handedness are associated with errors in curvature this phenotype was examined in the *Myo31DF* mutant. Loss of *Myo31DF* caused no significant reduction in the magnitude of the hindgut anterior curve when compared to the wildtype (Fig5.4). This indicates that, in some cases, these phenotypes are independent.

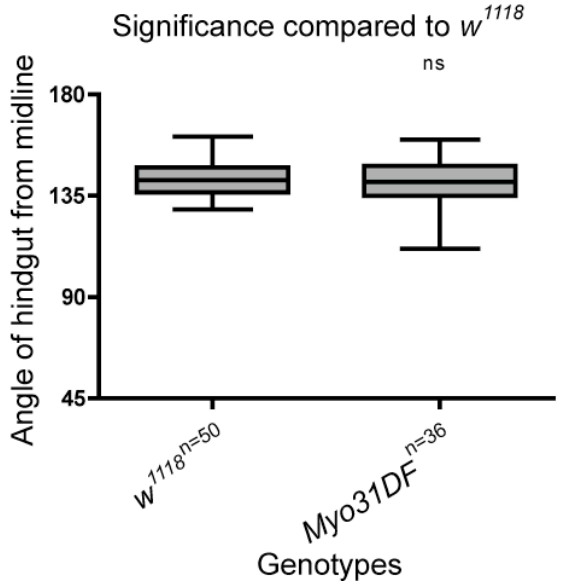

Figure 5.4: Loss of *Myo31DF* does not affect curvature.
The *Myo31DF* mutant does not display a significant reduction in hindgut curvature when compared to the wildtype. Statistical significance calculated using an unpaired t-test.

In the case of *Myo31DF* errors in rotation do not equate to errors in curvature (Fig5.4). It is, however, unclear if errors in rotation and curvature are linked in JAK/STAT mutants. By re-plotting the curvature measurements, in Figures 3.6 and 5.4, to show the direction of rotation it is possible to examine these phenotypes together (Fig5.5). Hindguts with a dextral rotation, in both loss of and ectopic JAK/STAT mutants, show a significant reduction in curvature when compared to wildtype. As wildtype and *Myo31DF* embryos have comparable curvature, *Myo31DF* was used as wildtype to statistically assess the curvature of JAK/STAT mutant hindguts with a sinistral rotation. Hindguts with a sinistral rotation, in both

loss of and ectopic JAK/STAT mutants, also display a significant reduction in curvature. This analysis shows that, in JAK/STAT mutants, errors in hindgut curvature are not dependent on the direction of rotation or vice versa (Fig5.5).

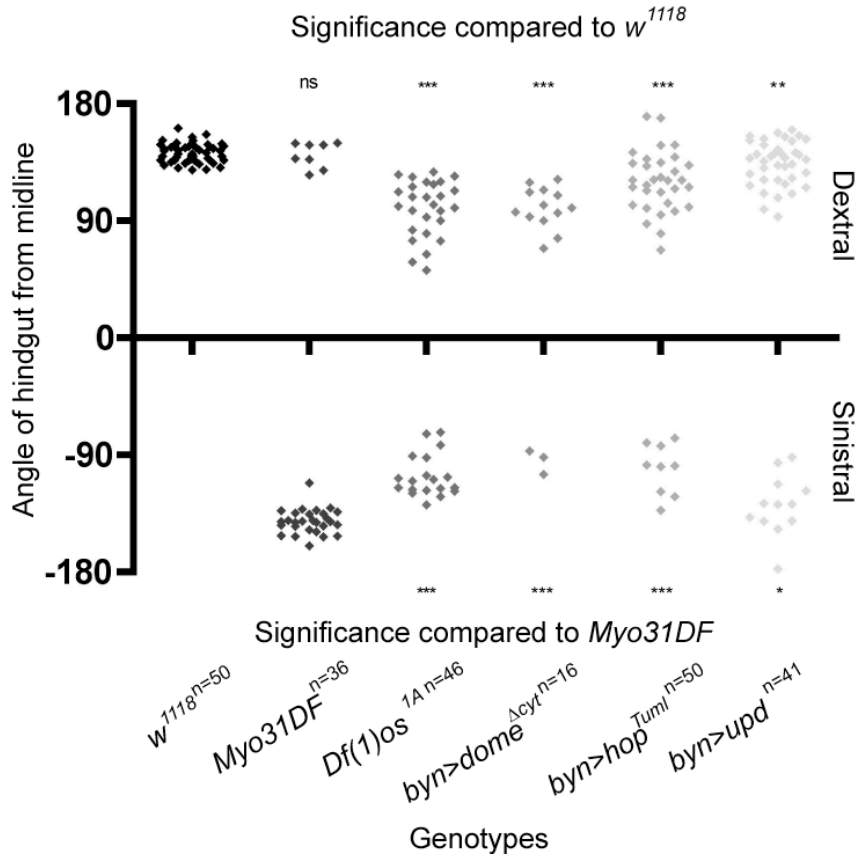

Figure 5.5: The effect of hindgut handedness on curvature in JAK/STAT mutants.

Angle measurements are those used in figures 3.6 and 5.4. Angle values are positive for hindguts with dextral rotation and negative for those with sinistral rotation. A statistical comparison of curvature in hindguts with dextral rotations has been made between mutants and wildtype. *Myo31DF* embryos with dextral rotation, show no significant (ns) reduction in curvature, while JAK/STAT loss-of-function do show a significant reduction (* p>0.0001) as do those with ectopic JAK/STAT activation *byn>hop^{Tuml}* (*** p>0.0001) and *byn>Upd* (** p>0.001). A statistical comparison of curvature in hindguts with sinistral rotation has been made between JAK/STAT mutants and *Myo31DF*. Again both loss of JAK/STAT function (*** p>0.0001) and JAK/STAT ectopic activation *byn>hop^{Tuml}* (*** p>0.0001) and *byn>upd* (* p>0.01) result in a significant reduction in the magnitude of hindgut curvature. Statistical significance calculated using an unpaired t-test.**

Loss of *Myo31DF* does not affect FasIII distribution indicating that it does not have a role in its localisation (Fig 5.6).

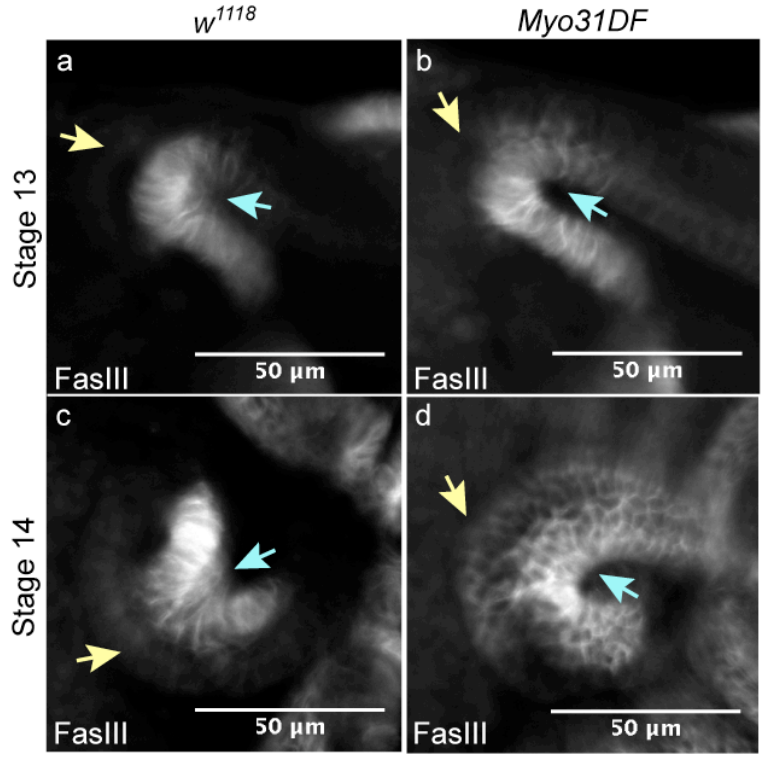

Figure 5.6: FasIII asymmetry is maintained in the *Myo31DF* mutant. Images represent a single confocal slice, the yellow arrow indicates outside of the curve and blue, the inside.
(a, c) At both stages 13 and 14 in the wildtype and (b, d) *Myo31DF* FasIII is present on the inside of the hindgut curve.

5.2.2 Spatial lateralisation of *FasIII* is required for correct hindgut handedness

Data presented in Chapter four described *FasIII* as a prospective JAK/STAT target required for correct hindgut curvature. Closer examination of *FasIII* loss-of-function embryos showed that these also had errors in hindgut handedness (Fig5.7c-d). Furthermore, errors in handedness were also observed in the *vari* loss-of-function embryos in which FasIII is ectopically lateralised, in a JAK/STAT-independent manner (Fig5.7e-f).

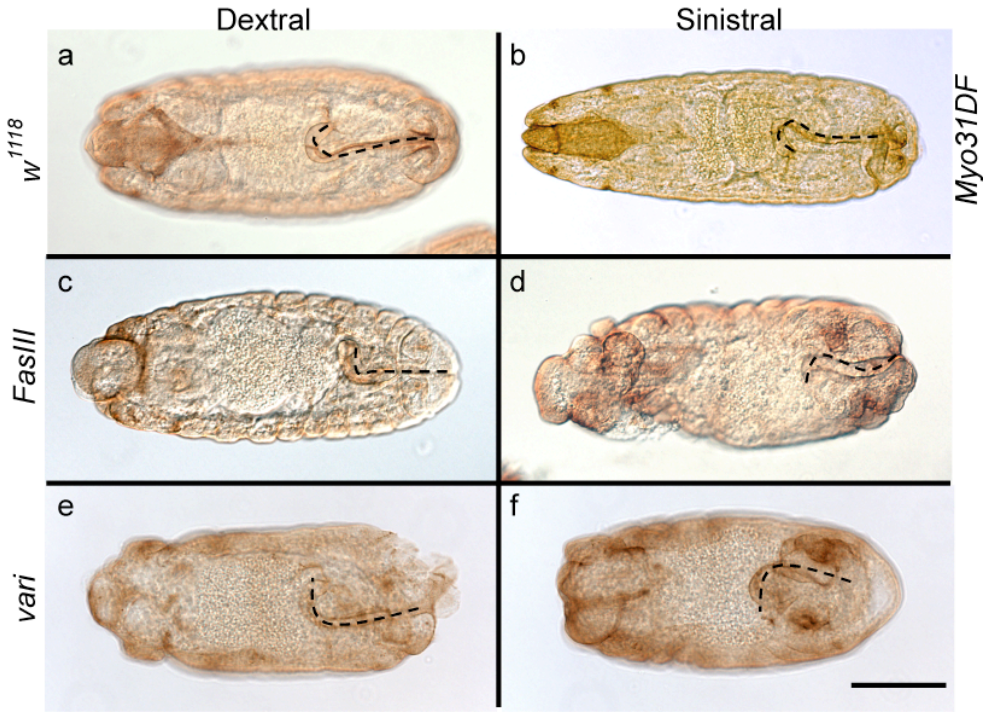

Figure 5.7: Loss of *FasIII* or *vari* causes defects in hindgut rotations.
(a) In the wildtype the hindgut undergoes a dextral rotation. (b) In *Myo31DF* it undergoes a sinistral rotation in the majority of cases. (c-d) Loss of *FasIII* causes the hindgut to undergo either dextral and sinistral rotations. (e-f) Loss of *vari* also causes the hindgut to undergo either dextral and sinistral rotations. Scale bar represents 100µm.

The proportion of rotation errors in the *vari* and *FasIII* mutant embryos are not as high as observed in the *Myo31DF* mutant (Fig5.8) nor the strongest JAK/STAT loss-of-function allele, $Df(1)os^{1A}$ (Fig5.3).

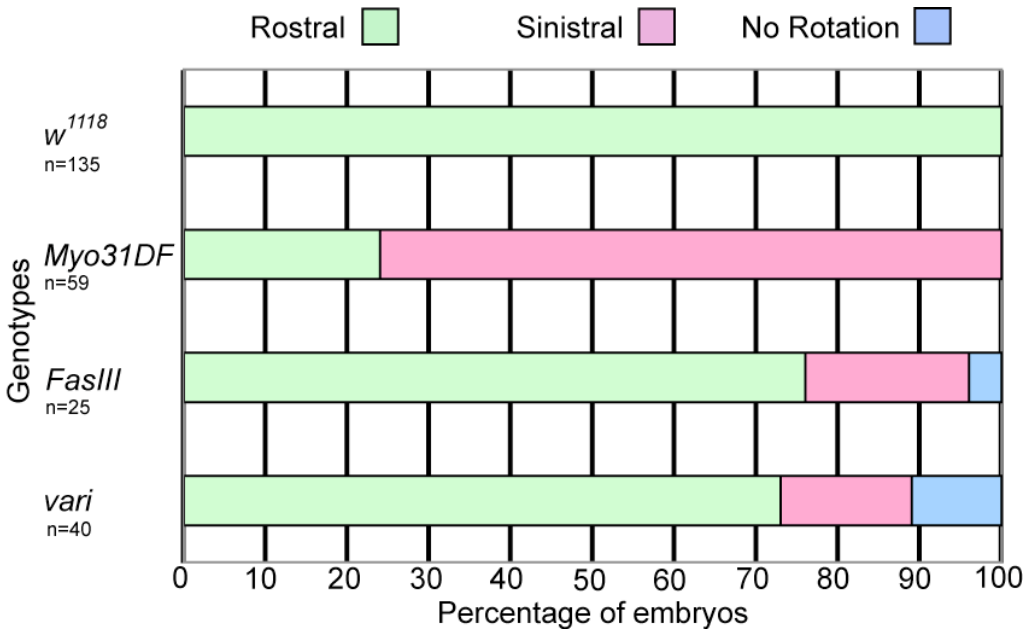

Figure 5.8: Quantification of hindgut rotation defects in *FasIII* and *vari* mutant embryos. In the wildtype the hindgut undergoes a dextral rotation with complete fidelity, this is lost in the *Myo31DF* mutant. Loss of *FasIII* and *vari* also causes sinistral hindgut rotations.

Work in Chapter four has shown that FasIII is capable of mediating cell adhesion. The cell adhesion molecule, DE-cad, has recently been suggested to have an important role in hindgut rotation (Taniguchi et al., 2011), described in 1.4.4. Examination of DE-cad protein distribution in the hindgut shows a novel asymmetry. Higher levels of DE-cad are detected along the outside length of the hindgut when compared to the inside. This is present before and after rotation and is opposed to lateralised FasIII (Fig5.9).

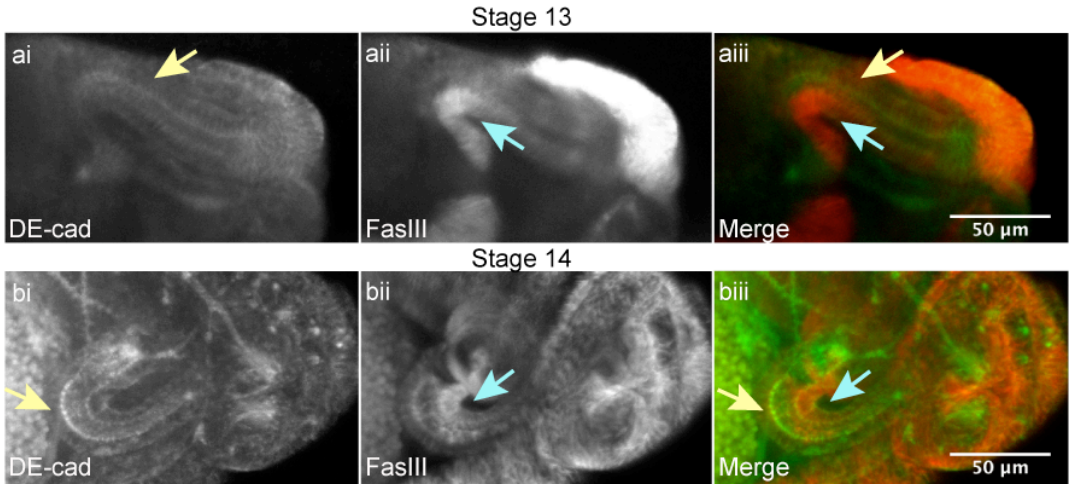

Figure 5.9: Asymmetry in FasIII and DE-cad during rotation. Images represent maximum intensity projections of multiple stacks, the yellow arrow indicates the outside of the curve and blue, the inside.
(ai, aiii) At stage 13 DE-cad appears enriched on the outside of the hindgut curve (aii-aiii) opposing FasIII. (bi-biii) This is also the case at stage 14.

Confocal cross-sections of the stage 14 hindgut show that FasIII and DE-cad are present in opposing domains around the diameter of the lumen (Fig5.10).

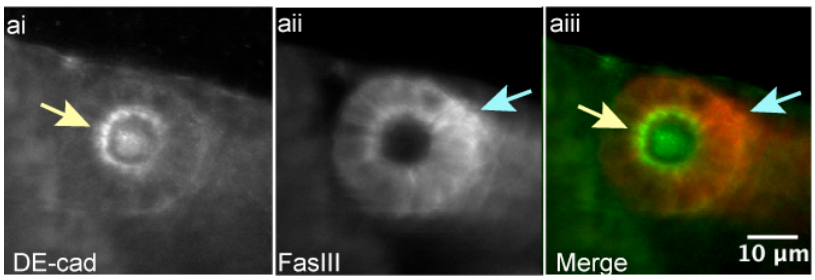

Figure 5.10: Asymmetry of FasIII and DE-cad in the lumen. Images represented are a single confocal slice of a stage 14 hindgut, the yellow arrow indicates the outside of the curve and blue, the inside.
(ai, aiii) DE-cad appears enriched on the outside curve of the hindgut in contrast to FasIII (aii-aiii).

The observed asymmetry of DE-cad is also apparent in *Df(1)os*^{1A} indicating that this distribution is independent of JAK/STAT signalling (Fig5.11). Given the role of DE-cad in the process of hindgut rotation (Taniguchi et al., 2011), its asymmetrical

enrichment, opposite lateral FasIII, may provide a further insight into the role of cell adhesion in rotation.

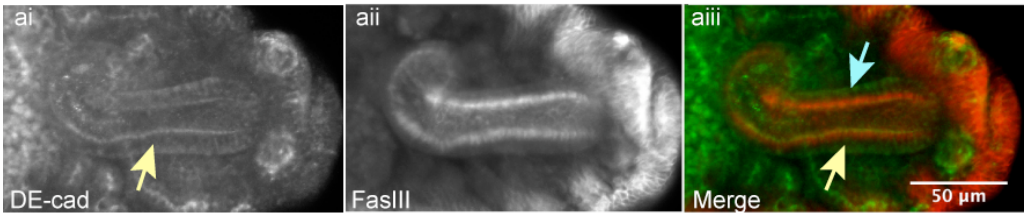

Figure 5.11: Asymmetry of FasIII and DE-cad in *Df(1)os^{1A}*. Images represents a maximum projection of multiple slices of a stage 14 embryo, the yellow arrow indicates the outside of the curve and blue, the inside.
(ai, aiii) In *Df(1)os^{1A}* DE-cad appears enriched on the outside of the hindgut curve. (ai-aii) As previously described, FasIII appears symmetric in *Df(1)os^{1A}*.

5.2.3 JAK/STAT signalling and FasIII affect hindgut rotation

To better understand the nature of JAK/STAT rotation defects, high resolution images of wildtype, *Df(1)os^{1A}* and *FasIII* loss-of-function mutant hindguts were examined. As discussed in 1.4.3, hindgut compartments are separated by morphologically-distinct sets of border cells, visualised by enriched Crb staining. The positioning of the lateral border cells can be used to visualise the rotation of the hindgut. In wildtype embryos, the lateral border cells undergo a twist in the LI (Fig5.12a). Strikingly, this twist is not apparent in *Df(1)os^{1A}* (Fig5.12b) or *FasIII* (Fig5.12c) mutants. While the significance of this observation is unclear, it links the observed rotation errors with a morphological defect in the hindgut.

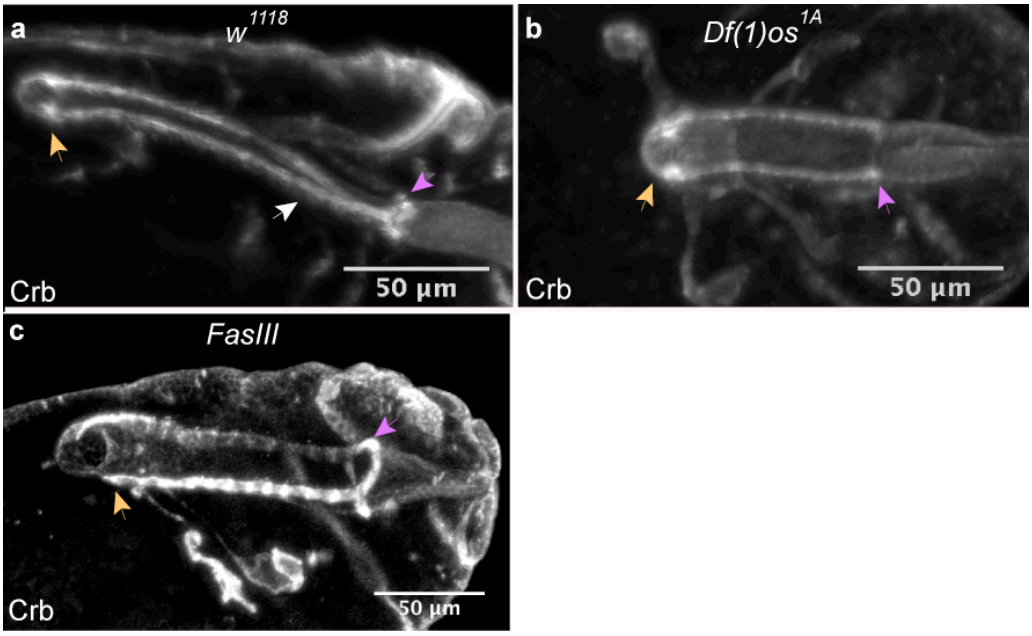

Figure 5.12: Errors in JAK/STAT and *FasIII* mutant hindgut twist. Maximum projections of multiple slices of stage 14 hindguts viewed laterally; orange arrow indicates the anterior border cell ring while the purple arrow indicates the posterior.
(a) In the wildtype the lateral border cells undergo a twist in the LI, white arrow. (b) In *Df(1)os*^{1A} and (c) the *FasIII* mutant, this does not occur.

The failure of lateral border cells to twist (Fig5.12) may be caused by an error in border cell positioning, discussed in 1.4.3. To investigate this, the localisation of En was examined. En is normally expressed by cells on the outside of the wildtype hindgut throughout development (Fig5.13).

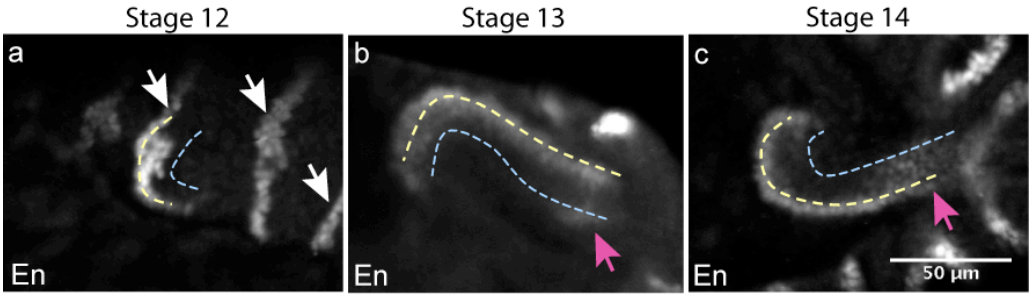

Figure 5.13: Asymmetry of En during hindgut development. Images displayed are a single confocal slice transecting the hindgut curve; the yellow line indicates the outside of the curve and blue line, the inside.

(a) At stage 12 En is found asymmetrically throughout the outside length of the hindgut, this should not be confused with En staining in ectodermal stripes, white arrows. (b) At stage 13 and (c) 14, En is also present on the outside length of the hindgut as well as in a symmetrically-positioned loop near the posterior, purple arrow.

In *Df(1)os*^{1A}, En is restricted to the outside of hindguts that have undergone both dextral (Fig5.14a) or sinistral rotation (Fig5.14b). This is consistent with previous reports that *en* expression is unaffected by the loss of JAK/STAT signalling (Johansen et al., 2003). En is integral in defining the LI-d and LI-v domains and lateral border cell positioning (Takashima and Murakami, 2001, Iwaki and Lengyel, 2002). As En is present, and expressed on the outside of the curve, in the JAK/STAT loss-of-function mutant it can be assumed that JAK/STAT signalling is not affecting the positioning of the lateral border cells. Therefore, JAK/STAT signalling is likely to be directly affecting hindgut rotation, presumably via FasIII.

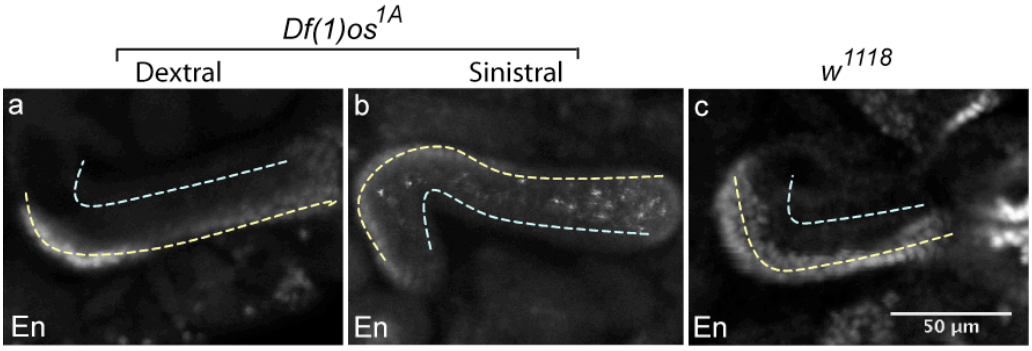

Figure 5.14: Asymmetry of En in *Df(1)os^{1A}* hindguts. Images represent a single confocal slice transecting the stage 14 hindgut curve; the yellow line indicates the outside of the curve and blue line, the inside.
(a) *Df(1)os^{1A}* hindguts with both dextral and (b) sinistral rotation show En staining on the outside of the hindgut. (c) This is also observed in the wildtype.

5.3 Discussion

Data presented in this chapter describe a novel role for the JAK/STAT pathway in mediating correct hindgut rotation through FasIII. Preliminary results indicate that both loss of or ectopic JAK/STAT signalling, and loss of *FasIII,* result in errors in the direction of rotation. This process appears to be downstream of the characterised regulator of hindgut handedness*, Myo31DF*. Furthermore, the novel enrichment of DE-cad, opposing lateralised FasIII, indicates that localised cell adhesion may be key for correct hindgut rotation.

No genetic interaction between *Myo31DF* and JAK/STAT signalling was observed and FasIII distribution is unaffected by loss of *Myo31DF*, indicating they operate idependently to mediate correct rotation, Interestingly, other known mediators of asymmetry may also provide clues to the unknown factor that contributes to the tight asymmetrical regulation of lateral FasIII, discussed in Chapter four. Sim is a transcription factor which, when lost, causes errors in the hindgut handedness. While not commented on by Maeda and colleagues, a *sim*/*LacZ* reporter appears to be expressed on the inside of the hindgut curve (Maeda et al., 2007). Unfortunately, using immunohistochemistry staining, Sim could not be observed in the hindgut (data not shown). In addition, while not investigated further, ubiquitous hindgut

Notch activation has been found to cause hindgut rotation defects (Iwaki and Lengyel, 2002). Notch activation is normally restricted to the LI-v, discussed in 1.4.3 (Takashima and Murakami, 2001, Iwaki and Lengyel, 2002). As postulated in Chapter 4, such an asymmetrically restricted factor could positively regulate FasIII expression. Due to their localisation, and mutant phenotypes, the investigation of Sim and Notch function in the context of JAK/STAT signalling and FasIII may lead to a further understanding of hindgut rotation and possibly generation of JAK/STAT and FasIII asymmetry.

In vertebrate models, symmetry is initially broken by asymmetrically-expressed factors which can be visualised prior to the establishment of physical markers of handedness (reviewed in Hamada et al., 2002, Tabin, 2006). This is in stark contrast to *Drosophila* where the most upstream mediator of hindgut handedness, so far described, *Myo31DF*, has been described as being uniformly expressed along both sides of the gut lumen (Hozumi et al., 2006). Excluding the unconfirmed asymmetry in Sim (Maeda et al., 2007), the distribution of FasIII is the first asymmetrically-distributed factor associated with establishing handedness in *Drosophila*. This may be important in understanding the differences and similarities in the mechanisms employed by vertebrate and invertebrate models in establishing asymmetry.

The observed errors in hindgut rotation, in both *FasIII* and *vari* mutants, indicate that the spatial regulation of FasIII lateralisation may be important in mediating rotation. However, the relevance of the role of Vari on FasIII localisation is not clear, based on a chronology of hindgut rotation. It is presumed that FasIII is only localised by Vari at the onset of SJ formation (Moyer and Jacobs, 2008) which occurs at stage 14 (Tepass and Hartenstein, 1994). This is after hindgut rotation. Indeed, an oversight of this work was not closely examining the timeline of FasIII lateralisation in the *vari* mutant. However, recent data show that SJs start forming as proteins begin to collect in stable complexes, at stage 13, prior to the presence of EM-visible structures (Oshima and Fehon, 2011). The effect of Vari on FasIII at stage 13 is not documented. However, the earlier onset of SJ formation, and

presumably the function of Vari on FasIII, may provide an explanation for the errors in the direction of hindgut rotation observed in the *vari* mutant.

I hypothesised earlier that hindgut rotation may require anterior/posterior patterning. Indeed, errors in the direction of hindgut rotation in JAK/STAT and *FasIII* mutants indicate that anterior localised factors are required for the fidelity of this process. A potential mechanism for FasIII in patterning rotation may be found in light of the recent model proposing a role for the cell adhesion molecule DE-cad in this process. Taniguchi and colleagues showed that the asymmetric subcellular localisation of DE-cad orchestrates a change in cell shape, the generation of PCC, sufficient to cause the physical rotation of the hindgut, discussed in 1.4.4 (Taniguchi et al., 2011). From the data presented in this thesis I hypothesise that the localised lateralisation of FasIII, and its previously proposed role in promoting tissue stability (Chapter four), may act to stabilise cell interactions, locally blocking the generation of PCC. This localised inhibition of PCC may be sufficient to determine the point at which the hindgut rotates (Fig5.15a). Either loss of lateral FasIII (Fig5.15b) or ectopic lateral FasIII (Fig5.15c) would change the manner in which PCC is spatially regulated. If this is the case, changing the spatial regulation of FasIII lateralisation may be sufficient to disrupt DE-cad function affecting the process, and perhaps the direction, of hindgut rotation. Considering this hypothesis, genotypes in which FasIII is ectopically lateralised would potentially cause a uniform block on PCC. Given the apparent requirement for PCC to generate rotation it is unclear how rotation would occur at all in these conditions. However, with the loss of DE-cad, PCC is also blocked yet rotation still occurs, in the majority of cases, albeit in a randomised manner (Taniguchi et al., 2011). This indicates that the generation of PCC is not an absolute requirement for rotation. Furthermore, both loss of DE-cad (Taniguchi et al., 2011) and changes in the spatial regulation of FasIII lateralisation, in either a JAK/STAT dependent or independent manner, are the only genotypes known to cause a failure of hindgut rotation in a small proportion of embryos. This similarity in phenotypes further indicates that DE-cad may be operating with JAK/STAT signalling and FasIII to mediate correct rotation. Lastly, the novel

observation of an asymmetry in DE-cad enrichment on the outside of the hindgut hints at a requirement for localised adhesion factors in the generation of PCC (Fig5.15d). The significance of this observation does, however, have to be further investigated.

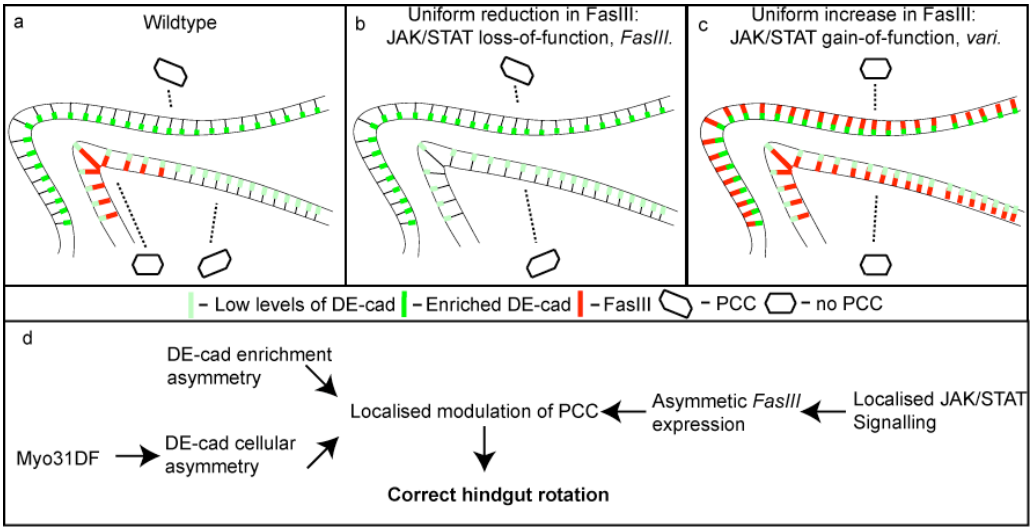

Figure 5.15: The effect of localised cell adhesion on hindgut rotation. Schematic of a stage 13 hindgut prior to rotation.

(a) In the wildtype, lateral FasIII on the inside of the hindgut blocks the generation of PCC. (b) Uniform lack of FasIII lateralisation, either through lack of *FasIII* or uniform sub-apical FasIII (not shown), results in an even distribution of PCC. (c) Uniform FasIII lateralisation, either through loss of *vari* or ectopic JAK/STAT signalling, results in an absence of any PCC. (d) The factors that may lead to localised patterning of PCC.

Data present in this thesis show a twist of the hindgut, visualised by the lateral border cells, in the LI, the region in which lateral FasIII is present. Furthermore, with the loss of FasIII or loss of lateralised FasIII, JAK/STAT loss-of-function, the twist is no longer apparent. This morphological defect is potentially consistent with a model in which JAK/STAT signalling and FasIII define the point of hindgut rotation, through regulating PCC (Fig5.15). However, it could be expected that the loss of a visible twist would result in a failure to rotate. In the genotypes examined, in the majority of cases, rotation does occur. The link between the two phenotypes, rotation and border cell twist, is therefore not clear. Further examination of the

presence, or position, of the lateral border cell twist in additional JAK/STAT and *vari* genotypes may help further understanding of these ideas.

To test the model proposed in figure 5.15, the effect of lateral FasIII on PCC, and cell shape, should be examined. Interestingly, discussions with members of the Matsuno lab, who undertook the DE-cad work, revealed that the observations of PCC were made on the dorsal, outside, of the hindgut prior to rotation (Ryo Hatori, Tokyo University of Science, personal communication). As these observations were made in a region opposing lateral FasIII, it is not known if PCC occurs on the inside of the hindgut. Examination of cell shape on the inside of the hindgut, and comparison to that on the outside, may indicate if lateralised FasIII has a role in blocking PCC. In addition, genetic interaction studies of *shg* (DE-cad), *FasIII* and JAK/STAT mutants should also be undertaken to elucidate if they operate via a shared mechanism.

The work presented so far shows that JAK/STAT signalling mediates local tissue stability, in the embryonic hindgut, through the lateralisation of the homophilic adhesion molecule FasIII. Experimental manipulation of localised lateral FasIII affects both hindgut rotation and curvature. The work in the next chapter examines the roles of JAK/STAT signalling, and lateralised FasIII, in additional *Drosophila* tissues.

6 The role of JAK/STAT signalling and FasIII elsewhere in *Drosophila* development

6.1 Introduction

The data presented in Chapters four and five describe FasIII as an effector of JAK/STAT signalling providing localised cell adhesion, which I hypothesise is important in rotation and the maintenance of curvature in the embryonic hindgut. To further investigate and consolidate these findings, JAK/STAT signalling and FasIII were examined in additional *Drosophila* tissues throughout development.

In the literature, there is an interesting correlation between JAK/STAT function and the distribution of FasIII. Two examples of this are in the testes and during oogenesis. In the testes the JAK/STAT pathway plays an important role in maintaining the stem cell niche (Kiger et al., 2001, Tulina and Matunis, 2001), the hub, a region where FasIII is highly expressed (Gonczy and DiNardo, 1996). During oogenesis, in the egg chamber, JAK/STAT signalling is required for BC migration and adhesion (Silver and Montell, 2001, Ghiglione et al., 2002, Beccari et al., 2002, Silver et al., 2005). described in 1.2.3, with FasIII being found exclusively between the PCs (Goode et al., 1996). While FasIII is regularly used to identify the hub and PCs, its function and relationship with JAK/STAT signalling in these locations is yet to be investigated. Of particular interest is the function of JAK/STAT signalling during BC migration. In this process, loss of JAK/STAT signalling reduces the number of BCs and JAK/STAT gain-of-function increases the number of BCs. This phenotype has widely been associated with changes in cell adhesion, largely thought to be mediated by DE-cad (Silver and Montell, 2001). Data was presented in Chapter four which characterised FasIII as a cell adhesion molecule, acting downstream of JAK/STAT signalling, and so its potential role in providing cohesion to the BC cluster was investigated.

In addition to the egg chamber, larval monolayer epithelial sheets, the imaginal discs, were also investigated. These are primordial tissues that form appendages in the adult and are readily dissected and imaged. The wing disc of 3rd instar larvae is a well-characterised model tissue with an extensively described fate map. It is used for the study of multiple processes, from the control of cell division (Justice et al., 1995, Johnston et al., 1999, Mukherjee et al., 2005) to the regulation of signal transduction (Baker, 1988, Doherty et al., 1996, Baonza et al., 2000). In the 3rd instar wing disc there are three distinct folds, two in the prospective hinge and one in the pouch. Interestingly the folds in the prospective hinge have been shown to express the JAK/STAT ligand *upd* (Mukherjee et al., 2005), resulting in the activation of the *10xSTATGFP* reporter throughout their length (Bach et al., 2007). Nothing is known about how these folds form or how their structure is maintained. Therefore, the wing disc hinge folds will provide a further epithelial model in which to examine the function of JAK/STAT signalling, and lateral FasIII, in maintaining tissue structure.

6.2 Results

6.2.1 FasIII is not downstream of the JAK/STAT pathway in the *Drosophila* egg chamber

The transcription factor *slbo* is expressed at low levels in the PCs and highly in the BCs at the posterior of the egg chamber prior to BC migration, stage 8 (Fig6.1ai-aii), and during BC migration, stage 9 (Fig6.1bi-bii), discussed in 1.2.4 (Rorth et al., 1998). Therefore the *slbo*-Gal4 driver provides a useful genetic tool for examining BC migration.

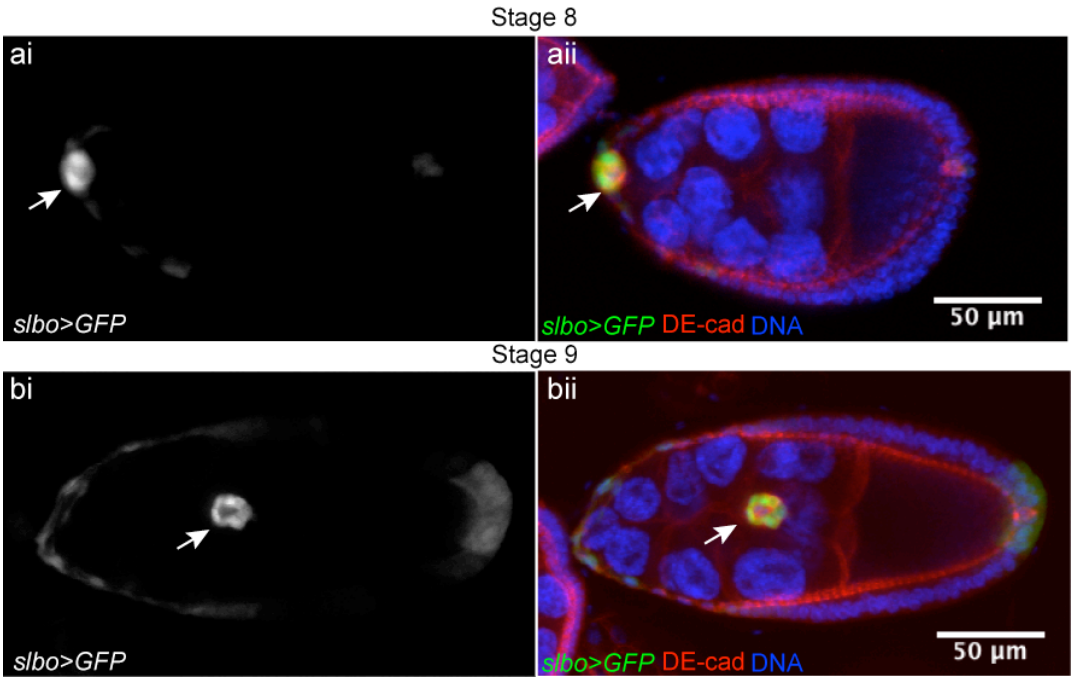

Figure 6.1: The expression pattern of *slbo* during BC migration. Images represent maximum projections of multiple confocal slices, white arrows mark border cells.
(ai-aii) At stage 8 border cells are found at the posterior of the egg chamber. (bi-bii) At stage 9 border cells are found migrating through the egg chamber nurse cells.

Examination of FasIII in the egg chamber, at both stage 8 (Fig6.2ai, aii) and stage 9 (Fig6.2ci-cii), confirms FasIII is present between the PCs where it spans the entire lateral membrane (Fig6.2bi-bii, di-dii). By comparison, Dlg is also present in PCs, however, its distribution is polarised (Fig6.2di-eii). Interestingly, this differing subcellular localisation of lateral FasIII and polarised Dlg, in the egg chamber, is reminiscent of the situation on the inside of the hindgut curve.

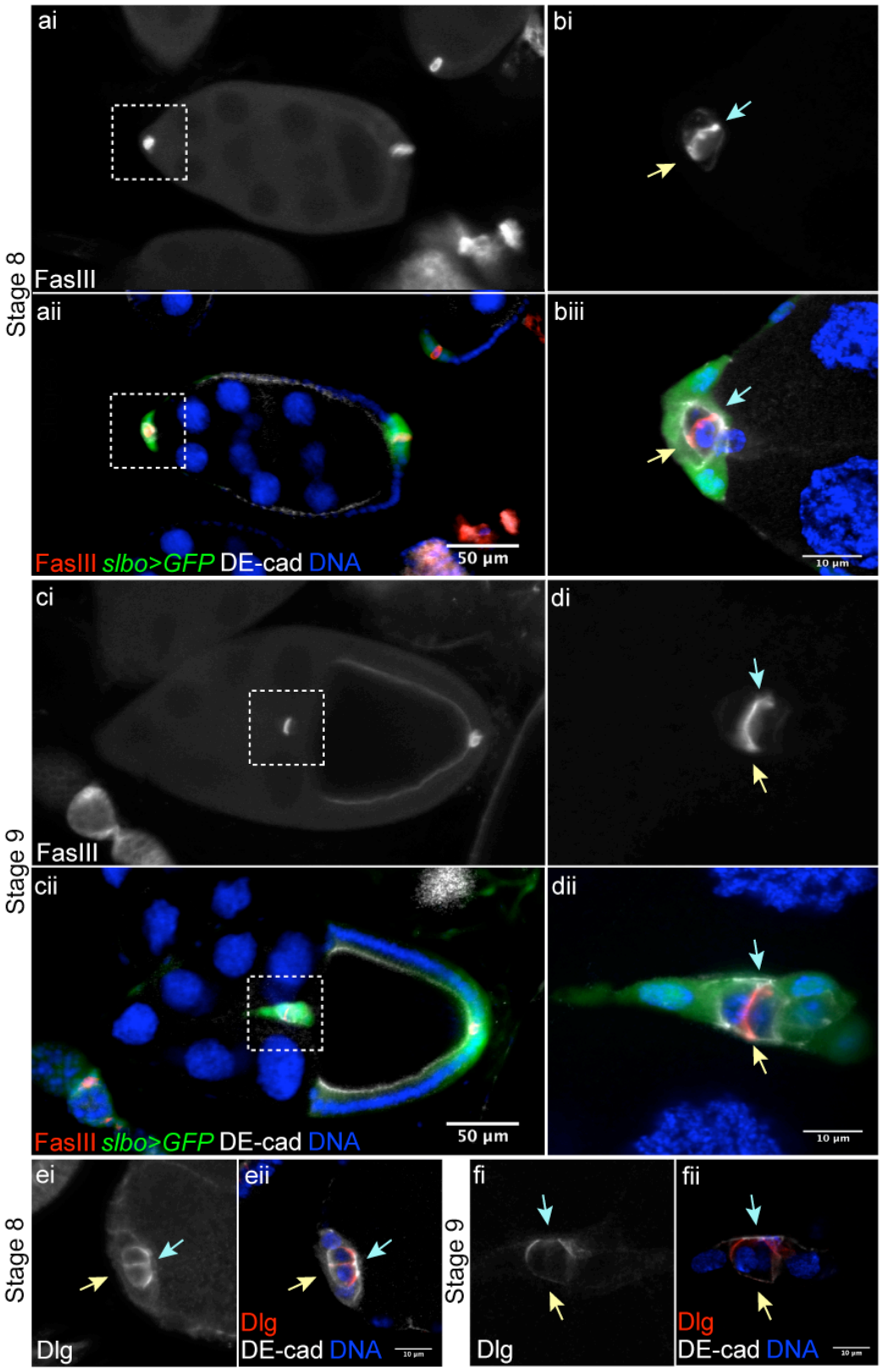
Stage 8
ai
FasIII
bi
aii
FasIII slbo>GFP DE-cad DNA
50 µm
biii
10 µm
Stage 9
ci
FasIII
di
cii
FasIII slbo>GFP DE-cad DNA
50 µm
dii
10 µm
Stage 8
ei
Dlg
eii
Dlg
DE-cad DNA
Stage 9
fi
Dlg
fii
Dlg
DE-cad DNA

Figure 6.2: FasIII is present laterally in the PCs. Images represent a single confocal slice, blue arrows mark the apical cell surface and yellow arrows mark the basal cell surface. Areas marked by a dashed box in ai-aii, ci-cii are enlarged in bi-bii, di-dii.
(ai-aii, bi-bii) FasIII is found lateralised between PCs at stage 8, (ci-cii, di-dii) and at stage 9. (ei-eii) Dlg is found in PCs localised to the apical surface at stage 8, (fi-fii) and stage 9.

In the embryonic hindgut, lateralised FasIII coincides with high levels of JAK/STAT signalling, however, this does not appear to be the case in the PCs. At both stage 8 (Fig6.3ai-biii) and stage 9 (Fig6.3ci-diii), the *10xSTATGFP* reporter is not highly expressed in the PCs, which contain lateral FasIII, but is stronger in the neighbouring BCs, which lack FasIII.

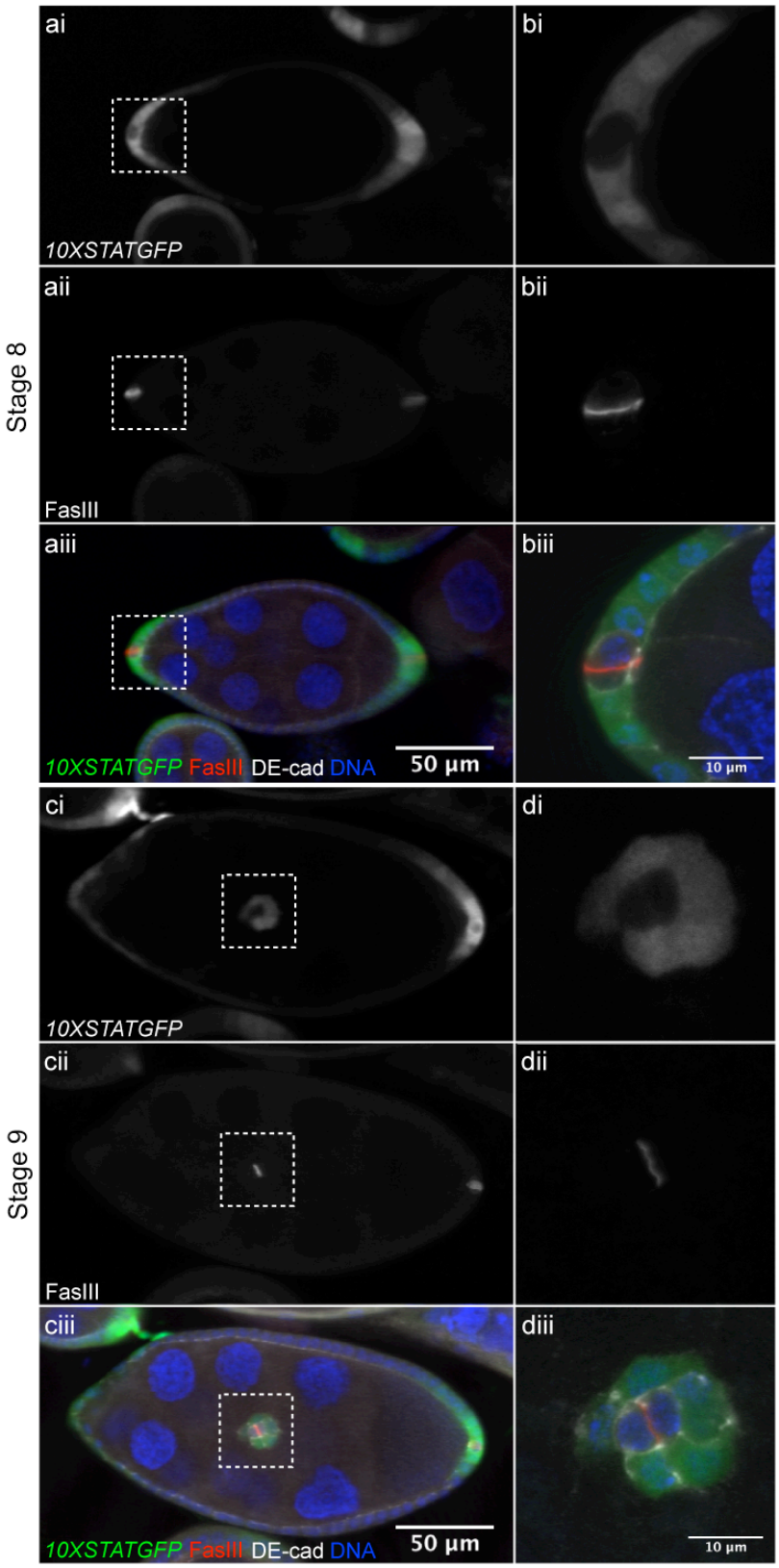
Stage 8
Stage 9
ai
bi
10XSTATGFP
aii
bii
FasIII
aiii
biii
10XSTATGFP FasIII DE-cad DNA
50 µm
10 µm
ci
di
10XSTATGFP
cii
dii
FasIII
ciii
diii
10XSTATGFP FasIII DE-cad DNA
50 µm
10 µm

Figure 6.3: Lack of coincidence of *10xSTATGFP* and FasIII during oogenesis. Images represent a single confocal slice. Areas marked by a dashed box in ai-aiii, ci-ciii are enlarged in bi-biii, di-diii.
(ai, aiii, bi, biii) At stage 8 *10xSTATGFP* is found in a gradient at the posterior and anterior of the egg chamber but appears absent from the PCs. (aii, aiii, bii, biii) FasIII appears to be localised between the PCs. (ci, ciii, di, diii) At stage 9 *10xSTATGFP* again appears in BCs but not PCs. (cii, ciii, dii, diii) FasIII again appears to be localised between the PCs.

Figure 6.3 indicates that FasIII may not be transcriptionally downstream of JAK/STAT signalling in the egg chamber. To confirm this, the abundance of FasIII protein was examined in different JAK/STAT backgrounds. Neither increased JAK/STAT signalling, *slbo>GFP, upd* (Fig6.4bi-bii), nor loss of JAK/STAT signalling, *slbo>GFP*, $dome^{\Delta cyt}$ (Fig6.4ci-cii) caused an appreciable change in the abundance or localisation of FasIII protein, when compared with the expression of a control UAS construct, *slbo>GFP*, *rhodopsin4*(*rh4*)-RNAi (Fig6.4ai-aii). Rh4 has no known interaction with the JAK/STAT pathway providing a good control to examine the non-specific effects of UAS expression. Taken together, these data indicate that FasIII is not a downstream effector of JAK/STAT signalling in the egg chamber and so this tissue was not examined further.

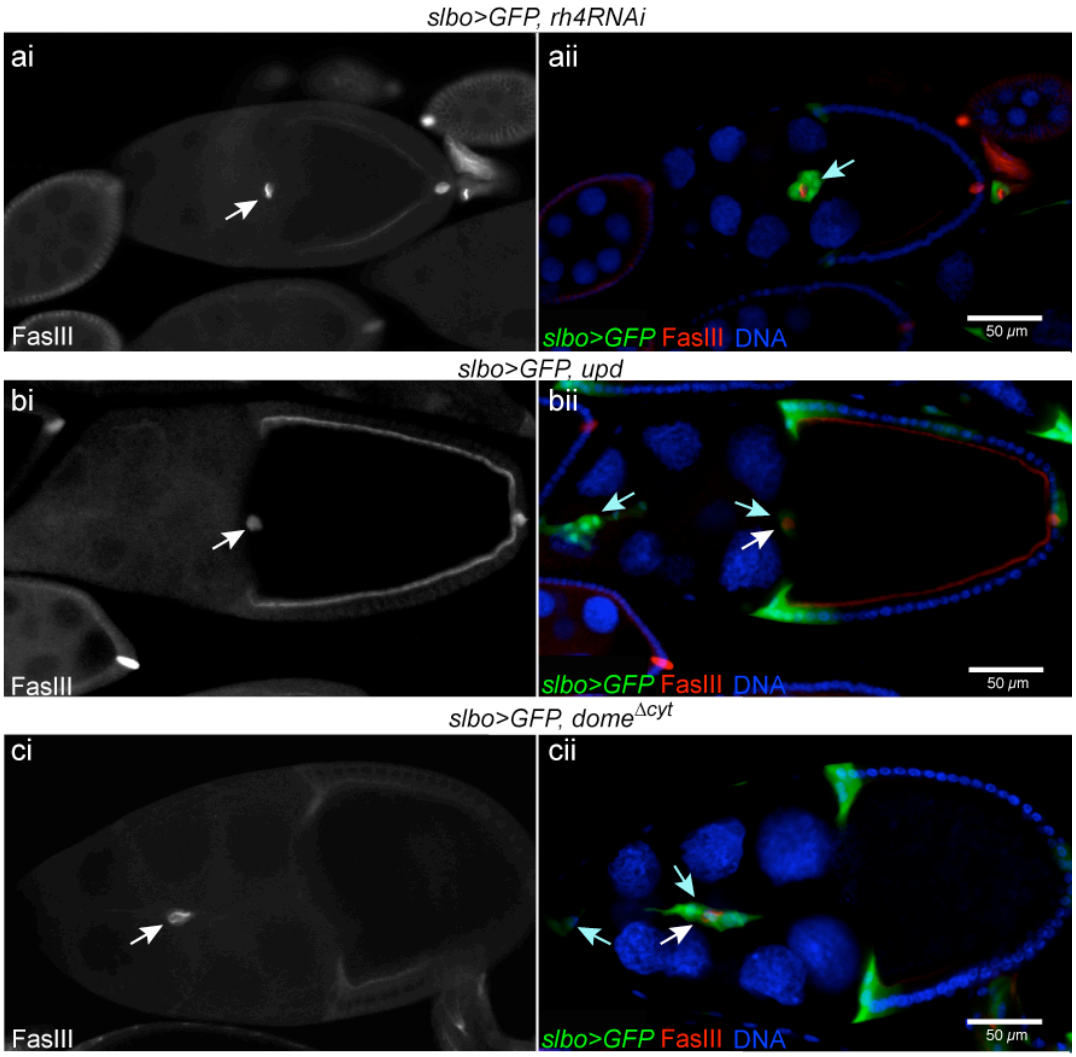

Figure 6.4: The effect of JAK/STAT signalling on FasIII abundance during oogenesis. Images represent a single confocal slice of a stage 9/early stage 10 egg chamber. White arrow indicates FasIII, blue arrow indicates migrating BCs.

(ai-aii) In the control, *slbo>GFP, rh4RNAi* FasIII is at the centre of the border cell cluster. (bi-bii) Increased JAK/STAT activation, *slbo>GFP, upd*, does not result in an increase of FasIII. (ci-cii) Loss of JAK/STAT signalling, *slbo>GFP, dome*$^{\Delta cyt}$, does not cause a reduction of FasIII.

6.2.2 A role for JAK/STAT and FasIII in wing disc fold structure

Given the proposed role of the JAK/STAT pathway, and lateral FasIII, in maintaining the integrity of embryonic hindgut curvature, it was hypothesised that a similar mechanism may have a role in maintaining other epithelial structures. One such epithelium, the 3rd instar larval wing disc, contains three distinct central folds;

two in the prospective hinge region, henceforth termed medial and proximal, and one in the pouch, termed distal (Fig6.5ai-aiv). Theoretically, the morphology of a curve and a fold require similar cell shape changes during formation and, presumably, similar mechanisms to maintain their structure (Fig6.7). Examination of JAK/STAT signalling in the wing disc confirms that the JAK/STAT reporter, *10xSTATGFP*, is expressed in the medial and proximal, but not the distal, folds (Fig6.7aii-aiv). Interestingly, FasIII protein is less restricted being detected throughout the wing disc (Fig6.5aiii-aiv).

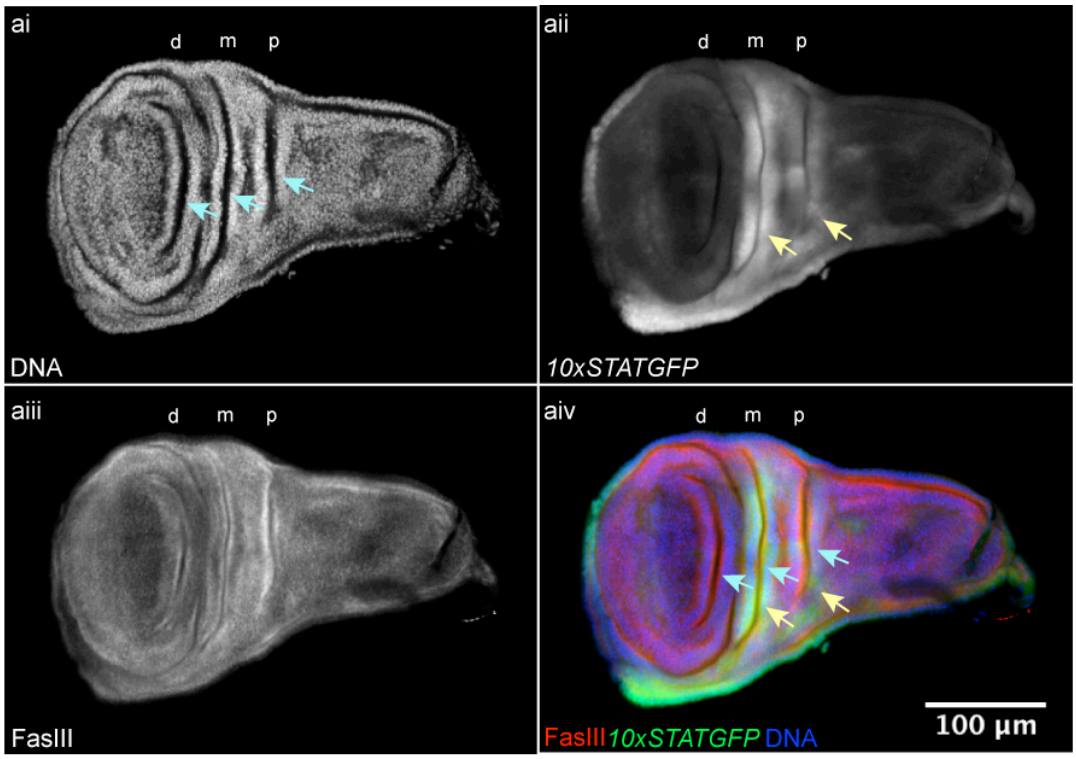

Figure 6.5: JAK/STAT signalling and FasIII in the wing disc. Images represent a single confocal slice of a laterally viewed wing disc.

(ai) The wing disc contains three folds, two in the prospective hinge, proximal (p) and medial (m) as well as one in the pouch, distal (d), blue arrows. (aii) The JAK/STAT reporter, *10xSTATGFP*, is expressed in m and p, yellow arrows. (aiii) FasIII is less restricted, being detected throughout the whole wing disc. (aiv) Merge of *10xSTATGFP*, FasIII and wing disc folds.

Figure 6.5 appears to show no close association between JAK/STAT signalling and FasIII in the wing disc. In the embryo, it is proposed that JAK/STAT signalling causes FasIII lateralisation, through increased expression. As such, optical cross-sections of the wing disc folds were made to examine the subcellular localisation of FasIII. From this view, the *10xSTATGFP* reporter appears enriched in cells at the base of the fold (Fig6.6ai-aiii). Furthermore, a greater proportion of FasIII protein appears lateralised in regions of high JAK/STAT activity and more sub-apical in the distal fold which lacks JAK/STAT signalling (Fig6.6aii-aiii). This indicates that, while the association between JAK/STAT signalling and FasIII is less striking than that observed in the embryo (Fig4.3), FasIII does appear to be lateralised in the presence of JAK/STAT signalling in the wing disc hinge folds. Based on these data, I propose that, while lower levels of FasIII are more widespread, JAK/STAT increases FasIII in the base of the proximal and medial folds resulting in its lateralisation.

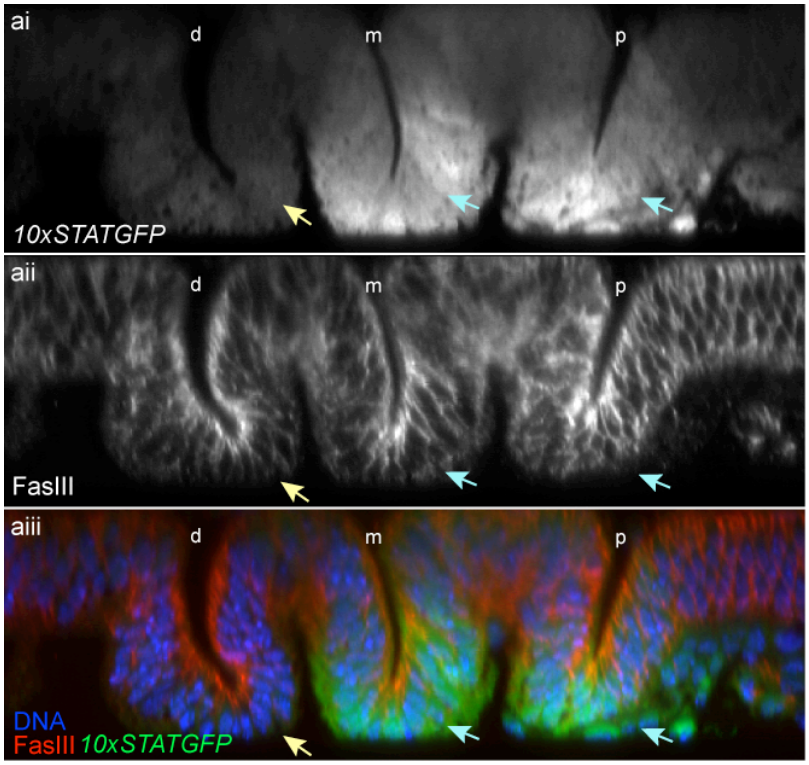

Figure 6.6: JAK/STAT signalling and FasIII in fold cross sections. Images represent an extended view of XZ confocal slices.
(ai) *10xSTATGFP* is localised in the base of folds m and p, compare blue and yellow arrows. (aii) FasIII appears to be more extensively lateralised in m and p when compared to fold d, compare blue and yellow arrows. (aiii) Merge showing overlay of *10xSTATGFP*, FasIII and wing disc folds.

The high levels of localised JAK/STAT signalling in the base of the wing disc folds is reminiscent of the localised signalling found on the inside of the hindgut curve. Indeed, the presence of lateralised FasIII in these regions provides circumstantial evidence that the pathway may have a similar role in both tissues (Fig6.7).

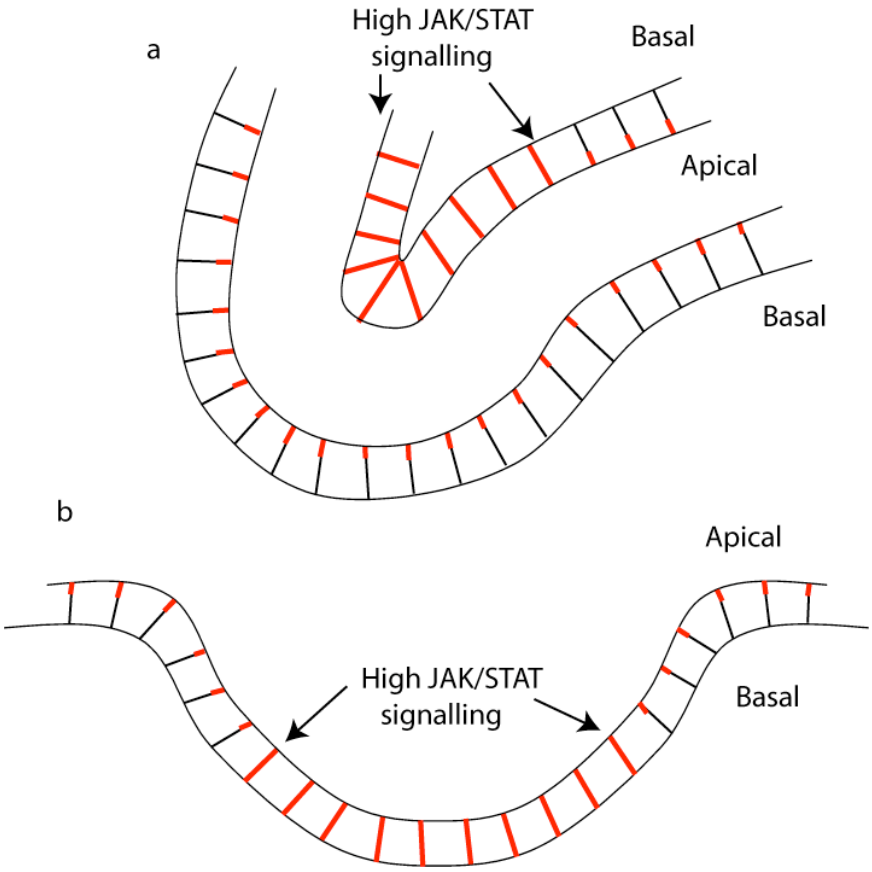

Figure 6.7: Schematic of the coincidence of JAK/STAT signalling and lateral FasIII in the hindgut and wing disc fold. Schematic not to scale.
(a) In the hindgut high levels of JAK/STAT signalling are found on the inside of the curve resulting in lateralised FasIII. (b) In the wing disc JAK/STAT signalling is found in the base of the hinge folds in the same region as lateralised FasIII.

To manipulate both JAK/STAT signalling and FasIII in the wing disc folds the *patched* (*ptc*)-Gal4 driver line was used. This enhancer trap is expressed along the centre of the entire wing disc, on the anterior side of the anterior/posterior compartment boundary (Chen and Struhl, 1996) (Fig6.8). The *ptc* domain, therefore, transects the wing disc hinge folds and the expression of the *10xSTATGFP* reporter (Fig6.8aii). This experimental setup is advantageous as it allows the genetic manipulation of a defined location, preserving the adjacent tissue as wildtype, hence, providing an internal experimental control.

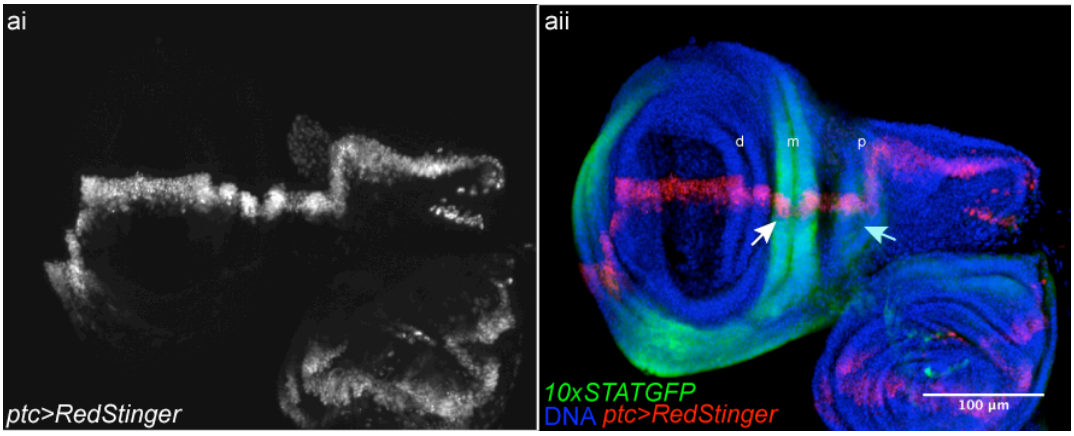

Figure 6.8: The *ptc*-Gal4 wing disc domain. Images represent a Z-projection of multiple slices. The *ptc* domain is visualised through the expression of *RedStinger*.
(ai) The *ptc* domain runs from the proximal to the distal extremes of the wing disc. (aii) The *ptc* domain transects the m and p folds.

Both JAK/STAT activity and *FasIII* expression can be effectively manipulated in the *ptc* domain. Knockdown of the JAK/STAT transcription factor, *stat92E*, *ptc>stat92E-RNAi*, results in a reduction of the expression of the *10xSTATGFP* reporter (Fig6.9b) while knockdown of *FasIII*, *ptc>FasIII-RNAi*, results in a reduction of FasIII protein staining (Fig6.9c), when compared to the wildtype (Fig6.9ai-aii). Conversely, ectopic pathway activation through expression of the wildtype JAK/STAT kinase, *hop*, *ptc>hop*, results in ectopic expression of the *10xSTATGFP* reporter (Fig6.9c) while ectopic *FasIII* expression, *ptc>FasIII*, causes an increase in FasIII protein (Fig6.9e), when compared to wildtype (Fig6.9ai-aii).

In a departure from hindgut and egg chamber experiments ectopic JAK/STAT pathway activation was mediated through the expression of wildtype *hop* rather than hop^{Tuml} or *upd*. Expression of these JAK/STAT components, in the *ptc* domain, resulted in lethality prior to the larval 3rd instar (data not shown, Victoria Wright, University of Sheffield, personal communication). Ptc is a receptor in the Hh pathway (Marigo et al., 1996) which has numerous, widespread roles during *Drosophila* development therefore has broad expression throughout development (reviewed in, Wicking et al., 1999). While overexpression of wildtype *hop* is

sufficient to activate the JAK/STAT pathway, in a ligand-independent manner (Fig6.9c), it has a weaker effect than overexpression of hop^{Tuml} or *upd* (Wojciech Stec, University of Sheffield, personal communication). This reduced activity appears to allow development to proceed until the 3rd instar.

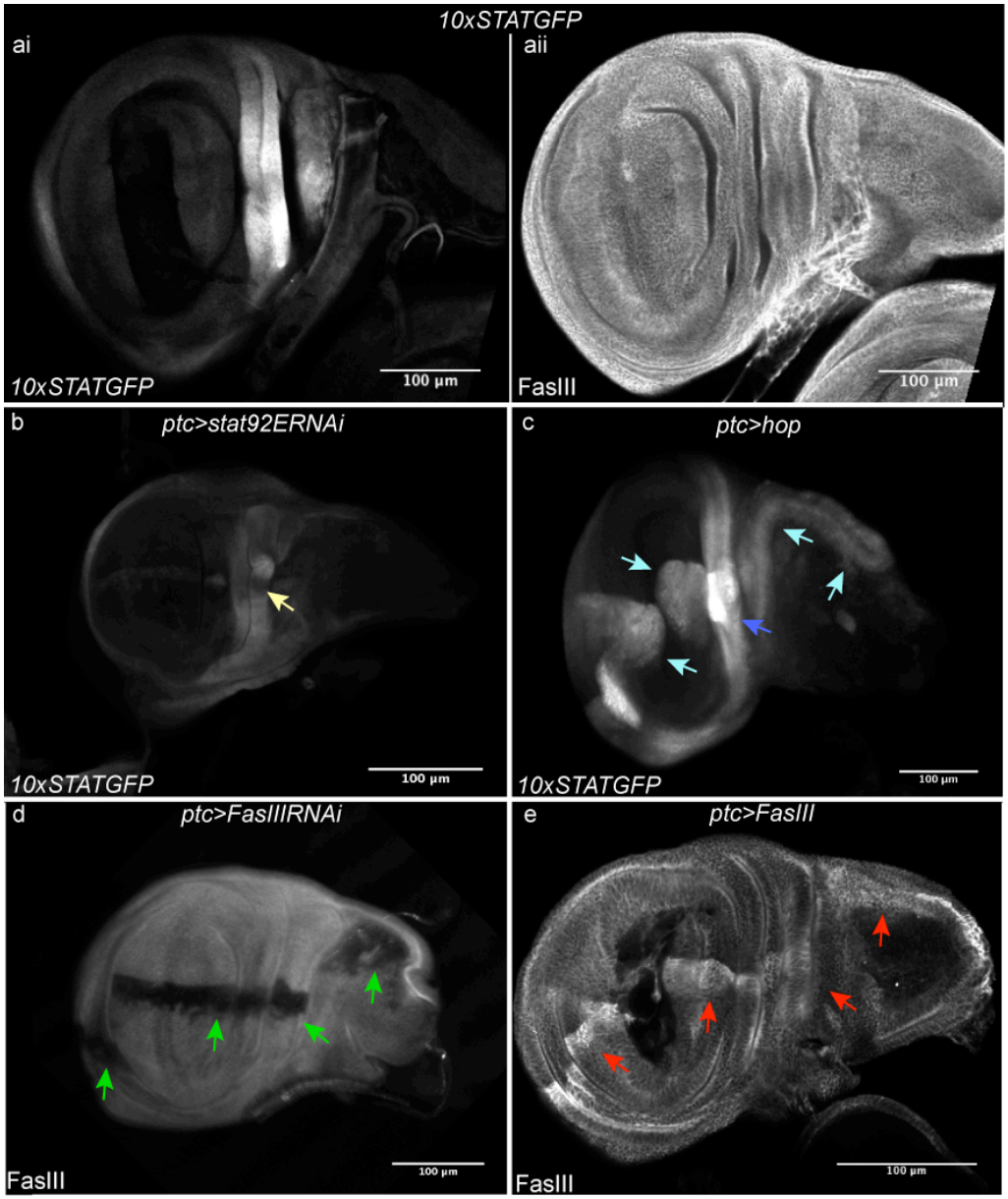
10xSTATGFP
ai
10xSTATGFP
100 µm
aii
FasIII
100 µm
b
ptc>stat92ERNAi
10xSTATGFP
100 µm
c
ptc>hop
10xSTATGFP
100 µm
d
ptc>FasIIIRNAi
FasIII
100 µm
e
ptc>FasIII
FasIII
100 µm

Figure 6.9: Modulation of JAK/STAT signalling and FasIII in the *ptc* domain. Images represent a single confocal slice.
(ai) In a wildtype background, *10xSTATGFP*, the *10xSTATGFP* reporter is uniform along the width of the hinge folds (aii) FasIII protein distribution expression is uniform across the wing disc. (b) Knockdown of the JAK/STAT pathway, *ptc>stat92E-RNAi*, causes loss of *10xSTATGFP* in the region intersecting the m and p folds, yellow arrow. (c) Ectopic pathway activation through the expression of wildtype *hop*, *ptc>hop*, causes ectopic *10xSTATGFP* expression along *ptc* domain, light blue arrows, and increased expression in the regions of endogenous JAK/STAT signalling, dark blue arrow. (d) Knockdown of *FasIII*, *ptc>FasIII-RNAi*, results in a loss of FasIII protein throughout the *ptc* domain. (e) Ectopic *FasIII* expression, *ptc>FasIII*, results in an increase in FasIII protein abundance in the *ptc* domain.

In the early embryo, FasIII expression is largely dependent on JAK/STAT signalling. Conversely, in the wing disc, the association between JAK/STAT signalling and FasIII is less striking (Fig6.5). However, subcellular FasIII does appear lateralised in regions of high JAK/STAT signalling (Fig6.6). To further investigate if FasIII levels are regulated by JAK/STAT signalling, FasIII protein abundance was examined upon the knockdown of the JAK/STAT pathway. Unexpectedly, this resulted in a reduction of FasIII staining along the length of the *ptc* domain (Fig6.10bi-bii), when compared to the wildtype (Fig6.10a). This suggests that loss of JAK/STAT signalling affects FasIII abundance in the wing disc. The extent of the reduction is, however, confusing as it is found beyond the regions of JAK/STAT signalling, as reported by *10xSTATGFP*. This indicates that stat92E may be operating in a ligand-independent manner away from the hinge region, an occurrence that has been previously described (Mukherjee et al., 2005). These workers also observed that loss of both *upd* and *hop* failed to block Stat92E function in the pouch (Mukherjee et al., 2005). Evidence from the mammalian field has shown that other signalling pathways, namely G-coupled protein receptors (GPCRs) (Pelletier et al., 2003), Wnt (Yamashita et al., 2002) and Notch (Kamakura et al., 2004), can activate STATs. Furthermore, in the early *Drosophila* embryo, gain-of-function Receptor Tyrosine Kinases (RTKs) can signal through Stat92E (Li and Li, 2003). While the relevance of the findings reported in these publications is unclear, in the context of FasIII in the wing disc, it shows precedents for JAK/STAT ligand-

independent signalling in this tissue. Further investigation should focus on upstream components of the JAK/STAT pathway to identify if the ligand-independent effect on *FasIII* expression requires the pathway kinase and receptor.

Although knockdown of *stat92E* causes a loss of *FasIII* in the wing disc, ectopic pathway activation does not result in a noticeable increase in FasIII abundance (Fig6.10ci-cii). This shows that increasing JAK/STAT signalling appears not to increase *FasIII* expression throughout the *ptc* domain. However, when viewed from this perspective, a role for JAK/STAT signalling in causing ectopic FasIII lateralisation cannot be discounted.

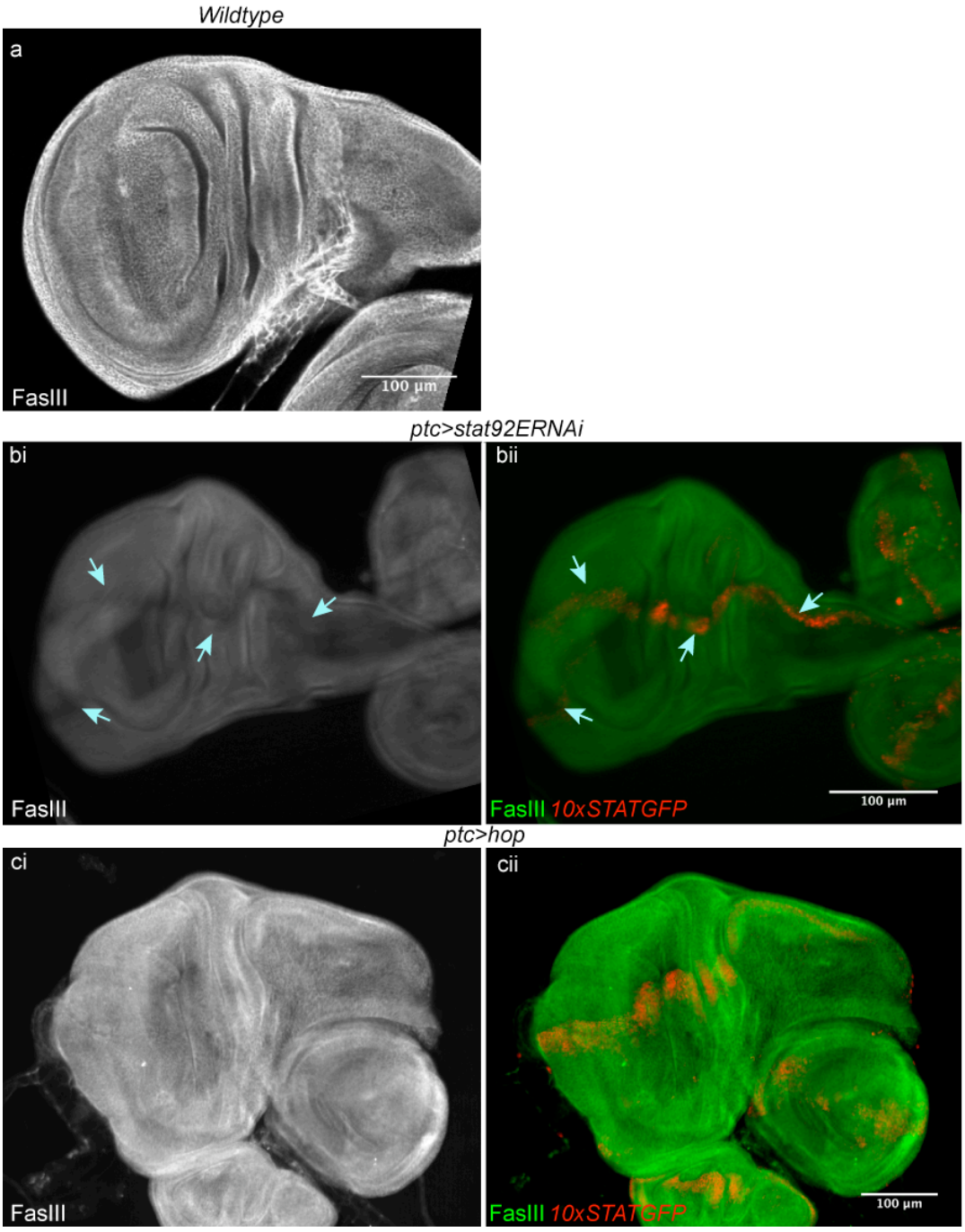

Figure 6.10: The effect of JAK/STAT signalling on FasIII in the wing disc. Images represent a single confocal slice.

(a) In the wildtype FasIII staining appears uniform throughout the wing disc (bi-bii) Knock down of JAK/STAT signalling, *ptc>stat92E-RNAi* causes a reduction in FasIII staining throughout the *ptc* domain. (ci-cii) Ectopic JAK/STAT signalling, *ptc>hop,* does not appear to affect FasIII staining.

Given the putative role of the JAK/STAT pathway and FasIII in maintaining the hindgut curve, it was hypothesised that they could also function in providing structure to the wing disc folds. To test this, the structure of the folds was examined upon the knockdown of *FasIII* and JAK/STAT. Nuclear staining was used to mark cells and so visualise the shape of the wing disc. Analysis of the observed phenotypes is based on the assumption that manipulating JAK/STAT signalling and FasIII is unlikely to affect the subcellular localisation of the nuclei. Knockdown of *FasIII* causes a disruption of the medial fold, *ptc>FasIII-RNAi* (Fig6.11b). Knockdown of JAK/STAT signalling causes a more drastic phenotype with the disruption of both medial and proximal folds, *ptc>stat92E-RNAi* (Fig6.11c), when compared to the control, *ptc>rh4-RNAi* (Fig6.11a). The observed JAK/STAT phenotype, in the medial and proximal folds, is consistent with the pathway being active in these locations (Fig6.5aii, Fig6.6ai). The disruption of the medial fold with the knockdown of *FasIII*, while more subtle than the JAK/STAT phenotype, is consistent with a role for FasIII operating downstream of the pathway in the wing disc. This less penetrant phenotype may be a result of experimental variation caused by different levels of knockdown.

Ectopic expression of *FasIII*, *ptc>FasIII,* (Fig6.11d) or activation of the JAK/STAT pathway, *ptc>hop,* (Fig6.11e) causes a widening of the distal fold, in the pouch, when compared to the control (Fig6.11a).

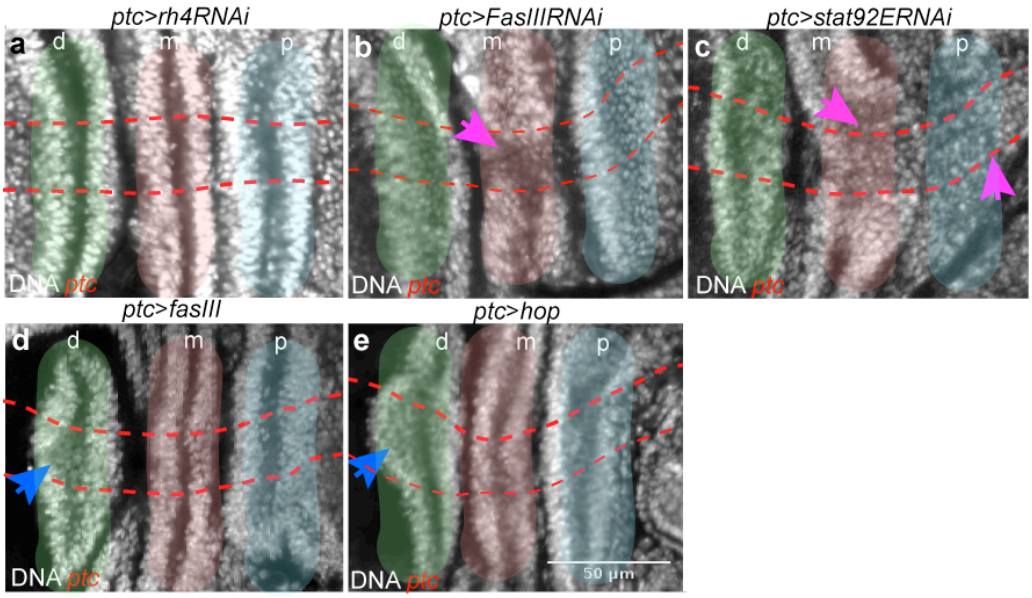

Figure 6.11. The effect of FasIII and JAK/STAT signalling on the morphology of wing disc folds. Images represent a single confocal slice, the *ptc* region marked with red lines. Distal (d) fold highlighted in green, medial (m) in red and proximal (p) in blue.

(a) In the control, *ptc>rh4-RNAi*, all folds exhibit the same morphology, (b) Knockdown of *FasIII*, *ptc>FasIII-RNAi,* causes a loss in the magnitude of the m fold, purple arrow. (c) Loss of JAK/STAT signalling, *ptc>stat92E-RNAi*, causes a loss in the magnitude of both m and p folds, purple arrows. (d) Ectopic FasIII expression, *ptc>FasIII*, causes an increase in the magnitude of the d fold, blue arrow. (e) Ectopic JAK/STAT signalling, *ptc>hop*, also causes an increase in the magnitude of the d fold, blue arrow.

To gain a better understanding of how the folds change with the knockdown of *Stat92E* and *FasIII* cross-sections of these regions were examined. Knockdown of *Stat92E* caused a noticeable reduction in the magnitude of the medial and proximal folds within the *ptc* domain (Fig6.12a, c) which appear shallower when compared to a region out of the *ptc* domain (Fig6.12a-b). Within the wing disc the *ptc* domain is present in a gradient, this presumably results in a reduction in the amount of *ptc* expression and, as such, a reduction of RNAi expression. Within this region *Stat92E* knockdown still effect fold morphology albeit less drastically with only the proximal fold appearing shallower (Fig6.12d). Cross sections of *FasIII* knockdown also confirms the earlier experiment with loss of the medial fold within the *ptc* domain

(Fig6.12e, gi and gii) when compared to a region outside the *ptc* domain (Fig6.12e-fii).

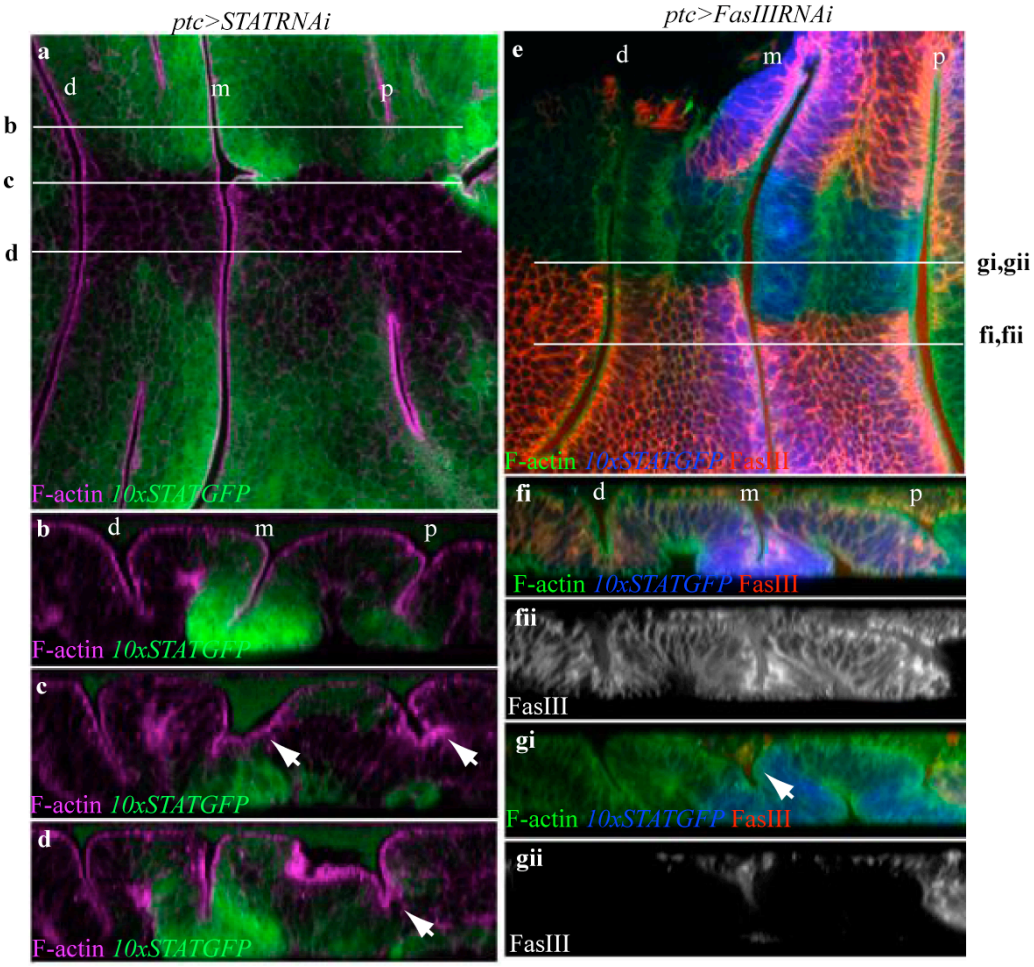

Figure 6.12: Cross section analysis of wing disc folds in *ptc* knockdown.

(a) Knockdown of *Stat92E* causes loss of the medial (m) and proximal fold in the *ptc* domain. This is marked through the loss of the *10xSTATGFP* reporter. (b) Cross sections out of the *ptc* domain show three folds of comparable magnitude. (c) In the *ptc* domain the m and p folds appear noticeably shallower, white arrows. (d) In the gradient of the *ptc* domain the d fold is noticeably shallower, white arrow. (e) Knockdown of *FasIII* causes a reduction in the magnitude of the medial fold in the *ptc* domain. This is marked through the loss of FasIII protein staining. (fi-fii) Cross sections out of the *ptc* domain show three folds of comparable magnitude. (gi-gii) In the *ptc* domain the medial fold appears shallower.

To confirm the observation that JAK/STAT signalling and FasIII affect the morphology of the wing disc hinge folds, both were knocked down in the broader *zfh2* domain which extends across the length of the medial fold (Whitworth and Russell, 2003) (Fig6.17). Due to the increased area of misexpression, it would be expected that this would have a greater effect than knockdown in the more restricted *ptc* domain. Indeed, both knockdown of *FasIII*, *zfh2>FasIII-RNAi* (Fig6.13b), and *stat92E*, *zfh2>stat92E-RNAi* (Fig6.13c), causes a drastic disruption of the medial fold, when compared to the control, *zfh2>rh4-RNAi* (Fig6.13a). This provides further evidence that FasIII operates in a similar manner to JAK/STAT signalling in the wing disc folds.

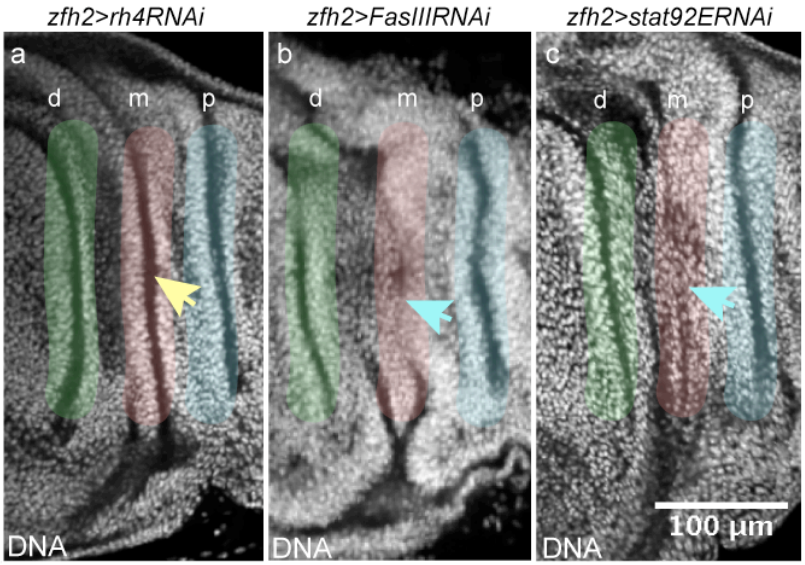

Figure 6.13: The effect of *FasIII* and JAK/STAT signalling on fold morphology in the *zfh2* domain. Images represent a single confocal slice. Distal (d) fold highlighted in green, medial (m) in red (which corresponds to the *zfh2* Gal4 expression domain) and proximal (p) in blue.
(a) The m fold is not affected in the control, *zfh2>rh4-RNAi*, yellow arrow (b) Knockdown of *FasIII*, *zfh2>FasIII-RNAi* results in a disruption of the m fold, blue arrow. (c) Knockdown of JAK/STAT signalling, *zfh2>stat92E-RNAi*, also causes a disruption of the m fold, blue arrow.

Lastly, the wing disc fold phenotype was examined through the generation of clones. This technique generates a mosaic of wildtype and mutant tissue through the stochastic induction of mitotic clones leading to the expression of a mutant Stat92E

protein. Clones were very rarely found to span the wing disc folds. This was only observed once, a small clone was found to span the medial fold (Fig6.14aii, b), causing disruption in its morphology (Fig6.14ai, b).

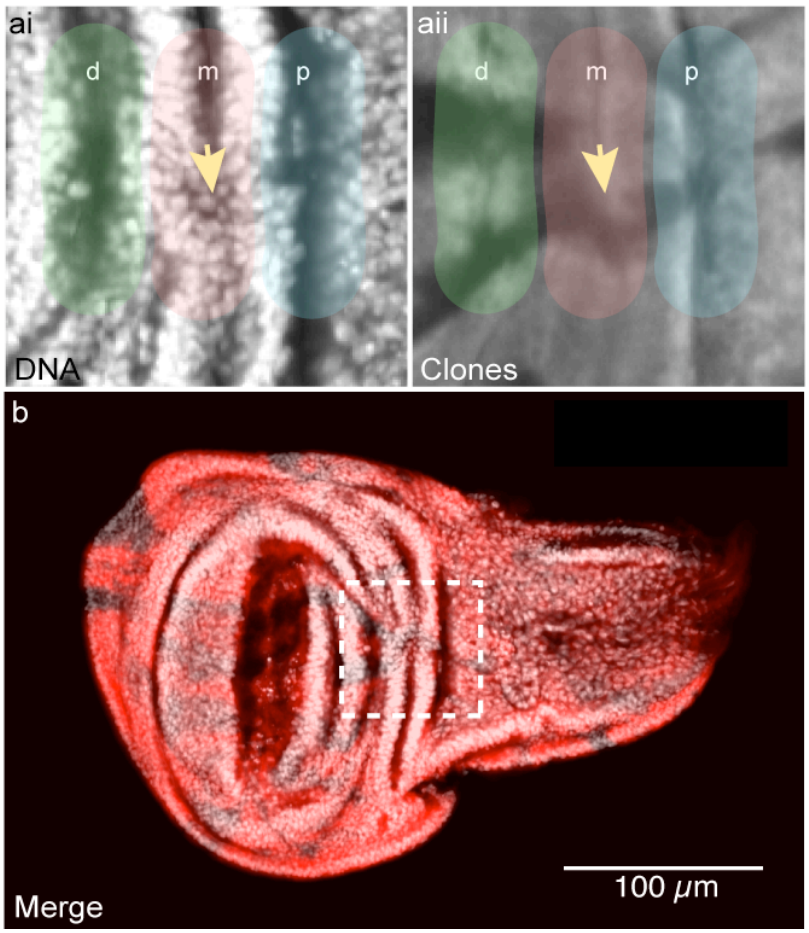

Figure 6.14: The medial wing disc fold is reduced in a JAK/STAT loss of function clone. S*tat92E* loss of function clones are marked with loss of grey (ai-aii) and red in (b). Distal (d) fold highlighted in green, medial (m) in red and proximal (p) in blue.
(ai-aii) A clone spanning the medial fold causes a reduction in its magnitude. (b) Merge of clone marker and wing disc morphology.

Based on the hindgut model, in which JAK/STAT signalling via FasIII acts to maintain curve morphology, it is hypothesised that a similar process is occurring to maintain fold structure in the wing disc. However, it has previously been shown that the JAK/STAT pathway is required in the wing disc for cell proliferation

(Mukherjee et al., 2005). Indeed, the changes in wing disc fold magnitude could be attributed to changes in cell number. Loss of JAK/STAT signalling may lead to a reduction in proliferation, resulting in a reduction of fold magnitude. Conversely, ectopic JAK/STAT signalling may result in increased cell proliferation, resulting in an increase in fold magnitude. A previous study, on JAK/STAT signalling in the wing disc, has shown that in the 1st and 2nd instar larvae JAK/STAT signalling has a pro-proliferative role. Conversely, in the 3rd instar larvae the JAK/STAT pathway acts in an anti-proliferative manner (Mukherjee et al., 2005). As the hinge folds are not formed until the 3rd instar it is unlikely that the JAK/STAT pathway is acting in a pro-proliferative manner in the wing disc folds. Furthermore, FasIII is characterised as an adhesion molecule which has never been associated with proliferation, with data in this thesis indicating this is not the case (Fig4.16), and largely phenocopies JAK/STAT signalling in the wing disc. While circumstantial, this further suggests that JAK/STAT signalling and FasIII operate in a structural, rather than a proliferative, role in the wing disc hinge folds.

To confirm that JAK/STAT signalling is not affecting wing disc hinge fold structure, via cell proliferation, mitosis in response to ectopic JAK/STAT activation was examined. In the wildtype wing disc, there is no apparent increase in cells stained with the mitosis marker, H3 phospho (S10), in regions marked with the *10xSTATGFP* reporter (Fig6.15ai-aii). Furthermore, when wildtype *hop* is expressed in the *ptc* domain, there is no noticeable increase in proliferating cells in the hinge region (Fig6.15bi-bii). This data provides a further indication that the effect of JAK/STAT signalling, on wing disc fold morphology, is more likely to be structural, rather than proliferative.

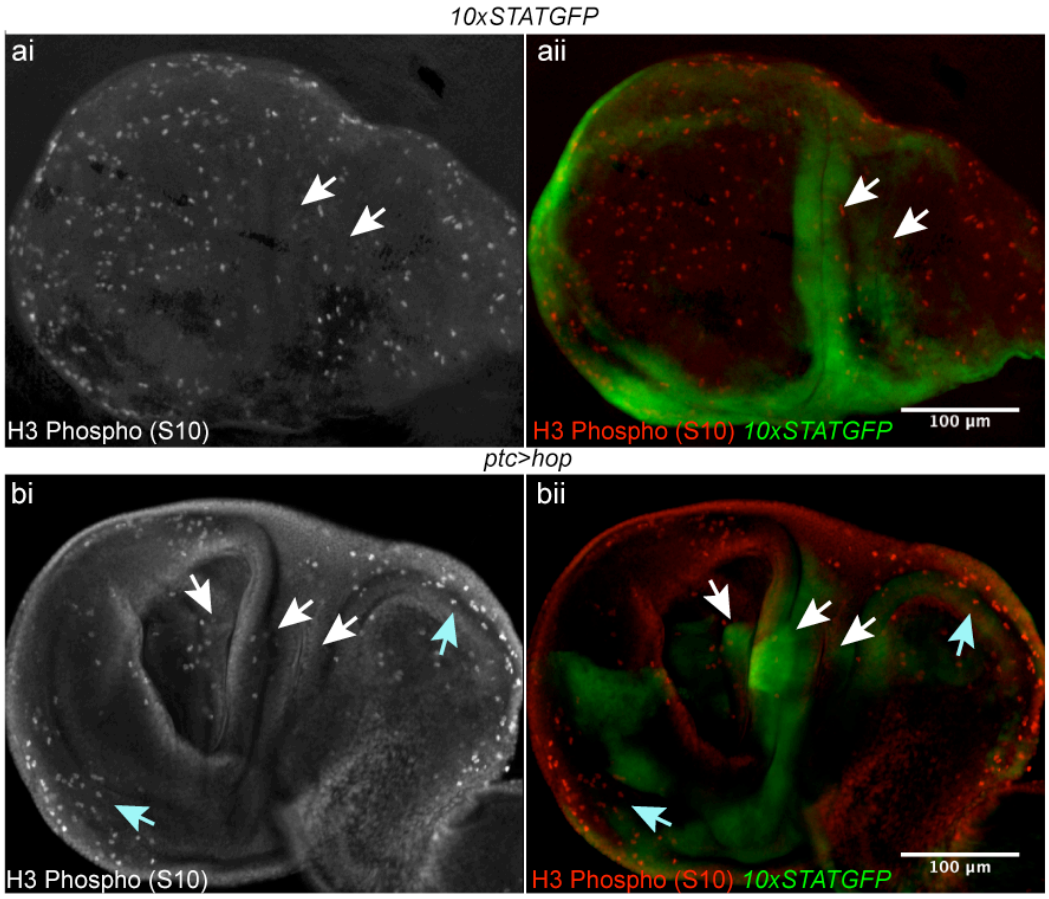

Figure 6.15: JAK/STAT signalling and cell division in the wing disc. Images represent a single confocal slice. Mitotic cells are marked with H3 Phospho (S10).
(ai-aii) In the wildtype, *10xSTATGFP*, there does not appear to be an enrichment of dividing cells overlying *10xSTATGFP* in the hinge, white arrows. (bi-bii) With ectopic JAK/STAT activation, *ptc>hop*, there also does not appear to be an enrichment of dividing cells overlying *10xSTATGFP* in the hinge region, white arrows. However there does seem to be an increase in dividing cells overlying *10xSTATGFP* in regions away from the hinge, blue arrows.

6.2.3 Wing hinge defects may be causative of JAK/STAT outstretched phenotype

The wing disc is a primordial tissue that forms the wing in the later *Drosophila* adult. The subsequent ramifications of defects in the structure of the wing disc hinge folds is unknown. To investigate this problem, adult flies with wing disc hinge defects were examined. In the wildtype (Fig6.19a) and control, *ptc>rh4-RNAi,* (Fig6.16a) the adult *Drosophila* holds its wings back against its abdomen.

Knockdown of *stat92E, ptc>stat92E-RNAi*, resulted in a severe outstretched phenotype, in which the adult holds its wings away from its abdomen (Fig6.16b). Furthermore, knockdown of *FasIII* also resulted in an abnormal wing posture in which the wings appear slightly outstretched, as well as rotated (Fig6.16c). To further test the requirement for JAK/STAT signalling and *FasIII* in adult wing posture, knockdowns in the *zfh2* domain were examined. Unfortunately, knockdown of *stat92E*, *zfh2>stat92E-RNAi,* resulted in lethality, when grown at either 18°C or 25°C, and so could not be analysed. Loss of *FasIII*, *zfh2>FasIII-RNAi*, resulted in a rotated wing posture (Fig6.16f), when compared to the control, *zfh2>rh4-RNAi,* (Fig6.16d). These data indicate that the correct structure of the 3rd instar larval wing disc prospective hinge folds, mediated by JAK/STAT signalling and FasIII, may be important for the development of the correct adult wing posture.

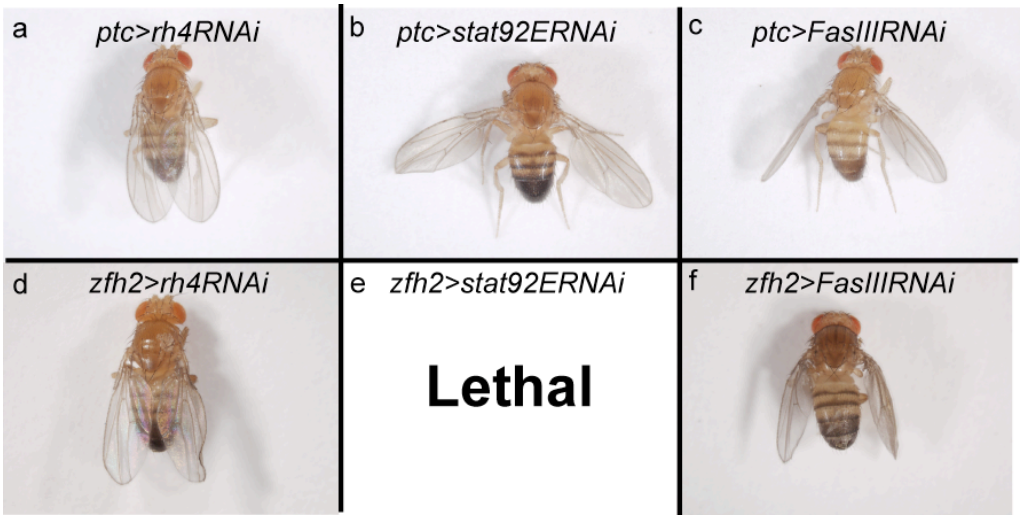

Figure 6.16: Wing disc posture in knockdown of *stat92E* and *FasIII*. Images are of male flies. (a) Knockdown of *rh4* in the *ptc* domain, *ptc>rh4-RNAi*, does not affect wing posture (0/112). (b) Knockdown of *stat92E* in the *ptc* domain, *ptc>stat92E-RNAi*, results in a severe outstretch phenotype (male – 20/22, female – 19/20). (c) Knockdown of *FasIII* in the *ptc* domain, *ptc>FasIII-RNAi*, results in a subtle outstretched phenotype (male 22/27, female 31/36). (d) Knockdown of *rh4* in the *zfh2* domain, *zfh2>rh4-RNAi*, does not affect wing posture (male – 0/44, female – 0/35). (e) Knockdown of *stat92E* in the *zfh2* domain, *zfh2>stat92E-RNAi*, causes lethality. (f) Knockdown of *FasIII* in the *zfh2* domain, *zfh2>FasIII-RNAi*, results in a rotated wing posture phenotype (male – 16/27, female – 19/34).

In addition to the *zfh2* and *ptc* Gal4 drivers previously described, numerous other *Drosophila* lines are available which express in the developing wing. *Daughterless* (*da*) is ubiquitous throughout development (Cronmiller and Cummings, 1993), *apterous* (*ap*) is expressed primarily in the pouch (Calleja et al., 1996), *Distal-less* (*Dll*) and *vestigial* (*vg*) are expressed through the centre of the pouch (Simmonds et al., 1995) and *MS1096* is expressed in the proximal pouch (Capdevila and Guerrero, 1994) (Fig6.17).

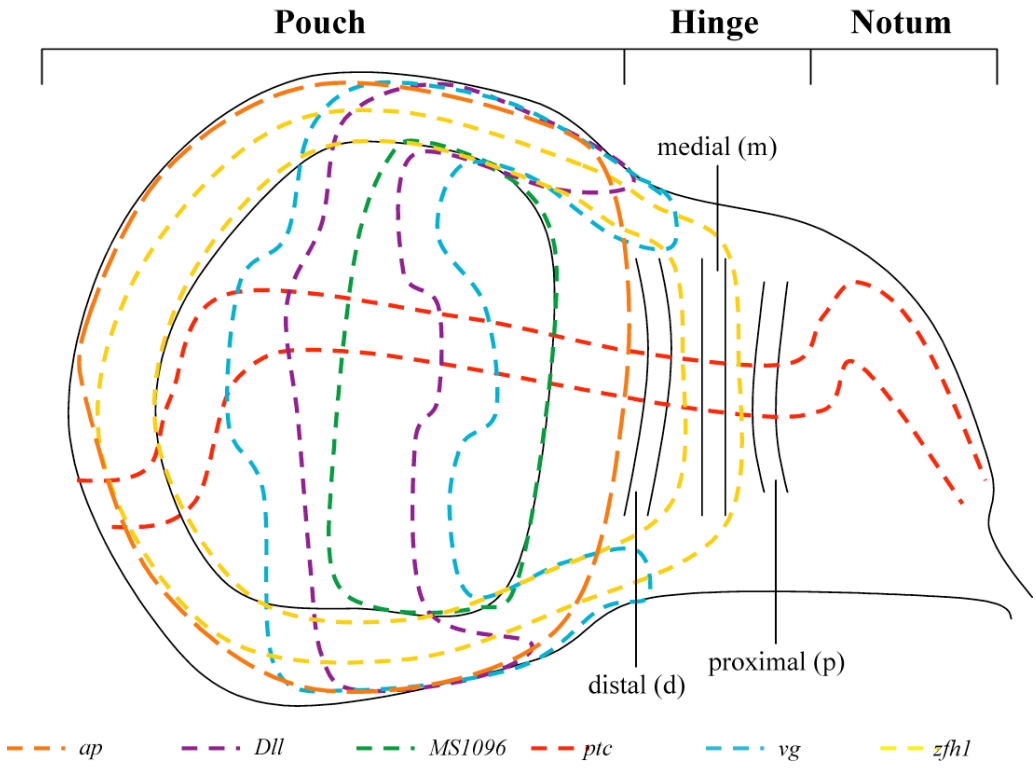

Figure 6.17: Schematic of Gal4 expression domains.

***Ap*, orange, is expressed throughout the whole pouch, both *Dll*, purple, and *vg*, blue, are expressed in a domain at the centre of the pouch and *MS1096*, green, is expressed in the proximal pouch. As previously described, *ptc*, red, is expressed from distal to proximal through the pouch, hinge and notum while *zfh2*, yellow, is expressed in a ring around the outside of the pouch encompassing the central fold in the hinge. *Da* is expressed throughout the entire wing disc, not shown.**

To examine further the role of FasIII in wing development, the Gal4 drivers, described in figure 6.16, were used to misexpress both *FasIII* and *FasIII-RNAi*. Either knockdown or overexpression of *FasIII* in the pouch, mediated by *Dll* and *vg*, had no discernable adult wing phenotype (Fig6.18g-l). Knockdown in the MS1096 domain did (Fig6.18n), however, produce a small wing phenotype when compared to overexpression and the control (Fig6.18m, o). Interestingly, both knockdown with *ap* and *da* (Fig6.18b, e) as well as overexpression with *ap* (Fig6.18f) caused a drastic crumpled wing phenotype when compared to the controls (Fig6.18a, d). Overexpression of *FasIII* with *da*-Gal4 caused lethality. The crumpled wing phenotype is intriguing as the adult structures give the appearance of a newly eclosed fly. These results appear to show that affecting tissue-wide adhesion, either through loss of, or an increase in, FasIII can drastically affect adult wing development. While not independently verified through this work, the folded wing phenotype is reminiscent of the published wing morphology caused by the overexpression of *upd* or *upd2* using the *MS1096*-Gal4 (Hombria et al., 2005). Here the wings appear smaller and crumpled when compared to the wildtype. While the significance of these findings is unknown, the similarity of the *FasIII* and JAK/STAT overexpression phenotypes further consolidates a model in which FasIII operates as an effector of JAK/STAT signalling. Furthermore, while it is difficult to analyse wing posture in flies with disrupted wing morphology, mediated by *ap* and *da* (Fig6.18b, e-f), wing posture with knockdown and overexpression of *FasIII* in the pouch, mediated by *Dll vg* and MS1096 (Fig6.18g-o), is normal. This indicates that only levels of FasIII in the hinge are important for the development of wing posture (Fig6.16).

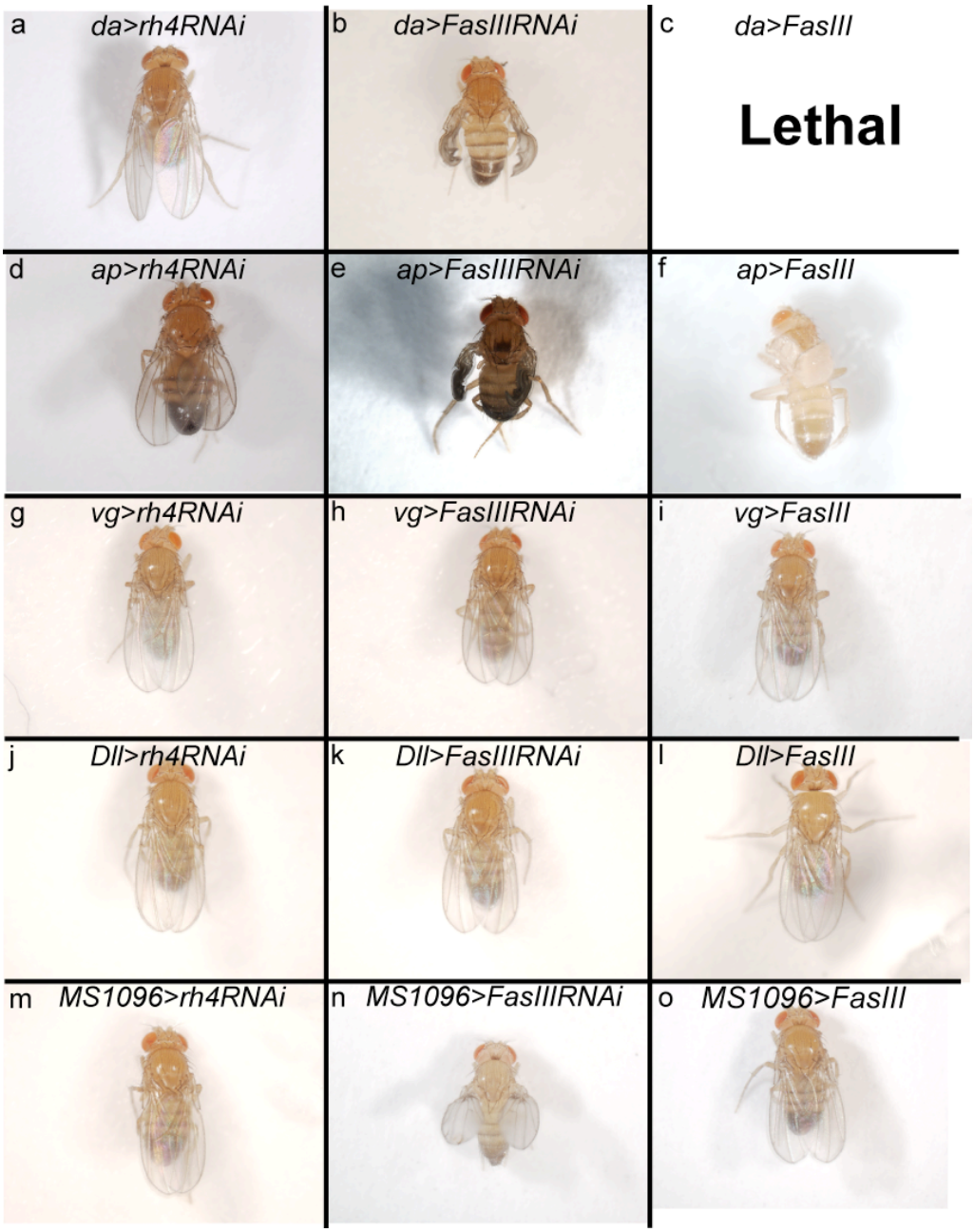
a da>rh4RNAi
b da>FasIIIRNAi
c da>FasIII
Lethal
d ap>rh4RNAi
e ap>FasIIIRNAi
f ap>FasIII
g vg>rh4RNAi
h vg>FasIIIRNAi
i vg>FasIII
j Dll>rh4RNAi
k Dll>FasIIIRNAi
l Dll>FasIII
m MS1096>rh4RNAi
n MS1096>FasIIIRNAi
o MS1096>FasIII

Figure 6.18: The effect of knockdown and overexpression of *FasIII* in the wing. Images represented are male flies.
(a-c) Ubiquitous knockdown, *da>FasIII-RNAi* (male – 21/36, female 12/24), causes a crumpled wing phenotype when compared to the control, *da>rh4-RNAi* (male – 0/42, female 0/38), overexpression caused lethality. (d-e) Knockdown, *ap>FasIII-RNAi* (male – 10/19, female 18/27), and overexpression, *ap>FasIII*, in the pouch caused a crumpled wing phenotype when compared to the control, *ap>rh4-RNAi* (male – 0/22, female – 0/27). (g-l) Knockdown, *vg>FasIII-RNAi* (male – 0/37, female – 0/37/) *Dll>FasIII-RNAi* (male – 0/21, female – 0/28), and overexpression, *vg>FasIII* (male – 0/36, female – 0/35) *Dll>FasIII* (male – 0/24, female 0/35), in the centre of the pouch caused no phenotype when compared to the controls, *vg>rh4* |(male – 0/31, female – 0/39) *Dll>rh4-RNAi* (male – 0/42, female – 0/42). (m-o) Knockdown *MS1096>FasIII-RNAi* (male – 6/11, female – 59/67), in the proximal pouch caused a small wing phenotype while overexpression, *MS1096>FasIII* (male – 0/29, female – 0/41), and the control, *MS1096>rh4* (male – 0/30, female 0/47), appeared normal.

The described outstretched wing postures, especially apparent with knockdown of *stat92E*, are reminiscent of a historic fly line. The first JAK/STAT allele was generated through an X-ray mutagenesis screen in 1930 by Hermann J Müller (Muller, 1930) who went on to collect the 1946 Nobel Prize in Physiology or Medicine (Shampo and Kyle, 1999). One of the phenotypes attributed to the locus was an abnormal adult wing posture. The wings of these flies were "outstretched", held away from the fly's body (Fig6.19b) rather than flush and parallel to its abdomen (Fig6.19a). This mutation was named *outstretched* (*os*), based on this phenotype, and is still known as such in Flybase (www.flybase.org). Half a century on, the locus was further investigated and renamed *unpaired*, a name by which it is more commonly known, based on its embryonic expression pattern (Carroll and Scott, 1986). Later the gene was cloned and identified as the first *Drosophila* JAK/STAT cytokine ligand (Harrison et al., 1998). While the occurrence of the outstretched phenotype is used to validate genes that modulate JAK/STAT signalling (Callus and Mathey-Prevot, 2002), the mechanism by which it arises is unknown.

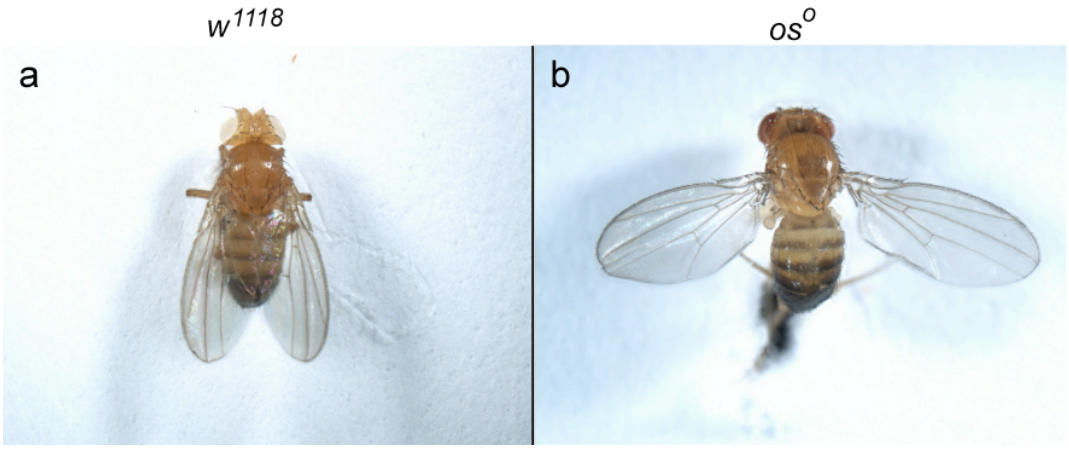

Figure 6.19: The JAK/STAT outstretched wing phenotype. Images represent male flies. (a) In the wildtype the wings are held back against the body (b) In the *os^{o}* allele the wings are held out away from the body.

Due to the nature of the *os^{o}* abnormal wing posture it is widely assumed that it is caused by a defect in the wing hinge region of the adult fly. As knockdown of JAK/STAT signalling (Fig6.11c, Fig6.13c) causes errors in wing disc hinge folds and an outstretched adult wing posture (Fig6.16b), reminiscent of *os ^{o}* (Fig6.19b), the wing disc folds of this historic allele were examined. The *os^{o}* mutant wing disc hinge shows a disruption of the proximal fold, (Fig6.20b), when compared to the wildtype (Fig6.20a). This evidence indicates that defects in the wing disc hinge, mediated by either JAK/STAT signalling or FasIII, are likely to be causative of the *os^{o}* phenotype.

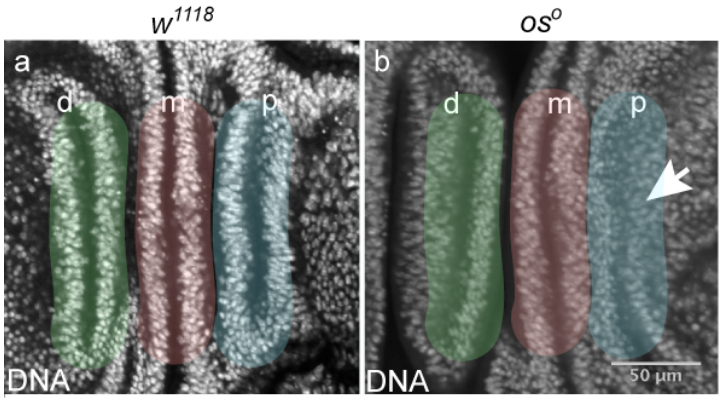

Figure 6.20: Wing disc hinge defects in the *os^{o}* mutant. Images represent a single confocal slice. Distal (d) fold highlighted in green, medial (m) in red and proximal (p) in blue.
(a) In the wildtype all folds exhibit the same morphology. (b) In the *os^{o}* mutant p is disrupted.

6.2.4 Examination of the *os^{o}* regulatory elements

Mutants lacking any of the core JAK/STAT components are lethal prior to adulthood. Given the homozygous, viable nature of the *os^{o}* allele it is likely that this represents a hypomorphic mutation in which *upd* regulatory elements, rather than *upd* itself, have been lost. Examination of *upd* expression in the wildtype wing disc hinge, by *in situ* hybridisation, shows mRNA in three distinct regions; two in the medial fold and one in the proximal (Fig6.21a). In the *os^{o}* allele *upd* expression in the proximal fold is lost (Fig6.21b) (images courtesy of Shriui Hou and Martin Zeidler). As would be expected, this loss of *upd* equates to loss of the *10xSTATGFP* reporter in the proximal fold (Fig6.21d), when compared to wildtype (Fig6.21c). These observations are consistent with previous findings showing a disruption of the proximal fold in the *os^{o}* allele (Fig6.20).

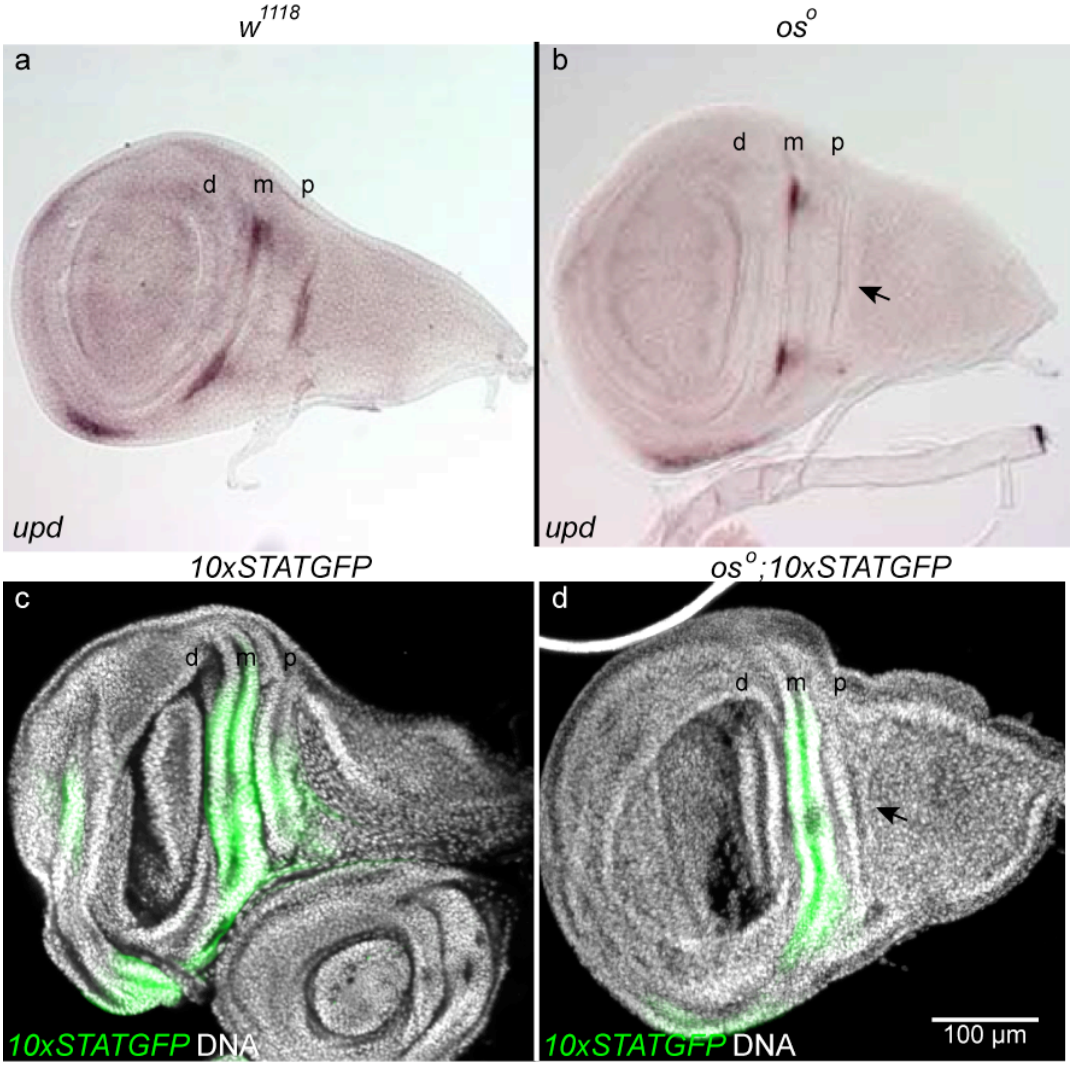

Figure: 6.21: JAK/STAT wing disc activity in *os°*.

(a) In the wildtype wing disc hinge *upd* expression, visualised by *in-situ* hybridisation, is found in two regions of the medial fold and one in the proximal fold. (c) The localisation of *upd* closely corresponds to expression of *10xSTATGFP*. (b) In the *os°* mutant the expression of *upd* is lost in the proximal fold, black arrow. (d) The loss of *upd* in *os°* results in loss of *10xSTATGFP* in the proximal fold, black arrow. *Upd in-situ* hybridisation images, a and b, courtesy of Shirui Hou and Martin Zeidler.

The loss of an *upd* regulatory element is likely to be due to a lesion generated through the x-ray irradiation; this may lie close to the *upd* gene itself. To attempt to identify this, transgenic *Drosophila* lines were used in which the intergenic region, approximately 20kb, between *upd* and *upd3* was divided into 17 sections and cloned

upstream of Gal4 (kind gift of Stephen Brown). Due to the proximity of these constructs to *upd* they may contain regulatory elements required for its expression. Unfortunately not all constructs were available; the ones used are written in red in the schematic below (Fig6.22).

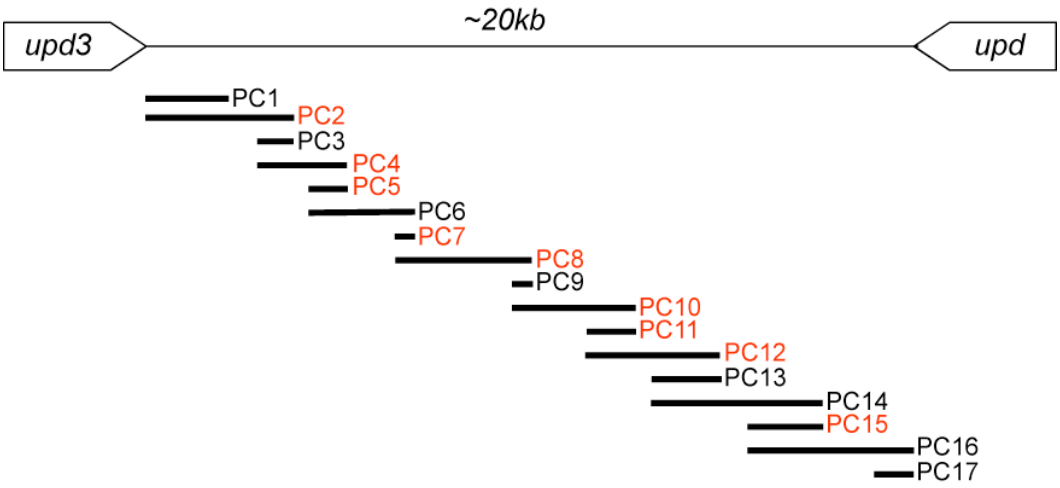

Figure 6.22: Schematic of the constructs made within the *upd3* – *upd* intergenic region. Drawing not to scale.
Constructs used are written red the others were not available.

If the expression of a reporter, driven by one of these constructs, is found in the wing disc proximal fold then the key regulatory element, and the lesion in os^{o}, required for *upd* expression may lie within this genetic region. All available stocks were crossed to UAS-*RedStinger*, with only PC12 identified as driving expression in the wing disc. Here, expression of the reporter, was found in both the hinge and notum (Fig6.23e).

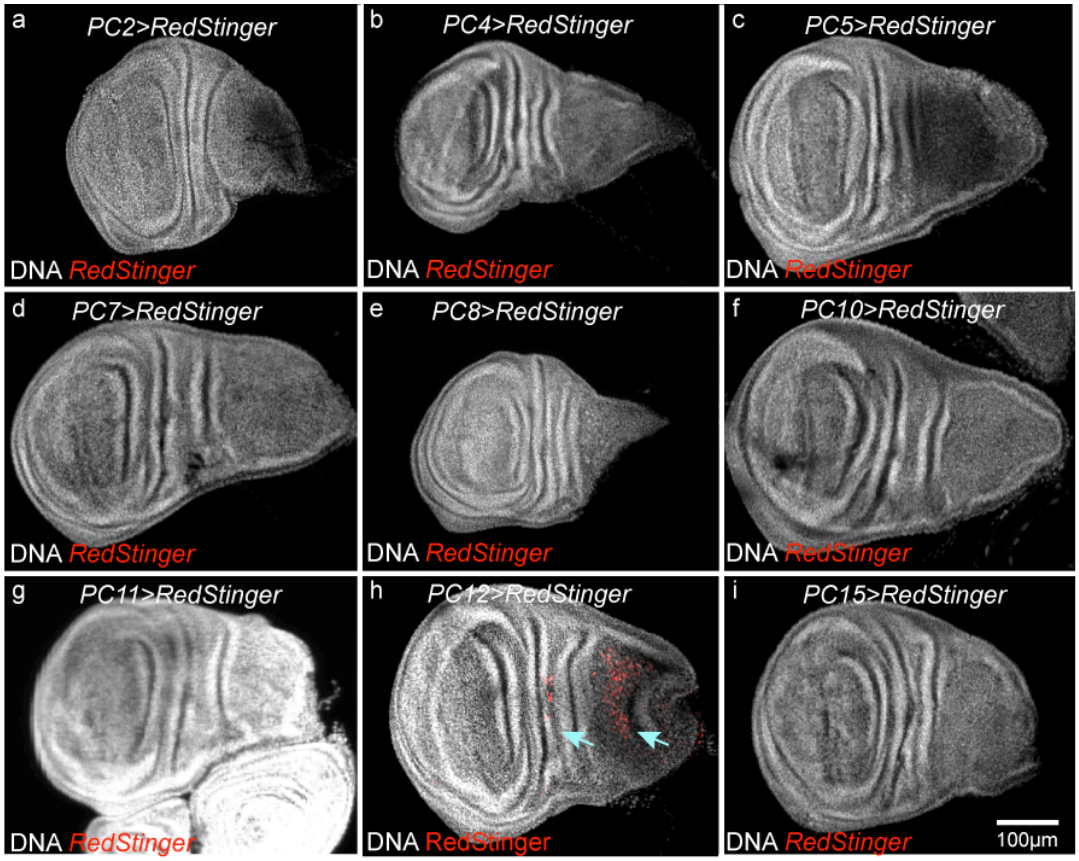

Figure 6.23: Expression domains of the *upd*, *upd3* intergenic Gal4 constructs. Images represent a single confocal slice.

(a-g, i) No *RedStinger* expression was detected in the wing disc of the majority of constructs (h) Only line PC12 drove expression of *RedStinger* which was detected in the hinge and notum, blue arrows.

Closer examination of the PC12 shows that the hinge expression is in a region between the medial and proximal folds (Fig6.24ai-aii). Comparison with a *upd* enhancer trap, E132>*RedStinger*, shows that this may be in a different location to endogenous *upd* expression which is found in distinct regions of the medial and proximal folds (Fig6.24bi-bii).

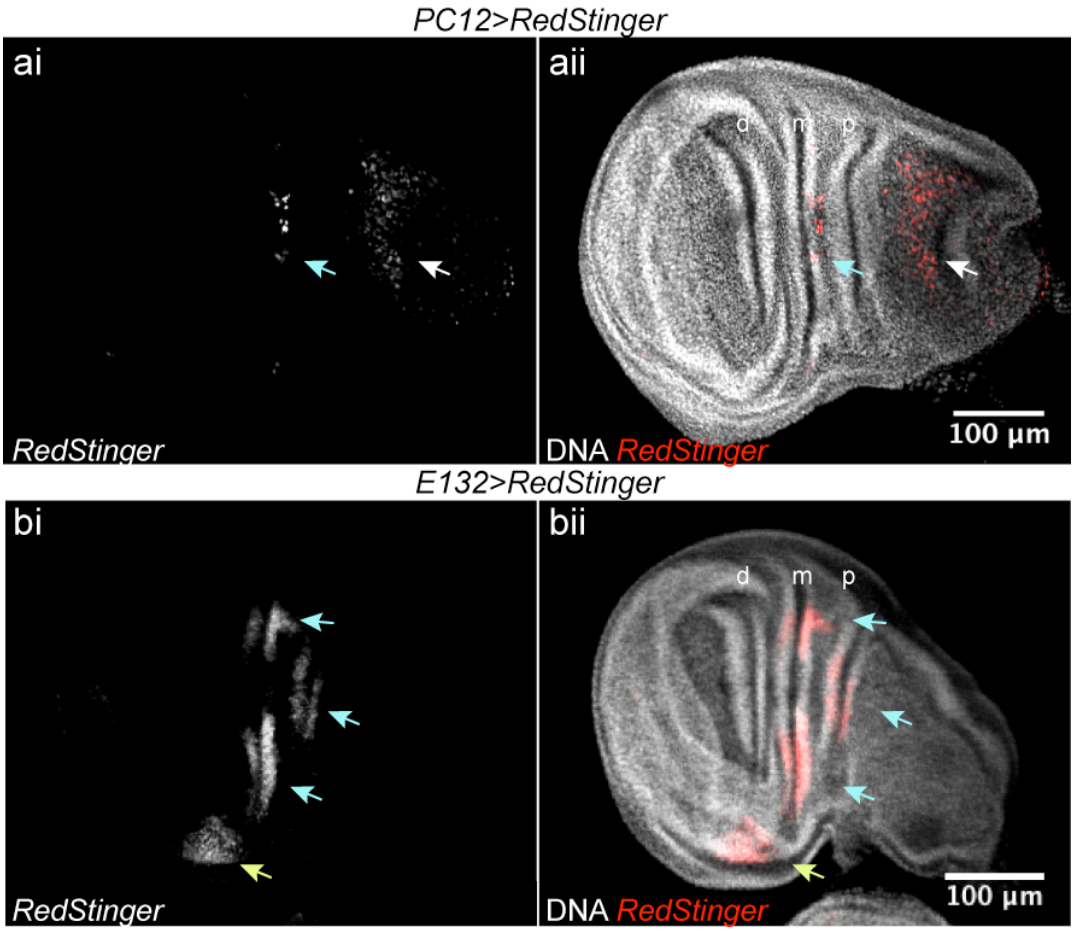

Figure 6.24: A comparison of PC12 and *upd* expression. Images represent a single confocal slice (ai-aii) PC12 drives expression of *RedStinger* in the hinge region, blue arrow, and the notum, yellow arrow.
(bi-bii) *Upd* expression, through the E132 enhancer trap, drives expression of *RedStinger* in the medial and proximal folds, blue arrows, and the pouch, yellow arrow.

To confirm that the expression observed in PC12 does not drive the distal expression of *upd, upd* was knocked down in this region, *PC12>Upd-RNAi*. If this population of cells does produce the Upd required to correctly form the proximal hinge fold then the cell autonomous knockdown of *upd* in them should result in an outstretched adult phenotype. While nothing is known about *upd3* function in the wing disc, given the cytological location of PC12, knockdown of *upd3* was undertaken to confirm this was not having an effect, *PC12>upd3-RNAi*. Both knockdown of *upd* and *upd3* failed to result in an outstretched adult phenotype (Fig6.25). This shows

that the *upd* regulatory element in *PC12* is not required for the expression of endogenous *upd* in the proximal fold. Furthermore, this indicates that the region identified by PC12 is not where the lesion in os^{o} is likely to be.

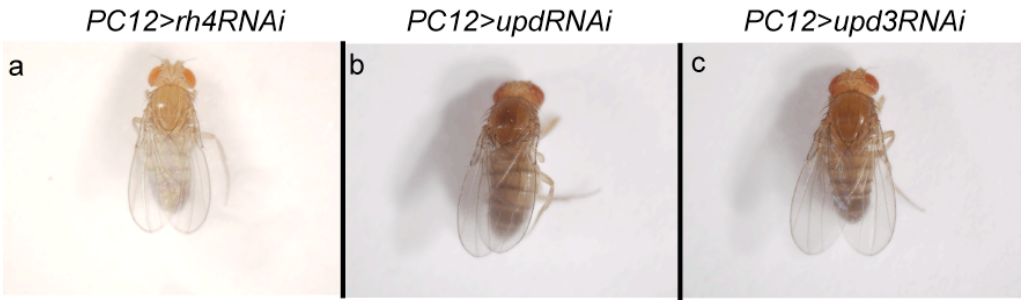

Figure 6.25: Knockdown of *upd* and *upd3* in PC12. Images are of male flies.
(a) Knockdown of *rh4* in *PC12*, *PC12>rh4*, does not affect wing posture (male – 0/39, female 0/40). (b) Knockdown of *upd* in *PC12*, *PC12>Upd-RNAi,* does not affect wing posture (male – 0/35, female – 0/40). (c) Knockdown of *upd3* in *PC12*, *PC12>upd3-RNAi*, also does not affect wing posture (male – 0/53, female – 0/36).

6.3 Discussion

In this chapter, the role of FasIII as a JAK/STAT effector has been examined in two further *Drosophila* tissues, the egg chamber and the 3rd instar wing disc. The data presented show that, while the coincidence of lateral FasIII and JAK/STAT signalling in the egg chamber is intriguing, FasIII does not function downstream of the pathway in this tissue. In the wing disc, I have shown a novel role for JAK/STAT signalling in providing structure to folds of the prospective hinge region. In this situation, lateralised FasIII appears to be an effector of pathway activity as both loss of, and ectopic, JAK/STAT pathway activation or *FasIII* expression results in changes in the magnitude of the wing disc folds. Furthermore, these data provide a better understanding of the abnormal wing posture exhibited by the historic os^{o} allele.

In the egg chamber, it was confirmed that FasIII is lateralised between the two PCs. However, JAK/STAT signalling is high in the adjacent BCs but not the PCs themselves. The disjunction of FasIII and the JAK/STAT pathway was confirmed as

FasIII protein abundance and localisation was neither increased, with ectopic JAK/STAT activation, nor reduced with loss of pathway activity. These observations are consistent with the dynamics of JAK/STAT signalling in the egg chamber. It is known that *upd* is expressed solely from the PCs, signalling to the adjacent follicle cells, defining them as BCs (Beccari et al., 2002, Xi et al., 2003). This places lateral FasIII in the wrong context to be either downstream of the JAK/STAT pathway or a pathway effector. A similar situation is present in the testes. Here JAK/STAT signalling is required to maintain stem cell identity. FasIII is present solely within the hub, the testes stem cell niche. As with the egg chamber, *upd* expression is tightly regulated, restricted to the hub with the signal being received in the adjacent germline stem cells and cyst progenitor cells (Kiger et al., 2001, Tulina and Matunis, 2001). Again, this places FasIII in the cells from which the JAK/STAT signal originates, rather than in those that receive it. This indicates that the relationship between JAK/STAT signalling and FasIII in the testes is analogous to that in the egg chamber.

To further elucidate the function of JAK/STAT signalling and FasIII in epithelia, folds of the 3rd instar wing disc were investigated. Examination of the *10xSTATGFP* reporter showed that pathway activity is localised at the base of the medial and proximal folds. In this region FasIII appears lateralised, a situation analogous to the embryonic hindgut where JAK/STAT activity is localised asymmetrically and coincides with lateralised FasIII. Knockdown, and loss, of both JAK/STAT signalling and *FasIII* affects the morphology of the medial and proximal folds in the prospective wing disc hinge. It is tempting to state that this shows that JAK/STAT signalling and FasIII are required to maintain the structure of these folds. However, while it is evident that JAK/STAT signalling and FasIII are required in the folds, these data do not provide a clear indication of a mechanism by which these phenotypes occur. There is no published description of the timeline of fold formation. From the data generated through this work, it is unclear if the folds initially form in the absence of JAK/STAT signalling and FasIII then degenerates, similar to the hindgut curve, or if the folds fail to form at all. The ideal method to

examine this problem would be to live image the development of folds in each mutant background (Aldaz et al., 2010). Temporal data of fold dynamics would provide an understanding of wildtype fold formation and why this is aberrant in the mutant backgrounds.

A further phenotype observed, in the wing disc, is the increase in the magnitude of the distal fold with ectopic JAK/STAT activation or *FasIII* expression. While providing further evidence that JAK/STAT signalling is operating through FasIII, the phenotype itself is hard to explain. The distal fold is found in the pouch rather than the prospective hinge and does not experience JAK/STAT signalling or exhibit lateralised FasIII. These differences indicate that its formation and maintenance are likely to depend on a different mechanism. The manner in which ectopic JAK/STAT signalling and *FasIII* expression can affect its magnitude do, however, indicate that its morphology is sensitive to predicted JAK/STAT and FasIII mediated changes in tissue stability.

An unexpected result of this work is the potential identification of the cause of the outstretched wing posture in the historic os^{o} allele. The abnormal outstretched wing posture appears to correlate with the loss of the proximal wing disc fold, a consequence of losing the proximal expression of *upd*. Targeted knockdown of JAK/STAT signalling and *FasIII* appears also to affect wing posture, indicating that the correct structure of the wing disc folds is important for this aspect of adult wing development. The manner in which different wing postures arise, through different genetic manipulations, may lead to a further understanding of how the adult wing hinge develops. In os^{o} and *ptc>stat92E-RNAi* the wing disc proximal fold is greatly reduced correlating with a severe outstretched wing posture. Reduction of the entire wing disc medial fold alone, *zfh2>FasIII-RNAi*, correlates with a rotated wing posture, rather than an outstretched phenotype. Interestingly, *ptc>FasIII-RNAi*, only appears to affect a small region of the medial wing disc fold. This genetic background caused an intermediate phenotype where the wings are both slightly rotated and outstretched. These data indicate that defects in the structure of both the

wing disc proximal and medial folds correlate with alterations in adult wing posture, albeit, in different capacities. An obvious continuation of this study is to examine adult wildtype and mutant wing hinges. This work may identify the adult structures derived from the 3rd instar wing disc folds. Such observations could be important in understanding the manner in which the wing disc primordial folds map to the adult structures and how the different genetic backgrounds cause variations of adult phenotypes. Furthermore, an examination of the pupal primordial wing should also be undertaken. While the data in this thesis indicate that there is a correlation between the wing disc prospective hinge and adult wing posture, further development occurs during metamorphosis. An understanding of how these structures change over time, both in the wildtype and mutants, would be required to support the data and conclusions presented in this thesis. Of further interest, and to better understand the development of wing posture, would be the examination of other members of the *Drosophila* genus. Over the years numerous *Drosophila* species have been collected and maintained as lab stocks. Of these *Drosophila talamancana* is the only species whose wildtype wing posture is outstretched rather than held back against the abdomen (Maxi Polihronakis Richmond, University of California *Drosophila* Stock Center, personal communication). Examination of both the wing disc hinge and adult wing hinge structure of *talamancana* may provide insight into the role of the wing disc hinge folds in the development of wing posture.

While the correct development of wing posture is poorly understood, a number of alleles have been noted as having an abnormal wing posture. Fly models for human degenerative diseases such as Parkinson's disease mutants, *parkin* (*park*) and *PTEN-induced putative kinase 1* (*Pink1*) (Greene et al., 2003, Clark et al., 2006, Park et al., 2006), and oculopharyngeal muscular dystrophy, *nuclear poly(A)-binding protein (PABPN1*) (Chartier et al., 2006), display a degeneration of adult flight muscles manifesting as both held up and droopy wing phenotypes. However, wing phenotypes only become visible a number of days after eclosion (Greene et al., 2003, Park et al., 2006, Chartier et al., 2006) while the defects observed in both JAK/STAT and *FasIII* genetic backgrounds are immediately apparent. While these

phenotypes are different from those described in this thesis the examination of muscle development in flies with outstretched wings should be undertaken to discount this as being causative of the phenotype. In addition, numerous other alleles are also known as having abnormal wing postures. These were almost exclusively described by the pioneers of *Drosophila* research in the era of Herman J Müller, some examples of which are *aeroplane (ae)* – on the second chromosome (Quelprud, 1931), *spread* (*sprd*) – on the third chromosome, *Dichaete* (*D*) – on the third chromosome (Bridges et al., 1923) and *taxi* (*tx*) – on the third chromosome (Collins, 1928). Of these, only *ae* has undergone further examination with modern techniques. The *ae* wing posture (Quelprud, 1931) bears a striking similarity to the *os* allele, which is on the X chromosome (Muller, 1930). Examination of the flight musculature of the *ae* allele shows that this appears normal indicating that abnormal muscle development is not causative of the phenotype (Soanes and Bell, 1999). It is suspected that *ae* is a hypomorphic allele of the homeotic gene *teashirt* (*tsh*) (Soanes et al., 2001), much like *os* is a hypomorphic allele of *upd*. Interestingly, *tsh* is expressed in the wing disc hinge region (Soanes et al., 2001); this is consistent with an association between JAK/STAT signalling and the hinge. Investigating whether there is any genetic interaction between JAK/STAT signalling and *tsh* may lead to a further understanding of the correct formation of wing posture.

The characterisation of the os^{o} allele provides a starting point from which to examine the manner in which *upd* is regulated. Through understanding why the phenotype occurs, and through the identification of subtle changes in its expression, *upd* regulatory elements may be identified. While preliminary attempts in this thesis were unsuccessful, a more diligent approach could be attempted. This should initially be undertaken through the detailed sequencing and comparison of the *upd* locus in wildtype and os^{o} to identify any loss of sequence. It could be assumed that this region would contain the regulatory elements required for the specific spatial expression of *upd*, which is lost in os^{o}.

7 Discussion

7.1 Introduction

The work in this thesis describes a novel role for the JAK/STAT pathway in affecting epithelial morphology through regulating the homophilic adhesion molecule FasIII. JAK/STAT signalling is required to increase localised *FasIII* expression resulting in FasIII protein lateralisation. Evidence from the embryonic hindgut and the 3rd instar larval wing disc indicates that lateralised FasIII increases tissue stability maintaining epithelial structures during development. Previously I have described the significance of these results in the relevant biological systems. In this chapter I will relate the relevance of these findings to the wider literature and discuss the scope for future work.

7.2 The role of JAK/STAT and FasIII in epithelial tissues

7.2.1 JAK of all trades?

Data presented within Chapters three, four and five show that the JAK/STAT pathway is integral for correct morphogenesis of the *Drosophila* embryonic hindgut. Loss of, or ectopic pathway activation results in curvature (Chapters three and four), handedness (Chapter five) and elongation defects (Johansen et al., 2003b). An interesting discussion point is the relationship of these phenotypes and how the pathway may directly, or indirectly, affect them.

The role of JAK/STAT signalling in co-ordinating cell migration is well conserved from the slime mould, *Dictyostelium discoideum* (reviewed in, Kawata, 2011), through *Drosophila* germ cells (Brown et al., 2006) and border cells (Silver and Montell, 2001, Silver et al., 2005) to immune chemotaxis and cancer metastasis (reviewed in, Wu and Zhou, 2009, Ara and Declerck, 2010). However, in addition to the hindgut (Johansen et al., 2003b), there is only one documented case of the pathway coordinating convergent extension movements. During zebrafish gastrulation STAT3 mediates convergent extension movements through regulating components of the PCP pathway (Yamashita et

al., 2002, Miyagi et al., 2004). In vertebrate systems the role of the PCP pathway in co-ordinating convergent extension is well established in numerous processes including gastrulation, neural plate migration and cochlea elongation (Wallingford et al., 2000, reviewed in Goodrich and Strutt, 2011). In *Drosophila*, the JAK/STAT pathway has been associated with regulation of the core PCP protein *four-jointed* (*fj*), an interaction which is key in establishing the polarity of ommatidial rotation in the eye (Zeidler et al., 1999). However, the *Drosophila* PCP pathway is yet to be associated with convergent extension movements and has been shown not to have a role in germband extension in the embryo (Blankenship et al., 2006). Furthermore, loss of both core and upstream PCP components does not affect hindgut rotation (Taniguchi et al., 2011) or hindgut morphogenesis (Samantha Warrington, Sheffield University, personal communication). This indicates that the PCP pathway is not operating as an effector of JAK/STAT signalling during hindgut elongation. As such, based on the published literature, it is hard to rationalise a direct role for the JAK/STAT pathway in driving hindgut convergent extension movements. Within this thesis, the further characterisation of the spatial regulation of JAK/STAT signalling places pathway activity away from the region of cell rearrangement. Furthermore, in the wildtype, the localisation of JAK/STAT signalling, and lateral FasIII, are correctly spatially regulated to effect curvature and handedness. Indeed, errors in convergent extension may be a side effect of changes in FasIII-mediated cell adhesion which could impede cell rearrangement. While this hypothesis can be rationalised for ectopic JAK/STAT signalling, inducing lateralised FasIII resulting in widespread tissue stability, it is unclear how a reduction in convergent extension occurs with the loss of lateralised FasIII in JAK/STAT loss-of-function hindguts. To better understand this problem a comprehensive analysis of hindgut length in *FasIII* and *vari* mutants, in which lateral FasIII is changed in a JAK/STAT-independent manner, is required. Furthermore, to satisfactorily understand hindgut elongation, detailed timelapse microscopy of cell rearrangement in the wildtype, JAK/STAT, *FasIII* and *vari* mutant embryos should be undertaken. Lastly, there are undoubtedly additional JAK/STAT pathway effectors in the hindgut, the identification and characterisation of which will lead to a better understanding of the association between curvature, rotation and elongation.

7.2.2 The sequential organisation of development

JAK/STAT signalling and lateral FasIII have been described throughout this thesis as having a role in preserving already formed epithelial structures. This is a functionally important, and largely overlooked, aspect of developmental biology. Due to the stepwise progression of development, structures are often formed and must then be maintained as morphogenesis occurs around them. Few examples have been examined such as the vertebrate gut and heart tube in which tissues connected to the organs act to maintain tissue structures, discussed in 7.3.1 (Taber et al., 2010, Savin et al., 2011). Indeed the scope and requirement for this type of mechanism is likely to be conserved in various tissues in different model organisms.

7.3 Analogies with vertebrate models

7.3.1 The morphogenesis of vertebrate tubular organs

Curved looping tubular structures are conserved throughout nature and various mechanisms affect their morphogenesis. Here I will discuss the development of the vertebrate heart tube and gut, comparing these systems with the *Drosophila* embryonic hindgut.

The vertebrate heart tube (HT) is initially found as a bilateral structure (Fig7.1b) that undergoes a looping process important for the formation of the final multi-chamber organ. The first morphological event is a dextral bending of the tube to form a “c” shape (Fig7.1d) (reviewed in, Manner, 2000). Integral to this initial looping are external tissues, two supportive tissues, the ventral splanchnopleure (SPL) membrane and the dorsal mesocardium (DMC) (Fig7.1a) as well as the caudal omphalomesenteric veins (Ovs) (these later form the right and left atria) (Fig7.1c) (Taber et al., 2010). It is believed that both the SPL and Ovs put pressure on the HT forcing it to bend; loss of both SPL and Ovs membrane causes a failure to loop or a reversal of looping (Voronov and Taber, 2002, Voronov et al., 2004). The pressure exerted by the SPL and Ovs is initially resisted by the DMC, generating torsion and causing twist. This pressure eventually dissipates

when the DMC ruptures allowing the final establishment of the "c" shape (Taber et al., 2010). While these external influences are important *in vivo* the HT does, however, show a capacity to loop *ex vivo* indicating the role of intrinsic effectors (Manning and McLachlan, 1990). Evidence shows that the cytoskeletal network may be key to this process as asymmetric inhibition of actin polymerisation causes the HT to loop in the opposing direction to which inhibition is applied (Itasaki et al., 1991, Latacha et al., 2005). Consistent with a role for the cytoskeleton in looping is an asymmetric enrichment of actin bundles (Shiraishi et al., 1992, Latacha et al., 2005), non-muscle myosin (NMHC-II) (Linask and Vanauker, 2007, Lu et al., 2008) and Flectin (a NMHC-II associated structural protein) (Lu et al., 2008) in the HT (Fig7.1a,c).

The primordial vertebrate gut is a looped endodermally-derived tube divided into the foregut, midgut and hindgut. This is connected to the dorsal body cavity via a tissue known as the dorsal mesentery (DM) (Fig7.1e). During midgut elongation a hairpin structure is formed which later undergoes a counter-clockwise 90º turn followed by a further 180º twist, forming the presumptive small intestine (Davis et al., 2008). This looping initially requires the correct tilting of the gut tube which is mediated by the connective DM tissue (Fig7.1e-f). In mouse and chick Nodal (TGF-ß) signalling results in asymmetric expression of *Pitx2*, and subsequently *Insulin gene enhancer protein* (*Isl-1*), on the left of the DM (Davis et al., 2008). In the chick, asymmetric signalling results in high levels of cell adhesion via increased N-cadherin (Fig7.1e-f), an adherens junction adhesive molecule, as well as a contraction in the ECM surrounding the cells (Kurpios et al., 2008). These effects on cell adhesion and ECM contraction result in changes in cell shape from cuboidal to columnar causing the gut to tilt (Davis et al., 2008). Once formed, the maintenance of the looped gut appears dependent on the presence of the DM, loss of which results in uncoiling (Savin et al., 2011). In *Xenopus*, the upstream role of PITX2 is conserved, however, looping appears to be caused by asymmetric gut elongation rather than changes in cell shape (Muller et al., 2003). Furthermore, in zebrafish both Nodal, known as *south-paw*, signalling and PITX2 are conserved. These function to induce asymmetric mesoderm migration which mediates gut looping (Horne-Badovinac et al., 2001, Horne-Badovinac et al., 2003).

As discussed throughout the thesis, morphogenesis of the hindgut is an epithelial-intrinsic process, however both the vertebrate gut and HT rotation and looping require the application of external forces for morphogenesis applied by the DM or OV and SPL respectively. A further difference is the reliance on the ECM surrounding the organ to provide structural support. At present there is no evidence in the literature to suggest the ECM has a role in hindgut morphogenesis or that the JAK/STAT contributes to the formation of the ECM. An interesting similarity, however, is the inherent asymmetry of structural cell components in all these structures; F-actin, NMHC-II and Flectin in the HT (Fig7.1a,c), the adhesion molecule N-cadherin in the gut DM (Fig7.1e-f) and FasIII in the hindgut (Fig7.2g). While these asymmetrically-distributed components have an active role in morphogenesis in the vertebrate system, FasIII appears to have a passive role in maintaining the structure of the *Drosophila* hindgut.

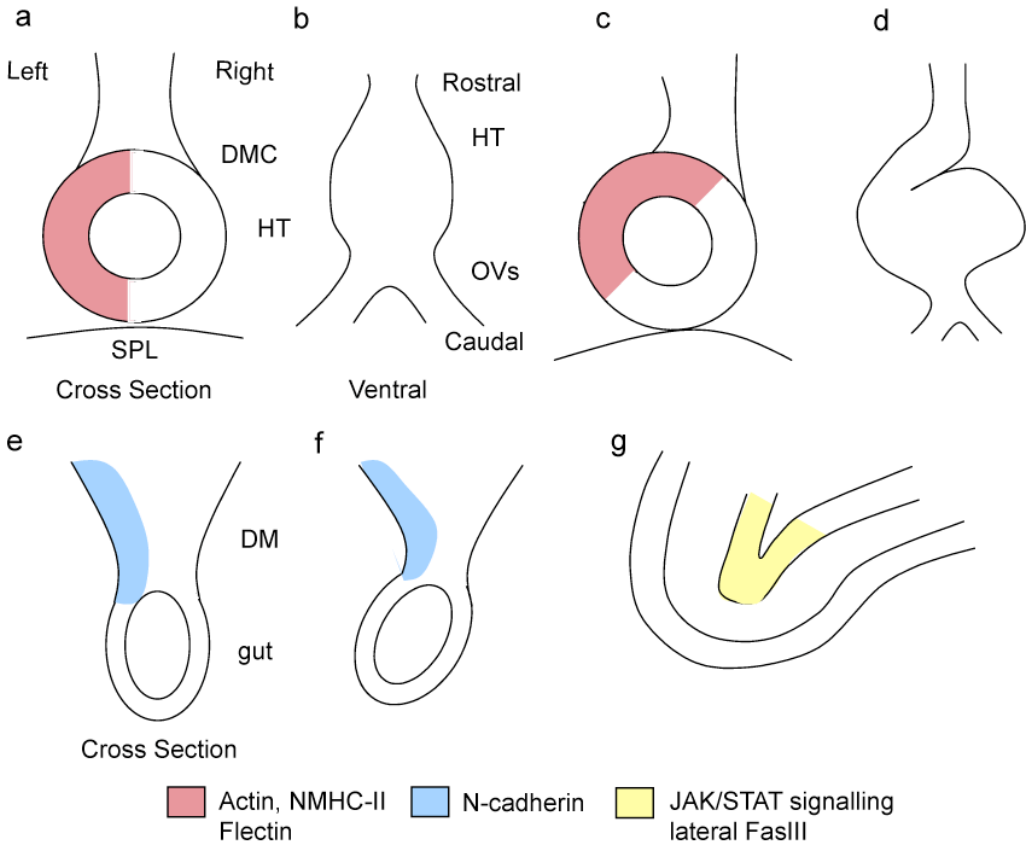

Figure 7.1: Anatomy and localised factors in tubular organ morphogenesis. Schematics not drawn to scale.

(a) The cross-section of the HT. The SPL is connected ventrally and the DMC dorsally. Actin, NHMC-II and Flectin are found on the inside of the HT. (b) Ventral view of the HT with the Ovs connected caudally. (c) The HT twists due to the combined effects of the SPL, OVs and DMC as well as actin, NMHC-II and Flectin. (d) Once rotation is complete the HT forms a "c" shape when viewed from ventral. (e) The vertebrate gut, is connected to the DM which asymmetrically expresses N-cadherin. (f) The effects of N-cadherin and changes in cell shape cause the gut to tilt, a process integral to correct gut rotation. (g) The *Drosophila* embryonic hindgut, as characterised in this thesis. Asymmetric JAK/STAT signalling and lateralised FasIII have a role in maintaining curvature.

7.3.2 The maintenance of vertebrate tubular organs

In addition to the morphogenesis of tubular organs, much may be learnt from tissues that require structural support to maintain their function; the mouse aorta provides a good example of such an organ. The pressure of blood pumped through the aorta places a large amount of both shearing and axial stress on the epithelium of the lumen (reviewed in,

Lehoux et al., 2006). Important to withstanding this is the underlying elasticity of the ECM. Loss of both elastin (Li et al., 1998, Wagenseil et al., 2010) and fibrillin, which provides a scaffold on which the elastin forms (Carta et al., 2006), drastically disrupts the morphology of the aorta. The elasticity provided by elastin and fibrillin is also required in alveoli to conserve their morphology (Wendel et al., 2000, Shifren et al., 2007). As well as being a tubular structure the aorta also contains a curve analogous to the *Drosophila* embryonic hindgut (Fig7.1g). Of interest in the aortic curve is the distribution of PECAM-1 (CD31). PECAM-1 is an Ig-domain family homophilic adhesion protein found in many haematopoetic lineages as well as the endothelia. In these tissues PECAM-1 is involved in the immune response and maintenance of the vascular barrier (reviewed in Privratsky et al., 2010). While FasIII has no clear human homologue (reviewed in Banerjee et al., 2006), it does have features in common with PECAM-1, in that both are single pass transmembrane adhesion proteins with extracellular Ig domains. Examination of PECAM-1 distribution shows that it is enriched on the inside of the aortic arch (Simon Culhmann and Paul Evans, University of Sheffield, personal communication) (Fig7.2) in a similar spatial context to FasIII in the *Drosophila* hindgut. While the significance of this asymmetry has not been characterised it is known that aorta in PECAM-1 knockout mice are susceptible to sheer stress (Tzima et al., 2005). This indicates a reduction in the integrity of the aorta. Current data indicate that loss of integrity is due to failure of PECAM-1 acting as a mechanosensor. In response to pressure PECAM-1 activates Src signalling resulting in changes to integrin-mediated adhesion (Davies, 1997, Tzima et al., 2005). While this is an accepted role of PECAM-1, it would be of interest to examine if the intercellular adhesive properties of PECAM-1 also contribute to maintaining the integrity of the aorta.

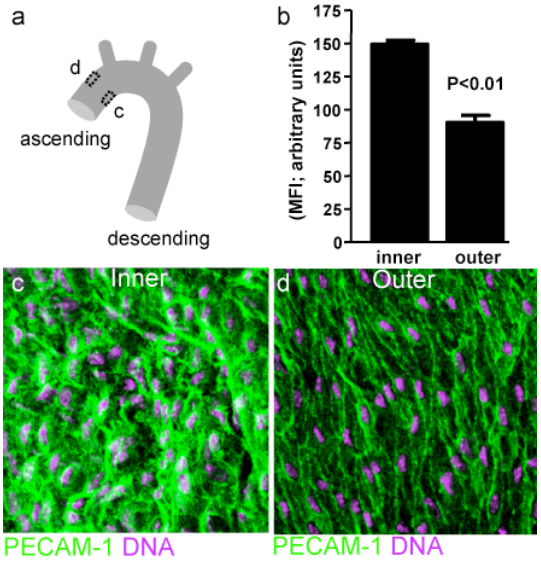

Figure 7.2: PECAM-1 in the mouse aorta. Figure courtesy of Simon Culhmann and Paul Evans. (a) Schematic of the mouse aorta indicating the places at which PECAM-1 levels were measured. (b) PECAM-1 staining is significantly higher on the inner side of the aorta than the outer. (c-d) Staining of PECAM-1 on the inside and outside of mouse aorta.

7.4 Future study

7.4.1 Quantifying *in vivo* stress

One limitation of this work was the inability to quantify the suspected "strain" placed on the hindgut curve during the morphogenesis. In *Drosophila*, an *in vivo* method of demonstrating tension in a tissue is the observation of recoil or relaxation in response to physical disruption. The visualised recoil is as a result of the dissipation of stored potential energy. One technique used for this type of study is laser ablation which generates physical cuts in tissue. This method has been used to great effect in demonstrating the role of the actomyosin cytoskeleton in creating force in the epithelium during germband extension (Fernandez-Gonzalez et al., 2009) and ventral furrow formation (Martin et al., 2010). In addition to these accessible tissues, laser ablation has been used in a subcutaneous manner demonstrating the role of discrete cell populations in effecting tissue migration during tracheal morphogenesis (Caussinus et al., 2008). An alternative to laser ablation is the use of genetic ablation to selectively kill cells at different locations in the hindgut, creating a lesion. This has been successfully undertaken

through the ectopic expression of exogenous factors which drive cell death such as the ricin A (Hidalgo et al., 1995) and diphtheria toxins (Lin et al., 1995) or pro-apoptotic genes such as *reaper* (*rpr*) and *head involution defective* (*hid*) (Grether et al., 1995). While theoretically possible, both techniques have their limitations. Due to the inaccessible location of the hindgut, in the centre of the embryo, it is unlikely that laser ablation would be a practical tool to undertake this type of study. Furthermore, genetic ablation relies on appropriate hindgut region-specific Gal4 drivers to create spatially controlled lesions. Identifying, or generating, a line with the correct specificity may provide challenging. Despite these potential experimental options the hypothesised strain placed on the hindgut is likely to be caused by cell rearrangement and changes in cell shape. These events are unlikely to accrue the type of stored energy observed during germband extension, ventral furrow formation or tracheal morphogenesis. Therefore, hindgut tissue strain may not be identifiable using laser or genetic ablation.

An additional method used to examine forces at a molecular level is Atomic Force Microscopy (AFM). This is a multipurpose technique used to quantify the interactions and relative movement of closely associated molecules (reviewed in, Lal and John, 1994). The relative movement of objects can be used to further understand the inherent strains and stresses in biological systems. Current AFM set-ups require physical contact with the sample limiting the *in vivo* application of this technique to the hindgut. There are, however, methods being developed in the Matsuno lab to allow the dissection and *ex vivo* examination of the embryonic hindgut (Ryo Hatori, Tokyo University of Science, personal communication). This may provide accessible biological material that may be assessed by AFM. Examination of wildtype, JAKSTAT, *FasIII* and *vari* mutant alleles may provide a quantitative measurement of the resistance to strain provided by asymmetrically-distributed lateral FasIII.

7.4.2 Maintaining or tightening curvature?

In silico models are an additional tool for assessing *in vivo* processes where direct experimentation is technically difficult. Continuing work in the lab has developed a two-dimensional computer model for hindgut curvature. To summarise, the *in silico* model

accepts the premise that biological tissues possess similar properties to fluids, including a requirement to reach a surface tension equilibrium (Beysens et al., 2000) following the Differential Adhesion Hypothesis (DAH) (Steinberg, 1963). Based on assumptions of the interplay between surface tension and adhesion (Manning et al., 2010, reviewed in, Lecuit and Lenne, 2007) the model was devised to examine the effect on the morphology of an already formed curve in response to an increase in local cell adhesion, caused by lateral FasIII. Simulations using this model suggest that the homophilic adhesive properties of FasIII may operate to actively tighten the hindgut curve (Fig7.3) (video 7.1) (Joseph Barry, EMBL Heidelberg, personal communication).

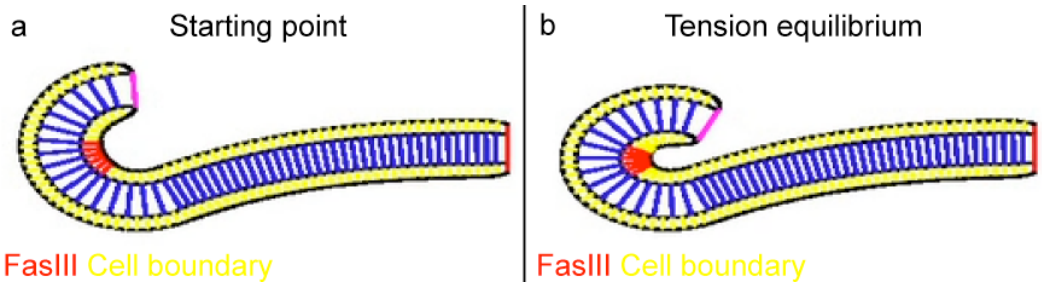

Figure 7.3: *In silico* 2-D model of the effect of FasIII on hindgut curvature. Data and model courtesy of Joseph Barry.
(a) The model is established a pre-formed curve. (b) Based on set parameters for energy, adhesion and surface tension the model is allowed to reach its minimal energy state of tension equilibrium. Based on the input parameters this results in a tightening of the pre-formed curve.

Video 7,1: *In silico* 2-D model of the effect of FasIII on hindgut curvature. Data and model courtesy of Joseph Barry.
A video showing the sequential steps required for the model to move from the defined start point to its minimal energy state of tension equilibrium.

This analysis suggests that alteration of intercellular adhesion may be sufficient to modulate hindgut curvature without the requirement of addition factors. However, this contradicts the interpretation of the current biological data presented in this thesis, in which FasIII is hypothesised to passively maintain curvature. It is possible that failure to tighten the curve may have been misinterpreted as a failure to maintain curvature. Regardless, the generation of *in silico* simulations has shed further light on the possible

function of FasIII in the hindgut. Further *in vivo* experimentation is required, however, to differentiate between the two models.

Recent work from the Matsuno lab has developed an *in silco* model to examine hindgut rotation (Taniguchi et al., 2011). The formula used to generate this model contains a component accounting for tissue surface tension indicating that surface tension may also have a role in hindgut rotation. As the model described above is two dimensional it will not be possible to examine the role of asymmetric FasIII on rotation using it in its current form. However, it would be of interest to examine, in the Matsuno model, how asymmetric FasIII lateralistaion modulates DE-cad mediated rotation.

7.4.3 Additional roles for JAK/STAT signalling and homophilic Ig adhesion molecules

Given the apparent widespread loss of FasIII in the embryo, following the loss of JAK/STAT signalling, it is likely that JAK/STAT control of FasIII may play a role in other processes. In the embryo the JAK/STAT pathway has roles in the morphogenesis of the foregut (Johansen et al., 2003a, Li et al., 2003, Josten et al., 2004), tracheal pits (Binari and Perrimon, 1994, Hou et al., 1996, Li et al., 2003), posterior spiracles (Brown et al., 2001, Lovegrove et al., 2006) and during germband extension (Bertet et al., 2009). FasIII also appears abundant within these regions. It would be of interest to investigate if FasIII is lateralised in a JAK/STAT-dependent manner in these locations and if loss of *FasIII* causes any morphological defects in these structures.

Lastly, the asymmetry of the adhesion molecule PECAM-1 in the mouse aorta is an intriguing observation. To further characterise the mouse aorta as a system analogous to the *Drosophila* embryonic hindgut, a continuation of this work should establish if PECAM-1 is downstream of the mammalian JAK/STAT pathway. While some evidence from an *in vitro* endothelial cell model indicates that JAK/STAT signalling can affect PECAM-1 levels, albeit negatively, (Neria et al., 2007) conflicting data also suggests that PECAM-1 can regulate JAK/STAT signalling. In *in vivo* mouse models PECAM-1 physically interacts with, and positively regulates phosphorylation of, STAT3 and

STAT5 (Ilan et al., 2001, Carrithers et al., 2005). Ultimately, the aorta-specific characterisation of the interactions between JAK/STAT signalling and PECAM-1, as well as an understanding the role of PECAM-1 in maintaining aorta structure, may lead to a better understanding of the extent to which localised adhesion is conserved in maintaining epithelial structures.

8 References

1. Agaisse, H., Petersen, U. M., Boutros, M., Mathey-Prevot, B. & Perrimon, N. Signaling role of hemocytes in Drosophila JAK/STAT-dependent response to septic injury. *Dev Cell* **5**, 441-450 (2003).
2. Ainsworth, C., Wan, S. & Skaer, H. Coordinating cell fate and morphogenesis in Drosophila renal tubules. *Philos Trans R Soc Lond B Biol Sci* **355**, 931-937 (2000).
3. Aldaz, S., Escudero, L. M. & Freeman, M. Live imaging of Drosophila imaginal disc development. *Proc Natl Acad Sci U S A* **107**, 14217-14222 (2010).
4. Ando, R., Hama, H., Yamamoto-Hino, M., Mizuno, H. & Miyawaki, A. An optical marker based on the UV-induced green-to-red photoconversion of a fluorescent protein. *Proc Natl Acad Sci U S A* **99**, 12651-12656 (2002).
5. Ara, T. & Declerck, Y. A. Interleukin-6 in bone metastasis and cancer progression. *Eur J Cancer* **46**, 1223-1231 (2010).
6. Arbouzova, N. I., Bach, E. A. & Zeidler, M. P. Ken & barbie selectively regulates the expression of a subset of Jak/STAT pathway target genes. *Curr Biol* **16**, 80-88 (2006).
7. Arbouzova, N. I. & Zeidler, M. P. JAK/STAT signalling in Drosophila: insights into conserved regulatory and cellular functions. *Development* **133**, 2605-2616 (2006).
8. Assemat, E., Bazellieres, E., Pallesi-Pocachard, E., Le Bivic, A. & Massey-Harroche, D. Polarity complex proteins. *Biochim Biophys Acta* **1778**, 614-630 (2008).
9. Azam, M. et al. Interleukin-3 signals through multiple isoforms of Stat5. *EMBO J* **14**, 1402-1411 (1995).
10. Bach, E. A. et al. GFP reporters detect the activation of the Drosophila JAK/STAT pathway in vivo. *Gene Expr Patterns* **7**, 323-331 (2007).
11. Bach, E. A., Vincent, S., Zeidler, M. P. & Perrimon, N. A sensitized genetic screen to identify novel regulators and components of the Drosophila janus kinase/signal transducer and activator of transcription pathway. *Genetics* **165**, 1149-1166 (2003).
12. Bachmann, A., Draga, M., Grawe, F. & Knust, E. On the role of the MAGUK proteins encoded by Drosophila varicose during embryonic and postembryonic

development. *BMC Dev Biol* **8**, 55 (2008).

13. Baeg, G. H., Lin, X., Khare, N., Baumgartner, S. & Perrimon, N. Heparan sulfate proteoglycans are critical for the organization of the extracellular distribution of Wingless. *Development* **128**, 87-94 (2001).
14. Baeg, G. H., Zhou, R. & Perrimon, N. Genome-wide RNAi analysis of JAK/STAT signaling components in Drosophila. *Genes Dev* **19**, 1861-1870 (2005).
15. Baker, N. E. Transcription of the segment-polarity gene wingless in the imaginal discs of Drosophila, and the phenotype of a pupal-lethal wg mutation. *Development* **102**, 489-497 (1988).
16. Baksa, K., Parke, T., Dobens, L. L. & Dearolf, C. R. The Drosophila STAT protein, stat92E, regulates follicle cell differentiation during oogenesis. *Dev Biol* **243**, 166-175 (2002).
17. Banerjee, S., Sousa, A. D. & Bhat, M. A. Organization and function of septate junctions: an evolutionary perspective. *Cell Biochem Biophys* **46**, 65-77 (2006).
18. Baonza, A., de Celis, J. F. & Garcia-Bellido, A. Relationships between extramacrochaetae and Notch signalling in Drosophila wing development. *Development* **127**, 2383-2393 (2000).
19. Barolo, S., Castro, B. & Posakony, J. W. New Drosophila transgenic reporters: insulated P-element vectors expressing fast-maturing RFP. *Biotechniques* **36**, 436-40, 442 (2004).
20. Baumgartner, S. et al. A Drosophila neurexin is required for septate junction and blood-nerve barrier formation and function. *Cell* **87**, 1059-1068 (1996).
21. Beccari, S., Teixeira, L. & Rorth, P. The JAK/STAT pathway is required for border cell migration during Drosophila oogenesis. *Mech Dev* **111**, 115-123 (2002).
22. Behr, M., Riedel, D. & Schuh, R. The claudin-like megatrachea is essential in septate junctions for the epithelial barrier function in Drosophila. *Dev Cell* **5**, 611-620 (2003).
23. Beitel, G. J. & Krasnow, M. A. Genetic control of epithelial tube size in the Drosophila tracheal system. *Development* **127**, 3271-3282 (2000).
24. Belenkaya, T. Y. et al. Drosophila Dpp morphogen movement is independent of dynamin-mediated endocytosis but regulated by the glypican members of heparan

sulfate proteoglycans. *Cell* **119**, 231-244 (2004).

25. Bellen, H. J. et al. The Drosophila gene disruption project: progress using transposons with distinctive site specificities. *Genetics* **188**, 731-743 (2011).
26. Bellen, H. J. et al. The BDGP gene disruption project: single transposon insertions associated with 40% of Drosophila genes. *Genetics* **167**, 761-781 (2004).
27. Bertet, C., Rauzi, M. & Lecuit, T. Repression of Wasp by JAK/STAT signalling inhibits medial actomyosin network assembly and apical cell constriction in intercalating epithelial cells. *Development* **136**, 4199-4212 (2009).
28. Betz, A., Lampen, N., Martinek, S., Young, M. W. & Darnell, J. E. J. A Drosophila PIAS homologue negatively regulates stat92E. *Proc Natl Acad Sci U S A* **98**, 9563-9568 (2001).
29. Betz, A., Ryoo, H. D., Steller, H. & Darnell, J. E. STAT92E is a positive regulator of Drosophila inhibitor of apoptosis 1 (DIAP/1) and protects against radiation-induced apoptosis. *Proceedings of the National Academy of Sciences* **105**, 13805 (2008).
30. Beysens, D. A., Forgacs, G. & Glazier, J. A. Cell sorting is analogous to phase ordering in fluids. *Proc Natl Acad Sci U S A* **97**, 9467-9471 (2000).
31. Bina, S., Wright, V. M., Fisher, K. H., Milo, M. & Zeidler, M. P. Transcriptional targets of Drosophila JAK/STAT pathway signalling as effectors of haematopoietic tumour formation. *EMBO Rep* **11**, 201-207 (2010).
32. Binari, R. & Perrimon, N. Stripe-specific regulation of pair-rule genes by hopscotch, a putative Jak family tyrosine kinase in Drosophila. *Genes Dev* **8**, 300-312 (1994).
33. Blair, S. S. Cell signaling: wingless and glypicans together again. *Curr Biol* **15**, R92-4 (2005).
34. Blankenship, J. T., Backovic, S. T., Sanny, J. S., Weitz, O. & Zallen, J. A. Multicellular rosette formation links planar cell polarity to tissue morphogenesis. *Dev Cell* **11**, 459-470 (2006).
35. Bourouis, M. & Jarry, B. Vectors containing a prokaryotic dihydrofolate reductase gene transform Drosophila cells to methotrexate-resistance. *EMBO J* **2**, 1099-1104 (1983).

36. Bowerman, B. Embryonic polarity: protein stability in asymmetric cell division. *Curr Biol* **10**, R637-41 (2000).
37. Brand, A. H. & Perrimon, N. Targeted gene expression as a means of altering cell fates and generating dominant phenotypes. *Development* **118**, 401-415 (1993).
38. Bridges, C. B., Morgan, T. H. & Washington, C. I. o. The third-chromosome group of mutant characters of Drosophila melanogaster. (1923).
39. Broeck, J. V. Insect G protein-coupled receptors and signal transduction. *Arch Insect Biochem Physiol* **48**, 1-12 (2001).
40. Bronner, G. et al. Sp1/egr-like zinc-finger protein required for endoderm specification and germ-layer formation in Drosophila. *Nature* **369**, 664-668 (1994).
41. Brown, S., Hu, N. & Hombria, J. C. Identification of the first invertebrate interleukin JAK/STAT receptor, the Drosophila gene domeless. *Curr Biol* **11**, 1700-1705 (2001).
42. Brown, S., Hu, N. & Hombria, J. C. Novel level of signalling control in the JAK/STAT pathway revealed by in situ visualisation of protein-protein interaction during Drosophila development. *Development* **130**, 3077-3084 (2003).
43. Brown, S., Zeidler, M. P. & Hombria, J. E. JAK/STAT signalling in Drosophila controls cell motility during germ cell migration. *Dev Dyn* **235**, 958-966 (2006).
44. Calleja, M., Moreno, E., Pelaz, S. & Morata, G. Visualization of gene expression in living adult Drosophila. *Science* **274**, 252-255 (1996).
45. Callus, B. A. & Mathey-Prevot, B. SOCS36E, a novel Drosophila SOCS protein, suppresses JAK/STAT and EGF-R signalling in the imaginal wing disc. *Oncogene* **21**, 4812-4821 (2002).
46. Campos-Ortega, J. A. & Hartenstein, V. The embryonic development of Drosophila melanogaster. xvii, 405 (1997).
47. Capdevila, J. & Guerrero, I. Targeted expression of the signaling molecule decapentaplegic induces pattern duplications and growth alterations in Drosophila wings. *EMBO J* **13**, 4459-4468 (1994).
48. Carrithers, M. et al. Enhanced susceptibility to endotoxic shock and impaired STAT3 signaling in CD31-deficient mice. *Am J Pathol* **166**, 185-196 (2005).
49. Carroll, S. B. & Scott, M. P. Zygotically active genes that affect the spatial

expression of the fushi tarazu segmentation gene during early Drosophila embryogenesis. *Cell* **45**, 113-126 (1986).

50. Carta, L. et al. Fibrillins 1 and 2 perform partially overlapping functions during aortic development. *J Biol Chem* **281**, 8016-8023 (2006).
51. Castonguay, L. A., Bryant, S. H., Snow, P. M. & Fetrow, J. S. A proposed structural model of domain 1 of fasciclin III neural cell adhesion protein based on an inverse folding algorithm. *Protein Sci* **4**, 472-483 (1995).
52. Caussinus, E., Colombelli, J. & Affolter, M. Tip-cell migration controls stalk-cell intercalation during Drosophila tracheal tube elongation. *Curr Biol* **18**, 1727-1734 (2008).
53. Cavdar Koc, E., Burkhart, W., Blackburn, K., Moseley, A. & Spremulli, L. L. The small subunit of the mammalian mitochondrial ribosome. Identification of the full complement of ribosomal proteins present. *J Biol Chem* **276**, 19363-19374 (2001).
54. Celniker, S. E. et al. Unlocking the secrets of the genome. *Nature* **459**, 927-930 (2009).
55. Chartier, A., Benoit, B. & Simonelig, M. A Drosophila model of oculopharyngeal muscular dystrophy reveals intrinsic toxicity of PABPN1. *EMBO J* **25**, 2253-2262 (2006).
56. Chen, H. W. et al. mom identifies a receptor for the Drosophila JAK/STAT signal transduction pathway and encodes a protein distantly related to the mammalian cytokine receptor family. *Genes Dev* **16**, 388-398 (2002).
57. Chen, Y. & Struhl, G. Dual roles for patched in sequestering and transducing Hedgehog. *Cell* **87**, 553-563 (1996).
58. Chiba, A., Snow, P., Keshishian, H. & Hotta, Y. Fasciclin III as a synaptic target recognition molecule in Drosophila. *Nature* **374**, 166-168 (1995).
59. Clark, I. E. et al. Drosophila pink1 is required for mitochondrial function and interacts genetically with parkin. *Nature* **441**, 1162-1166 (2006).
60. Cohen, G. M. Caspases: the executioners of apoptosis. *Biochem J* **326**, 1-16 (1997).
61. Collas, P. The current state of chromatin immunoprecipitation. *Mol Biotechnol* **45**, 87-100 (2010).
62. Collins, J. L. Taxi wings, a new useful III chromosome mutant in Drosophila

melanogaster. *American Naturalist* 127-136 (1928).

63. Corish, P. & Tyler-Smith, C. Attenuation of green fluorescent protein half-life in mammalian cells. *Protein Eng* **12**, 1035-1040 (1999).
64. Cowan, C. M., Shepherd, D. & Mudher, A. Insights from Drosophila models of Alzheimer's disease. *Biochem Soc Trans* **38**, 988-992 (2010).
65. Cronmiller, C. & Cummings, C. A. The daughterless gene product in Drosophila is a nuclear protein that is broadly expressed throughout the organism during development. *Mech Dev* **42**, 159-169 (1993).
66. Davies, P. F. Overview: temporal and spatial relationships in shear stress-mediated endothelial signalling. *J Vasc Res* **34**, 208-211 (1997).
67. Davis, N. M. et al. The chirality of gut rotation derives from left-right asymmetric changes in the architecture of the dorsal mesentery. *Dev Cell* **15**, 134-145 (2008).
68. Dawson, M. A. et al. JAK2 phosphorylates histone H3Y41 and excludes HP1alpha from chromatin. *Nature* **461**, 819-822 (2009).
69. Devergne, O., Ghiglione, C. & Noselli, S. The endocytic control of JAK/STAT signalling in Drosophila. *J Cell Sci* **120**, 3457-3464 (2007).
70. Dietzl, G. et al. A genome-wide transgenic RNAi library for conditional gene inactivation in Drosophila. *Nature* **448**, 151-156 (2007).
71. Doherty, D., Feger, G., Younger-Shepherd, S., Jan, L. Y. & Jan, Y. N. Delta is a ventral to dorsal signal complementary to Serrate, another Notch ligand, in Drosophila wing formation. *Genes Dev* **10**, 421-434 (1996).
72. Dong, X. et al. ebi regulates epidermal growth factor receptor signaling pathways in Drosophila. *Genes Dev* **13**, 954-965 (1999).
73. Dostert, C. et al. The Jak-STAT signaling pathway is required but not sufficient for the antiviral response of drosophila. *Nat Immunol* **6**, 946-953 (2005).
74. Dubreuil, R., Byers, T. J., Branton, D., Goldstein, L. S. & Kiehart, D. P. Drosophilia spectrin. I. Characterization of the purified protein. *J Cell Biol* **105**, 2095-2102 (1987).
75. Ekengren, S. et al. A humoral stress response in Drosophila. *Curr Biol* **11**, 1479 (2001).
76. Elkins, T., Hortsch, M., Bieber, A. J., Snow, P. M. & Goodman, C. S. Drosophila

fasciclin I is a novel homophilic adhesion molecule that along with fasciclin III can mediate cell sorting. *J Cell Biol* **110**, 1825-1832 (1990).

77. Faivre-Sarrailh, C. et al. Drosophila contactin, a homolog of vertebrate contactin, is required for septate junction organization and paracellular barrier function. *Development* **131**, 4931-4942 (2004).
78. Fehon, R. G., Dawson, I. A. & Artavanis-Tsakonas, S. A Drosophila homologue of membrane-skeleton protein 4.1 is associated with septate junctions and is encoded by the coracle gene. *Development* **120**, 545-557 (1994).
79. Fernandez-Gonzalez, R., Simoes Sde, M., Roper, J. C., Eaton, S. & Zallen, J. A. Myosin II dynamics are regulated by tension in intercalating cells. *Dev Cell* **17**, 736-743 (2009).
80. Ferrus, A., Llamazares, S., de la Pompa, J. L., Tanouye, M. A. & Pongs, O. Genetic analysis of the Shaker gene complex of Drosophila melanogaster. *Genetics* **125**, 383-398 (1990).
81. Firmbach-Kraft, I., Byers, M., Shows, T., Dalla-Favera, R. & Krolewski, J. J. tyk2, prototype of a novel class of non-receptor tyrosine kinase genes. *Oncogene* **5**, 1329-1336 (1990).
82. Fraichard, S., Bouge, A. L., Chauvel, I. & Bouhin, H. Tenectin, a novel extracellular matrix protein expressed during Drosophila melanogaster embryonic development. *Gene Expr Patterns* **6**, 772-776 (2006).
83. Fuss, B. & Hoch, M. Notch signaling controls cell fate specification along the dorsoventral axis of the Drosophila gut. *Curr Biol* **12**, 171-179 (2002).
84. Fuss, B., Josten, F., Feix, M. & Hoch, M. Cell movements controlled by the Notch signalling cascade during foregut development in Drosophila. *Development* **131**, 1587-1595 (2004).
85. Fuss, B. et al. Control of endoreduplication domains in the Drosophila gut by the knirps and knirps-related genes. *Mech Dev* **100**, 15-23 (2001).
86. Gee, K., Guzzo, C., Che Mat, N. F., Ma, W. & Kumar, A. The IL-12 family of cytokines in infection, inflammation and autoimmune disorders. *Inflamm Allergy Drug Targets* **8**, 40-52 (2009).
87. Ghanim, M. & White, K. P. Genotyping method to screen individual Drosophila

embryos prior to RNA extraction. *Biotechniques* **41**, 414, 416, 418 (2006).

88. Ghiglione, C. et al. The Drosophila cytokine receptor Domeless controls border cell migration and epithelial polarization during oogenesis. *Development* **129**, 5437-5447 (2002).
89. Gilbert, M. M., Weaver, B. K., Gergen, J. P. & Reich, N. C. A novel functional activator of the Drosophila JAK/STAT pathway, unpaired2, is revealed by an in vivo reporter of pathway activation. *Mech Dev* **122**, 939-948 (2005).
90. Gonczy, P. & DiNardo, S. The germ line regulates somatic cyst cell proliferation and fate during Drosophila spermatogenesis. *Development* **122**, 2437-2447 (1996).
91. Goode, S., Melnick, M., Chou, T. B. & Perrimon, N. The neurogenic genes egghead and brainiac define a novel signaling pathway essential for epithelial morphogenesis during Drosophila oogenesis. *Development* **122**, 3863-3879 (1996).
92. Goodrich, L. V. & Strutt, D. Principles of planar polarity in animal development. *Development* **138**, 1877-1892 (2011).
93. Green, R. B., Hatini, V., Johansen, K. A., Liu, X. J. & Lengyel, J. A. Drumstick is a zinc finger protein that antagonizes Lines to control patterning and morphogenesis of the Drosophila hindgut. *Development* **129**, 3645-3656 (2002).
94. Greene, J. C. et al. Mitochondrial pathology and apoptotic muscle degeneration in Drosophila parkin mutants. *Proc Natl Acad Sci U S A* **100**, 4078-4083 (2003).
95. Grether, M. E., Abrams, J. M., Agapite, J., White, K. & Steller, H. The head involution defective gene of Drosophila melanogaster functions in programmed cell death. *Genes Dev* **9**, 1694-1708 (1995).
96. Grote, K., Luchtefeld, M. & Schieffer, B. JANUS under stress--role of JAK/STAT signaling pathway in vascular diseases. *Vascul Pharmacol* **43**, 357-363 (2005).
97. Grueber, W. B. et al. Projections of Drosophila multidendritic neurons in the central nervous system: links with peripheral dendrite morphology. *Development* **134**, 55-64 (2007).
98. Guarente, L., Yocum, R. R. & Gifford, P. A GAL10-CYC1 hybrid yeast promoter identifies the GAL4 regulatory region as an upstream site. *Proc Natl Acad Sci U S A* **79**, 7410-7414 (1982).
99. Halder, G., Callaerts, P. & Gehring, W. J. Induction of ectopic eyes by targeted

expression of the eyeless gene in Drosophila. *Science* **267**, 1788-1792 (1995).

100. Hamada, H., Meno, C., Watanabe, D. & Saijoh, Y. Establishment of vertebrate left-right asymmetry. *Nat Rev Genet* **3**, 103-113 (2002).
101. Han, C., Belenkaya, T. Y., Wang, B. & Lin, X. Drosophila glypicans control the cell-to-cell movement of Hedgehog by a dynamin-independent process. *Development* **131**, 601-611 (2004).
102. Hao, I., Green, R. B., Dunaevsky, O., Lengyel, J. A. & Rauskolb, C. The odd-skipped family of zinc finger genes promotes Drosophila leg segmentation. *Dev Biol* **263**, 282-295 (2003).
103. Harrison, D. A., Binari, R., Nahreini, T. S., Gilman, M. & Perrimon, N. Activation of a Drosophila Janus kinase (JAK) causes hematopoietic neoplasia and developmental defects. *EMBO J* **14**, 2857-2865 (1995).
104. Harrison, D. A., McCoon, P. E., Binari, R., Gilman, M. & Perrimon, N. Drosophila unpaired encodes a secreted protein that activates the JAK signaling pathway. *Genes Dev* **12**, 3252-3263 (1998).
105. Hartenstein, V. Atlas of drosophila development. (1993).
106. Hatini, V., Green, R. B., Lengyel, J. A., Bray, S. J. & Dinardo, S. The Drumstick/Lines/Bowl regulatory pathway links antagonistic Hedgehog and Wingless signaling inputs to epidermal cell differentiation. *Genes Dev* **19**, 709-718 (2005).
107. Hayashi, T. & Murakami, R. Left-right asymmetry in Drosophila melanogaster gut development. *Dev Growth Differ* **43**, 239-246 (2001).
108. He, J. & Zhang, Y. Janus kinase 2: an epigenetic 'writer' that activates leukemogenic genes. *J Mol Cell Biol* **2**, 231-233 (2010).
109. Hendzel, M. J. et al. Mitosis-specific phosphorylation of histone H3 initiates primarily within pericentromeric heterochromatin during G2 and spreads in an ordered fashion coincident with mitotic chromosome condensation. *Chromosoma* **106**, 348-360 (1997).
110. Henriksen, M. A., Betz, A., Fuccillo, M. V. & Darnell, J. E. J. Negative regulation of STAT92E by an N-terminally truncated STAT protein derived from an alternative promoter site. *Genes Dev* **16**, 2379-2389 (2002).

111. Hidalgo, A., Urban, J. & Brand, A. H. Targeted ablation of glia disrupts axon tract formation in the Drosophila CNS. *Development* **121**, 3703-3712 (1995).
112. Hijazi, A. et al. boudin is required for septate junction organisation in Drosophila and codes for a diffusible protein of the Ly6 superfamily. *Development* **136**, 2199-2209 (2009).
113. Hoch, M. & Pankratz, M. J. Control of gut development by fork head and cell signaling molecules in Drosophila. *Mech Dev* **58**, 3-14 (1996).
114. Hombria, J. C., Brown, S., Hader, S. & Zeidler, M. P. Characterisation of Upd2, a Drosophila JAK/STAT pathway ligand. *Dev Biol* **288**, 420-433 (2005).
115. Hombria, J. C. & Sotillos, S. JAK/STAT signalling: STAT cannot play with Ken and Barbie. *Curr Biol* **16**, R98-100 (2006).
116. Horne-Badovinac, S. et al. Positional cloning of heart and soul reveals multiple roles for PKC lambda in zebrafish organogenesis. *Curr Biol* **11**, 1492-1502 (2001).
117. Horne-Badovinac, S., Rebagliati, M. & Stainier, D. Y. A cellular framework for gut-looping morphogenesis in zebrafish. *Science* **302**, 662-665 (2003).
118. Hou, X. S., Melnick, M. B. & Perrimon, N. Marelle acts downstream of the Drosophila HOP/JAK kinase and encodes a protein similar to the mammalian STATs. *Cell* **84**, 411-419 (1996).
119. Hozumi, S. et al. Head region of unconventional myosin I family members is responsible for the organ-specificity of their roles in left-right polarity in Drosophila. *Dev Dyn* **237**, 3528-3537 (2008).
120. Hozumi, S. et al. An unconventional myosin in Drosophila reverses the default handedness in visceral organs. *Nature* **440**, 798-802 (2006).
121. Ilan, N. et al. Pecam-1 is a modulator of stat family member phosphorylation and localization: lessons from a transgenic mouse. *Dev Biol* **232**, 219-232 (2001).
122. Improta, T. et al. Transcription factor ISGF-3 formation requires phosphorylated Stat91 protein, but Stat113 protein is phosphorylated independently of Stat91 protein. *Proc Natl Acad Sci U S A* **91**, 4776-4780 (1994).
123. Itasaki, N., Nakamura, H., Sumida, H. & Yasuda, M. Actin bundles on the right side in the caudal part of the heart tube play a role in dextro-looping in the embryonic chick heart. *Anat Embryol (Berl)* **183**, 29-39 (1991).

124. Iwaki, D. D., Johansen, K. A., Singer, J. B. & Lengyel, J. A. drumstick, bowl, and lines are required for patterning and cell rearrangement in the Drosophila embryonic hindgut. *Dev Biol* **240**, 611-626 (2001).
125. Iwaki, D. D. & Lengyel, J. A. A Delta-Notch signaling border regulated by Engrailed/Invected repression specifies boundary cells in the Drosophila hindgut. *Mech Dev* **114**, 71-84 (2002).
126. Johansen, K. A., Green, R. B., Iwaki, D. D., Hernandez, J. B. & Lengyel, J. A. The Drm-Bowl-Lin relief-of-repression hierarchy controls fore- and hindgut patterning and morphogenesis. *Mech Dev* **120**, 1139-1151 (2003).
127. Johansen, K. A., Iwaki, D. D. & Lengyel, J. A. Localized JAK/STAT signaling is required for oriented cell rearrangement in a tubular epithelium. *Development* **130**, 135-145 (2003).
128. Johnson, A. N., Mokalled, M. H., Haden, T. N. & Olson, E. N. JAK/Stat signaling regulates heart precursor diversification in Drosophila. *Development* **138**, 4627-4638 (2011).
129. Johnston, L. A., Prober, D. A., Edgar, B. A., Eisenman, R. N. & Gallant, P. Drosophila myc regulates cellular growth during development. *Cell* **98**, 779-790 (1999).
130. Josten, F., Fuss, B., Feix, M., Meissner, T. & Hoch, M. Cooperation of JAK/STAT and Notch signaling in the Drosophila foregut. *Dev Biol* **267**, 181-189 (2004).
131. Justice, R. W., Zilian, O., Woods, D. F., Noll, M. & Bryant, P. J. The Drosophila tumor suppressor gene warts encodes a homolog of human myotonic dystrophy kinase and is required for the control of cell shape and proliferation. *Genes Dev* **9**, 534-546 (1995).
132. Kallio, J. et al. Eye transformer is a negative regulator of Drosophila JAK/STAT signaling. *FASEB J* **24**, 4467-4479 (2010).
133. Kamakura, S. et al. Hes binding to STAT3 mediates crosstalk between Notch and JAK-STAT signalling. *Nat Cell Biol* **6**, 547-554 (2004).
134. Karsten, P., Hader, S. & Zeidler, M. P. Cloning and expression of Drosophila SOCS36E and its potential regulation by the JAK/STAT pathway. *Mech Dev* **117**, 343-346 (2002).

135. Kawata, T. STAT signaling in Dictyostelium development. *Dev Growth Differ* **53**, 548-557 (2011).
136. Khare, N. & Baumgartner, S. Dally-like protein, a new Drosophila glypican with expression overlapping with wingless. *Mech Dev* **99**, 199-202 (2000).
137. Kiger, A. A., Jones, D. L., Schulz, C., Rogers, M. B. & Fuller, M. T. Stem cell self-renewal specified by JAK-STAT activation in response to a support cell cue. *Science* **294**, 2542-2545 (2001).
138. Kispert, A., Herrmann, B. G., Leptin, M. & Reuter, R. Homologs of the mouse Brachyury gene are involved in the specification of posterior terminal structures in Drosophila, Tribolium, and Locusta. *Genes Dev* **8**, 2137-2150 (1994).
139. Klar, A. J. & Halvorson, H. O. Studies on the positive regulatory gene, GAL4, in regulation of galactose catabolic enzymes in Saccharomyces cerevisiae. *Mol Gen Genet* **135**, 203-212 (1974).
140. Klemenz, R., Weber, U. & Gehring, W. J. The white gene as a marker in a new P-element vector for gene transfer in Drosophila. *Nucleic Acids Res* **15**, 3947-3959 (1987).
141. Kose, H., Rose, D., Zhu, X. & Chiba, A. Homophilic synaptic target recognition mediated by immunoglobulin-like cell adhesion molecule Fasciclin III. *Development* **124**, 4143-4152 (1997).
142. Koster, M. & Hauser, H. Dynamic redistribution of STAT1 protein in IFN signaling visualized by GFP fusion proteins. *Eur J Biochem* **260**, 137-144 (1999).
143. Kurpios, N. A. et al. The direction of gut looping is established by changes in the extracellular matrix and in cell:cell adhesion. *Proc Natl Acad Sci U S A* **105**, 8499-8506 (2008).
144. Kwon, E. J. et al. Transcriptional regulation of the Drosophila raf proto-oncogene by Drosophila STAT during development and in immune response. *J Biol Chem* **275**, 19824-19830 (2000).
145. Lal, R. & John, S. A. Biological applications of atomic force microscopy. *Am J Physiol* **266**, C1-21 (1994).
146. Langevin, J. et al. Drosophila exocyst components Sec5, Sec6, and Sec15 regulate DE-Cadherin trafficking from recycling endosomes to the plasma membrane. *Dev*

Cell **9**, 365-376 (2005).

147. Laprise, P. et al. Yurt, Coracle, Neurexin IV and the Na(+),K(+)-ATPase form a novel group of epithelial polarity proteins. *Nature* **459**, 1141-1145 (2009).
148. Laprise, P. et al. Epithelial polarity proteins regulate Drosophila tracheal tube size in parallel to the luminal matrix pathway. *Curr Biol* **20**, 55-61 (2010).
149. Latacha, K. S. et al. Role of actin polymerization in bending of the early heart tube. *Dev Dyn* **233**, 1272-1286 (2005).
150. Laval, M., Bel, C. & Faivre-Sarrailh, C. The lateral mobility of cell adhesion molecules is highly restricted at septate junctions in Drosophila. *BMC Cell Biol* **9**, 38 (2008).
151. Lecuit, T. & Lenne, P. F. Cell surface mechanics and the control of cell shape, tissue patterns and morphogenesis. *Nat Rev Mol Cell Biol* **8**, 633-644 (2007).
152. Lehoux, S., Castier, Y. & Tedgui, A. Molecular mechanisms of the vascular responses to haemodynamic forces. *J Intern Med* **259**, 381-392 (2006).
153. Lengyel, J. A. & Iwaki, D. D. It takes guts: the Drosophila hindgut as a model system for organogenesis. *Dev Biol* **243**, 1-19 (2002).
154. Li, D. Y. et al. Elastin is an essential determinant of arterial morphogenesis. *Nature* **393**, 276-280 (1998).
155. Li, J. et al. Patterns and functions of STAT activation during Drosophila embryogenesis. *Mech Dev* **120**, 1455-1468 (2003).
156. Li, J. & Li, W. X. Drosophila gain-of-function mutant RTK torso triggers ectopic Dpp and STAT signaling. *Genetics* **164**, 247-258 (2003).
157. Lin, D. M., Auld, V. J. & Goodman, C. S. Targeted neuronal cell ablation in the Drosophila embryo: pathfinding by follower growth cones in the absence of pioneers. *Neuron* **14**, 707-715 (1995).
158. Linask, K. K. & Vanauker, M. A role for the cytoskeleton in heart looping. *ScientificWorldJournal* **7**, 280-298 (2007).
159. Liu, X., Kiss, I. & Lengyel, J. A. Identification of genes controlling malpighian tubule and other epithelial morphogenesis in Drosophila melanogaster. *Genetics* **151**, 685-695 (1999).
160. Loren, C. E. et al. A crucial role for the Anaplastic lymphoma kinase receptor

tyrosine kinase in gut development in Drosophila melanogaster. *EMBO Rep* **4**, 781-786 (2003).

161. Lovegrove, B. et al. Coordinated control of cell adhesion, polarity, and cytoskeleton underlies Hox-induced organogenesis in Drosophila. *Curr Biol* **16**, 2206-2216 (2006).
162. Lu, W. et al. Cellular nonmuscle myosins NMHC-IIA and NMHC-IIB and vertebrate heart looping. *Dev Dyn* **237**, 3577-3590 (2008).
163. Luschnig, S., Batz, T., Armbruster, K. & Krasnow, M. A. serpentine and vermiform encode matrix proteins with chitin binding and deacetylation domains that limit tracheal tube length in Drosophila. *Curr Biol* **16**, 186-194 (2006).
164. Maeda, R. et al. Roles of single-minded in the left-right asymmetric development of the Drosophila embryonic gut. *Mech Dev* **124**, 204-217 (2007).
165. Makki, R. et al. A short receptor downregulates JAK/STAT signalling to control the Drosophila cellular immune response. *PLoS Biol* **8**, e1000441 (2010).
166. Manner, J. Cardiac looping in the chick embryo: a morphological review with special reference to terminological and biomechanical aspects of the looping process. *Anat Rec* **259**, 248-262 (2000).
167. Manning, A. & McLachlan, J. C. Looping of chick embryo hearts in vitro. *J Anat* **168**, 257-263 (1990).
168. Manning, M. L., Foty, R. A., Steinberg, M. S. & Schoetz, E. M. Coaction of intercellular adhesion and cortical tension specifies tissue surface tension. *Proc Natl Acad Sci U S A* **107**, 12517-12522 (2010).
169. Marigo, V., Davey, R. A., Zuo, Y., Cunningham, J. M. & Tabin, C. J. Biochemical evidence that patched is the Hedgehog receptor. *Nature* **384**, 176-179 (1996).
170. Martin, A. C., Gelbart, M., Fernandez-Gonzalez, R., Kaschube, M. & Wieschaus, E. F. Integration of contractile forces during tissue invagination. *J Cell Biol* **188**, 735-749 (2010).
171. Miller, A. S., Cottam, D. M. & Milner, M. J. Cell-cell and cell-substrate adhesion in cultured Drosophila imaginal disc cells. *In Vitro Cell Dev Biol Anim* **36**, 180-187 (2000).
172. Miyagi, C. et al. STAT3 noncell-autonomously controls planar cell polarity during

zebrafish convergence and extension. *J Cell Biol* **166**, 975-981 (2004).

173. Mohler, W. A. & Blau, H. M. Gene expression and cell fusion analyzed by lacZ complementation in mammalian cells. *Proc Natl Acad Sci U S A* **93**, 12423-12427 (1996).
174. Montell, D. J., Rorth, P. & Spradling, A. C. slow border cells, a locus required for a developmentally regulated cell migration during oogenesis, encodes Drosophila C/EBP. *Cell* **71**, 51-62 (1992).
175. Morata, G., Macias, A., Urquia, N. & Gonzalez-Reyes, A. Homoeotic genes. *Semin Cell Biol* **1**, 219-227 (1990).
176. Morgan, D. et al. Inversin, a novel gene in the vertebrate left-right axis pathway, is partially deleted in the inv mouse. *Nat Genet* **20**, 149-156 (1998).
177. Morgan, N. S., Heintzelman, M. B. & Mooseker, M. S. Characterization of myosin-IA and myosin-IB, two unconventional myosins associated with the Drosophila brush border cytoskeleton. *Dev Biol* **172**, 51-71 (1995).
178. Morgan, N. S., Skovronsky, D. M., Artavanis-Tsakonas, S. & Mooseker, M. S. The molecular cloning and characterization of Drosophila melanogaster myosin-IA and myosin-IB. *J Mol Biol* **239**, 347-356 (1994).
179. Morgan, T. H. SEX LIMITED INHERITANCE IN DROSOPHILA. *Science* **32**, 120-122 (1910).
180. Moyer, K. E. & Jacobs, J. R. Varicose: a MAGUK required for the maturation and function of Drosophila septate junctions. *BMC Dev Biol* **8**, 99 (2008).
181. Mukherjee, T., Hombría, J. C. G. & Zeidler, M. P. Opposing roles for Drosophila JAK/STAT signalling during cellular proliferation. *Oncogene* **24**, 2503-2511 (2005).
182. Muller, H. J. Types of visible variations induced by X-rays inDrosophila. *Journal of Genetics* **22**, 299-334 (1930).
183. Muller, J. K., Prather, D. R. & Nascone-Yoder, N. M. Left-right asymmetric morphogenesis in the Xenopus digestive system. *Dev Dyn* **228**, 672-682 (2003).
184. Muller, P., Kuttenkeuler, D., Gesellchen, V., Zeidler, M. P. & Boutros, M. Identification of JAK/STAT signalling components by genome-wide RNA interference. *Nature* **436**, 871-875 (2005).

185. Nagafuchi, A., Shirayoshi, Y., Okazaki, K., Yasuda, K. & Takeichi, M. Transformation of cell adhesion properties by exogenously introduced E-cadherin cDNA. *Nature* **329**, 341-343 (1987).
186. Nakato, H., Futch, T. A. & Selleck, S. B. The division abnormally delayed (dally) gene: a putative integral membrane proteoglycan required for cell division patterning during postembryonic development of the nervous system in Drosophila. *Development* **121**, 3687-3702 (1995).
187. Nelson, K. S., Furuse, M. & Beitel, G. J. The Drosophila Claudin Kune-kune is required for septate junction organization and tracheal tube size control. *Genetics* **185**, 831-839 (2010).
188. Neria, F. et al. Mechanisms of endothelial cell protection by blockade of the JAK2 pathway. *Am J Physiol Cell Physiol* **292**, C1123-31 (2007).
189. Niewiadomska, P., Godt, D. & Tepass, U. DE-Cadherin is required for intercellular motility during Drosophila oogenesis. *J Cell Biol* **144**, 533-547 (1999).
190. Noordermeer, J., Klingensmith, J., Perrimon, N. & Nusse, R. dishevelled and armadillo act in the wingless signalling pathway in Drosophila. *Nature* **367**, 80-83 (1994).
191. Nusslein-Volhard, C. & Wieschaus, E. Mutations affecting segment number and polarity in Drosophila. *Nature* **287**, 795-801 (1980).
192. Oda, H., Uemura, T., Harada, Y., Iwai, Y. & Takeichi, M. A Drosophila homolog of cadherin associated with armadillo and essential for embryonic cell-cell adhesion. *Dev Biol* **165**, 716-726 (1994).
193. Oshima, K. & Fehon, R. G. Analysis of protein dynamics within the septate junction reveals a highly stable core protein complex that does not include the basolateral polarity protein Discs large. *J Cell Sci* **124**, 2861-2871 (2011).
194. Park, J. et al. Mitochondrial dysfunction in Drosophila PINK1 mutants is complemented by parkin. *Nature* **441**, 1157-1161 (2006).
195. Parnas, D., Haghighi, A. P., Fetter, R. D., Kim, S. W. & Goodman, C. S. Regulation of postsynaptic structure and protein localization by the Rho-type guanine nucleotide exchange factor dPix. *Neuron* **32**, 415-424 (2001).
196. Patel, N. H. et al. Expression of engrailed proteins in arthropods, annelids, and

chordates. *Cell* **58**, 955-968 (1989).

197. Patel, N. H., Snow, P. M. & Goodman, C. S. Characterization and cloning of fasciclin III: a glycoprotein expressed on a subset of neurons and axon pathways in Drosophila. *Cell* **48**, 975-988 (1987).
198. Paul, S. M., Ternet, M., Salvaterra, P. M. & Beitel, G. J. The Na+/K+ ATPase is required for septate junction function and epithelial tube-size control in the Drosophila tracheal system. *Development* **130**, 4963-4974 (2003).
199. Pelletier, S., Duhamel, F., Coulombe, P., Popoff, M. R. & Meloche, S. Rho family GTPases are required for activation of Jak/STAT signaling by G protein-coupled receptors. *Mol Cell Biol* **23**, 1316-1333 (2003).
200. Polesello, C., Roch, F., Gobert, V., Haenlin, M. & Waltzer, L. Modeling cancers in Drosophila. *Prog Mol Biol Transl Sci* **100**, 51-82 (2011).
201. Privratsky, J. R., Newman, D. K. & Newman, P. J. PECAM-1: conflicts of interest in inflammation. *Life Sci* **87**, 69-82 (2010).
202. Quelle, F. W. et al. Cloning of murine Stat6 and human Stat6, Stat proteins that are tyrosine phosphorylated in responses to IL-4 and IL-3 but are not required for mitogenesis. *Mol Cell Biol* **15**, 3336-3343 (1995).
203. Quelprud, T. aeroplane, a second chromosome recessive wing mutant in Drosophila melanogaster. *Hereditas* **15**, 97-119 (1931).
204. Raju, T. N. The Nobel chronicles. 1933: Thomas Hunt Morgan (1866-1945). *Lancet* **353**, 157 (1999).
205. Raju, T. N. The Nobel chronicles. 1995: Edward B Lewis (b 1918), Christiane Nusslein-Volhard (b 1942), and Eric Francis Wieschaus (b 1947). *Lancet* **356**, 81 (2000).
206. Riechmann, V. & Ephrussi, A. Axis formation during Drosophila oogenesis. *Curr Opin Genet Dev* **11**, 374-383 (2001).
207. Rivas, M. L., Cobreros, L., Zeidler, M. P. & Hombria, J. C. Plasticity of Drosophila Stat DNA binding shows an evolutionary basis for Stat transcription factor preferences. *EMBO Rep* **9**, 1114-1120 (2008).
208. Rorth, P. Initiating and guiding migration: lessons from border cells. *Trends Cell Biol* **12**, 325-331 (2002).

209. Rorth, P. et al. Systematic gain-of-function genetics in Drosophila. *Development* **125**, 1049-1057 (1998).
210. Rozen, S. & Skaletsky, H. Primer3 on the WWW for general users and for biologist programmers. *Methods Mol Biol* **132**, 365-386 (2000).
211. Sakatsume, M. et al. The Jak kinases differentially associate with the alpha and beta (accessory factor) chains of the interferon gamma receptor to form a functional receptor unit capable of activating STAT transcription factors. *J Biol Chem* **270**, 17528-17534 (1995).
212. San Martin, B. & Bate, M. Hindgut visceral mesoderm requires an ectodermal template for normal development in Drosophila. *Development* **128**, 233-242 (2001).
213. Sanson, B., White, P. & Vincent, J. P. Uncoupling cadherin-based adhesion from wingless signalling in Drosophila. *Nature* **383**, 627-630 (1996).
214. Savin, T. et al. On the growth and form of the gut. *Nature* **476**, 57-62 (2011).
215. Schindler, C. & Plumlee, C. Inteferons pen the JAK-STAT pathway. *Semin Cell Dev Biol* **19**, 311-318 (2008).
216. Scita, G. & Di Fiore, P. P. The endocytic matrix. *Nature* **463**, 464-473 (2010).
217. Shampo, M. A. & Kyle, R. A. Hermann Muller--Nobel Prize for contributions to genetics. *Mayo Clin Proc* **74**, 242 (1999).
218. Shandala, T., Kortschak, R. D., Gregory, S. & Saint, R. The Drosophila dead ringer gene is required for early embryonic patterning through regulation of argos and buttonhead expression. *Development* **126**, 4341-4349 (1999).
219. Shi, S. et al. JAK signaling globally counteracts heterochromatic gene silencing. *Nat Genet* **38**, 1071-1076 (2006).
220. Shi, S. et al. Drosophila STAT is required for directly maintaining HP1 localization and heterochromatin stability. *Nat Cell Biol* **10**, 489-496 (2008).
221. Shifren, A., Durmowicz, A. G., Knutsen, R. H., Hirano, E. & Mecham, R. P. Elastin protein levels are a vital modifier affecting normal lung development and susceptibility to emphysema. *Am J Physiol Lung Cell Mol Physiol* **292**, L778-87 (2007).
222. Shiraishi, I., Takamatsu, T., Minamikawa, T. & Fujita, S. 3-D observation of actin filaments during cardiac myofibrinogenesis in chick embryo using a confocal laser

scanning microscope. *Anat Embryol (Berl)* **185**, 401-408 (1992).

223. Shuai, K. et al. Interferon activation of the transcription factor Stat91 involves dimerization through SH2-phosphotyrosyl peptide interactions. *Cell* **76**, 821-828 (1994).
224. Shuai, K., Schindler, C., Prezioso, V. R. & Darnell, J. E. J. Activation of transcription by IFN-gamma: tyrosine phosphorylation of a 91-kD DNA binding protein. *Science* **258**, 1808-1812 (1992).
225. Silver, D. L., Geisbrecht, E. R. & Montell, D. J. Requirement for JAK/STAT signaling throughout border cell migration in Drosophila. *Development* **132**, 3483-3492 (2005).
226. Silver, D. L. & Montell, D. J. Paracrine signaling through the JAK/STAT pathway activates invasive behavior of ovarian epithelial cells in Drosophila. *Cell* **107**, 831-841 (2001).
227. Silver, D. L. & Montell, D. J. A new trick for Cyclin-Cdk: activation of STAT. *Dev Cell* **4**, 148-149 (2003).
228. Simmonds, A. J., Brook, W. J., Cohen, S. M. & Bell, J. B. Distinguishable functions for engrailed and invected in anterior-posterior patterning in the Drosophila wing. *Nature* **376**, 424-427 (1995).
229. Simoes Sde, M. et al. Rho-kinase directs Bazooka/Par-3 planar polarity during Drosophila axis elongation. *Dev Cell* **19**, 377-388 (2010).
230. Simoes, S. et al. Compartmentalisation of Rho regulators directs cell invagination during tissue morphogenesis. *Development* **133**, 4257-4267 (2006).
231. Singer, J. B., Harbecke, R., Kusch, T., Reuter, R. & Lengyel, J. A. Drosophila brachyenteron regulates gene activity and morphogenesis in the gut. *Development* **122**, 3707-3718 (1996).
232. Snow, P. M., Bieber, A. J. & Goodman, C. S. Fasciclin III: a novel homophilic adhesion molecule in Drosophila. *Cell* **59**, 313-323 (1989).
233. Snow, P. M., Patel, N. H., Harrelson, A. L. & Goodman, C. S. Neural-specific carbohydrate moiety shared by many surface glycoproteins in Drosophila and grasshopper embryos. *J Neurosci* **7**, 4137-4144 (1987).
234. Soanes, K. H. & Bell, J. B. Rediscovery and further characterization of the

aeroplane (ae) wing posture mutation in Drosophila melanogaster. *Genome* **42**, 403-411 (1999).

235. Soanes, K. H. et al. Identification of a regulatory allele of teashirt (tsh) in Drosophila melanogaster that affects wing hinge development. An adult-specific tsh enhancer in Drosophila. *Mech Dev* **105**, 145-151 (2001).
236. Sotillos, S., Diaz-Meco, M. T., Moscat, J. & Castelli-Gair Hombria, J. Polarized subcellular localization of Jak/STAT components is required for efficient signaling. *Curr Biol* **18**, 624-629 (2008).
237. Sotillos, S., Espinosa-Vazquez, J. M., Foglia, F., Hu, N. & Hombria, J. C. An efficient approach to isolate STAT regulated enhancers uncovers STAT92E fundamental role in Drosophila tracheal development. *Dev Biol* **340**, 571-582 (2010).
238. Speder, P., Adam, G. & Noselli, S. Type ID unconventional myosin controls left-right asymmetry in Drosophila. *Nature* **440**, 803-807 (2006).
239. St Johnston, D. & Nusslein-Volhard, C. The origin of pattern and polarity in the Drosophila embryo. *Cell* **68**, 201-219 (1992).
240. Starz-Gaiano, M., Melani, M., Meinhardt, H. & Montell, D. Interpretation of the UPD/JAK/STAT morphogen gradient in Drosophila follicle cells. *Cell Cycle* **8**, 2917-2925 (2009).
241. Starz-Gaiano, M., Melani, M., Wang, X., Meinhardt, H. & Montell, D. J. Feedback inhibition of Jak/STAT signaling by apontic is required to limit an invasive cell population. *Dev Cell* **14**, 726-738 (2008).
242. Steinberg, M. S. Reconstruction of tissues by dissociated cells. Some morphogenetic tissue movements and the sorting out of embryonic cells may have a common explanation. *Science* **141**, 401-408 (1963).
243. Stork, T. et al. Organization and function of the blood-brain barrier in Drosophila. *J Neurosci* **28**, 587-597 (2008).
244. Strigini, M. et al. The IgLON protein Lachesin is required for the blood-brain barrier in Drosophila. *Mol Cell Neurosci* **32**, 91-101 (2006).
245. Strong, R. K., Vaughn, D. E., Bjorkman, P. J. & Snow, P. M. Expression and crystallization of a soluble form of Drosophila fasciclin III. *J Mol Biol* **241**, 483-487

(1994).

246. Taber, L. A., Voronov, D. A. & Ramasubramanian, A. The role of mechanical forces in the torsional component of cardiac looping. *Ann N Y Acad Sci* **1188**, 103-110 (2010).
247. Tabin, C. J. The key to left-right asymmetry. *Cell* **127**, 27-32 (2006).
248. Takahashi, T. & Shirasawa, T. Molecular cloning of rat JAK3, a novel member of the JAK family of protein tyrosine kinases. *FEBS Lett* **342**, 124-128 (1994).
249. Takashima, S. & Murakami, R. Regulation of pattern formation in the Drosophila hindgut by wg, hh, dpp, and en. *Mech Dev* **101**, 79-90 (2001).
250. Tanentzapf, G. & Tepass, U. Interactions between the crumbs, lethal giant larvae and bazooka pathways in epithelial polarization. *Nat Cell Biol* **5**, 46-52 (2003).
251. Taniguchi, K. et al. Chirality in planar cell shape contributes to left-right asymmetric epithelial morphogenesis. *Science* **333**, 339-341 (2011).
252. Tefferi, A. & Gilliland, D. G. The JAK2V617F tyrosine kinase mutation in myeloproliferative disorders: status report and immediate implications for disease classification and diagnosis. *Mayo Clin Proc* **80**, 947-958 (2005).
253. Tepass, U. Adherens junctions: new insight into assembly, modulation and function. *Bioessays* **24**, 690-695 (2002).
254. Tepass, U. & Hartenstein, V. The development of cellular junctions in the Drosophila embryo. *Dev Biol* **161**, 563-596 (1994).
255. Tepass, U., Theres, C. & Knust, E. crumbs encodes an EGF-like protein expressed on apical membranes of Drosophila epithelial cells and required for organization of epithelia. *Cell* **61**, 787-799 (1990).
256. Tiklova, K., Senti, K. A., Wang, S., Graslund, A. & Samakovlis, C. Epithelial septate junction assembly relies on melanotransferrin iron binding and endocytosis in Drosophila. *Nat Cell Biol* **12**, 1071-1077 (2010).
257. Tsai, Y. C. & Sun, Y. H. Long-range effect of upd, a ligand for Jak/STAT pathway, on cell cycle in Drosophila eye development. *Genesis* **39**, 141-153 (2004).
258. Tuinstra, E. J., De Jong, G. & Scharloo, W. Lack of response to family selection for directional asymmetry in Drosophila melanogaster: left and right are not distinguished in development. *Proc Biol Sci* **241**, 146-152 (1990).

259. Tulina, N. & Matunis, E. Control of stem cell self-renewal in Drosophila spermatogenesis by JAK-STAT signaling. *Science* **294**, 2546-2549 (2001).
260. Tzima, E. et al. A mechanosensory complex that mediates the endothelial cell response to fluid shear stress. *Nature* **437**, 426-431 (2005).
261. Valentino, L. & Pierre, J. JAK/STAT signal transduction: regulators and implication in hematological malignancies. *Biochem Pharmacol* **71**, 713-721 (2006).
262. Van de Bor, V., Zimniak, G., Cerezo, D., Schaub, S. & Noselli, S. Asymmetric localisation of cytokine mRNA is essential for JAK/STAT activation during cell invasiveness. *Development* **138**, 1383-1393 (2011).
263. Vidal, O. M., Stec, W., Bausek, N., Smythe, E. & Zeidler, M. P. Negative regulation of Drosophila JAK-STAT signalling by endocytic trafficking. *J Cell Sci* **123**, 3457-3466 (2010).
264. Vogl, C. et al. Transcriptome analysis reveals a major impact of JAK protein tyrosine kinase 2 (Tyk2) on the expression of interferon-responsive and metabolic genes. *BMC Genomics* **11**, 199 (2010).
265. Voronov, D. A., Alford, P. W., Xu, G. & Taber, L. A. The role of mechanical forces in dextral rotation during cardiac looping in the chick embryo. *Dev Biol* **272**, 339-350 (2004).
266. Voronov, D. A. & Taber, L. A. Cardiac looping in experimental conditions: effects of extraembryonic forces. *Dev Dyn* **224**, 413-421 (2002).
267. Wagenseil, J. E. et al. The importance of elastin to aortic development in mice. *Am J Physiol Heart Circ Physiol* **299**, H257-64 (2010).
268. Wallingford, J. B. et al. Dishevelled controls cell polarity during Xenopus gastrulation. *Nature* **405**, 81-85 (2000).
269. Wang, S. et al. Septate-junction-dependent luminal deposition of chitin deacetylases restricts tube elongation in the Drosophila trachea. *Curr Biol* **16**, 180-185 (2006).
270. Weigel, D., Jurgens, G., Kuttner, F., Seifert, E. & Jackle, H. The homeotic gene fork head encodes a nuclear protein and is expressed in the terminal regions of the Drosophila embryo. *Cell* **57**, 645-658 (1989).
271. Weigel, D., Seifert, E., Reuter, D. & Jackle, H. Regulatory elements controlling

expression of the Drosophila homeotic gene fork head. *EMBO J* **9**, 1199-1207 (1990).

272. Wendel, D. P., Taylor, D. G., Albertine, K. H., Keating, M. T. & Li, D. Y. Impaired distal airway development in mice lacking elastin. *Am J Respir Cell Mol Biol* **23**, 320-326 (2000).
273. Whitworth, A. J. Drosophila models of Parkinson's disease. *Adv Genet* **73**, 1-50 (2011).
274. Whitworth, A. J. & Russell, S. Temporally dynamic response to Wingless directs the sequential elaboration of the proximodistal axis of the Drosophila wing. *Dev Biol* **254**, 277-288 (2003).
275. Wicking, C., Smyth, I. & Bale, A. The hedgehog signalling pathway in tumorigenesis and development. *Oncogene* **18**, 7844-7851 (1999).
276. Wilks, A. F. et al. Two novel protein-tyrosine kinases, each with a second phosphotransferase-related catalytic domain, define a new class of protein kinase. *Mol Cell Biol* **11**, 2057-2065 (1991).
277. Wingen, C., Stumpges, B., Hoch, M. & Behr, M. Expression and localization of clathrin heavy chain in Drosophila melanogaster. *Gene Expr Patterns* **9**, 549-554 (2009).
278. Wodarz, A., Hinz, U., Engelbert, M. & Knust, E. Expression of crumbs confers apical character on plasma membrane domains of ectodermal epithelia of Drosophila. *Cell* **82**, 67-76 (1995).
279. Wolpert, L. et al. Principles of Development. (2006).
280. Wright, V. M., Vogt, K. L., Smythe, E. & Zeidler, M. P. Differential activities of the Drosophila JAK/STAT pathway ligands Upd, Upd2 and Upd3. *Cell Signal* **23**, 920-927 (2011).
281. Wu, L. H. & Lengyel, J. A. Role of caudal in hindgut specification and gastrulation suggests homology between Drosophila amnioproctodeal invagination and vertebrate blastopore. *Development* **125**, 2433-2442 (1998).
282. Wu, V. M. & Beitel, G. J. A junctional problem of apical proportions: epithelial tube-size control by septate junctions in the Drosophila tracheal system. *Curr Opin Cell Biol* **16**, 493-499 (2004).

283. Wu, V. M. et al. Drosophila Varicose, a member of a new subgroup of basolateral MAGUKs, is required for septate junctions and tracheal morphogenesis. *Development* **134**, 999-1009 (2007).
284. Wu, Y. & Zhou, B. P. Inflammation: a driving force speeds cancer metastasis. *Cell Cycle* **8**, 3267-3273 (2009).
285. Xi, R., McGregor, J. R. & Harrison, D. A. A gradient of JAK pathway activity patterns the anterior-posterior axis of the follicular epithelium. *Dev Cell* **4**, 167-177 (2003).
286. Yamamoto, K. et al. Stat4, a novel gamma interferon activation site-binding protein expressed in early myeloid differentiation. *Mol Cell Biol* **14**, 4342-4349 (1994).
287. Yamashita, S. et al. Stat3 Controls Cell Movements during Zebrafish Gastrulation. *Dev Cell* **2**, 363-375 (2002).
288. Yan, R., Small, S., Desplan, C., Dearolf, C. R. & Darnell, J. E. J. Identification of a Stat gene that functions in Drosophila development. *Cell* **84**, 421-430 (1996).
289. Yoon, W. H., Meinhardt, H. & Montell, D. J. miRNA-mediated feedback inhibition of JAK/STAT morphogen signalling establishes a cell fate threshold. *Nat Cell Biol* **13**, 1062-1069 (2011).
290. Zeidler, M. P., Perrimon, N. & Strutt, D. I. The four-jointed gene is required in the Drosophila eye for ommatidial polarity specification. *Curr Biol* **9**, 1363-1372 (1999).
291. Zeidler, M. P., Perrimon, N. & Strutt, D. I. Polarity determination in the Drosophila eye: a novel role for unpaired and JAK/STAT signaling. *Genes Dev* **13**, 1342-1353 (1999).
292. Zhong, Z., Wen, Z. & Darnell, J. E. J. Stat3: a STAT family member activated by tyrosine phosphorylation in response to epidermal growth factor and interleukin-6. *Science* **264**, 95-98 (1994).

Re-print Permission

December 2, 2011

Richard Wells
Sheffield University

Mdp08rew@sheffield.ac.uk

Dear Richard,

In response to your request regarding permission to adapt the following material:

Item:	Figures on pp. 29-33
Title:	*Atlas of* Drosophila *Development*
Author:	Volker Hartenstein
Copyright date:	1993

To be used in:

Title:	PhD Thesis
Author:	Richard Wells
Publication date:	2012

I confirm that we are willing to grant non-exclusive rights in the English language, subject to the following conditions:

1. Full acknowledgment shall be made to the source and correct references given. Copyright holder is Cold Spring Harbor Laboratory Press.
2. Permission of the author is obtained where possible.
3. Permission is limited to the proposed publication, on a non-exclusive, ***one-time-only basis***, with distribution rights in the English language only. This permission relates to publication in the English language for print and online rights only. ***Rights do not apply to revised editions.***

*Please note that we do not grant blanket permissions for future editions or translations. If you need any of the aforementioned, please reapply and include details of usage.

By Carol C. Brown **Date: 12/2/11**
For Cold Spring Harbor Laboratory Press, 500 Sunnyside Blvd., Woodbury NY 11797, USA